CHARACTERISTICS OF COUPLED NONGRAY RADIATING GAS FLOWS

WITH ABLATION PRODUCT EFFECTS ABOUT BLUNT BODIES

DURING PLANETARY ENTRIES

by

KENNETH SUTTON

A thesis submitted to the Graduate Faculty of
North Carolina State University at Raleigh
in partial fulfillment of the
requirements for the degree of
Doctor of Philosophy

DEPARTMENT OF MECHANICAL AND AEROSPACE ENGINEERING

RALEIGH

1 9 7 3

APPROVED BY:

Chairman of Advisory Committee

ABSTRACT

SUTTON, KENNETH. Characteristics of Coupled Nongray Radiating Gas Flows
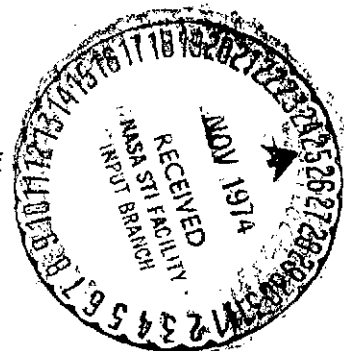with Ablation Product Effects about Blunt Bodies during Planetary En-
tries. (Under the direction of FREDERICK OTTO SMETANA).

A computational method is developed for the fully-coupled solution
of nongray, radiating gas flows with ablation product effects about
blunt bodies during planetary entries. The treatment of radiation ac-
counts for molecular band, continuum, and atomic line transitions with
a detailed frequency dependence of the absorption coefficient. The
ablation of the entry body is solved as part of the solution for a
steady-state ablation process.

Application of the developed method is shown by results at typical
conditions for unmanned, scientific probes during entry to Venus. The
radiative heating rates along the downstream region of the body can,
under certain conditions, exceed the stagnation point value. The ra-
diative heating to the body is attenuated in the boundary layer at the
downstream region of the body as well as at the stagnation point of the
body.

Results from a study of the radiating, inviscid flow about spheri-
cally-capped, conical bodies during planetary entries are presented
and show that the nondimensional, radiative heating distributions are
nonsimilar with entry conditions. Therefore, extreme caution should be
exercised in attempting to extrapolate results from known distributions
to other entry conditions for which solutions have not yet been obtained.

BIOGRAPHY

Kenneth Sutton was ████████████████████████████████. He was reared in Jacksonville, Florida and graduated from Andrew Jackson High School in 1957. He attended Jacksonville University for two years before transferring to the University of Florida where he received the degree of Bachelor of Mechanical Engineering in 1962.

After graduating, he accepted a position with the Langley Research Center of the National Aeronautics and Space Administration in Hampton, Virginia. He received his graduate education through the NASA Graduate Study Program. In 1963 he returned to the University of Florida and received the degree of Master of Engineering in 1964. He began night studies in 1964 with the Tidewater Extension Center of George Washington University and received the degree of Master of Science in Governmental Administration in 1967. He entered North Carolina State University at Raleigh in 1968 to begin advanced studies in the Department of Mechanical and Aerospace Engineering. He returned to the Langley Research Center in 1969 where he performed the analysis presented in this thesis.

He is presently assigned to the Advanced Entry Analysis Branch of the Spacecraft Systems Division at the Langley Research Center. He is a member of the American Institute of Aeronautics and Astronautics and the American Society of Mechanical Engineers. He is registered as a Professional Engineer by the State of Florida.

ACKNOWLEDGEMENTS

The author wishes to express his appreciation to the National

Aeronautics and Space Administration for its continued support of his

graduate studies and for supporting the research presented in the

thesis.

The author wishes to thank the members of his advisory committee

for their help and cooperation. He is especially grateful to Dr.

Frederick O. Smetana for his assistance and patience during the

author's studies and research investigation.

Special appreciation is extended to Mr. Gerald D. Walberg of the

Langley Research Center for proposing the topic of the research inves-

tigation, for his continued support of the investigation, and for his

consultation on many technical matters. The author is appreciative of

the technical consultation given to him by members of the Langley

Research Center: Dr. Walter B. Olstad, Mr. Linwood B. Callis, Dr.

Robert E. Boughner, Mr. Ralph A. Falanga, Mr. John T. Suttles, and

Dr. G. Louis Smith. Also, the author is grateful for the technical

assistance by members of the Aerotherm Corporation: Mr. William E.

Nicolet, Dr. Robert M. Kendall, and Mr. Eugene P. Bartlett.

The author is grateful for the pleasant conversation, encourage-

ment, and technical assistance extended to him by his office colleagues,

Mr. Randolph A. Graves, Jr., and Mr. E. Vincent Zoby. Special gratitude

is expressed to Mr. Bennie W. Cocke, Jr. of the Langley Research Center

for his guidance and help in the author's earlier career. Also,

TABLE OF CONTENTS

LIST OF TABLES

LIST OF FIGURES

LIST OF SYMBOLS

A	parameter defined by eq. 21
a	sonic velocity, see eq. 49
B	parameter defined by eq. 22
B_ν	Planck function
C	parameter defined by eq. 23
C_1	parameter defined by eq. A4
C_2	parameter defined by eq. A5 or eq. 35
C_3	parameter defined by eq. A6 or eq. 36
c_p	specific heat
$\bar{c}_p$	specific heat parameter defined by eq. 61
D	parameter defined by eq. 24
D_{ij}	binary diffusion coefficient for ith and jth chemical species
$\bar{D}$	self-diffusion coefficient of a reference species
E	parameter defined by eq. 25
E_n	exponential integral of order n
E_3	exponential integral of order 3
F^R	divergence of radiative flux defined by eq. 26
F_i	diffusion factor of ith chemical species in a given chemical system, see eq. 57
f	represents the variables p,u,v, or h in eqs. 37 to 39
f	stream function for boundary-layer equations, defined by eq. 70
g_i	metric coefficient for ith coordinate, used herein as $g_1=\lambda$, $g_2=1$, $g_3=r$ (see eqs. 6 to 8)
H	total enthalpy, $h+u^2/2$, in boundary-layer equations

h	enthalpy
$\bar{h}$	enthalpy parameter defined by eq. 61
h^*	Planck constant
h_a^o	heat of formation of undecomposed ablation material
I_ν	monochromatic radiation intensity
j_i	diffusional mass flux of chemical element i, see eq. 58
K	body curvature parameter defined by eq. 9
$\bar{K}_i$	mass fraction of chemical element i
k	thermal conductivity
ℓ	differential line element in eqs. 6 and 7
M	molecular weight
m_a	ablation rate of the heatshield
P_1	thermodynamic variable defined by eqs. 31 and 48
P_3	thermodynamic variable defined by eqs. 32 and 49
p	pressure
q^C	convective heat flux, see eq. 60
q^R	radiative heat flux
q_{cond}	heat flux conducted into the heatshield
Re_θ	momentum thickness Reynolds number for boundary layer
Rn	nose radius of body at s=0, see Figure 3
r	radial distance from axis of symmetry of body, see Figure 3
r_b	body radius from axis of symmetry, see Figure 3
S	transformed s coordinate for inviscid-layer equations, defined by eq. 15
SF	stream function for inviscid-layer equations, defined by eq. 45

s	coordinate along the body surface, see Figure 3
T	transformed t coordinate defined by eq. 15
$\overline{T}$	temperature
$\overline{T}_\delta$	temperature at $y=\delta$ in inviscid flow field
t	time
t_υ	dummy variable of monochromatic optical depth in eqs. 76 to 78
u	velocity tangent to body surface, see Figure 3
V_∞	free-stream velocity
V_e	entry velocity
v	velocity normal to body surface, see Figure 3
W	weight of entry probe
W/C_dA	ballistic coefficient where the drag coefficient, C_d, is for area, A, of the probe's base
x_i	general coordinates, used herein as $x_1=s$, $x_2=y$, and $x_3=\phi$ (see eqs. 6 and 7)
$\overline{x}_j$	mole fraction of chemical species j
Y	transformed y coordinate, defined by eq. 15
y	coordinate normal to the body surface, see Figure 3
z_j	quantity for jth chemical species defined by eq. 59
$\overline{z}_i$	quantity for ith chemical element defined by eq. 59
z	distance along axis of symmetry of body
z	function for the exponential integral of order n, $E_n(z)$
α_{ij}	mass fraction of chemical element i in chemical species j
β	difference between the angle of the shock wave and the angle of the body surface, see Figure 3
γ	angle between a ray and the normal for radiation flux in eq. 71

γ_e entry angle

δ shock stand-off distance of inviscid layer

δ^* boundary-layer displacement thickness defined by eq. 2

δ^t total thickness of shock layer defined by eq. 1

ε_ν monochromatic emissivity defined by eqs. 76 and 78

ε_w emissivity of the heatshield

η transformed y coordinate for boundary-layer equations, defined by eq. 69

θ angle of body surface relative to axis of symmetry of body, see Figure 3

θ_c cone half angle for a spherically-capped, conical body

λ curvature parameter defined by eq. 9

λ_δ value of λ at y=δ

μ viscosity in boundary-layer equations

μ_1 parameter defined by eq. 59

μ_2 parameter defined by eq. 59

μ_ν monochromatic linear absorption coefficient corrected for induced emission

$\bar{\mu}_\nu$ μ_ν for molecular band transitions, defined by eq. 81

ν radiation frequency

ξ transformed s coordinate for boundary-layer equations, defined by eq. 69

ρ density

$\rho\varepsilon_d$ turbulent eddy diffusivity

$\rho\varepsilon_h$ turbulent eddy conductivity

$\rho\varepsilon_m$ turbulent eddy viscosity

σ Stefan-Boltzmann constant

τ_ν monochromatic optical depth defined by eq. 75

τ_w aerodynamic shear at the wall

ϕ azimuth angle, see Figure 3

Ω solid angle

subscripts

a   refers to the ablation material

c   refers to the char of the decomposed ablation material

e   refers to the boundary-layer edge

g   refers to the pyrolysis gas of the decomposed ablation material

i,j   refers to the ith or jth chemical species or chemical element

o   refers to stagnation-point values, s=0

s   refers to conditions behind a normal shock wave

w   refers to the body wall

∞ refers to free-stream conditions

δ refers to conditions at $y=\delta$ in the inviscid layer

ν refers to radiation frequency

superscripts

C,L   refers to continuum transitions, including molecular band transitions, or line transitions in eq. 79

1,2   refers to the first or second step in the two-step numerical method for the radiating, inviscid flow solution

+,-   refers to the direction of the radiative flux (+ refers to the radiative flux toward the shock wave and - refers to the radiative flux toward the body)

prime   refers to dimensional quantities in the section of Radiating, Inviscid Flow Field Solution

INTRODUCTION

One of the major scientific endeavors of the present day is the exploration of the planets by unmanned and manned spacecraft. The present technique for planetary entry is to use atmospheric friction as a brake to slow the spacecraft from hypersonic speeds. During hypersonic entry the gas around the body in the formed shock layer is heated by the dissipated kinetic energy. In order for the spacecraft to survive, the main body of the spacecraft will be protected from this source of intense heat by the use of an ablative heat shield material. The speeds required for planetary entries will be well in the excess of the parabolic speed in order to reduce trip times for interplanetary travel. The temperatures of the heated gas behind a shock wave associated with these high-speed entries are sufficient for gas radiation to be a major contributor to the heating of the spacecraft. The inclusion of radiative heating in the energy equation of flow field solutions causes a strong coupling between the radiative transport, the inviscid shock layer, the boundary layer, and the ablative heat shield analyses. Computational methods for the solution of this complex flow phenomena are required before heat shields can be designed to survive during planetary entries at speeds in excess of parabolic speed.

At entry speeds less than parabolic speed the radiative heating is negligible and convection through the boundary layer is the dominant mode of heat transport to the body. The neglect of radiative transport uncouples the inviscid flow equations and the boundary layer equations; however, the boundary layer analysis and the heat shield analysis are

still coupled. Extensive analyses for boundary layers with mass injection have been conducted over the years so that the necessary inputs to the heat shield analysis for convective heating and mass diffusion can be determined without a coupled solution of the equations.

At entry speeds in excess of parabolic speed the radiative transport cannot be neglected and the radiative heating can be much more dominant than convective heating. In general, the radiative transport in a gas is governed by integral equations involving the absorption coefficient integrated over both radiation frequency spectrum and three-dimensional space. The absorption coefficient is dependent on the temperature, density, and the number density of the species present in the gas (ref. 1, page 721). Thus, the radiative transport is dependent on the thermodynamic profiles throughout the gas layer between the shock wave and body. The absorption of radiation by the cooler gas in the boundary layer will change the thermodynamic profiles in the boundary layer and affect the convective heating and mass diffusion to the heat shield. In early studies, the incident radiation to the spacecraft was taken as the radiation from the inviscid shock layer. Later studies have shown that the boundary layer, with and without injection of abla-tion products, can absorb radiation and reduce the incident radiative heating to the spacecraft. For high-speed planetary entry, the solution of the flow field equations and the heat shield analysis is very complex because of the coupling of radiative transport.

The radiative transport to the stagnation region of blunt bodies for entries into air has been the primary interest for most studies of

radiating flow fields with ablation product effects. The interest for entries into air was due to Earth reentry after exploration of the Earth's moon and preliminary studies for Earth reentry after exploration of Mars. There is a need for investigation of the radiating flow field in other gaseous atmospheres because of the increased interest in exploration of other planets (Venus, Jupiter, etc.). The emphasis on the stagnation region was due to a simplification of the solution and because the radiative heating was considered to be greatest in this region. However, the recent results by Olstad (ref. 2) and by Callis (ref. 3) for an inviscid, radiating flow field have shown that the radiative heating to the flank regions of blunted-conical bodies can equal or exceed the radiative heating to the stagnation region. As discussed by Page (ref. 4), most of the heat shield surface and weight is downstream of the stagnation region and valid treatment of fully-coupled solutions is needed downstream of the stagnation region along cone flanks or over spherical noses. Anderson (ref. 5) states the need for additional solutions of the coupled radiative problem with ablation product effects to complement the existing results. These points illustrate the need for a method of calculating the fully-coupled radiating flow field, with ablation product effects, around the entire body and for entries into atmospheres of arbitrary gases.

The purpose of the present study is to investigate and develop a computational method for a fully-coupled solution of the radiating flow field, with ablation products injection, about blunt bodies for entries into arbitrary gas mixtures. Basically, the method is to separate the

radiating flow field into an outer inviscid layer and an inner boundary layer with injected ablation products; then, the two solutions are coupled by the radiative transport through both layers and by the boundary layer displacement thickness for mass injection. The radiative flux is included in the energy equation of both the inviscid solution and the boundary layer solution. As previously stated, the fully-coupled formulation for radiating planetary entry is very complex and all approaches require varying degrees of approximation in order to obtain a solution. By separating the two different layers of flow, a better treatment should be possible for the solution of each layer.

A second-order, time-asymptotic technique is used for the solution of the inviscid shock layer. The set of unsteady governing equations is hyperbolic, thus the technique is valid in both the subsonic and super-sonic regions of the inviscid flow about the body. A computer program for a numerical solution of the technique is developed in the study. An equilibrium thermodynamic subroutine and a detailed radiative trans-port subroutine are included in the computer program so that arbitrary gas mixtures can be considered. Moretti and Abbett (ref. 6) used a time-asymptotic technique for an inviscid flow solution without radia-tion in a perfect gas and Callis (refs. 3 and 7) used a time-asymptotic technique for a radiating, inviscid flow solution in air.

The solution of the inner gas layer is for a nonsimilar, multi-component boundary layer with mass injection, unequal diffusion coef-ficients, and arbitrary chemical species. The numerical, integral matrix method of Barlett and Kendall (ref. 8) is used for the boundary

layer solution and there is an existing computer program called BLIMP. In the computer program, the thermodynamic properties and transport properties (viscosity, etc.) are calculated as part of the solution. The injection rate of ablation products can be either prespecified or calculated during the solution for a steady-state ablation process. The computer program is modified in the present study to account for radiative transport within the boundary layer.

The radiative transport solution for coupling the inviscid layer and the boundary layer is for a nongray gas with molecular band, continuum, and atomic line transitions. The integration over the radiation spectrum uses a detailed frequency dependence of the absorption coeffieients and the tangent slab approximation is used for integration over physical space. An existing computer program (RAD/EQUIL) of the numerical method by Nicolet (ref. 9) is used for the solution of the radiative transport. In addition to using this program for coupling the flow fields, an extensive modification of the program is made so that it can be used efficiently as a subroutine in the developed computer program for the inviscid radiating layer.

The application of the present developed method is shown by a study of typical points on an entry trajectory for Venus. To the author's knowledge, there are no published results for a fully-coupled radiating solution with ablation products injection at either the stagnation or downstream regions on a body for Venusian entry. The validity of the method is investigated by a comparison with published results for Earth entry.

REVIEW OF LITERATURE

The review of literature is restricted to prior studies which
present the more pertinent results for the radiating flow about blunt
bodies with ablation products injection. The fully-coupled solution of
radiating flow with ablation analysis is a complex problem and involves
many disciplines; therefore, a detailed review of the entire field for
the thermal analysis during planetary entry is not presented. A good
review and extensive reference list for radiating shock layers is given
by Anderson (ref. 5). Similarly, a review of ablative heat shields for
planetary entries is given by Walberg and Sullivan (ref. 10). These two
articles provide a good review of the present technology of radiative
heating and ablation analysis for high-speed planetary entry. For
additional discussions of the background information presented in the
Introduction on planetary gas dynamics and planetary entry, the reader
is referred to references 4 and 11 to 15. Information on trajectory
analysis for planetary missions is available in reference 16. A dis-
cussion on types of heat shield materials and ablation mechanisms is
given in reference 17. A good analysis on the coupling between the
boundary layer and a charring ablator is given by Kendall et al., (ref.
18).

The remaining sections of the literature survey present more
detailed information which is pertinent to an analysis of the radiating
flow about blunt bodies. The first section discusses features of radi-
ation transport modeling. The second section is a discussion on radia-
ting flow field analyses. In addition to flows about blunt bodies, a

discussion is presented on significant and applicable results from stagnation region analyses. Finally, a section is presented on the thermal analyses for Venusian entry.

Radiation Transport Modeling

An atom or molecule in a high-temperature gaseous medium can emit and absorb radiation at a frequency characteristic of some transition from one quantum state to another and each specie has an absorption spectrum which can be expressed in terms of an absorption coefficient. Because of quantum transtions, the absorption coefficient is a function of frequency. Radiation of a given frequency travels in physical space a distance (radiation mean free path) before being absorbed. (The above description is from reference 1, page 721.) Thus, the radiative transport in a gaseous medium is a function of frequency and distance and the equation for the total radiative transport is an integral over both frequency spectrum and physical space.

The solution for a radiating flow field is a set of integro-differential equations and approximations are used to solve this complex system of equations. One of the approximations deals with the spatial aspect of radiative transport. The absorption of radiation at a point in the flow field is a function of the emitted radiation from surrounding fluid elements; and, since radiation travels a distance before being absorbed, the radiative transport is a three-dimensional problem in space. To reduce the complexity of the solution, the "tangent slab approximation"

is usually used for radiating flow fields. This approximation treats the gas layer as a one-dimensional slab in calculation of the radiative transport. The radiative heat flux is neglected except in the direction normal to either the body or shock wave.

Garrett (ref. 19), after a review of the studies of references 20 to 22, states the error introduced by the approximation should be less than 5 percent at the stagnation point. Page (ref. 4), in a discussion of the three-dimensional effects, concludes that the tangent slab approximation is sufficiently accurate for engineering calculations when the shock-layer thickness is small compared to the curvature (~1/12). Page's conclusions are based primarily on the studies by Chien (ref. 23) and by Wilson (ref. 24). The study by Wilson was a comparison of the tangent slab approximation with an exact three-dimensional numerical calculation at the stagnation and downstream regions of a blunted, conical body for a typical Earth reentry. The error for the tangent slab approximation was 15 percent at the stagnation region and less error at the conical region. The tangent slab approximation is used in the present study.

In radiation transport modeling, the gas may be treated as transparent, gray, or nongray. A transparent gas is assumed to emit radiation but not absorb radiation. The treatment of a gray or nongray gas allows both emission and absorption. However, the absorption coefficient is assumed constant over the frequency spectrum for a gray gas. A frequency dependence of the absorption coefficient, either approximate or in detail, is included for a nongray gas. Anderson (ref. 5) traces the

historical development of radiating flow fields and shows the progression from transparent, continuum only, uncoupled calculations used by early investigators to the nongray, continuum and line, coupled energy calculations which are current today. As discussed by Anderson, a gray gas analysis is not sufficiently accurate for reentry applications and the gas should be treated as nongray.

The frequency dependence of absorption coefficient for a nongray gas is treated in detail or by a "step-model". In a step model, the frequency dependence is broken into a number of discrete steps (see, for example, references 7 and 25 to 27). The number of steps are generally from two to nine. The calculation of the radiative heat flux involves an integral over frequency and using a step-model will simplify the integration. However, the injection of ablation products into the flow field increases the number of species to be considered and there is a rapid change in chemical composition in the boundary layer. A step-model has to be constructed for the particular gas composition and the addition of ablation products will complicate the construction. Boughner (ref. 25) had difficulty in developing a general step-model for a CO_2-N_2 mixture; and, the developed step-model was only valid over a restricted and narrow range of conditions. The difficulty was due to molecular band radiation.

The radiative heat flux with ablation product effects has been calculated for a nongray gas and the frequency dependence of absorption coefficient was considered in detail (see, for example, references 19, 28, and 29). There are computer programs for calculating the detailed,

nongray radiative transport of which the ones used primarily for reentry application are RATRAP, developed by Wilson (ref. 30); SPECS, developed by Thomas (ref. 31); and RAD/EQUIL, developed by Nicolet (refs. 9 and 32). Suttles (ref. 33) made a comparison of these programs in a recent study and concluded that the RAD/EQUIL program depended on fewer approximations, included more detail, and required less computer time than RATRAP and SPECS. The RAD/EQUIL program is used in the present study.

As discussed by Penner and Olfe (ref. 13), radiation is coupled to the conservation equations by the radiation pressure, radiation energy density, and radiation energy transfer. The radiation pressure and radiation energy density are usually negligible and can be neglected even when the radiation energy transfer is very important. The two terms can be and are neglected in solutions which deal primarily with radiative heating (refs. 13 and 34). Therefore, the coupling between radiation and the conservation equations is due to the divergence of the radiative heat flux in the energy equation.

For additional information on radiation and radiative transport, the interested reader is referred to the numerous available books. Two good books with which the author is most familiar are by Penner (ref. 35) and by Penner and Olfe (ref. 13). Radiative heating is considered in the book on gas dynamics by Vincenti and Kruger (ref. 34). Also, references 36 to 38 present analyses of radiative transport for high-temperature gases.

Radiating Flow Fields

The interest of the present study is the radiating flow field about blunt bodies; therefore, the flow in both the stagnation region and the downstream region has to be considered. Also, the prior studies which included ablation product effects have been for the stagnation region. A discussion and literature survey are presented first on the pertinent results from analyses of stagnation-region flow; then a discussion and literature survey are presented for flow about blunt bodies.

Flow at Stagnation Region

The recent doctoral thesis by Garrett (ref. 19) presents a detailed review of the various methods used for solving the radiating flow field at the stagnation region. Also, the various methods of solution are discussed in the papers by Goulard et al (ref. 39) and by Anderson (ref. 5). The reader is referred to these papers for a description of the solutions. Only the pertinent results will be presented here.

The earlier studies by Howe and Viegas (ref. 40) and by Hoshizaki and Wilson (refs. 41 and 42) have shown there is a coupling between radiative and convective heating and that radiation from the higher-temperature inviscid region can be absorbed by the lower-temperature viscous region. Later studies have shown that the ablation products injected into the flow field from ablative heat shields can significantly reduce the radiative heating to the body (refs. 19, 22, 28, 29, 43, and 44). These studies were for Earth reentry except a limited part of the study by Wilson (ref. 44) was for Jovian entry. Hoshizaki and

Lasher (ref. 22) state that atomic carbon from the ablation products is the principle absorber and Smith et al. (ref. 28) show that carbon monoxide can also significantly absorb the radiation from the radiating shock layer.

The recent thesis by Garrett (ref. 19) presents a comparison of the results at the stagnation region for air injection and ablation product injection. Garrett uses an implicit finite difference method for a solution at the stagnation-point of a blunt body and treats the entire shock layer as viscous. The results of Garrett show that massive injection of ablation products from a carbon phenolic heat shield into air reduced the radiative heating to the body by 40 percent; but, massive injection of air only reduced the radiative heating by 15 percent. A comparison of results presented by Garrett for solutions from various studies showed that ablation products reduce the radiative heating; but, there were significant differences in the magnitude of the reduction.

Smith et al. (ref. 28) used a method for the stagnation region which is similar to the method in the present study. That is, separating the inviscid layer and the boundary layer and then coupling the two by the radiative transport. The study was for Earth reentry with ablation product effects. The derivation of the boundary layer equations included the radiative heat flux in the energy equation and was for moderate and strong blowing. However, the results presented did not include the radiative heat flux in the energy equation for the boundary layer and was only for strong blowing. The solution of the equations was by numerical methods and Dr. Smith has stated there are difficulties in

extending the solution to include radiative heat flux in the boundary-layer energy equation and to include moderate blowing. The problem has not been solved.* The study by Smith et al. did show that the basic method is valid and in the present study the treatment of the boundary-layer solution is much better than the approximate method used by Smith et al.

Hoshizaki and Lasher (ref. 22) treated the entire shock layer as viscous and stated the advantage is that it eliminates the necessity of matching the radiative heat flux at the inviscid-viscid interface. Garrett (ref. 19) treated the entire layer as viscous and there were irregularities in the enthalpy profiles at the inviscid-viscid interface for strong blowing. The enthalpy profiles come from the energy equation and this equation is where the radiative transport is coupled to the flow equations. In the present study, the coupling is not a direct matching of the radiative heat flux at the interface. The radiative heat flux to be coupled in the energy equation of the boundary layer is taken from the solution of the radiative transport over the entire shock layer. The magnitude of the radiative heat flux from the boundary layer toward the inviscid layer is small compared to the flux toward the boundary layer from the inviscid layer (see, for example, ref. 28). Thus, in the present method the solution for the radiating inviscid layer is solved once and an iteration is only required between the boundary layer solution and radiative transport solution.

---

*Personal communication with Dr. G. Louis Smith, Langley Research Center, Hampton, Virginia

Garrett (ref. 19) and Rigdon et al. (ref. 29) state the need for properly calculating the thermodynamic properties of the ablation products. In the present study, the thermodynamic properties are calculated during the solution for both the inviscid region and the boundary layer and arbitrary gases can be considered.

As illustrated by the comparisons presented by Garrett (ref. 19), there are discrepancies for the magnitude of radiative heating reduction due to ablation effects even for the stagnation region. The existing results are primarily for Earth reentry and calculations need to be performed for other planetary entries. Anderson (ref. 5) states that realistic calculations for radiative heating to entry vehicles should definitely account for ablation effects and additional radiative coupled analyses with ablation effects should be made in order to complement the existing results.

Flow about Blunt Bodies

There have been a number of studies and numerical solutions for the radiative heating with ablation effects at the blunt-body stagnation region but solutions for the downstream regions of the flow field are not so advanced. The few studies which have considered the radiating flow about blunt bodies have shown that radiative heating at the flank regions of hemisphere-conical bodies can be a large fraction and even exceed the radiative heating at the stagnation point (refs. 2, 3, 45, and 46). These studies were for Earth reentry, used a step-model for the radiative transport, and did not include ablation product effects.

The study by Olstad (ref. 2) was for an inviscid shock layer with the solution of the flow field by the method developed by Maslen (ref. 47) but modified for radiative transport. The method of Maslen is based on the flow being parallel to the shock wave and uses a von Mises transformation. This method uncouples the y-momentum equation. However, the method is not strictly valid at the stagnation region. The study by Olstad was for the Earth reentry of blunted-conical bodies with cone half angles of 30, 45, and 60 degrees. A step-model was used for the radiative transport. The results showned that the radiative heating along the cone flanks was comparable to the stagnation region values for the larger cone angles. Olstad also presented some preliminary results for air injection into the shock layer. These solutions were performed by using the Maslen method for an inner inviscid layer. The results showed that the air injection was more effective in reducing the radiative heating at the stagnation region than at the downstream region. The enthalpy profiles of the inner inviscid layer give the appearance of a boundary layer but are a result of absorption of the radiant energy emitted by the outer inviscid layer.

Callis (ref. 3) investigated the radiating, inviscid flow about long blunt bodies by using a time-asymptotic technique. A discussion of this technique is given below. The study by Callis was for Earth reentry and a step-model was used for the radiative transport. The body shapes were spherically capped cones. The results showed that for larger cone angles (60 degrees half angle) the inviscid radiative heating rates were in excess of the stagnation values over a large portion of the flank region.

Callis states that this increase in heating rates along the cone flanks
could pose a serious thermal protection problem.

Chou (ref. 46) presents an approximate method for the flow about
blunt bodies in which the entire layer is considered to be viscous. The
solution is based on an approximate method for nonsimilar terms, the
specie continuity equation is neglected, the density-viscosity product
is constant, and the wall conditions are for constant mass injection and
temperature along the body. An equation is developed for the nonsimilar-
ity of the tangential velocity and Chou states that the validity of the
equation cannot be defined rigorously and the physcial reason for the
successful application is not clear. The application of the method was
for Earth reentry and the injected gas was air. However, radiative
transport was not considered for the air injection cases. A comparison
was made with the method of Olstad (ref. 2) for inviscid radiating flow.
The check cases were supplied by Dr. Olstad and Chou states that his
method is valid when the results are compared. However, there is some
question about the manner in which the results are being compared and
the comparison may not be as good as shown by Chou. The disagreement
over the comparison of the results has not been resolved.*

Prior solutions for the radiating flow about blunt bodies did not
include ablation product effects and were for Earth reentry. The need
for a fully-coupled solution with ablation products for arbitrary gases
can be illustrated by the studies of Tauber (refs. 48 and 49) and Tauber

---

*Personal communications with Dr. W. B. Olstad, Langley Research
Center, Hampton, Virginia

and Wakefield (ref. 50). These studies were for planetary entry into Jupiter, Saturn, Uranus, and Neptune with a nominal atmospheric composition of 85 percent hydrogen and 15 percent helium (mole fraction). The basis for the thermal analysis is presented in the paper by Tauber and Wakefield. These studies had to rely on stagnation-point results for the thermal analysis at the downstream regions. Results from the solutions for Earth reentry and the limited results by Wilson (ref. 44) for H_2-He mixture were used. This recourse had to be used because of the lack of results for flow around bodies with ablation product effects and the lack of results for entry into planets other than Earth. Additional discussion of this problem is given by Page (ref. 4).

There is no method which is generally accepted as being best, even when radiative transport is not included, for the shock layer solution around hypersonic blunt bodies (ref. 39). This point is shown in the paper by Perry and Pasiuk (ref. 51) in which numerous solutions are compared and are compared with experimental data. There is considerable scatter between the different solutions even in the region of subsonic flow. The solution used in the present study for the radiating, inviscid layer is a numerical method of a time-asymptotic technique.

Prior studies have used the time-asymptotic technique for the solution of an inviscid flow field (see, for example, refs. 3, 6, 52 and 53). The time-asymptotic technique retains the time dependent terms in the governing equations of the flow field and permits the time to increase until steady-state conditions are reached. By retaining the time dependent terms, the set of governing equations is hyperbolic and the same

computational method can be used in both the subsonic and supersonic regions of the flow along the body. The development of the technique is due to the studies by Von Neumann and Richtmyer (ref. 54), by Lax (ref. 55), and by Lax and Wendroff (ref. 56). The present method for the solution of the radiating, inviscid flow field is based on the studies of Moretti and Abbett (ref. 6), Callis (ref. 3), and MacCormack (refs. 57 and 58).

Moretti and Abbett (ref. 6) applied the time-asymptotic technique to flow around blunt bodies without radiative transport. The advantages of the method over other methods are discussed briefly by Moretti and Abbett (ref. 6) and more fully by Moretti and Abbett (ref. 59). A comparison of their results with the data presented by Perry and Pasiuk showed the method to be as accurate in matching the experimental data as any other method. Also, it was shown that the shock wave can be treated as a discontinuity and thereby reduce the number of mesh points required in an accurate numerical solution.

Callis (ref. 7), applied the time-asymptotic technique to stagnation-point solutions and Callis (ref. 3), applied the technique for flow about long blunt bodies. The solutions were for radiating, inviscid flow and showed the time-asymptotic technique to be valid for radiating flow fields. Callis stresses the need for treating the shock wave as a discontinuity. In addition to reducing the number of mesh points, the property profiles are more accurately defined for the radiative transport.

In the studies by Callis, and by Moretti and Abbett, a Taylor series
expansion with the first three terms retained was used for the advance-
ment of the flow field variables in time. Thus, the solutions are of
second-order accuracy in time and require first-order and second-order
time derivatives of the flow field variables. A method of second-order
accuracy has been developed by MacCormack (refs. 57 and 58) which re-
quires only the first-order time derivatives of the flow field variables.
Basically, the method involves a two-step process for the advancement in
time with the spatial derivatives of the flow field variables taken in
alternate directions. The general method of MacCormack is used in the
present study and is described further in the section on Analysis.
Anderson (ref. 60) compared the two methods of time advancement in a
time-asymptotic technique for the steady-state, nonequilibrium, flow in
a nozzle and states the method developed by MacCormack to require fewer
computations and 30 percent less computer time for identical results.

The studies by Moretti and Abbett, by Callis, and by MacCormack
have shown the numerical methods for the time-asymptotic technique to
be convergent, stable, and insensitive to initial guesses. A numerical
method of second-order accuracy for the time-asymptotic technique and
a discontinuous shock wave is used in the present study for the radiating,
inviscid flow field solution.

Thermal Analyses for Venusian Entry

The fully-coupled solution for the radiating flow field with abla-
tion product effects has been investigated in several studies for Earth

reentry (refs. 19, 22, 28, 29, 43, and 44) and Wilson (ref. 44) investi-
gated a solution for Jupiter entry. These solutions were for the stag-
nation region of the body. At present, there are no published results
for a fully-coupled solution with ablation product effects at either the
stagnation or downstream regions for Venusian entry. A good review of
the present state of technology of thermal analyses and ablation analyses
for Venusian entry is given by Walberg and Sullivan (ref. 10).

The primary emphasis at the present time is for unmanned exploration
of Venus. A description of the exploration and the scientific experi-
ments is presented in references 61 to 64. Additional information on
trajectories, body shapes, and body sizes for unmanned entries is given
in references 65 to 69. The entry velocities range from 10 to 15 km/s
with the velocities for peak radiative heating being from 7 to 13 km/s.
The range of stagnation-point pressure on the body is 1 to 10 atmospheres.
The exploration of Venus is a multi-probe, entry mission with one large
probe and three small probes. The nominal body for the probes is a
spherically capped, conical shape with a .34 meter nose radius and a 60
degree half angle for the large probe and a .14 meter nose radius and a
45 degree half angle for the small probes.

Models of the Venusian atmosphere are given in references 62, 63,
and 70. The data for the models are primarily from the flights of
Mariner V and Venera 4. Carbon dioxide is the major gas component for
the Venusian atmosphere with up to 10 percent by volume of nitrogen.

Reviews of analytical and experimental studies of the radiative
heating for Venusian entry and for gas compositions similar to Venusian

atmosphere are presented in references 10, 25, 39, and 71. Therefore, a complete review of the literature will not be given. The results of a recent experimental study in a shock tube for the convective and radiative heating in air and in a .90 CO_2 - .10 N_2 mixture (mole fraction) are presented by Livingston and Williard (ref. 72). A review of the existing studies shows there is a difference in the radiative transport between air and CO_2/N_2 mixtures. The CO_2/N_2 mixtures begin to radiate at a lower temperature than air because of molecular band transitions, primarily CN and CO. At velocities less than 10 km/s the radiative heating can be as much as a factor of 10 greater than air. However, at velocities above 10 km/s the radiative heating is comparable in the two types of gases because of the domination of the atomic processes present.

A detailed study of radiative heating in CO_2/N_2 mixtures is presented in the thesis by Boughner (ref. 25). However, atomic line transitions were neglected and only flight velocities from 8.5 to 10.5 km/s were considered. Most of the study was for a mixture of 50 percent CO_2 and 50 percent N_2 (mole fraction) and the results showed the emission spectrum to be dominated by the CO(4+) band system and the red and violet bands of CN.

Deacon and Rumpel (ref. 71) present results for the radiative heating of a .80 CO_2 - .20 N_2 mixture (by mole fraction) at flight velocities from 5 to 16.5 km/s. The important radiators were found to be CO(4+) band system, continuum from carbon, and atomic transitions of neutral carbon. This study was for a constant property layer. Deacon and Rumpel states that to correct for a nonadiabatic layer the corrections

from air studies would have to be applied due to the lack of data for
CO_2/N_2 mixtures.

Spiegel et al. (ref. 69), present results for the thermal protection
of a spacecraft during a Venusian entry. This investigation was for a
completely uncoupled solution. In the study it was assumed: the shock
layer is isothermal, no coupling between radiative and convective heating,
no radiation absorption by ablation products, and no radiation cooling.
The study was for a spherically capped, conical body with a .15 m nose
radius and a 60 degree cone half angle. The heat-shield material was
high-density phenolic nylon. The results show the radiative heating at
a location on the cone flank to be greater by a factor of two than the
stagnation-point value. Also, the ablation rates of the heat-shield
material are comparable for the cone flank and the stagnation point.
These results need to be verified by a fully-coupled solution.

A recent, but unpublished, analysis has been conducted by the
present author and R. A. Falanga for the fully-coupled, radiating, flow
field solution with ablation products injection at the stagnation point
of a blunt body for Venusian entry.* The method of solution was similar
to the present method except the radiating, inviscid, flow field solution
was by the method of Falanga and Sullivan (ref. 73) and can only be used
in the subsonic region of flow about a blunt body. The results of this
recent study were that the boundary layer with ablation products injec-
tion will reduce the radiative heating to the body by 35 percent at

_____

*Publication pending in Journal of Spacecraft and Rocket.

velocities of 9.86 and 11.18 km/s; but, the reduction was only 14 percent at a velocity of 8.11 km/s. The injection rates were for the steady-state ablation of a high-density, phenolic-nylon, material.

METHOD OF ANALYSIS

The radiating flow field about the entry body is separated into an outer layer where the inviscid flow equations are applicable and an inner viscous layer where the boundary layer equations are applicable. The divergence of the radiative flux is included in the energy equation for the solution of each layer and the boundary layer is coupled to the inviscid shock layer by the radiative transport through both layers and by the boundary layer displacement thickness. This coupling of the boundary layer solution to the inviscid shock layer solution is illustrated by the temperature profile shown in Figure 1. The inviscid flow field is displaced from the wall by the boundary-layer displacement thickness and the boundary-layer profiles are used out to the point where the boundary-layer edge values and their derivatives equal the inviscid layer values. For the boundary-layer solution, the radiative transport is calculated from the mated profiles for the entire layer. The total thickness of the flow field now becomes

$$\delta^t = \delta + \delta^* \tag{1}$$

where δ is the thickness of the inviscid shock layer (shock stand-off distance) and δ^* is the boundary layer displacement thickness calculated from

$$\delta^* = \int_0^{y_e} \left(1 - \frac{\rho u}{\rho_e u_e} \right) dy + \frac{1}{\rho_e u_e r_b} \int_0^s (\rho v)_w r_b ds \tag{2}$$

The first term on the RHS of the expression is the usual term for the displacement thickness of a compressible boundary layer without mass injection and is due to the retardation of the flow in the boundary

layer. The second term is the increase in displacement thickness due to mass injection at the wall for around the body.

The methods of solution of the inviscid flow field, the boundary layer, and the radiative transport are presented in sub-sections of the Method of Analysis. The solution for the radiating, inviscid flow field about a blunt body was developed in the present study and the development of the flow field equations and the numerical method is described in detail. A second-order, time-asymptotic technique is used for the solution. The solution of the inner viscous layer is for a nonsimilar, multicomponent boundary layer with mass injection, unequal diffusion coefficients, and arbitrary chemical species. An existing computer program (BLIMP) is used for the boundary layer solution with modifications made in the present study for coupling the radiative transport and mating the solution to the inviscid flow field. The radiative transport solution is for a nongray gas with molecular band, continuum, and line transitions. An existing computer program (RAD/EQUIL) is used for the solution. In addition to using RAD/EQUIL for coupling the radiative transport through the entire layer, an extensive modification of the program was made in the present study so that it could be used effectively as a subroutine in the developed computer program for the radiative, inviscid flow field.

The radiating, inviscid flow field solution is calculated only once for the fully coupled solution; but, an iteration is required to couple the boundary layer solution to the inviscid flow solution because of inclusion of the radiative heat flux in the boundary layer and locating

the boundary layer edge in the inviscid flow field. The boundary layer solution is assumed not to affect the inviscid layer solution through higher order effects such as recalculating the inviscid solution for an "effective" body composed of the original body plus the displacement thickness. Also, the radiative heat flux from the boundary layer toward the inviscid layer is small compared to the flux from the inviscid layer toward the boundary layer. Thus, the inviscid layer solution should be only slightly affected by the boundary layer solution. The boundary conditions for the boundary layer edge are the appropriate values and their derivatives at the match point in the inviscid flow solution and are not the values at the wall condition of the inviscid flow solution.

The calculation procedure for the fully-coupled solution is shown in Figure 2. The steps in the procedure are:

1. An inviscid, radiating solution is calculated from trajectory data.

2. A boundary layer solution with uncoupled radiative transport is calculated using the inviscid wall values for the boundary layer edge conditions. For steady-state ablation, the radiative heating to the wall is taken as the inviscid wall value.

3. The profiles from the inviscid solution and the boundary layer solution are mated and the radiative transport is calculated for the entire layer.

4. A boundary layer solution with coupled radiative transport is calculated using the values at the match point of the two layers for the boundary layer edge values.

5. Steps 3 and 4 are repeated until the radiative transport through the

layer, the match point condition, and the ablation rates (for steady-state ablation) converge.

The inviscid flow field and the boundary layer solutions are for the flow around a body and the coupling of the two layers and the convergence of the final solution is applied at each location around the body.

The solutions of the radiating inviscid flow, the boundary layer, and the radiative transport for the total layer are calculated by separate computer programs which are coupled through the iteration procedure. Approximately nine hours of total computer time are required for a fully coupled solution about a body and the computer storage requirements for the radiative transport program, the radiating inviscid flow program, and the boundary layer program are 56000_8, 115000_8, and 256000_8, respectively. No attempt has been made to combine the programs into a single computer program because of the large storage requirements and the large computational time.

The effect of the boundary-layer displacement thickness on the inviscid flow solution and subsequent effect on the boundary layer solution could be accounted for by repeating the series of calculations as required until convergence. The computational time for such a procedure would be excessive. Also, the shape of a body is changing during a high velocity entry due to the ablation of the heatshield. Accounting for these shape changes in a solution would require an extensive series of iterations. In the present study, the body shape is the shape prior to entry.

The rate and elemental mass fractions for the mass injection of the ablation products into the boundary layer can be either prespecified or

calculated during a solution for steady-state ablation of a heatshield.
The equations for the wall boundary conditions in the boundary layer
solution includes the necessary mass and energy balances for steady-state
ablation. Steady-state ablation is a good representation of the ablation
phenomena at entry conditions where significant radiative heating is pre-
sent and is better than a specification of the mass injection rate.
Steady-state ablation is used for the representation of the ablation of
the heatshield for the Venusian entry solutions.

Radiating, Inviscid Flow Field Solution

A time-asymptotic technique is used for the solution of the radia-
ting inviscid flow field; therefore, the analysis is based on the equa-
tions of conservation of mass, momentum, and energy for unsteady flow.
The conditions for which the present analysis is carried out are that
the flow is axisymmetric, inviscid, and nonconducting; the gas is in
local thermodynamic and chemical equilibrium; the tangent slab approxi-
mation is valid for the radiative transport; and, the shock wave is a
discrete surface.

The conservation equations expressed in vector notation are

Mass:

$$\frac{\partial \rho}{\partial t} + \nabla \cdot (\rho \vec{V}) = 0 \tag{3}$$

Momentum:

$$\frac{\partial \vec{V}}{\partial t} + \vec{V} \cdot \nabla \vec{V} - \frac{1}{\rho} \nabla p = 0 \tag{4}$$

Energy:

$$\rho\frac{\partial h}{\partial t} + \rho\vec{V}\cdot\nabla h + \nabla\cdot\vec{q}^R - \frac{\partial p}{\partial t} - \vec{V}\cdot\nabla p = 0 \tag{5}$$

Equations 3 thru 5 are for a general, orthogonal, curvilinear coordinate system. The coordinate system for high speed entries can be either body oriented (direct method) or shock orientated (inverse method). The body-orientated, coordinate system as shown in Figure 3 is used in the present analysis.

Equations 3 thru 5 are transformed to the present, body-orientated, coordinate system by using relationships for vector operations as given in reference 74. The necessary metric coefficients, g_i, for the coordinate transformation are determined from the length of a differential line element and the general expression is

$$(d\ell)^2 = g_1^{\ 2}(dx_1)^2 + g_2^{\ 2}(dx_2)^2 + g_3^{\ 2}(dx_3)^2 \tag{6}$$

The expression for the present s, y, ϕ coordinate system is

$$(d\ell)^2 = \lambda^2(ds)^2 + (dy)^2 + r^2(d\phi)^2 \tag{7}$$

Comparing this expression to the general expression, the required metric coefficients are

$$\left.\begin{aligned} g_1 &= \lambda \\ g_2 &= 1 \\ g_3 &= r \end{aligned}\right\} \tag{8}$$

where

$$\left.\begin{aligned} r &= y \cos\theta + \int_0^s \sin\theta\ ds \\ \lambda &= 1 + Ky \end{aligned}\right\} \tag{9}$$

$$K = -\frac{d\theta}{ds}$$

<div align="right">(9)(concl.)</div>

The angle θ is a function of the coordinate s and the magnitude of the angle and the functional relation to s is known from the specification of the body shape.

By knowing the metric coefficients and using the relationships given in reference 74, the vector operations in equations 3 thru 5 can be carried out and the equations determined for the present coordinate system. Applying the axisymmetric conditions that the velocity and all gradients in the ϕ direction are zero, the conservation equations become

Mass:

$$\frac{\partial \rho}{\partial t} + \frac{1}{\lambda} \frac{\partial(\rho u)}{\partial s} + \frac{\rho u}{r} \sin \theta + \frac{\partial(\rho v)}{\partial y} + \rho v\left(\frac{K}{\lambda} + \frac{\cos \theta}{r}\right) = 0 \qquad (10)$$

s-momentum:

$$\frac{\partial u}{\partial t} + \frac{u}{\lambda} \frac{\partial u}{\partial s} + v \frac{\partial u}{\partial y} + \frac{Kuv}{\lambda} + \frac{1}{\rho\lambda} \frac{\partial p}{\partial s} = 0 \qquad (11)$$

y-momentum:

$$\frac{\partial v}{\partial t} + \frac{u}{\lambda} \frac{\partial v}{\partial s} + v \frac{\partial v}{\partial y} - \frac{Ku^2}{\lambda} + \frac{1}{\rho} \frac{\partial p}{\partial y} = 0 \qquad (12)$$

Energy:

$$\frac{\partial h}{\partial t} + \frac{u}{\lambda} \frac{\partial h}{\partial s} + v \frac{\partial h}{\partial y} - \frac{1}{\rho} \frac{\partial p}{\partial t} - \frac{u}{\rho\lambda} \frac{\partial p}{\partial s} - \frac{v}{\rho} \frac{\partial p}{\partial y} + \frac{1}{\rho}\left[\frac{\partial q^R}{\partial y} + q^R\left(\frac{K}{\lambda} + \frac{\cos \theta}{r}\right)\right] = 0$$

<div align="right">(13)</div>

The bracketed term of equation 13 is the divergence of the radiative flux with the application of the tangent slab approximation. In the tangent slab approximation, the derivative of the radiative flux in the y direction is considered in the solution but the derivative in the s

direction is neglected. The parameters in this section of the report are non-dimensionalized by

$$
s = \frac{s'}{Rn'} \qquad p = \frac{p'}{\rho_\infty' V_\infty'^2} \qquad q^R = \frac{q^R}{\rho_\infty' V_\infty'^3}
$$

$$
y = \frac{y'}{Rn'} \qquad h = \frac{h'}{V_\infty'^2} \qquad t = \frac{t'}{(Rn'/V_\infty')}
$$

$$
r = \frac{r'}{Rn'} \qquad \rho = \frac{\rho'}{\rho_\infty'}
$$

$$(14)$$

where the subscript ∞ refers to the free stream value and the prime to dimensional quantities.

The value of y at the shock wave will vary with the s location around the body and will also vary with time because the shock wave is moving during the solution until a steady-state solution (final solution) is obtained. It is convenient in the solution to fix the location of the shock wave and this is accomplished by the transformation

$$
\begin{aligned}
T &= t \\
S &= s \\
Y &= \frac{y}{\delta}
\end{aligned}
$$

$$(15)$$

where

$$
\delta = f(S, T)
$$

The quantity δ is the shock stand-off distance and the transformation of equations 15 gives Y=0 for y=0 and Y=1 for y=δ. The inviscid flow field is now a rectangular coordinate system of length one for the Y-coordinate and a length for the S-coordinate as specified by the body shape. The value of S is zero at the centerline of the body. The differential

relationships to transform equations 10 thru 13 from the s, y, t coordinate system to the S, Y, T system are

$$\frac{\partial(\ )}{\partial t} = \frac{\partial(\ )}{\partial T} - \frac{Y}{\delta} \frac{\partial \delta}{\partial T} \frac{\partial(\ )}{\partial Y}$$

$$\frac{\partial(\ )}{\partial s} = \frac{\partial(\ )}{\partial S} - \frac{Y}{\delta} \lambda_\delta \tan \beta \frac{\partial(\ )}{\partial Y}$$

$$\frac{\partial(\ )}{\partial y} = \frac{1}{\delta} \frac{\partial(\ )}{\partial Y}$$

(16)

The quantity λ_δ is the value of λ evaluated at y equals δ. Hereafter, subscript notation is used to denote partial differentiation with respect to the variables S, Y, and T.

Applying the transformation of equations 16, the conservation equations 10 thru 13 become

Mass:

$$\rho_T = -\left(A\rho_Y + \frac{u}{\lambda} \rho_S - Bu_Y + \frac{\rho}{\lambda} u_S + \frac{\rho}{\delta} v_Y + C\right)$$

(17)

S-momentum:

$$u_T = -\left(Au_Y + \frac{u}{\lambda} u_S - \frac{B}{\rho^2} p_Y + \frac{1}{\rho\lambda} p_S + D\right)$$

(18)

Y-momentum:

$$v_T = -\left(Av_Y + \frac{u}{\lambda} v_S + \frac{1}{\delta\rho} p_Y - E\right)$$

(19)

Energy:

$$h_T = -\left(Ah_Y + \frac{u}{\lambda} h_S - \frac{1}{\rho} p_T - \frac{A}{\rho} p_Y - \frac{u}{\rho\lambda} p_S + \frac{F^R}{\rho}\right)$$

(20)

where

$$A = \frac{v}{\delta} - \frac{Y}{\delta} \delta_T - \frac{uY}{\delta\lambda} \lambda_\delta \tan \beta$$

(21)

$$B = \frac{\rho Y}{\delta\lambda} \lambda_\delta \tan \beta$$

(22)

$$C = \frac{\rho u}{r} \sin \theta + \rho v \left(\frac{K}{\lambda} + \frac{\cos \theta}{r} \right) \tag{23}$$

$$D = \frac{Kuv}{\lambda} \tag{24}$$

$$E = \frac{Ku^2}{\lambda} \tag{25}$$

$$F^R = \frac{1}{\delta} q_Y^R + q^R \left(\frac{K}{\lambda} + \frac{\cos \theta}{r} \right) \tag{26}$$

$$\lambda = 1 + K\delta Y \tag{27}$$

$$\lambda_\delta = 1 + K\delta \tag{28}$$

The mass equation, equation 17, is now changed from density as the dependent variable to pressure as the dependent variable. This is accomplished by using the state equation in the functional form

$$h = h(p,\rho)$$

to obtain the differential relations

$$
\left.
\begin{aligned}
h_T &= \left(\frac{\partial h}{\partial p} \right)_\rho p_T + \left(\frac{\partial h}{\partial \rho} \right)_p \rho_T \\[2mm]
h_S &= \left(\frac{\partial h}{\partial p} \right)_\rho p_S + \left(\frac{\partial h}{\partial \rho} \right)_p \rho_S \\[2mm]
h_Y &= \left(\frac{\partial h}{\partial p} \right)_\rho p_Y + \left(\frac{\partial h}{\partial \rho} \right)_p \rho_Y
\end{aligned}
\right\} \tag{29}
$$

Using the differential relations of equations 29 and combining equations 17 and 20, a new equation for the conservation of mass is obtained in the form

Mass:

$$p_T = -\left[Ap_Y + \frac{u}{\lambda} p_S + P_3 \left(\frac{\rho}{\lambda} u_S - Bu_Y + \frac{\rho}{\delta} v_Y + C \right) - \frac{F^R}{P_1 \rho} \right] \tag{30}$$

where

$$P_1 = \frac{1}{\rho} - \left(\frac{\partial h}{\partial p}\right)_\rho \tag{31}$$

$$P_3 = \frac{1}{P_1} \left(\frac{\partial h}{\partial \rho}\right)_p \tag{32}$$

The values for the thermodynamic variables of ρ, P_1, and P_3 are determined by the conditions of chemical equilibrium for the gas with the specification of the elemental mass fractions of the gas and the two thermodynamic state variables of pressure and enthalpy. The dependent variable in the mass equation was changed from density to pressure as the dependent variable because density cannot be used as one of the specified thermodynamic state variables in the chemical equilibrium program used in the present study. Any two of the equations 17, 20, or 30 can be used in the inviscid flow solution depending on the method used for the thermodynamic state.

The basic equations for the solution of the radiating, inviscid flow field are equations 18 thru 28 and equations 30 thru 32. The terms

$$\frac{\rho u \sin \theta}{r} , \quad \frac{\rho v \cos \theta}{r} , \quad \text{and} \quad \frac{q^R \cos \theta}{r}$$

which appear in equations 23 and 26 are indeterminant at the centerline, $S=0$, and are evaluated by the L'Hospital rule.

The solution for the location of the shock wave and the flow field variables along the shock wave ($Y=1$) is by a method using a quasi, one-dimensional, unsteady characteristic solution and the Rankine-Hugoniot equations for a moving shock. This method is discussed by Moretti and

Abbett (ref. 6) and by Callis (ref. 7). A derivation of the equations
for the characteristic solution is presented in Appendix A. The equation
for a right running characteristic is

$$\frac{dY}{dT} = A + \frac{\sqrt{P_3}}{\delta}$$

(33)

and the compatibility equation is

$$\frac{dv}{dT} + \frac{1}{\rho\sqrt{P_3}} \frac{dp}{dT} = C_2 + \frac{C_3}{\rho\sqrt{P_3}}$$

(34)

where

$$C_2 = -\left(\frac{u}{\lambda} v_S - E\right)$$

(35)

$$C_3 = -\left[\frac{u}{\lambda} p_S + P_3\left(\frac{\rho}{\lambda} u_S + C\right) - \frac{F^R}{P_1\rho} - P_3 Bu_Y\right]$$

(36)

The set of derived equations for the radiating, inviscid flow
field about a blunt axisymmetric body is solved by the numerical methods
presented below. In addition to the complete body solution, a separate
solution for only the stagnation point of a blunt body was obtained
in the present study and the equations are presented in Appendix B.

The concept of the time-asymptotic technique is to assume initial
values for the flow field variables and then to increment the variables
in time until the variables are invarient with time. Thus, the evolution
of the flow in time is followed until the flow obtains a steady-state
condition. The numerical method used in the present study to obtain
a solution is based on the two-step method of MacCormack and a description
of the numerical analysis for the method is given in references 57 and
58.

At time T the value of a variable is known at all locations in the flow field. The advancement of a variable from time T to $T+\Delta T$ (one iteration) is given by

$$f(S,Y,T+\Delta T) = f(S,Y,T) + f_T^{ave}\Delta T \qquad (37)$$

where

$$f_T^{ave} = (f_T^1 + f_T^2)/2 \qquad (38)$$

The symbol f represents the variable p, u, v, or h and the superscripts 1 and 2 refer to the first and second step in the two-step process. The time derivative, f_T, of the variable is calculated from the unsteady equations (equations 18, 19, 20, or 30) with finite differences used for the spatial derivatives. The calculation of f_T^{ave} and the advancement from T to $T+\Delta T$ is a two-step process as follows:

1. Compute f_T^1 at time T from the unsteady equations using forward differences for the spatial derivatives. Advance f by

$$f_{n+1} = f_n + f_T^1 \Delta T \qquad (39)$$

2. Compute f_T^2 at n+1 from the unsteady equations using the variables f_{n+1} and backward differences for the spatial derivatives. Then, compute the average value of the time derivative, f_T^{ave}, by equation 38 and advance the variable, f, to time $T+\Delta T$ by equation 37.

Step 1 is applied to each variable p, u, v and h at all S, Y locations before proceeding to step 2.

A modification to the basic method of MacCormack for the spatial derivatives is used in the present study. In the basic method, two-point, forward finite differences are used for the first step and two-

point, backward differences are used for the second step along all coordinates. In the present method, three-point, central finite differences are used for the derivatives with respect to the S-coordinate for both steps in the two-step process. Three-point, forward differences on the first step and three-point, central differences on the second step are used for the derivatives of h and u with respect to the Y-coordinate. The derivatives of p and v with respect to the Y-coordinate are the basic method of two-point forward on the first step and two-point backward on the second step. A Taylor series expansion is used for the derivation of the finite difference equations for unequal spacing of the nodal points along each coordinate. The same equations are also valid when equally spaced points are specified.

The above numerical method is used for all nodal points except the nodal points along the shock wave (Y=1). The flow field variables at the nodal points along the shock wave and the location of the shock wave are calculated by a numerical method using the equations from the quasi, one-dimensional, characteristics analysis and the Rankine-Hugoniot equations for a moving shock wave. The numerical method is illustrated by the diagram in Figure 4. At time T all the quantities are known and the properties at D, δ, and δ_T are desired at time T+ΔT. The solution procedure is as follows:

1. Assume a δ_T at time T+ΔT and use trapezoidal integration to determine δ by

$$\delta(T+\Delta T) = \delta(T) + \left[\delta_T(T) + \delta_T(T+\Delta T)\right] \frac{\Delta T}{2} \qquad (40)$$

The angle β is calculated by

$$\tan \beta(T+\Delta T) = \left(\frac{1}{\lambda_\delta} \frac{\Delta \delta}{\Delta S}\right)_{T+\Delta T} \tag{41}$$

2. The properties of p, u, v, and h at point D are calculated from the Rankine-Hugoniot equations for a moving shock with the known free-stream properties, the assumed δ_T, and calculated β.

3. Point B is located from the characteristics equation (eq. 33) by

$$\Delta Y = \left(A + \frac{\sqrt{P_3}}{\delta}\right)_{ave} \Delta T \tag{42}$$

where averaged properites of points B and D are used for the integration. The properties at point B are averaged properties of points A and C.

4. A value of v at point D is computed from the integration of the compatability equation (eq. 34) from point B to point D using averaged properties

$$v_D = v_B + \left(C_2 + \frac{C_3}{\rho\sqrt{P_3}}\right)_{ave} \Delta T - \left[\left(\frac{1}{\rho\sqrt{P_3}}\right)_{ave} (P_D - P_B)\right] \tag{43}$$

The value for p_D is the value calculated by the Rankine-Hugoniot equations in step 2.

5. The computed value of v_D from the compatibility equation is compared with the value calculated from the Rankine-Hugoniot equations in step 2. If the values for v_D do not match, then a new value for $\delta_T(T+\Delta T)$ is assumed and steps 1-5 are cycled until convergence.

The numerical method is applied at each time step for each S-coordinate

location beginning with the S=0 location. The method is converged at each S location before proceeding to the next location around the body. A Newton-Raphson method is used for successive guesses for δ_T after the first two guesses.

The value of the shock stand-off distance, δ, at each S location is checked by a mass balance. For the mass balance, the mass flow through a plane in the flow field at the particular S location is equal to the mass flow from the free stream through the shock wave up to the particular S location. The expression for δ from the mass balance is

$$\delta = \frac{r_b^2}{2(SF - r_b \cos \theta)} \tag{44}$$

where

$$SF = \int_0^1 (r\rho u)dY \tag{45}$$

To insure a mass balance for the converged solution, the shock stand-off distance at each S location is adjusted if necessary to the value from equation 44 as the solution approaches convergence.

The size of the time step for the advancement at each iteration is calculated by the use of the characteristic equation (eq. 33) in the form

$$\Delta T \leq \frac{\Delta Y}{A + (\sqrt{P_3}/\delta)} \tag{46}$$

This stability criterion is based on the Courant-Friedricks-Lewy condition and insures that the net slope is less than the characteristics slope for hyperbolic equations (ref. 75, chap. 9). Equation 46 is a

one-dimensional equation being used for a two-dimensional problem; however, the ΔY is smaller than ΔS in the problem and no stability problem was encountered. A time step is calculated at each nodal point in the flow field and the minimum value for the nodal points along a ray at a S-coordinate is used for all the points along that particular S-coordinate. There is a large variation in time steps around the body and using a varying time step around the body requires less iterations for convergnece than using a minimum time step for the entire flow field. Having a different time plane through the flow field did not affect the converged steady-state solution.

The radiative heat flux, the thermodynamic properties, and the solution of the Rankine-Hugoniot equations are calculated by using the computer program of Nicolet (refs. 9 and 32). A modified version of this program is used as subroutines to the computer program developed for the radiating, inviscid flow field. A discussion of the method of calculating the radiative heat flux and the modifications are presented in the sub-section of Radiative Transport. Large computational times are required for the calculation of the radiative heat flux and the thermodynamic properties; however, these parameters do not have to be updated at each iteration. A study was made and it was determined that the thermodynamic properties and radiative heat flux can be calculated every 50 to 100 iterations without affecting the converged solution but greatly reducing the computational time. For the iterations when the thermodynamic subroutine is not used, the density is calculated by

$$\Delta\rho = \Delta h + \frac{\left(P_1 - \frac{1}{\rho}\right)}{P_1 P_3}\Delta p \tag{47}$$

with the thermodynamic properties P_1 and P_3 held constant. The properties P_1 and P_3 are calculated by

$$P_1 = \frac{\bar{T}c_p}{\rho a^2 \left[\left(\frac{\partial \ln M}{\partial \ln \bar{T}}\right)_p - 1\right]} \tag{48}$$

$$P_3 = a^2 \tag{49}$$

where $\bar{T}$ is temperature, a is sonic velocity, M is molecular weight, and c_p is specific heat. The non-dimensionalization of the properties is given by

$$\bar{T} = \frac{\bar{T}'}{\bar{T}'_s} \qquad\qquad a = \frac{a'}{V'_\infty} \qquad\qquad c_p = \frac{c'_p}{(V'^2_\infty/\bar{T}'_s)} \tag{50}$$

where the subscript s refers to the conditions behind a normal shock. The expressions are derived from equations 31 and 32 by using thermodynamic relations. The necessary properties for calculating P_1 and P_3 by equations 48 and 49 are available from the thermodynamic subroutine. Pressure and enthalpy which are calculated by the unsteady equations are used as the two specified, thermodynamic state variables for the thermodynamic subroutine and the radiative heat flux subroutine. The solution of the Rankine-Hugoniot equations for a moving shock wave is calculated by the usual Rankine-Hugoniot equations with the velocities on either side of the shock made relative to a fixed shock location. As mentioned, a solution for the Rankine-Hugoniot equations is included in the program of Nicolet.

The initial values to begin a solution are calculated by assuming the shock wave is stationary and the shock stand-off distances around

the body are equal to the shock stand-off distance at the centerline
(S=0). The value at the centerline is calculated by a correlation from
reference 76 of $\delta = .78/\rho_s$ where ρ_s is the nondimensional density
behind a normal shock and δ is the nondimensional stand-off distance. The
flow field variables for the nodal points along the shock wave are calcu-
lated from the Rankine-Hugoniot equations. The variables for the wall nodal
points are calculated by assuming an isentropic expansion along the body
with a Newtonian pressure distribution. Values for intermediate points
in the flow field are calculated by linear interpolation of the shock
and body values.

The convergence of a solution is determined by checking the change
in enthalpy between iterations. The percentage change in enthalpy
between two successive iterations must be less than a specified small
value and this criterion must be met for a specified number of iterations.
The enthalpy at the body, shock, and midpoint along a ray at each S
location is checked.

A computer program was developed for the numerical solution of the
radiating, inviscid flow field. The program is written in FORTRAN IV
language for CDC 6000 series computers. A listing of the program is
given in Appendix C.

Boundary Layer Solution

The boundary layer equations are for a nonsimilar, multicomponent
boundary layer with mass injection, unequal diffusion coefficients, and
arbitrary chemical species. The solution of the equations is by a

numerical, integral matrix method and there is an existing computer program for the solution called BLIMP. Many types of complex, reactive boundary layer problems can be solved by the program and numerous publications are required for a complete description of the program and the concepts and methods used in a solution. A brief discussion is presented of the basic method and of the modifications to the program made in the present study. A list of the significant publications is given after the discussion of the basic method.

The present discussion of the basic method is from reference 8. The boundary layer equations for an s, y coordinate system of a blunt, axisymmetric body (see Figure 3) are

Mass:

$$\frac{1}{r_b} \frac{\partial(\rho u r_b)}{\partial s} + \frac{\partial(\rho v)}{\partial y} = 0 \tag{51}$$

s-momentum:

$$\rho u \frac{\partial u}{\partial s} + \rho v \frac{\partial u}{\partial y} = \frac{\partial}{\partial y}\left[(\mu + \rho \varepsilon_m)\frac{\partial u}{\partial y}\right] - \frac{\partial p}{\partial s} \tag{52}$$

y-momentum:

$$\frac{\partial p}{\partial y} = 0 \tag{53}$$

Energy:

$$\rho u \frac{\partial H}{\partial s} + \rho v \frac{\partial H}{\partial y} = -\frac{\partial}{\partial y}(q^C + q^R) \tag{54}$$

where

$$H = h + \frac{u^2}{2} \tag{55}$$

Species:

$$\rho u \frac{\partial \bar{K}_i}{\partial s} + \rho v \frac{\partial \bar{K}_i}{\partial y} = \frac{\partial}{\partial y}\left(\rho \varepsilon_d \frac{\partial \bar{K}_i}{\partial y} - J_i\right) \tag{56}$$

The species' conservation equation is solved in terms of elemental mass fraction, $\bar{K}_i$, rather than the species' mole fraction by the application of the Shvab-Zeldovich transformation. This transformation eliminates the chemical source term for chemical equilibrium and reduces the number of species' conservation equations from the number of species to the number of elements. For a boundary layer with ablation products injection, the number of species is typically from 20 to 50 whereas the number of elements is only 2 to 6.

The complexity of using unequal diffusion coefficients for a multicomponent mixture is reduced by a bifurcation approximation for the binary diffusion coefficients. The approximation is expressed as

$$D_{ij} \approx \frac{\bar{D}}{F_i F_j} \tag{57}$$

where $\bar{D}$ is the self-diffusion coefficient of a reference specie and F_i, F_j are the diffusion factors for species i and j. The F_i of a specie for a given chemical system can be determined by finding the set of diffusion factors that gives the minimum total system residual error and a method is presented in reference 77. The bifurcation approximation permits the diffusive flux of element i to be expressed explicitly in terms of properties and gradients of element i and of the system as a whole, but not of other elements. Also, the I(I-1)/2 binary diffusion coefficients are replaced by I diffusion factors where I is the number of chemical species.

The diffusional mass flux of element i in the species' conservation equation (eq. 56) can be expressed as

$$j_i = -\frac{\rho \bar{D} \mu_2}{\mu_1 M}\left[\frac{\partial \bar{Z}_i}{\partial y} + (\bar{Z}_i - \bar{K}_i)\frac{\partial \ln \mu_2}{\partial y}\right] \qquad (58)$$

by use of the bifurcation approximation and the definition of the new quantities

$$Z_j = \frac{M_j \bar{x}_j}{F_j \mu_2} \qquad\qquad \bar{Z}_i = \sum \alpha_{ij} Z_j$$

$$\mu_1 = \sum \bar{x}_j F_j \qquad\qquad \mu_2 = \sum \frac{M_j \bar{x}_j}{F_j} \qquad\qquad\Bigg\} \qquad (59)$$

The subscript j refers to species and the subscript i refers to elements. The quantity α_{ij} is the mass fraction of element i in species j and Z_j is a quantity which for unequal diffusion lies between a mass fraction and a mole fraction for species j.

The convective heat flux term q^C in the energy equation (eq. 54) is the sum of heat flux due to conduction, diffusion, turbulence, and dissipation of kinetic energy. Using the bifurcation approximation for the heat flux due to diffusion, the convective heat flux can be expressed by

$$q^C = -\Bigg\{(\rho \epsilon_m + \mu)\frac{\partial(u^2/2)}{\partial y} + (k + \rho \epsilon_h c_p)\frac{\partial \bar{\bar{T}}}{\partial y} + \rho \epsilon_d \left(\frac{\partial \bar{h}}{\partial y} - c_p \frac{\partial \bar{\bar{T}}}{\partial y}\right) + \frac{\rho \bar{D} \mu_2}{\mu_1 M}\left[\frac{\partial \bar{h}}{\partial y} - \right.$$

$$\left. \bar{c}_p \frac{\partial \bar{\bar{T}}}{\partial y} + (\bar{h} - h)\frac{\partial \ln \mu_2}{\partial y}\right]\Bigg\} \qquad (60)$$

where

$$\bar{h} = \sum Z_j h_j \qquad\qquad \bar{c}_p = \sum Z_j c_{p_j} \qquad (61)$$

The turbulent transport terms in the equations are expressed in the Boussinesq form of eddy viscosity, eddy diffusion, and eddy

conductivity. If turbulent transport is considered, the turbulent transport properties are included in the boundary layer equations when a prespecified Reynolds number is exceeded. The Reynolds number is based on edge properties and momentum thickness. A transition region between laminar flow to turbulent flow is not included.

The boundary conditions at the boundary layer edge are the specifications of u, H, and $\bar{K}_i$ and their derivatives with respect to the y-coordinate. The wall boundary conditions allow for the possibility of solving numerous types of problems and thus specification of different variables. However, all the variations include zero slip at the wall, $u_w = 0$, and involves in some form the assignment of values for mass injection rate, $(\rho v)_w$; wall enthalpy or wall temperature, h_w or $\bar{T}_w$; and elemental mass fractions at the wall, $\bar{K}_{i,w}$.

The equations of the wall boundary conditions for energy balance and elemental mass balance allow a solution for steady-state ablation of a heatshield. The energy balance is

$$-q_w^C - q_w^R - \sigma \epsilon_w \bar{T}_w^4 - (\rho v)_w h_w + m_g h_g + m_c h_c - q_{cond} = 0 \qquad (62)$$

where the subscripts g and c refer to the pyrolysis gas and char for ablation and q_{cond} is the heat conducted into the ablation material at the wall surface. For steady-state ablation

$$m_g h_g + m_c h_c - q_{cond} = m_a h_a^o \qquad (63)$$

where m_a is the total ablation rate, m_g plus m_c, and h_a^o is the heat of

formation of the undecomposed ablation material. Noting that

$$(\rho v)_w = m_a \tag{64}$$

then the surface energy balance for steady-state ablation is

$$-q_w^C - q_w^R - \sigma \varepsilon_w \bar{T}_w^4 + m_a (h_a^o - h_w) = 0 \tag{65}$$

The elemental mass balance is

$$m_g \bar{K}_{i,g} + m_c \bar{K}_{i,c} - (\rho v)_w \bar{K}_{i,w} - J_{i,w} = 0 \tag{66}$$

and, for steady-state ablation

$$m_g \bar{K}_{i,g} + m_c \bar{K}_{i,c} = m_a \bar{K}_{i,a} \tag{67}$$

thus, the elemental mass balance for steady-state ablation is

$$m_a (\bar{K}_{i,a} - \bar{K}_{i,w}) - J_{i,w} = 0 \tag{68}$$

A solution for steady-state ablation does not require knowledge of the in-depth response of the ablation material but only the surface interactions between the boundary layer and the ablation material. From equations 65 and 68, it is shown that the additional properties of the elemental mass fractions and heat of formation of the undecomposed ablation material and the wall emissivity are all that is required for a steady-state ablation solution. The solution of the surface balances gives the basic boundary conditions of injection rate, enthalpy, and elemental mass fractions at the wall.

An ξ, η coordinate system is used for the actual solution of the boundary-layer equations by the transformations of

$$
\left.
\begin{aligned}
\xi &= \int_0^s u_e \rho_e \mu_e r_b^2 \, ds \\[2mm]
\eta &= \frac{r_b u_e}{\sqrt{2\xi}} \int_0^y \rho \, dy
\end{aligned}
\right\}
\tag{69}
$$

and a stream function of

$$
f - f_w = \int_0^\eta \frac{u}{u_e} \, d\eta
\tag{70}
$$

The transformed equations will not be presented.

The numerical procedure for the solution of the boundary layer equations is an integral matrix method. The boundary layer is divided into strips in the normal direction (η coordinate) and the conservation equations are integrated across the strips. Across a strip, the primary dependent variables of velocity, total enthalpy, and elemental mass fractions and their derivatives with respect to η are related by Taylor series expansions with cubic or quadratic fits. Implicit, finite difference expressions are used for the derivatives in the streamwise direction (ξ coordinate). The set of simultaneous equations which includes the Taylor series, the conservation equations, and the boundary conditions are solved by general Newton-Raphson iteration using a matrix inversion technique involving successive matrix reductions.

Many aspects of the BLIMP program have been left out in the above discussion. Further information for the boundary layer method and the

BLIMP computer program is presented in the following references. The solution for the boundary layer equations is given in references 8, 18, 78, and 79. The solution is for an arbitrary, multicomponent gas mixture and the method for the thermodynamic properties for chemical equilibrium is given in reference 80 and the method for the mixture transport properties is given in reference 81. A method for considering a boundary layer for a blunt body solution with entropy layer is presented in reference 82. Information on the turbulent transport model is given in references 79, 82, and 83. User's manuals for the BLIMP program are references 84 to 86. The description of a companion analysis for in-depth response of an ablative heatshield is given in reference 87.

Modifications to the BLIMP program were necessary in the present study to clarify the coupling of radiative heating and to make the boundary layer edge conditions compatible with the inviscid flow field. The radiative heating was included in the formulation of the energy equation and in the coding of the BLIMP program; however, the values for the radiative heating were set to zero in the program and no provision was made to input the values. The term $(q^C + q^R)$ was considered as being only convective heating, since q^R was set to zero, and was used in expressions in the program which are only applicable for convective heating. When the radiative heating, q^R, is included in the term $(q^C + q^R)$ these expressions are invalid. There was a provision for inputing radiative heating to the wall, unattenuated by the boundary layer, for use in the wall energy balance for steady-state ablation. The convective heating for the energy balance was represented by the

term $(q^C + q^R)$ at the wall and if the radiative heating through the layer is included in the term by q^R then the radiative heating at the wall is accounted for twice and the energy balance is invalid. The BLIMP program was modified by re-defining certain expressions to clarify the difference between convective and radiative heating and to properly input the radiative heating at the nodal locations.

The derivatives for the edge boundary conditions are set in the BLIMP program as the usual boundary layer edge condition of

$$\left(\frac{\partial u}{\partial y}\right)_e = 0 \qquad \left(\frac{\partial H}{\partial y}\right)_e = 0 \qquad \left(\frac{\partial \bar{K}_i}{\partial y}\right)_e = 0$$

These boundary conditions consider that u, H, and $\bar{K}_i$ are invariant with y in the inviscid layer. The edge conditions of zero for the velocity and total enthalpy gradients may not be of sufficient accuracy and may give incorrect results for the boundary layer solution because of non-adiabatic effects when radiative transport is present and when an entropy layer is present in the inviscid flow field of a blunt body. There are several methods in BLIMP for considering the effect of an entropy layer for a blunt body and for these methods the derivatives are specified by appropriate values and not set to zero. However, the methods did not consider the effect on the derivatives for a non-adiabatic inviscid flow field from radiative transport and were not appropriate for the present study. The BLIMP program was modified in the present study so that the derivatives of velocity and total enthalpy with respect to the y coordinate can be specified by inputs and correctly transformed to the η coordinate. Also, a modification was made for specifying the total

enthalpy at the boundary layer edge around the body. These modifications allow for equating the boundary layer edge values with the values of the radiating, inviscid flow field at the match point in the flow field.

Radiative Transport Solution

The solution of the radiative transport is for a nongray gas with molecular band, continuum, and atomic line transitions. A detailed frequency dependence of the absorption coefficients is used in the integration over the radiation spectrum and the tangent slab approximation is used for integration over physical space. An existing computer program (RAD/EQUIL) by Nicolet (refs. 9 and 32) is used for the calculation of the radiative transport. The present section presents a brief discussion of the method and the modifications to the computer program when used as subroutines for the radiating, inviscid flow field solution.

The tangent slab approximation treats the radiative transport as a one-dimensional problem in the direction normal to the body. Thus, the equations for the radiative transport are derived for a gas confined between two infinite parallel boundaries and the property gradients of the gas are considered as zero except in the normal direction between the boundaries. For the present problem, the boundaries are the shock and the body and the normal direction is perpendicular to the body. The tangent slab approximation is applied locally at each location around the body. Note, the tangent slab approximation is used only for the radiative transport calculations and not for the gradients of the thermodynamic state and flow properties for the flow field solution.

The radiative heat flux across a surface at a point in the gas layer is

$$dq_\nu^R = I_\nu \cos \gamma \, d\Omega \tag{71}$$

where I_ν is the intensity, γ is the angle between a ray and the normal, and Ω is the solid angle. The basic equation for the intensity gradient along a ray for a gas in local thermodynamic equilibrium is

$$\frac{dI_\nu}{d\ell} = \mu_\nu \, (B_\nu - I_\nu) \tag{72}$$

where μ_ν is the linear absorption coefficient corrected for induced emission and B_ν is the Planck function. The solution of equations 71 and 72 at a point y in the gas layer for the directional, radiative heat flux is given by Nicolet in the form

$$\left. \begin{aligned} q_\nu^{R,+}(y) &= \pi \int_0^{\epsilon_b^+} B_\nu(\epsilon_\nu^+) \, d\epsilon_\nu^+ \\[2ex] q_\nu^{R,-}(y) &= \pi \int_0^{\epsilon_b^+} B_\nu(\epsilon_\nu^-) \, d\epsilon_\nu^- \end{aligned} \right\} \tag{73}$$

where heat fluxes into the slab at the boundaries are neglected. The net flux at point y is

$$q^R(y) = \int_0^\infty q^{R,+}(y) \, d\nu - \int_0^\infty q^{R,-}(y) \, d\nu \tag{74}$$

The plus sign in the superscripts referes to the heat flux in the direction toward the shock and the negative sign for the flux toward the body.

Nicolet solves the flux equation in a Planck function, B_ν, and emissivity, ε_ν, coordinate system where

$$\tau_\nu = \int_0^y \mu_\nu \, dy \qquad (75)$$

$$\left.\begin{array}{l} \varepsilon_\nu^+ = 1 - 2E_3(\tau_\nu - t_\nu), \quad t_\nu \leq \tau_\nu \\[3mm] \varepsilon_\nu^- = 1 - 2E_3(\tau_\nu - t_\nu), \quad t_\nu \geq \tau_\nu \end{array}\right\} \qquad (76)$$

where t_ν are the dummy values of optical depth and $E_n(z)$ is the exponential integral of order n. For the solution by Nicolet, the exponential integral of third order is approximated by

$$E_3(z) \approx \frac{\exp(-2z)}{2} \qquad (77)$$

and the expressions for emissivity become

$$\left.\begin{array}{l} \varepsilon_\nu^+ \approx 1 - \exp\,[2(t_\nu - \tau_\nu)] \\[3mm] \varepsilon_\nu^- \approx 1 - \exp\,[2(\tau_\nu - t_\nu)] \end{array}\right\} \qquad (78)$$

The spectral absorption coefficient for a gas mixture is in general

$$\mu_\nu = \sum \mu_i^C(\nu) + \sum \mu_j^L(\nu) \qquad (79)$$

where the first term is the continuum contribution with a summation over all continuum transitions and the second term is the line contribution with a summation over all line transitions. The absorption coefficients are calculated in the RAD/EQUIL program and the theoretical expressions,

approximations, and experimental data of the various transitions for the species are given in detail in the report of Nicolet (ref. 9). Transitions of the species N, C, H, O, H^-, C^-, N^-, O^-, H_2, C_2, N_2, O_2, NO, CO, CN, and N_2^+ are considered for the radiative transport.

In the computer program, the radiative heating is separated into heating due to continuum transitions and line transitions. The continuum contribution is calculated by using only the first term of equation 79 for the spectral absorption coefficient and then the line contribution is calculated by

$$q_\nu^{R,L} = q_\nu^R - q_\nu^{R,C} \tag{80}$$

where the total absorption coefficient is used for the q_ν^R value. The molecular transitions are treated as an "equivalent" continuum process by a bandless model in which the bands within each band system are smeared by

$$\bar{\mu}_\nu = \frac{\int_{\Delta\nu} \mu_\nu \, d\nu}{\Delta\nu} \tag{81}$$

where the frequency increments $\Delta\nu$ are selected so that $\bar{\mu}_\nu$ varies smoothly over the frequency spectrum of the band system. The molecular transitions are included in the continuum contribution to the radiative flux.

For the continuum calculations, the frequency spectrum in terms of photon energy ($h*\nu$) is divided into 48 frequency nodal points over the range 0 to 15 ev. The frequency nodal points are not equally spaced over the spectrum but are spaced to resolve the frequency variation of the absorption coefficient especially at photoionization edges. The

number of node points, frequency range, and spacing are inputs to the program and the above values were used in the present study.

The line grouping technique is used for the atomic line transitions. In this technique, the line transitions near a specified frequency value are grouped together and the radiative heating is given as that from the line group. However, each line within the group is treated individually and can assume unshifted Lorentz or Doppler line shapes or a combination of the two with the half widths including the Stark, resonance, and Doppler effects. The frequency grid for each line is composed of 13 nodal points and the grid is dependent upon the characteristics of the gas layer as well as the individual line. Twenty line groups with a total of 134 lines are used in the present study. The line groups are not connected over the frequency spectrum, but are spaced according to the frequency locations of the line transitions.

The thermodynamic properties and species concentrations required for the calculation of the spectral absorption coefficients and Planck functions are calculated in the computer program by a chemical equilibrium method from the specification across the spatial grid of the enthalpy (or temperature), pressure, and elemental mass fractions. Only the species as given above are used for the radiative transport calculations; but, additional species can be included in the chemical equilibrium calculation. A method for the solution of the Rankine-Hugoniot equations for shock waves is also included in the program. The methods for the chemical equilibrium solution and the Rankine-Hugoniot solution are given in the report by Nicolet. The calculation of the thermodynamic state is consistent throughout the fully-coupled solution because the

chemical equilibrium method is the same in both the RAD/EQUIL and the BLIMP programs.

Briefly, the solution procedure for the radiative transport is that the chemical equilibrium calculations are made for the specified spatial grid. The spectral absorption coefficients, Planck functions and optical depths are calculated. Then the emissivities are calculated and the transformation to the B_ν, ε_ν coordinates is made by knowing B_ν and ε_ν as a function of y. The heat flux equations are then integrated. Cubic integration formulas are used for all integrations except for the frequency integration of the continuum flux. These integrals are evaluated by linear formulas because of the discontinuity at photoionization edges.

The RAD/EQUIL computer program is used for the calculation of the radiative transport through the total layer from the coupling of the boundary layer to the inviscid layer. This is step 3 in the calculation procedure. Also, a modified version of the RAD/EQUIL program is used as a subroutine in the computer program for the radiating, inviscid flow field solution. The following comments refer to the modified version. A separation between the subroutines for the radiative transport calculations and the chemical equilibrium calculations was made in order that the chemical equilibrium calculations can be performed without calculating the radiative transport. The chemical equilibrium subroutine was modified by the addition of a routine to calculate the necessary thermodynamic properties for the evaluation of the P_1 and P_3 properties required for the inviscid flow solution. The required addition was

taken from the chemical equilibrium version in the BLIMP computer program. The method for calculating thermodynamic derivatives for the chemical equilibrium version in BLIMP is given in reference 80. Also, the storage requirement was reduced by deleting options which were not required, by reducing the maximum number of spatial nodal points, and by reducing the maximum number of chemical species in the chemical equilibrium solution. The modified version of the RAD/EQUIL program was then mated to the computer program for the radiating, inviscid flow field solution.

RESULTS AND DISCUSSION

A computational method has been developed for the fully-coupled solution of nongray, radiating gas flow with ablation product effects about blunt bodies during planetary entries. Application of the developed method is shown by results for Venusian entries. There are no published results for a fully-coupled solution of the radiating flow about ablating, planetary entry bodies; therefore, the validity of the present method is shown by comparing the results from solutions to sub-components of the method with published results of corresponding solutions.

The present method for the solution of an inviscid flow field is compared with existing methods for both non-radiating and radiating gas flows about blunt bodies during Earth reentry. Results from solutions by the present method for the radiating, inviscid flow about blunt bodies are also presented for planetary entries. The present method for a fully-coupled solution with ablation product effects is compared with an existing method for the stagnation point of blunt bodies for Earth reentry. Results from the present method are then presented for the fully-coupled solution about blunt bodies for Venusian entries.

Several comments are given about the presentation of the results. In the present coordinate system, the radiative heating directed toward the shock wave is positive and the radiative heating directed toward the body is negative. However, the radiative heating rates at the wall are given by positive values in the presentation of results. As stated in

the section of Radiative Transport Solution, the radiation contributions
by molecular band transitions are included in the continuum contribution
to the radiative heating. The total contributions of molecular band
transitions and continuum transitions are referred to by continuum
processes. The line grouping technique is used for the atomic line
transitions and the spectral distributions for the line transitions are
given by the contribution of the line group and not by the individual
lines.

Non-Radiating, Inviscid Air Solution

The present method for an inviscid flow field has been used to
obtain a solution for the nonradiating flow about a spherically capped,
conical body during an Earth reentry. The results are presented in
Figure 5 and are compared with results by the method of Inouye et al.
(ref. 88). The method of reference 88 is considered to be one of the
more accurate methods and provides a good means of evaluating the accu-
racy of the present method for an inviscid flow field solution.

The solution is for the free-stream conditions and body shape
given in Figure 5(a). The results for the shock shape at the forward
region of the body and the location of the sonic line are presented in
Figure 5(b). Figure 5(c) presents the results for the shock shape at
the downstream region of the body. Because the thickness of the shock
layer is much smaller than the dimensions of the body, a better means
of comparing the shock shape is the shock stand-off distance and these

results are presented in Figure 5(d). The results for the shock stand-off distance illustrate the inflection points in the shock shape around the body. The results from the present method are in good agreement with the results by the method of reference 88 for the shock shape, especially considering the inflection points, and for the sonic line location.

The results for the distribution of tangential velocity and pressure along the body are presented in Figures 5(e) and 5(f), respectively. The results from the present method are in good agreement with the results by the method of reference 88 even in the region of the over-expansion of the flow at the sphere-cone junction.

The good agreement between the present results and those by the method of reference 88 indicates the present method provides a good solution for the inviscid flow about a blunt body. Radiating flow is not treated by the method of reference 88.

Radiating, Inviscid Solutions About Blunt Bodies

Results are presented from solutions of the radiating, inviscid gas flow about blunt bodies during planetary entry. The present results for solutions of entries into the Earth's atmosphere are compared with existing methods.

The present method is compared with the method of Callis (ref. 3) for an Earth reentry and the results are presented in Figure 6. The free-stream conditions and body shape are given in Figure 6(a). The

distributions of the wall pressure and the shock stand-off distance are presented in Figures 6(b) and 6(c), respectively. The two methods are in good agreement for these parameters. The distribution of wall, radiative heating rate is presented in Figure 6(d). The results by the two methods are in reasonable agreement at the forward region of the body; however, there is a considerable difference between the methods at the downstream region of the body. The results by Callis are greater by a factor of two than the present results at the downstream region.

An analysis was done to explain the difference between the methods. The thermodynamic profiles of temperature and pressure and the shock stand-off distances from the results by Callis were used as inputs to the radiative transport program, (RAD/EQUIL), used in the present method. The results of this calculation are compared with the present results in Figure 6(e). As shown by the data, the distributions of wall, radiative heating rate is now in good agreement at the downstream region. A similar type of analysis had to be used by Suttles (ref. 89) in comparing his results with Callis for large stand-off distances at the stagnation point of blunt bodies. The radiative heating rates by Callis were greater than those of Suttles for larger stand-off distances.

Results from the present method and the method of Callis are in good agreement for nonradiating flow solutions. The difference between the methods for radiating flow is attributed to the radiation models. The radiation model used by Callis (refs. 3 and 7) was developed by Olstad (refs. 2 and 26) and is based on a "step-model" approximation for the frequency dependence of the absorption coefficient. It is

possible that this radiation model by Olstad treats the radiating gas as being too transparent.* Thus, more radiation is transmitted to the body and this effect would be more noticeable the greater the shock stand-off distance.

The present method was used to calculate the radiative heating rate to the stagnation point of a blunt body for a range of nose radii and the results are compared with the method of Callis (ref. 7) in Figure 7. The same radiation model was used by Callis in references 3 and 7. The results by Callis are greater than the present results and the difference increases with the shock stand-off distance (nose radius).

A solution was obtained for the same conditions as previously given in Figure 6(a), except the nose radius was increased to 2.0 meters. The distribution of radiative heating rate is presented in Figure 8. The results of Callis are 50 percent greater than the present results at the forward region of the body as well as the downstream region.

The stagnation-point heating rates from solutions by the present method and the method of Callis are compared with the methods of references 73 and 89 in Table I for two nose radii. The methods of references 73 and 89 can only be used for the flow in the subsonic region of a blunt body. For the smaller nose radius, the results agree within 15 percent. For the larger nose radius, the present results and those by references 78 and 89 agree within 5 percent; but, the result by Callis is 50 percent greater. The radiation model (RATRAP, ref. 30) used by

---

*Personal Communications with Dr. W. B. Olstad, Langley Research Center, Hampton, Virginia.

references 73 and 89 treats the frequency dependence of absorption co-
efficient in detail as does the present radiation model (RAD/EQUIL, ref.
9). As stated in the section Radiation Transport Modeling, Suttles (ref.
32) made a comparison of these radiation models and concluded that the
RAD/EQUIL program was the better model. The present method is in agree-
ment with other methods which use a detailed radiation model.

The previously available results for the radiating, inviscid flow
about blunt bodies have been provided by the analysis of Callis (ref. 3)
and Olstad (ref. 2). The step-model approximation developed by Olstad
was used in both methods for the treatment of radiation. Olstad uses
an approximate method for the solution of the flow field and the method
is inverse, shock shape specified, rather than direct, body shape speci-
fied, as the present method. For these reasons, the present method was
not compared with the method of Olstad. Since the same radiation model
was used by Olstad and Callis, the results of Olstad should not agree
with results by the present method.

The difference in the results between the present method and the
method of Callis (ref. 3) for the radiative heating rates is attributed
to the different radiation models used in the methods. The radiation
model used in the present method treats the frequency dependence of the
absorption coefficient in detail and is a more accurate model than the
step model used by Callis. From the above analysis, it is concluded
that the present method provides a good solution for the radiating,
inviscid gas flow about blunt bodies.

Callis (ref. 3) and Olstad (ref. 2) state that the nondimensional,
radiative heating rate distributions along blunt bodies are nonsimilar

with respect to body angle and nose radius. Suttles (ref. 89) states

that the nondimensional, radiative heating rate distribution along the

body at the subsonic region of flow for hemispheres to be relatively

insensitive to the size of the nose radius. These results are based on

entries into an air atmosphere. The heating rates along the body are

nondimensionalized by the stagnation-point value, $q_w^R/q_{w,o}^R$, and the dis-

tance along the body is nondimensionalized by the nose radius, s/Rn.

The present method was used to investigate the above mentioned

trends. The results presented are for spherically-capped, conical

bodies since this is the body shape presently being considered for plan-

etary entries. However, the present method is not restricted to this

type of body shape. Results from stagnation-point solutions are also

presented.

Results of radiative heating distributions from solutions for

entries into different atmospheres and different entry conditions are

presented in Figure 9. The results for the two entry conditions of the

CO_2-N_2 mixture are representative of entry tó Venus and the results for

the H_2-He mixture are representative of entry to Jupiter. Note that the

distributions are highly nonsimilar for the different cases. The results

for case C and D are for the same atmosphere but different entry condi-

tions; but, the distributions are nonsimilar. The present method can

be readily used for entries into atmospheres other than air.

A comparison of the stagnation-point, radiative heating rates for

entries in air and in a $.90CO_2-.10N_2$ mixture (by volume) is presented

in Figure 10. The radiative heating in the CO_2-N_2 mixture is much greater than in air at the lower velocities; but, the results are comparable at the higher velocities. The difference at the lower velocities is due to the molecular band radiation from the red and violet bands of cynrogen, CN(R) and CN(V), and the fourth positive band of carbon dioxide, CO (4+), in the CO_2-N_2 mixture. The atomic species are dominant at the higher velocities, greater temperature behind the shock wave, and the radiation from the continuum and line transitions is greater than from the molecular band systems.

As the radiating gas flows around a body there are two effects which can influence the radiative heating to the body. The volume of radiating gas increases, increased shock stand-off distance, which will increase the radiative heating. This effect is offset by the decrease in temperature as the gas expands around the body. The distributions of radiative heating along spherically-capped, conical bodies for entry in an air atmosphere are presented in Figure 11 for different body angles. The distributions are nonsimilar and the nondimensional radiative heating is greatest for the largest body angle. The shock stand-off distances and temperatures at a location on the conical portion of the body are also presented. Both the temperature and shock stand-off distance are greater for the larger body angle; thus, the greater the radiative heating. Note that the dimensional, stagnation-point heating rate is insensitive to the downstream body angle for spherically-capped, conical bodies. These results are in agreement with the trends presented by Callis (3) and Olstad (4).

The effect of body angle on the nondimensional, radiative heating distribution for entries to Venus is presented in Figure 12 for two entry conditions. As for air entry, the radiative heating rates along the conical region of the body are greater for the larger cone angle. Also, the stagnation-point, radiative heating rate is insensitive to the cone angle. As previously stated, the nondimensional, radiative heating distribution is nonsimilar with respect to entry conditions. For the 60° body, the radiative heating rates along the downstream region of the body exceed the stagnation-point value at the lower velocity entry. At the higher velocity entry, the radiative heating rate increases along the downstream region but does not exceed the stagnation-point value.

The effect of nose radius on the nondimensional, radiative heating distributions for an entry in air is presented in Figure 13. The distributions are slightly nonsimilar for the downstream region of the body. Callis (ref. 3) and Olstad (ref. 2) state the distributions to be nonsimilar and the present results are in agreement. However, the results of Callis and Olstad indicate a greater nonsimilarity than shown by the present results for an air entry. The reason is probably due to the radiation model used by Callis and Olstad which might be too transparent as previously discussed. In which case, the nose radius would have a greater effect than shown by the present results. Suttles (ref. 89) states the distributions along the subsonic flow region of the body to be similar with respect to nose radius. The present results are in agreement with Suttles since the distributions are similar for the forward region of the body, $s/Rn < 0.4$.

The effect of nose radius on the nondimensional, radiative heating distributions for entries to Venus is presented in Figure 14. The distributions are slightly nonsimilar for the downstream region of the body for the lower velocity entry. However, the distributions are highly nonsimilar for the higher velocity entry. For both entries, the distributions are similar at the forward region of the body up to approximately the sphere-cone junction.

The present results are based on a limited range of entry conditions and body shapes. This same situation applies to the studies by Callis (ref. 3), Olstad (ref. 2), and Suttles (ref. 89) for entries only in an air atmosphere. Based on the present results, the following trends seem to be generally prevalent. The nondimensional, radiative heating distributions ($q_w^R/q_{w,o}^R$ versus s/Rn) are nonsimilar with respect to entries in different atmospheres and with respect to entries in the same atmosphere at different entry conditions. The distributions are also nonsimilar with respect to body angle and nose radius. Extreme caution should be exercised in attempting to extrapolate the results from known distributions to other entry conditions or body shapes for which solutions have not yet been obtained. For large body angles, the radiative heating rates to the downstream region of a body can exceed the stagnation point value for certain entry conditions.

The exact composition of the Venusian atmosphere is unknown at present. The most recent data indicates the composition to be predominately CO_2 with up to 10 percent by volume of N_2. The effect of gas

composition for CO_2-N_2 mixtures on the radiative heating to the stagnation-point of a body is presented in Figure 15 for two entry conditions. For the higher velocity entry, the radiative heating rate varies by only 25 percent over the range of CO_2 content with the higher values occurring for the greater percentage of CO_2. For the lower velocity entry, the radiative heating rate can vary by a factor of 6 over the range of CO_2 content. This is due to the domination of radiation by the molecular band transitions of CO(4+), CN(V), and CN(R) at the lower velocity. For the composition of present interest for Venusian entry (less than 10 percent N_2), the effect of composition on the stagnation-point, radiative heating rate is negligible at the higher velocity; but, a 22 percent difference occurs with composition at the lower velocity.

Fully-Coupled, Stagnation Point, Solutions for Earth Reentry

The present method has been used to obtain fully-coupled solutions at the stagnation point of blunt bodies for Earth Reentry. The solutions are for mass injection at the wall of air and ablation products. The results from the present method are compared with the results given by Garrett (ref. 19).

The solutions were obtained for the free-stream conditions and mass injection rates presented in Table II. These conditions are representative of a manned spacecraft reentering the Earth's atmosphere after exploration of Mars. For the solutions, the wall conditions of the temperature and the rate and composition of the injected gas were prespecified. This procedure was used to be consistent with the method of

Garrett. The results from the present method and the results given by Garrett are presented in Table II.

The present results agree with the results of Garrett within 5 percent for the mass injection of ablation products and within 10 percent for the mass injection of air. This good agreement is better than has been previously shown in comparing any two methods (see ref. 19). As shown by the results, the mass injection of ablation products is twice as effective as the mass injection of air in reducing the radiative heatinging to the wall. The mass injection of ablation products reduced the radiative heating to the wall by 40 percent at the larger blowing rate.

The present results for the temperature profile and the radiative flux profile through the gas layer for a solution are compared with the results of Garrett in Figure 16. The specified conditions are given in Figure 16(a) and the temperature profile and radiative flux profile are given in Figure 16(b) and 16(c), respectively. The present results are in good agreement with the results of Garrett. For the present solution, spectral distributions of radiative heating toward the wall due to continuum processes and due to line processes are presented in Figures 16 (d) and 16(e) respectively. Spectral distributions were not given in the thesis by Garrett.

For the continuum processes, practically all radiation beyond 11 eV is absorbed within the boundary layer and is attributed to the atomic species being at a lower temperature in the boundary layer than in the inviscid layer. There is a slight absorption of radiation within the boundary layer between the spectral range of 4 to 10 eV but the effect

is offset by increased radiation emission in the spectral range of 1 to 4 eV. For the line processes, the radiation is sharply reduced in the spectral region of 7 to 11 eV. Part of this reduction for the line groups at 7.1, 8.4 and 9.4 eV is due to the absorption by the fourth positive band system of carbon monoxide, $CO(4+)$. The carbon monoxide is present in the boundary layer from the mass injection of ablation products. The present results for the spectral regions of absorption, or increased emission, within the boundary layer are in agreement with the results given in reference 28.

The good agreement of the present results with those given by Garrett (ref. 19) shows that the present method for a fully-coupled solution with ablation product effect provides a good solution at the stagnation point of a blunt body for Earth reentry. The method by Garrett can only be used at the stagnation point of a blunt body and has not been used for entries in atmospheres other than air.

Fully-Coupled Solutions for Venusian Entry

The present method was used to obtain solutions at typical conditions for unmanned, scientific probes during Venusian entry. One mission currently under study is a multi-probe entry with one large probe and three small probes which are spherically-capped, conical bodies. A description of this type of mission is presented in references 61 to 64. The entry probes are released from a spacecraft and are targeted to different locations on Venus.

The entry parameters and body shapes listed below were used to calculate nominal trajectories for use in the present analysis. The only small probe considered herein is the one entering at the steepest entry angle.

	Large Probe	Small Probe
Entry velocity, km/s	11.06	11.06
Entry angle, degrees	-42	-56
W/C_dA, kg/m^2	78.5	125.7
Weight, kg	158.8	22.7
Nose radius, m	.3429	.1397
Body half-angle, degrees	60	45
Base diameter, m	1.3716	.4064

The atmospheric model used for the Venusian atmosphere is that presented in reference 62 and the gas composition is 97 percent carbon dioxide and 3 percent nitrogen by volume. The calculated entry trajectories are presented in Figure 17.

The radiative heating rates at the stagnation point of the bodies were calculated along the trajectories to determine the location of peak radiative heating. The "stagnation-point" version of the developed, radiating inviscid flow program was used for these calculations. The results are presented in Figure 18 for the large and small probes. Even though the nose radius is smaller, the radiative heating to the small probe is greater due to the deeper penetration in the denser regions of the atmosphere at higher velocities. Solutions for the radiating, inviscid flow around the bodies were then obtained at the peak heating conditions and the stagnation-point values of radiative heating rates from these solutions are also presented in Figure 18. It is at these conditions for peak radiating heating that fully-coupled solutions with

ablation product effects were obtained for the radiating gas flow around the large and small probes. Hereafter, the solutions are referred to as large and small probes.

The ablation of the heatshield for the fully-coupled solution is represented by steady-state ablation of a carbon-phenolic material with elemental mass fractions of carbon, 0.851; oxygen, 0.110; hydrogen, 0.035; and nitrogen, 0.004. The ablation rates are solved for as part of the fully-coupled solution and are not prespecified.

The results from the fully-coupled solutions for the large and small probes are presented in Figures 19 and 20, respectively. The distribution along the body of radiative heating, convective heating, ablation rate, aerodynamic shear, and momentum thickness Reynolds number are presented. The spectral distribution of radiative heat flux due to continuum processes is also presented for two body locations.

For the large probe, the ablation rate decreases along the body in the nose region and reaches a nearly constant value along the afterbody (Figure 19(d)). As shown in Figure 19(c), the convective heating rate decreases along the afterbody but the radiative heating rate increases to values which exceed the stagnation-point value. The radiative heating to the wall is greater than the convective heating along the entire body. The total heating rate, radiative plus convective, along the afterbody is 30 to 40 percent less than the stagnation-point value. Thus, the decrease in convective heating rate along the afterbody negates the effect of the increase in radiative heating rate. The wall temperature resulting from the steady-state ablation is $3600^\circ K$, within 2 percent, along the body.

For the small probe, there is a decrease in the ablation rate along the afterbody (Figure 20(d)) and both the convective and radiative heating rates decrease along the afterbody (Figure 20(c)). The convective heating rate is greater than the radiative heating rate along the entire body. This result is opposite to the result obtained for the large probe. The total heating rate along the afterbody of the small probe is 40 to 60 percent less than the stagnation-point value. The wall temperature resulting from the steady-state ablation is 3700°K, within 2 percent, along the body.

The radiative heating rates from inviscid, radiating solutions are compared with the results for the fully-coupled solutions with steady-state ablation in Figures 19(b) and 20(b) for the large and small probes, respectively. The radiative heating rates from the fully-coupled solutions are less than the values from the inviscid, radiating solutions by 9 and 17 percent, respectively, for the large and small probes at the stagnation point of the bodies. These percent reductions are nearly constant along the bodies. The reduction in radiative heating is due to absorption of radiation within the boundary layer.

Spectral distributions of radiative heating toward the body due to continuum processes are presented in Figures 19(g) and 20(g), respectively, for the large and small probes. The spectral distributions are presented for the stagnation point and an afterbody location. As shown by the results, the absorption of radiation within the boundary layer occurs in the spectral range of 5 to 10 eV and is due to self absorption

of the fourth positive band system of carbon monoxide, CO(4+). At the
stagnation point of the small probe there is a slight increase in radi-
ative heating within the boundary layer at 2.5 eV and is due to the
Swan band system of diatomic carbon, $C_2(S)$. A similar effect was noted
at the other body locations for both the large and small probes, but the
effect was too small to be presented in the figures. The radiative
heating due to line processes was less than ten percent of the total
radiative heating at these entry conditions and spectral distributions
are not presented.

The fully-coupled solutions assumed laminar flow in the boundary
layer. Shown in Figures 19(f) and 20(f) are the distributions of mo-
mentum thickness Reynolds number around the bodies. If the critical
value for transition to turbulent flow is about 200, then the boundary
layer would be turbulent along the afterbody for both the large and
small probes. This could have an appreciable effect on the distribution
of convective heating, ablation rate, and aerodynamic shear.

A fully-coupled solution for the large probe with a turbulent
boundary layer was obtained and the results are compared with the lami-
nar case in Figure 21. A critical value of 200 for the momentum thick-
ness Reynolds number was used for transition to turbulent flow. As
expected, the convective heating rates, ablation rates, and aerodynamic
shears increased with transition to turbulent flow. The distribution
along the body of radiative heating was essentially the same for both
laminar and turbulent flow; thus, the turbulent boundary layer did not
appear to further attenuate the radiative heating even though the

boundary-layer thickness was 80 percent greater than for laminar flow. This phenomenon can be explained with the wall spectral distributions presented in Figure 21(d) for the turbulent and laminar solutions. For the turbulent boundary layer, there is an increase in the self absorption of the CO(4+) band system in the spectral range of 5 to 8 eV but this effect is offset by an increased emission of the $C_2(S)$ band system at 2.5 eV and the red band system of cynrogen, CN(R), at .6 to 2 eV. The spectral distribution at the boundary layer edge is essentially the same for both the turbulent and laminar boundary layers and was presented in Figure 19(g). While the radiative heating rates along the afterbody of the large probe are the same for a turbulent or a laminar boundary layer, the wall spectral distribution of the radiation is different for the two cases. It should not be inferred that the radiative heating to the body will be the same for a laminar or turbulent boundary layer for other entry conditions or body shapes.

A fully-coupled solution was obtained for free-stream conditions representative of a higher entry velocity than the nominal trajectories and the results are presented in Figure 22. The free-stream conditions and body shape are given in Figure 22(a). The body shape is the same as the large probe except the nose radius is slightly smaller. Here-after, this case is referred to as the high velocity entry.

As shown in Figure 22(c), the radiative heating rate is greater than the convective heating rate along the entire body. Unlike the large probe, there is only a slight increase in the radiative heating along the afterbody. The convective heating rate at the stagnation

point is slightly less than the values just downstream of the stagnation point and is due to an increased effect of blockage of convective heating by the mass injection of the ablation products. As shown in Figure 22(d), the ablation rate decreases along the body in the nose region. The ablation rate and total heating rate are nearly constant along the afterbody. The wall temperature resulting from the steady-state ablation is $3750^{\circ}K$, within 1 percent, along the body.

There is significant absorption of radiation within the boundary layer for the high velocity entry as shown by a comparison of results between the fully-coupled solution and an inviscid, radiating solution in Figure 22(b). The reduction in radiative heating rate is 25 percent at the stagnation point and 25 to 30 percent along the afterbody. Spectral distributions of radiative heating toward the body due to continuum processes are presented in Figure 22(g) for the stagnation point and an afterbody location. For the continuum processes, most of the absorption within the boundary layer occurs in the spectral region of 5 to 10 eV and is due mainly to self absorption of the CO(4+) band. There is an increase in radiative flux at 2.5 eV and is due to the $C_2(S)$ band. At the stagnation point there is absorption at photon energies greater than 10 eV and this absorption is attributed to atomic species within the cooler regions of the boundary layer. There is also absorption at the photoionization edge of carbon at 8.5 eV.

The radiative flux due to line processes is 50 percent of the total radiative flux at the nose region of the body and decreases to only 20 percent along the afterbody. Spectral distributions of the radiative

heating due to line processes for two locations at the nose region are presented in Figure 22(h). Absorption of line radiation within the boundary layer occurs only for the line groups in the ultraviolet at 7.1, 8.4, and 9.4 eV. The line radiation in the visible and infrared regions of the spectral, less than 2 eV, is not attenuated within the boundary layer.

The present results have shown that the radiative heating toward the body is attenuated in the boundary layer for Venusian entries. This attenuation will reduce the radiative heating to the body by 10 to 20 percent at entry conditions and body shapes which are presently considered as nominal. The reduction can be as large as 30 percent at higher velocity entries. The radiative heating toward the body is attenuated in the boundary layer at the downstream region of the body as well as at the stagnation point of the body.

SUMMARY AND CONCLUSIONS

A method is presented for the solution of the fully-coupled, nongray radiating gas flow about an ablating, planetary entry body. The solution is for a gas in chemical equilibrium and arbitrary gas mixtures can be considered. The treatment of radiation accounts for molecular band, continuum, and atomic line transitions with a detailed frequency dependence of the absorption coefficient. The ablation of the entry body is solved as part of the solution for a steady-state ablation process.

Application of the developed method is shown by results at typical conditions for unmanned, scientific probes during entry to Venus. The radiative heating toward the body is attenuated in the boundary layer for Venusian entries. This attenuation will reduce the radiative heating to the body by 10 to 20 percent at entry conditions and body shapes which are presently considered as nominal. The reduction can be as large as 30 percent at higher velocity entries. The attenuation of radiation within the boundary layer is primarily due to the self absorption of the fourth positive band system of carbon monoxide, $CO(4+)$, in the radiation spectral region of 5 to 10 eV. At high velocity entry, the attenuation of radiation also occurs for line transitions in the radiation spectral region of 7 to 10 eV.

Prior studies of fully-coupled solutions with ablation product effects have been for the stagnation point of a body for Earth reentry and have shown that the boundary layer with injection of ablation products is effective in reducing the radiative heating to the body. The

present results show that the boundary layer over an ablating body will reduce the radiative heating to the body for entries to Venus. Furthermore, the attenuation of radiation within the boundary layer occurs at downstream regions of the body as well as the stagnation point of the body.

Present results from a study of the radiating, inviscid flow about spherically-capped, conical bodies during planetary entries show that the nondimensional, radiative heating distributions ($q_w^R/q_{w,o}^R$ versus s/Rn) to be nonsimilar with respect to entries in different atmospheres and with respect to entries in the same atmosphere at different entry conditions. The distributions are also nonsimilar with respect to nose radius and downstream body angle. Therefore, extreme caution should be exercised in attempting to extrapolate the results from known distributions to other entry conditions for which solutions have not yet been obtained. The radiative heating rates to the downstream region of the body can exceed the stagnation-point value for certain entry conditions and body shapes.

EXTENSION OF PRESENT RESEARCH

An immediate extension of the present research can be made in the following areas:

1. Additional fully-coupled solutions are needed for a better evaluation of the thermal environment for Venusian entries. Solutions with a turbulent boundary layer are needed for the small probe and for higher velocity entries.

2. Solutions are needed for body shapes other than spherically-capped, conical bodies for Venusian entries. Future design may dictate a different shape and the results would be useful in evaluating the effects of such a change in shape.

3. A study is needed for the effect of composition for CO_2-N_2 mixtures on the radiative heating distribution along a body for Venusian entries.

4. Use the present results and results from additional solutions to develop correlations which can be easily used in parametric design studies for Venusian entries.

5. The present computational method needs to be extended to include a transient ablation analysis.

6. Use the present method to begin studies of entries to Saturn. Saturn is characteristic of the giant planets (Jupiter, Saturn, Uranus, and Neptune) and probably will be the first chosen for exploration by entry probes.

TABLE I. – STAGNATION-POINT, RADIATIVE HEATING

RATES FOR AIR ENTRY.

$V_\infty = 14.55$ km/s

$\rho_\infty = 2.252 \times 10^{-4}$ kg/m^3

$p_\infty = 16.16$ N/m^2

Method	$q_{w,o}^R$, MW/m^2	
	Rn = .3427 m	Rn = 3.427 m
Present method	16.17	28.80
Callis, Ref. 3	18.71	45.47
Suttles, Ref. 89	18.38	27.26
Falanga and Sullivan, Ref. 73	18.73	28.44

TABLE II. – RESULTS FROM FULLY-COUPLED, STAGNATION-POINT

SOLUTIONS WITH MASS INJECTION FOR AIR ENTRIES.

(a) V_∞ = 15.25 km/s ; ρ_∞ = 2.72 x 10^{-4} kg/m^3 ; p_∞ = 17.76 N/m^2

Rn = 3.048 m ; $\overline{T}_w$ = 3600° K

Injected gas		$q_{w,o}^R$, MW/m^2	
$(\rho v)_w$, kg/m^2-s	Composition	Present method	Garrett, Ref. 19
0	–	3980	4150
.415	air	3375	3740
.830	air	3090	3490
.415	ablation products*	2870	2770
.830	ablation products*	2560	2460

* $\overline{K}_C$=.9207; $\overline{K}_O$=.0491; $\overline{K}_H$=.0216; $\overline{K}_N$=.0086

(b) V_∞ = 15.25 km/s ; ρ_∞ = 1.77 x 10^{-4} kg/m^3 ; p_∞ = 12.26 N/m^2

Rn = 2.56 m ; $\overline{T}_w$ = 3840° K

Injected gas		$q_{w,o}^R$, MW/m^2	
$(\rho v)_w$, kg/m^2-s	Composition	Present method	Garrett, Ref. 19
0	–	2307	2540
.205	ablation products*	1710	1620

* $\overline{K}_C$=.923; $\overline{K}_O$=.058; $\overline{K}_H$=.018; $\overline{K}_N$=.001

–2–
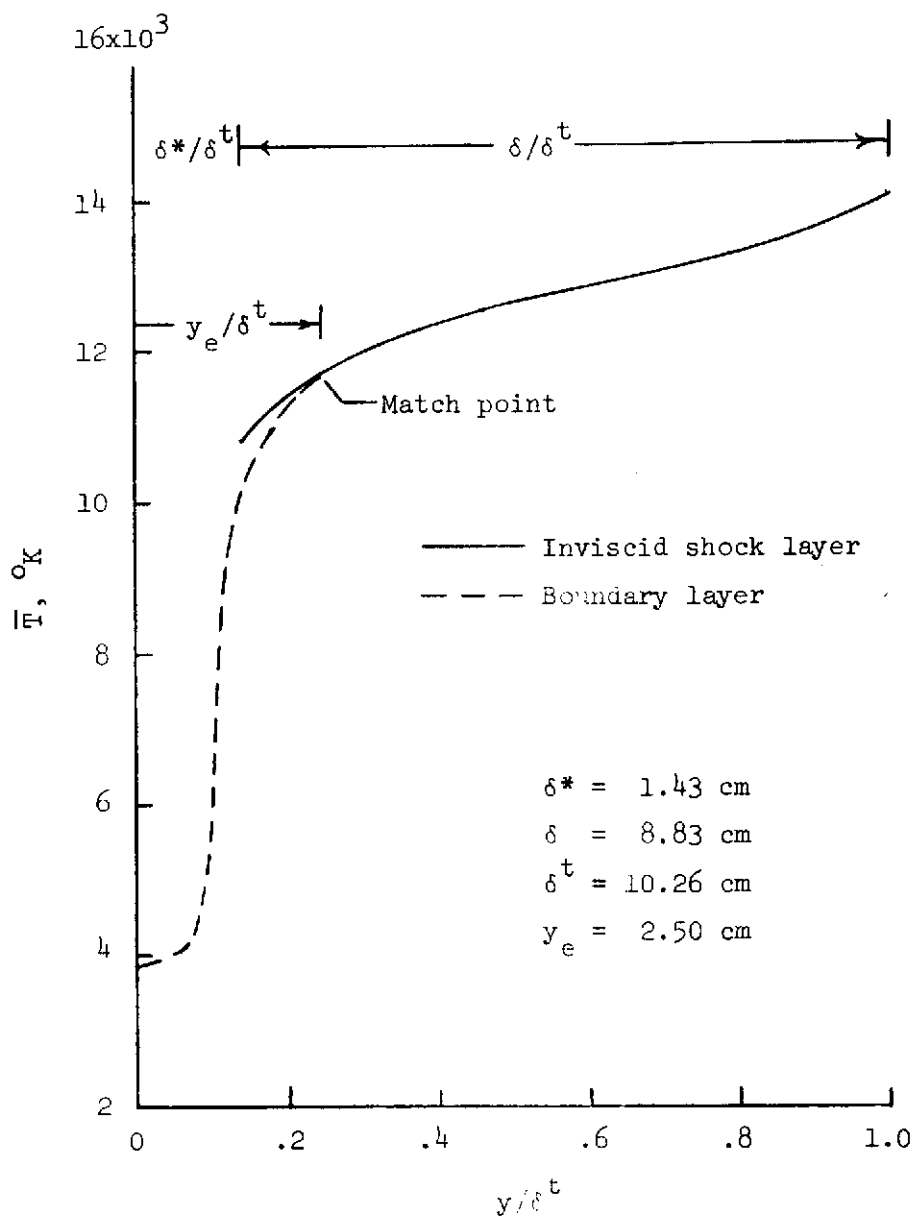
Figure 1. - Illustration of the mating of the boundary layer solution to the inviscid layer solution.
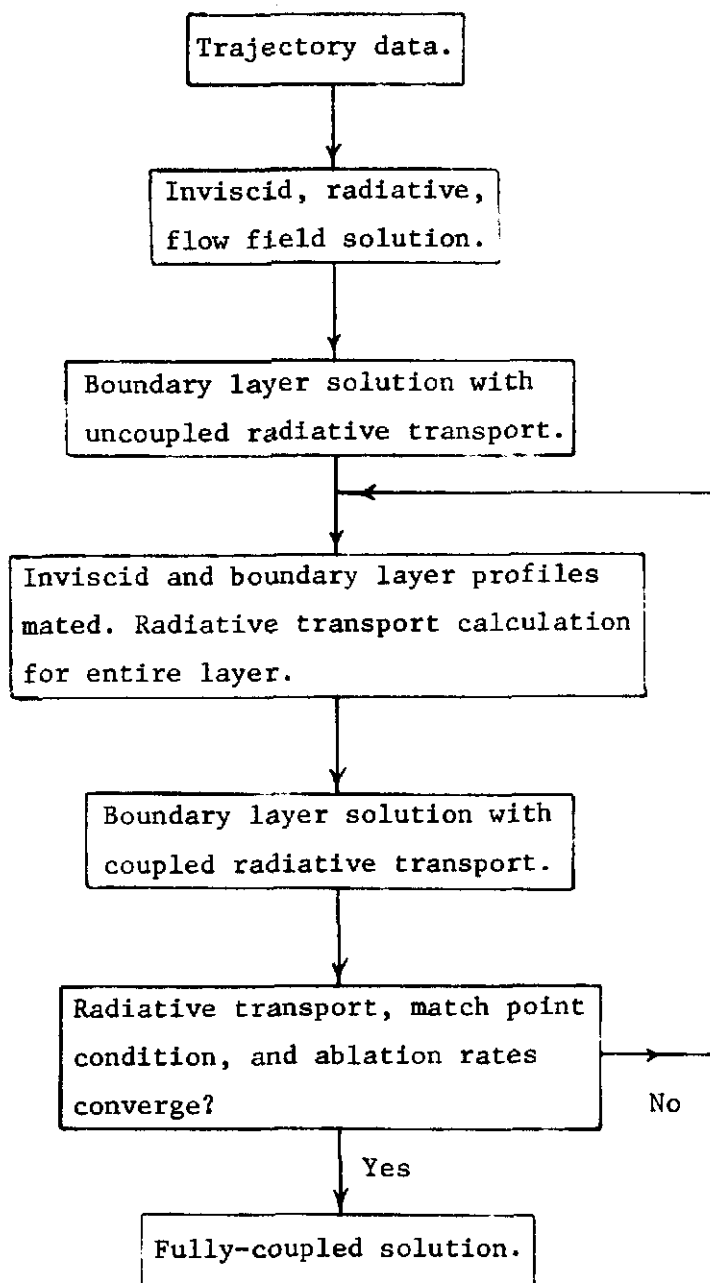
Figure 2. - Calculation procedure for the fully-coupled,
radiating, flow field solution.

Shock
wave

Body
surface

θ + β

θ

u

v

y

r

s

r_b

V_∞

axis of symmetry

Rn

δ
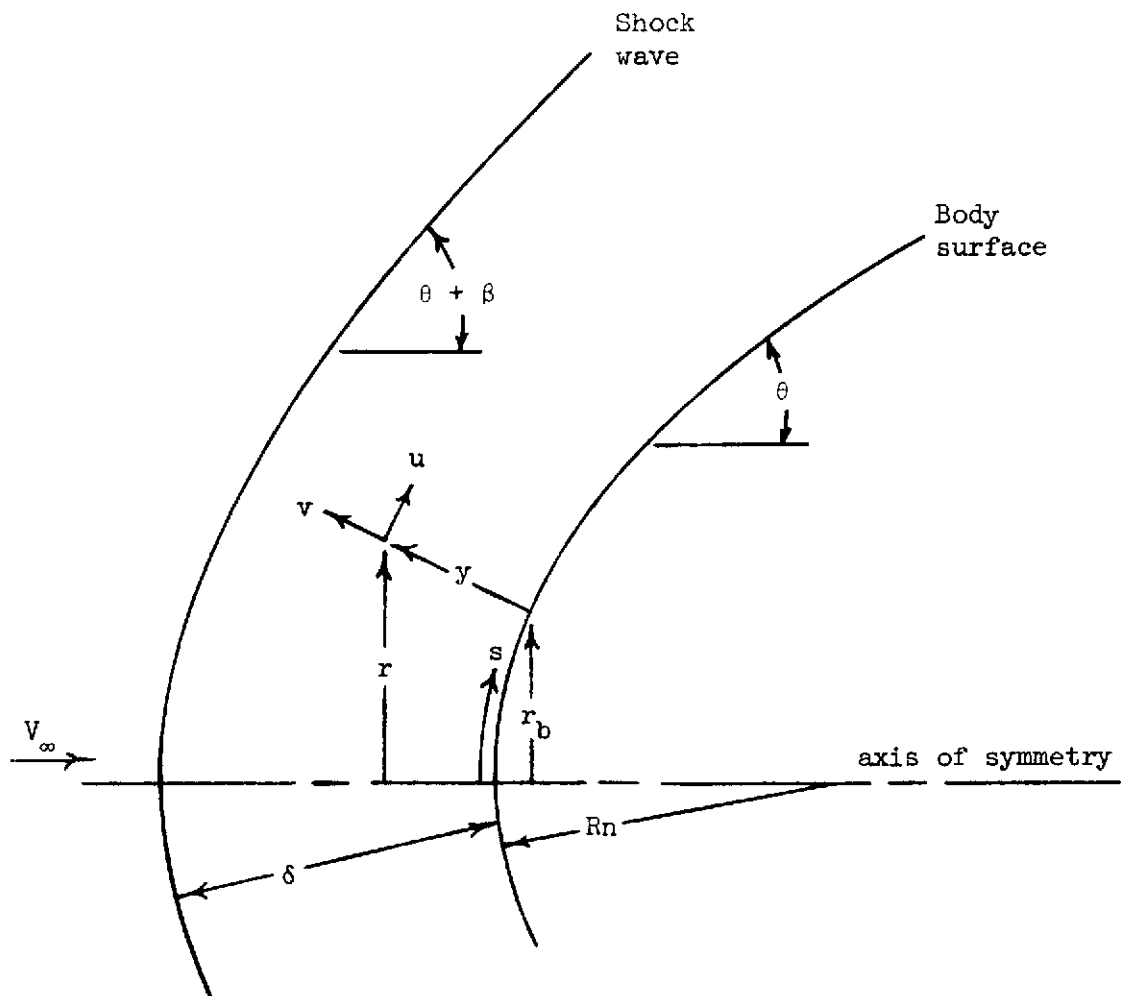
Coordinates

    s - Distance along body surface from axis of symmetry.

    y - Distance perpendicular to body surface.

    φ - Angle measured in plane normal to axis of symmetry.

Figure 3. - Flow field coordinate system for axisymmetric blunt body.
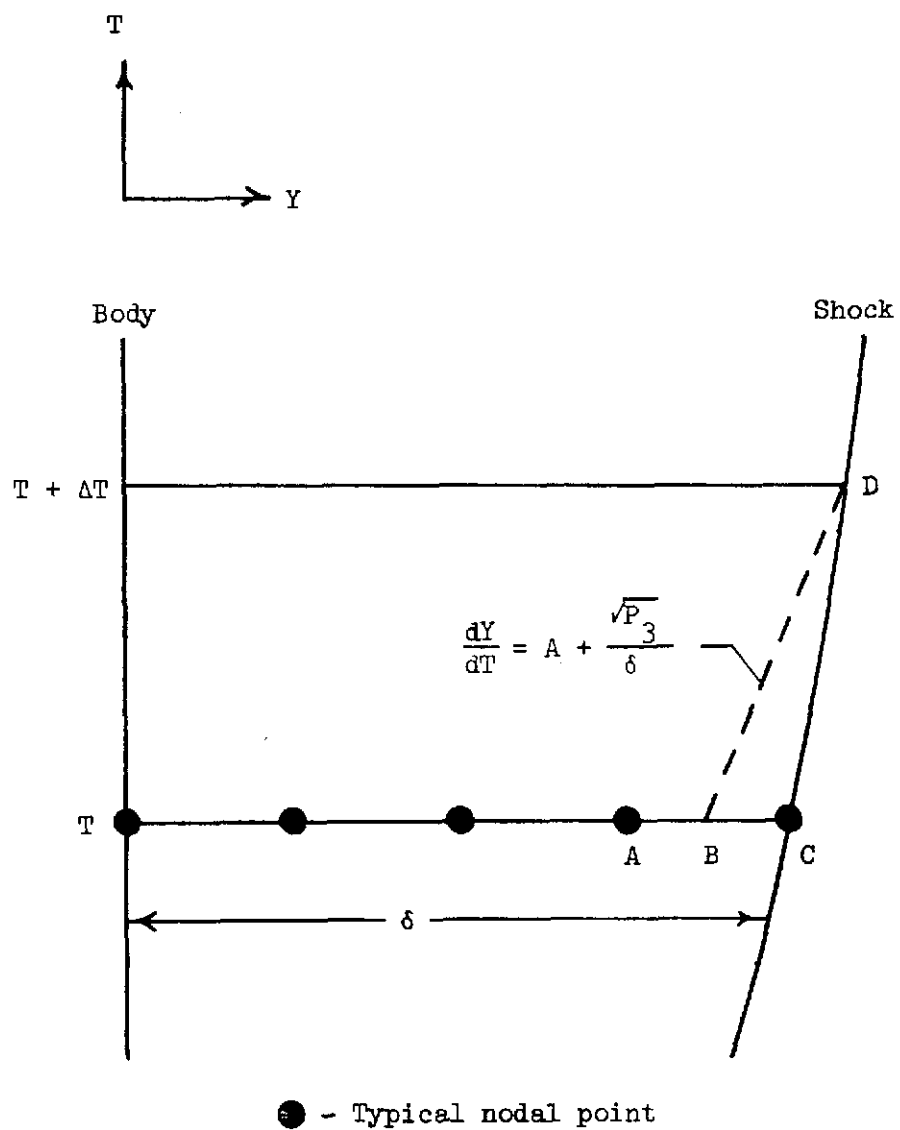
Figure 4. – Schematic of use of unsteady characteristics at shock wave.
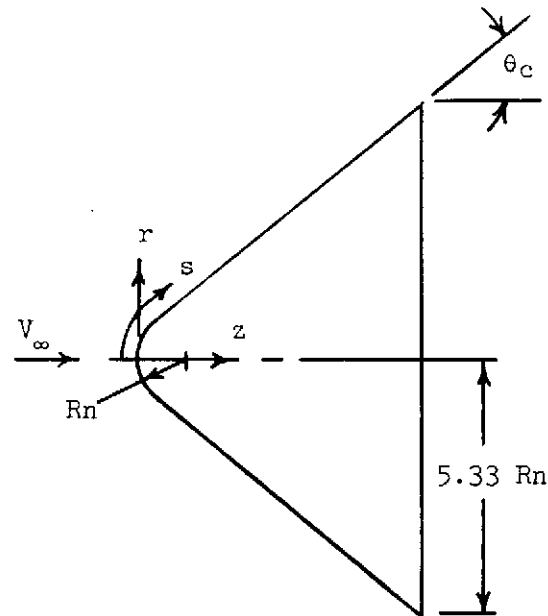
Gas composition by volume

$.79\ N_2 - .21\ O_2$ (air)

$V_\infty = 12.192$ km/s

$\rho_\infty = 3.15 \times 10^{-4}$ kg/m^3

$p_\infty = 22.6$ N/m^2

$h_\infty = 0.0$ J/kg

$Rn = 2.0$ m

$\theta_c = 40°$

(a) Free-stream conditions and body shape.

Figure 5. - Nonradiating, inviscid flow solution around a blunt body. Present method is compared with the method of Inouye et al. (ref. 88).
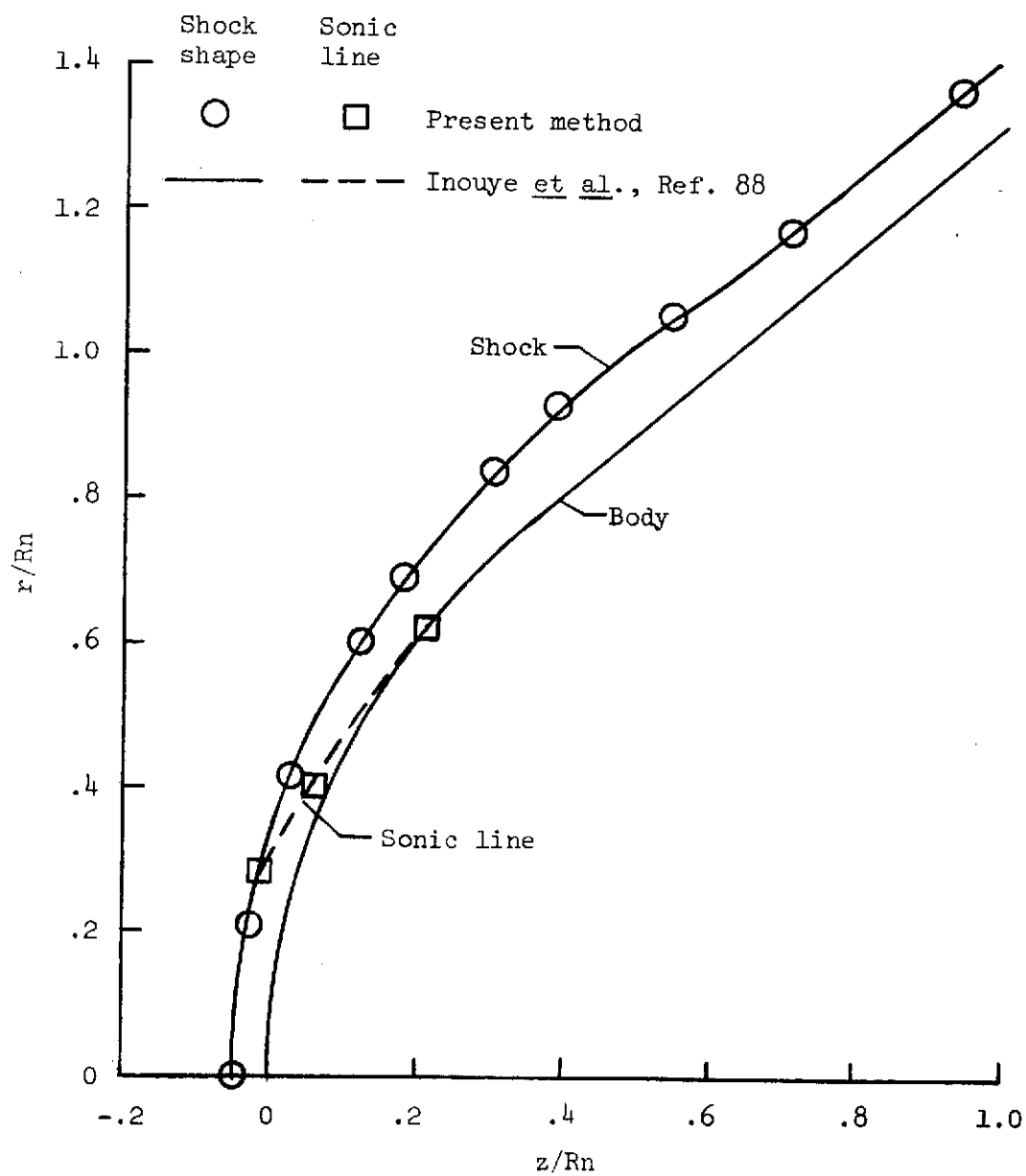
(b) Shock shape at forward region of body
and sonic line location.

Figure 5. - Continued.
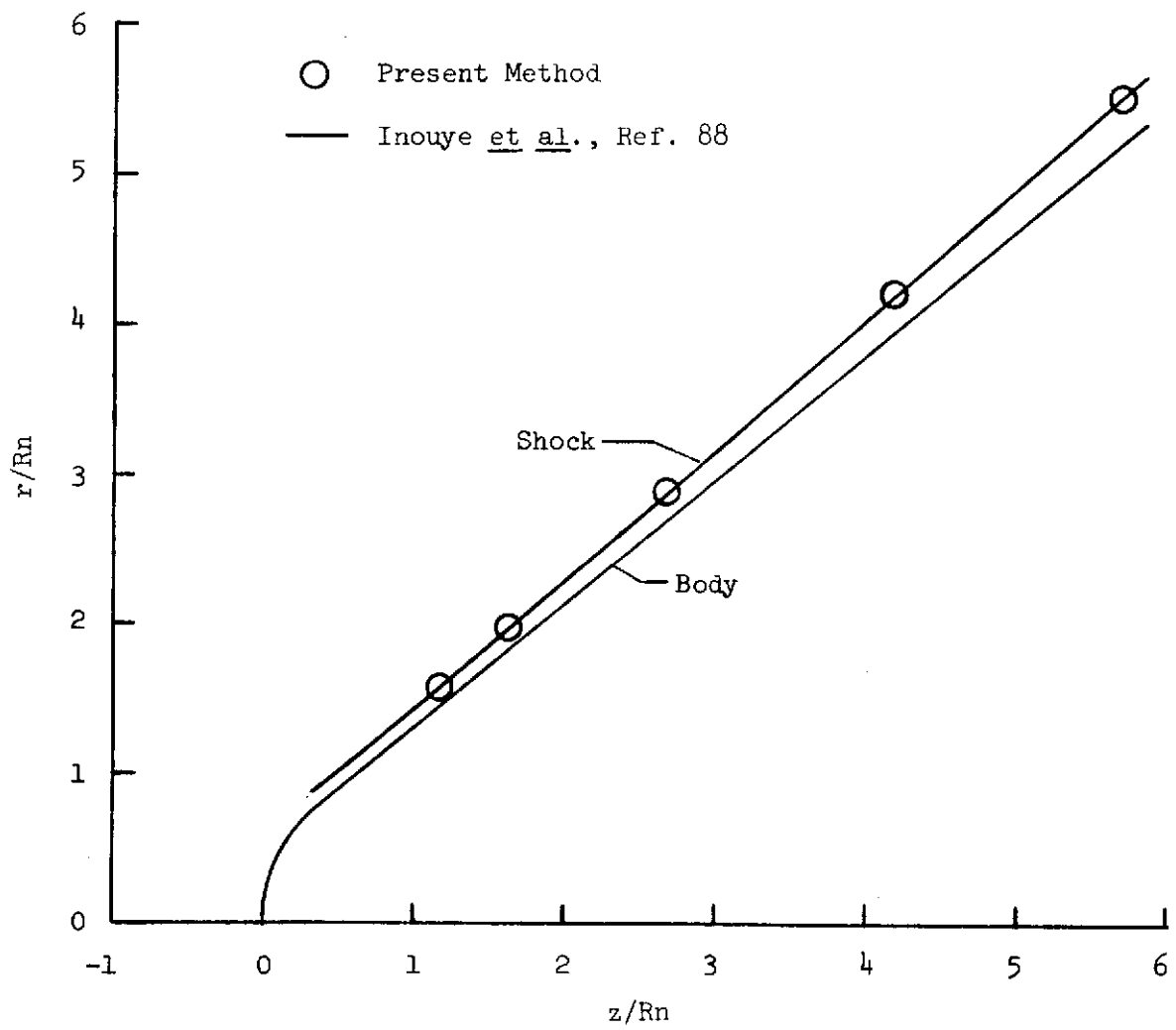
(c) Shock shape at downstream region of body.

Figure 5. - Continued.
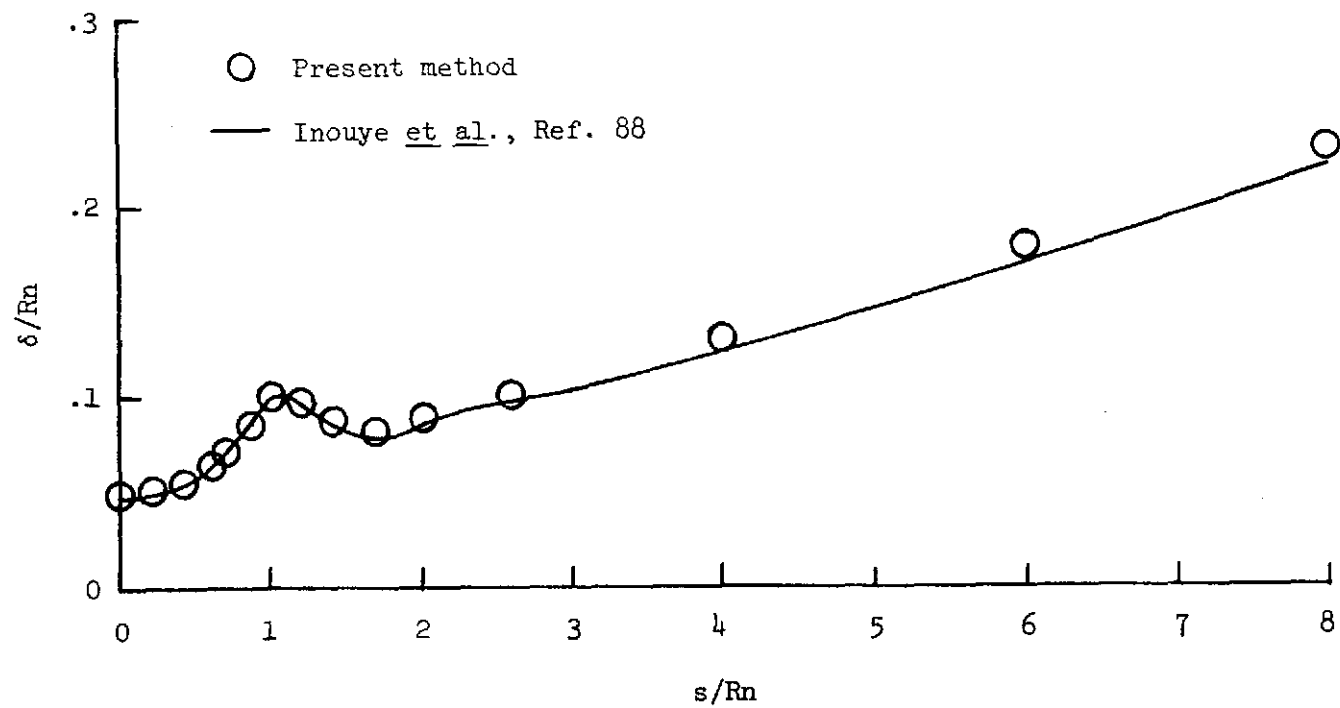
(d) Shock stand-off distance around body.

Figure 5. - Continued.
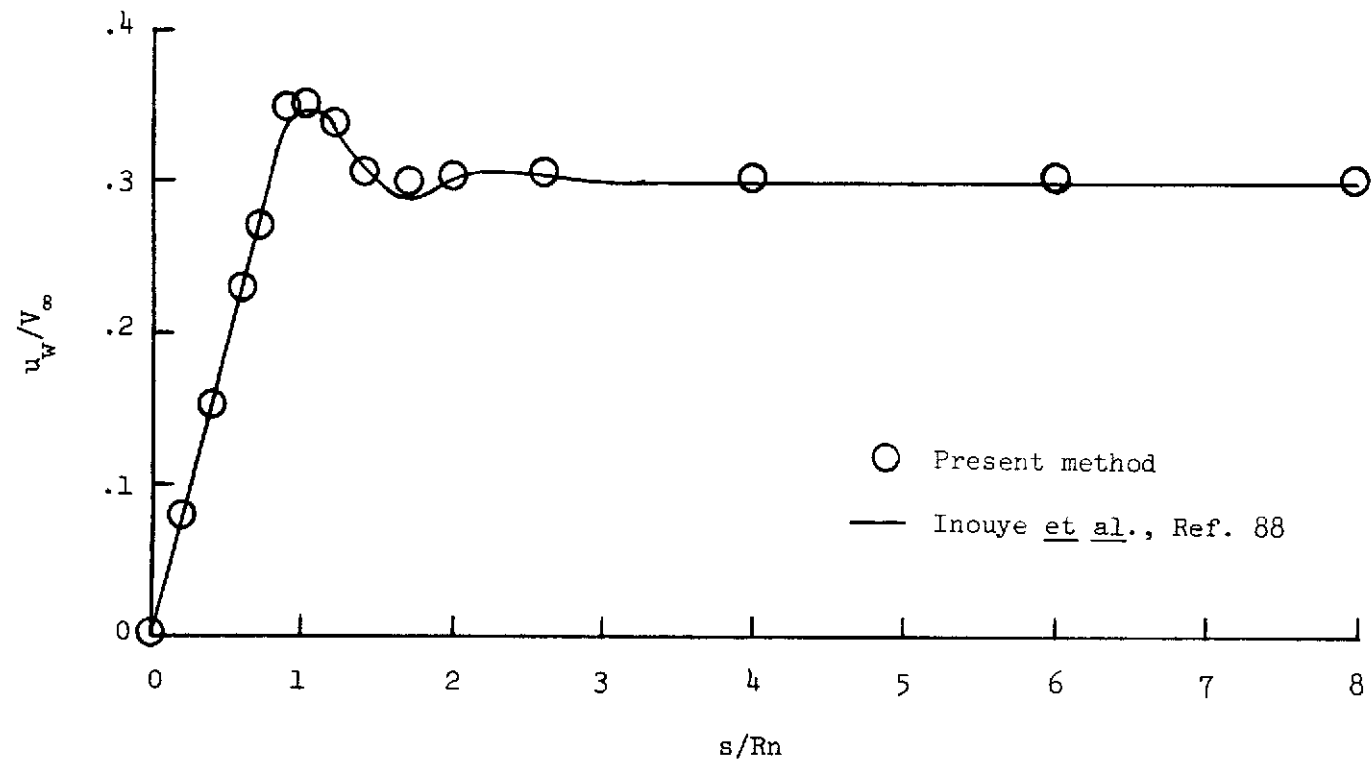
(e) Velocity distribution along body.

Figure 5. – Continued.
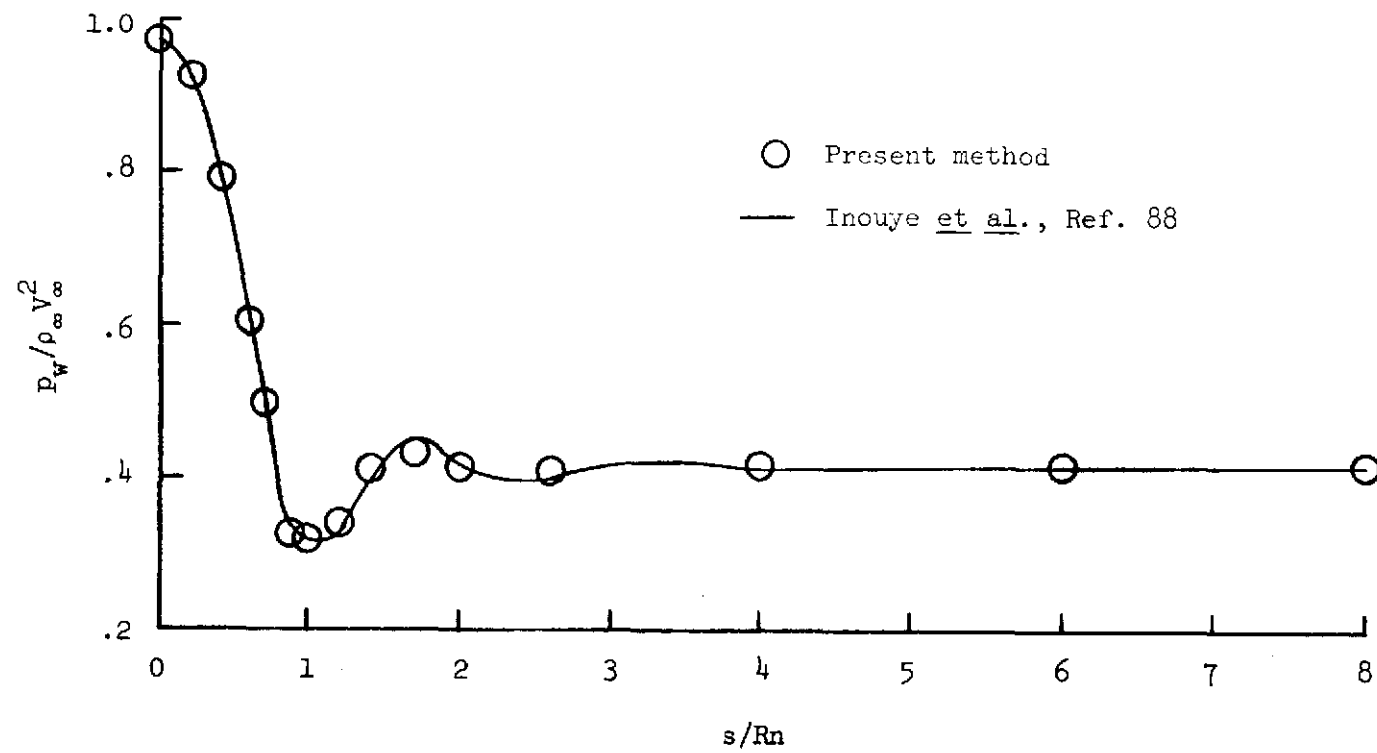
(f) Pressure distribution along body.

Figure 5. - Concluded.
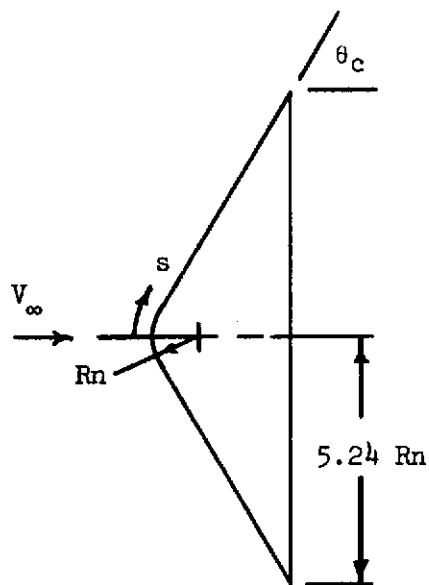
Gas composition by volume

$.79 \; N_2 - .21 \; O_2$ (air)

$V_\infty = 12.20$ km/s

$\rho_\infty = 2.74 \times 10^{-4}$ kg/m^3

$p_\infty = 20.0$ N/m^2

$h_\infty = 0.0$ J/kg

Rn $= 0.20$ m

$\theta_c = 60°$

(a) Free-stream conditions and body shape.

Figure 6. - Radiating, inviscid flow solution about a blunt body during Earth reentry. Present method is compared with the method of Callis (ref. 3).
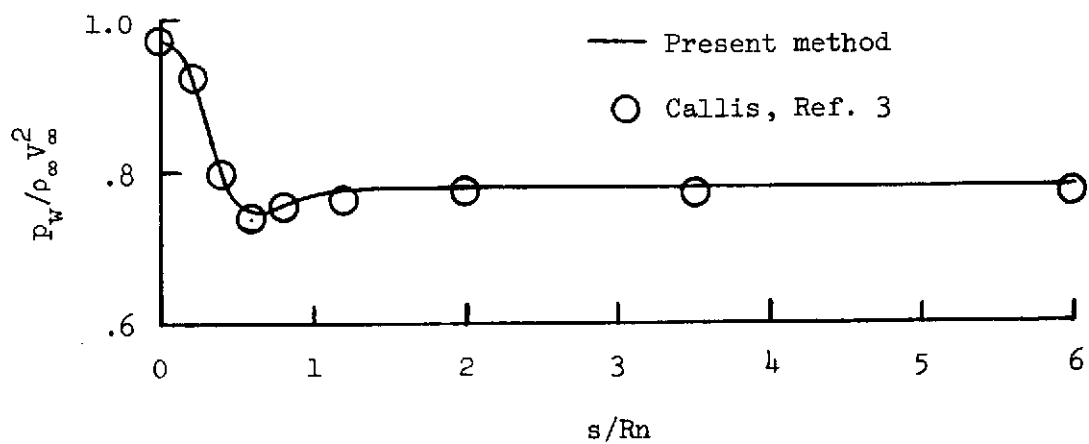
(b) Pressure distribution along body.
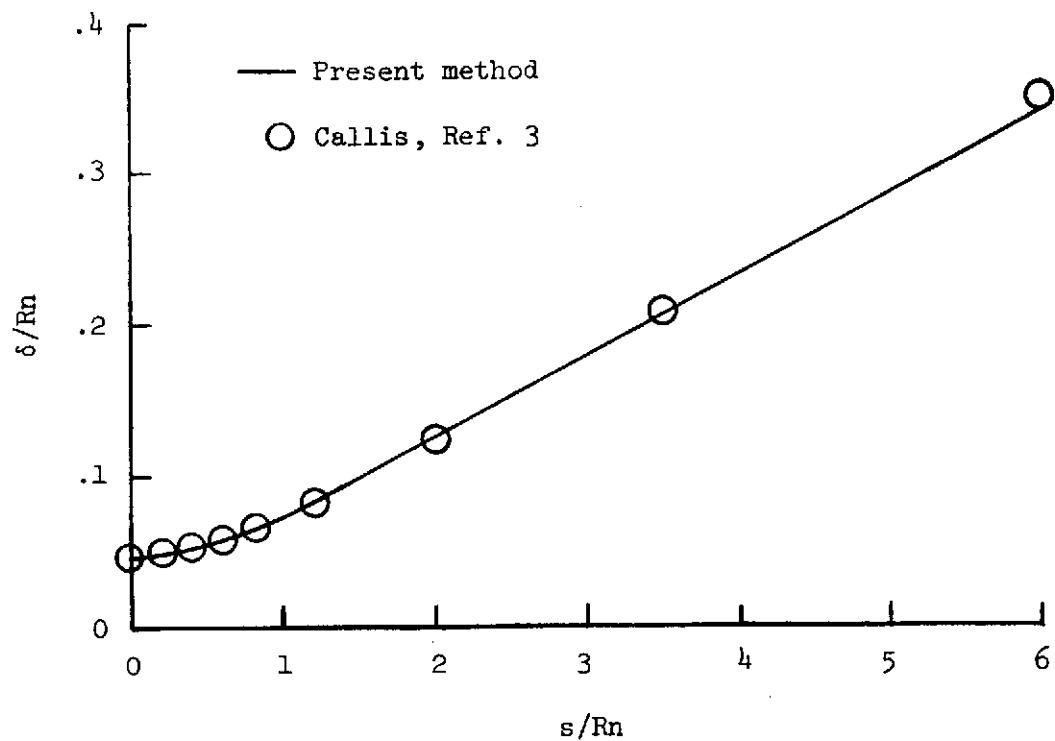
(c) Shock stand-off distance around body.

Figure 6. – Continued.
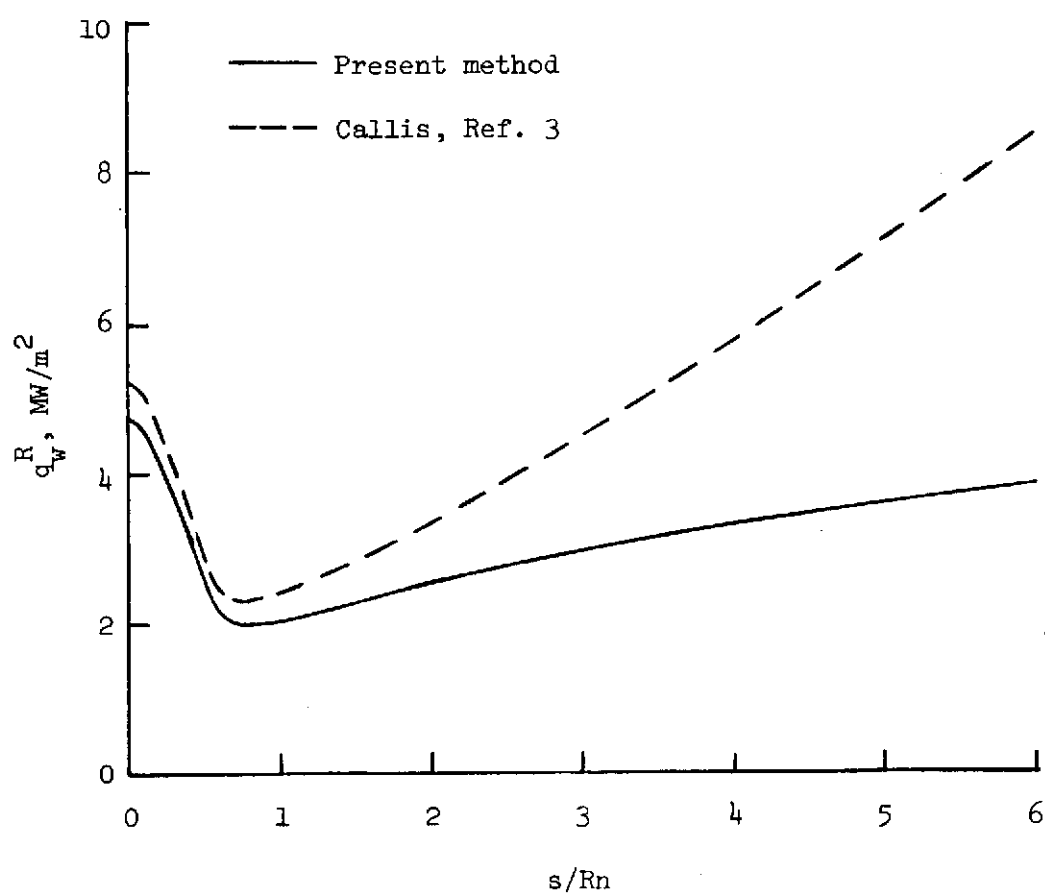
(d) Radiative heating along body.

Figure 6. - Continued.
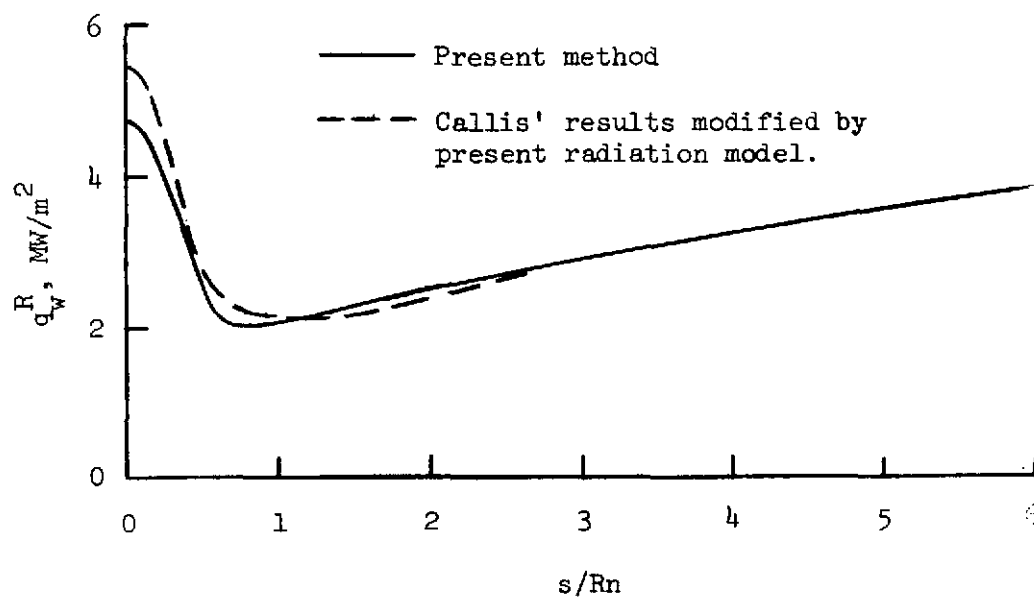
(e) Radiative heating along body.
Callis' results modified.

Figure 6. - Concluded.
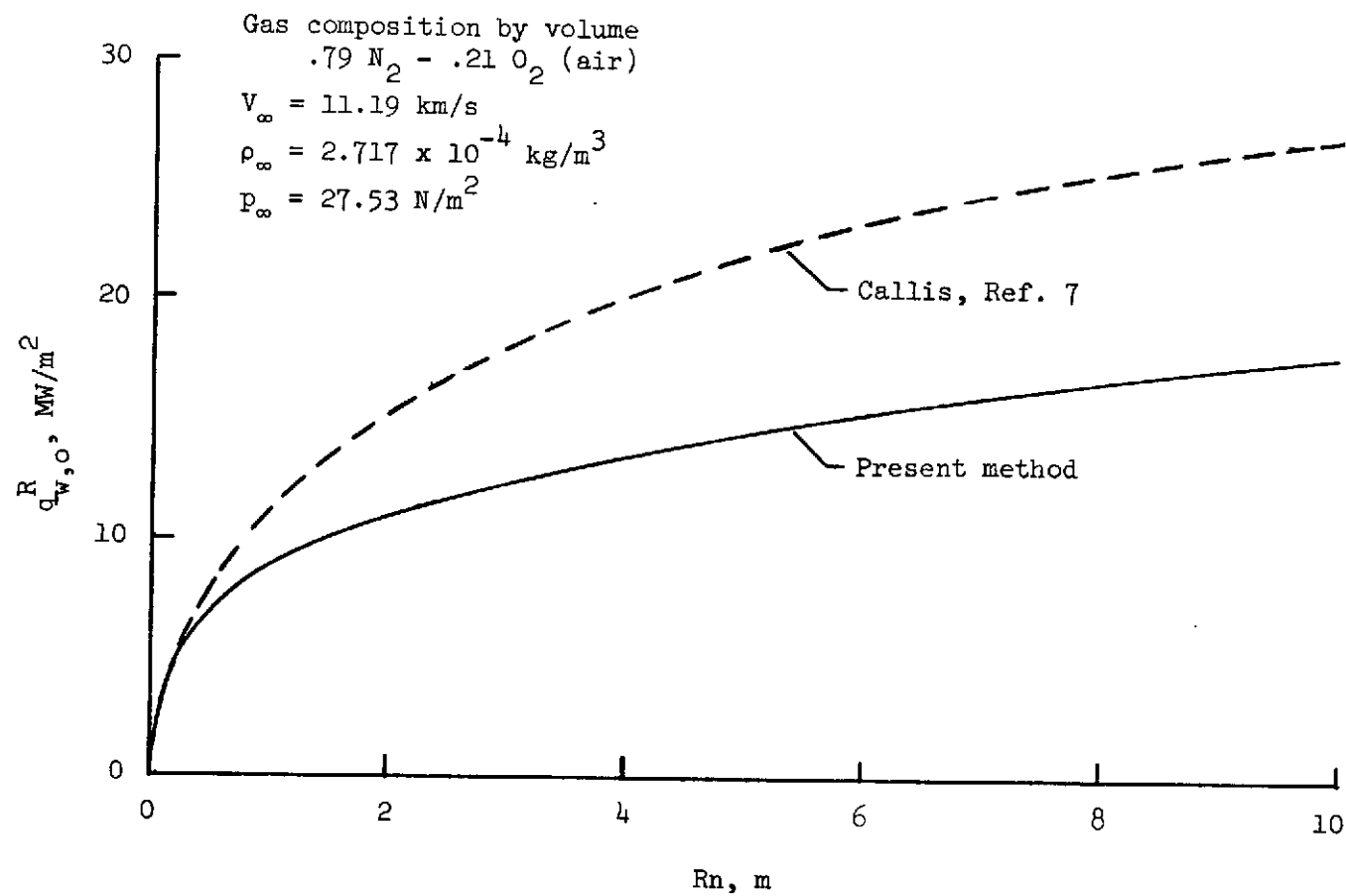
Figure 7. - Stagnation-point, radiative heating rates in an air
atmosphere as a function of nose radius. Present
results are compared with the method of Callis (ref. 7).
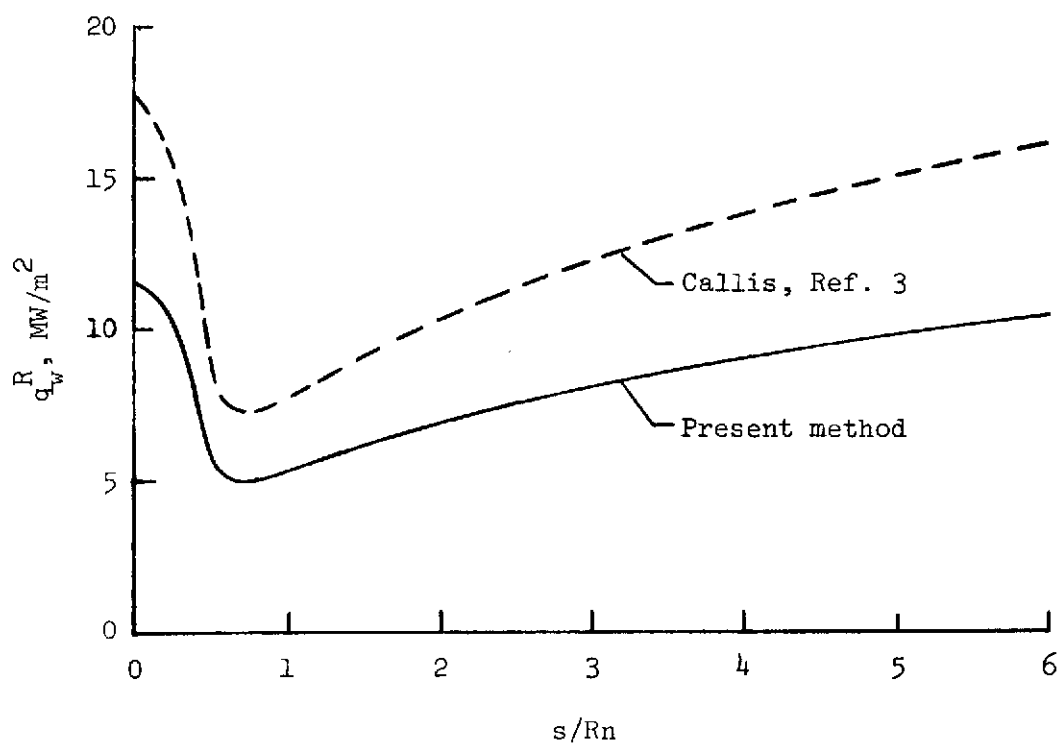
Figure 8. - Radiative heating distribution for free-stream
conditions and body shape given in Figure 6(a)
except Rn=2.0 m.   Present results are compared
with the method of Callis (ref. 3).

Case	Gas Composition*	V_∞, km/s	ρ_∞, kg/m^3	p_∞, N/m^2	h_∞, MJ/kg	$q_{w,o}^R$, MW/m^2
A	.79 N_2 - .21 O_2	12.200	2.744×10^{-4}	20.01	0	5.78
B	.85 H_2 - .15 He	50.000	5.700×10^{-3}	0	0	9668.00
C	.90 CO_2 - .10 N_2	8.740	3.294×10^{-3}	130.59	-8.43	4.44
D	.90 CO_2 - .10 N_2	11.175	2.850×10^{-3}	117.30	-8.43	35.70

* by volume
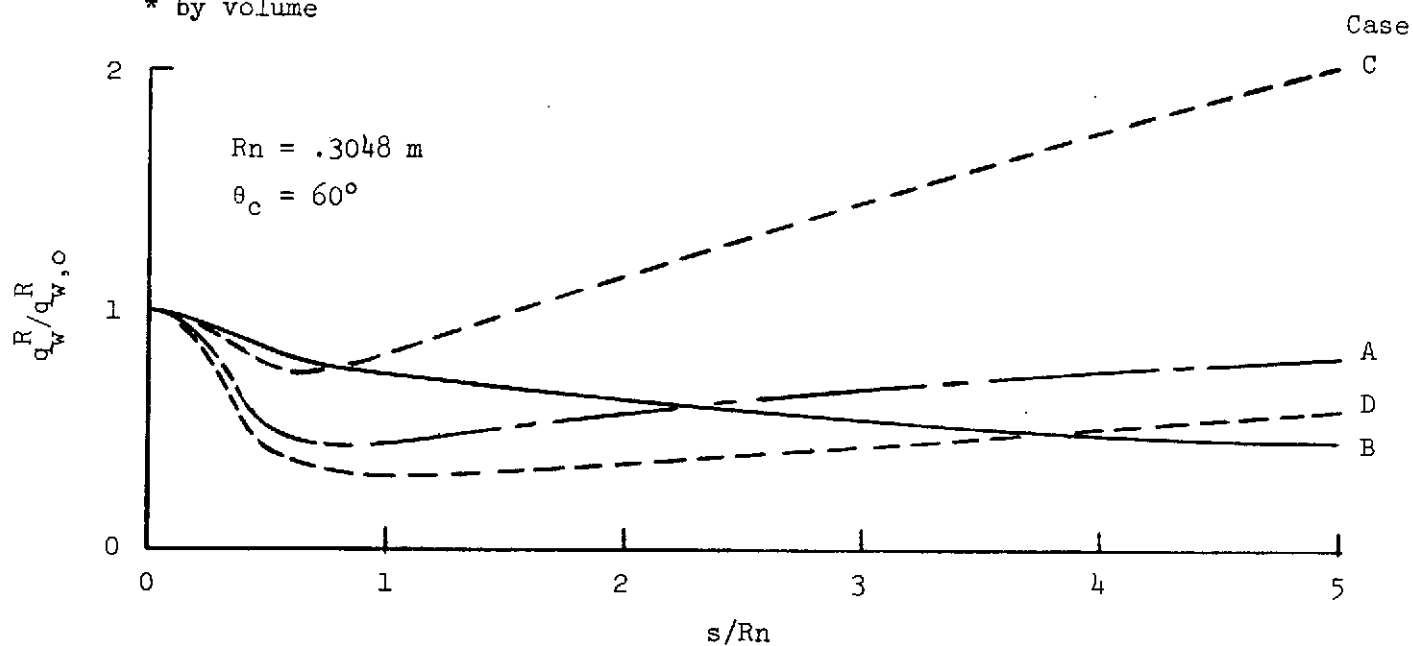
Figure 9. – Radiative heating distributions along a spherically-capped, conical body from radiating, inviscid flow solutions for entries in different atmospheres and different free-stream conditions.
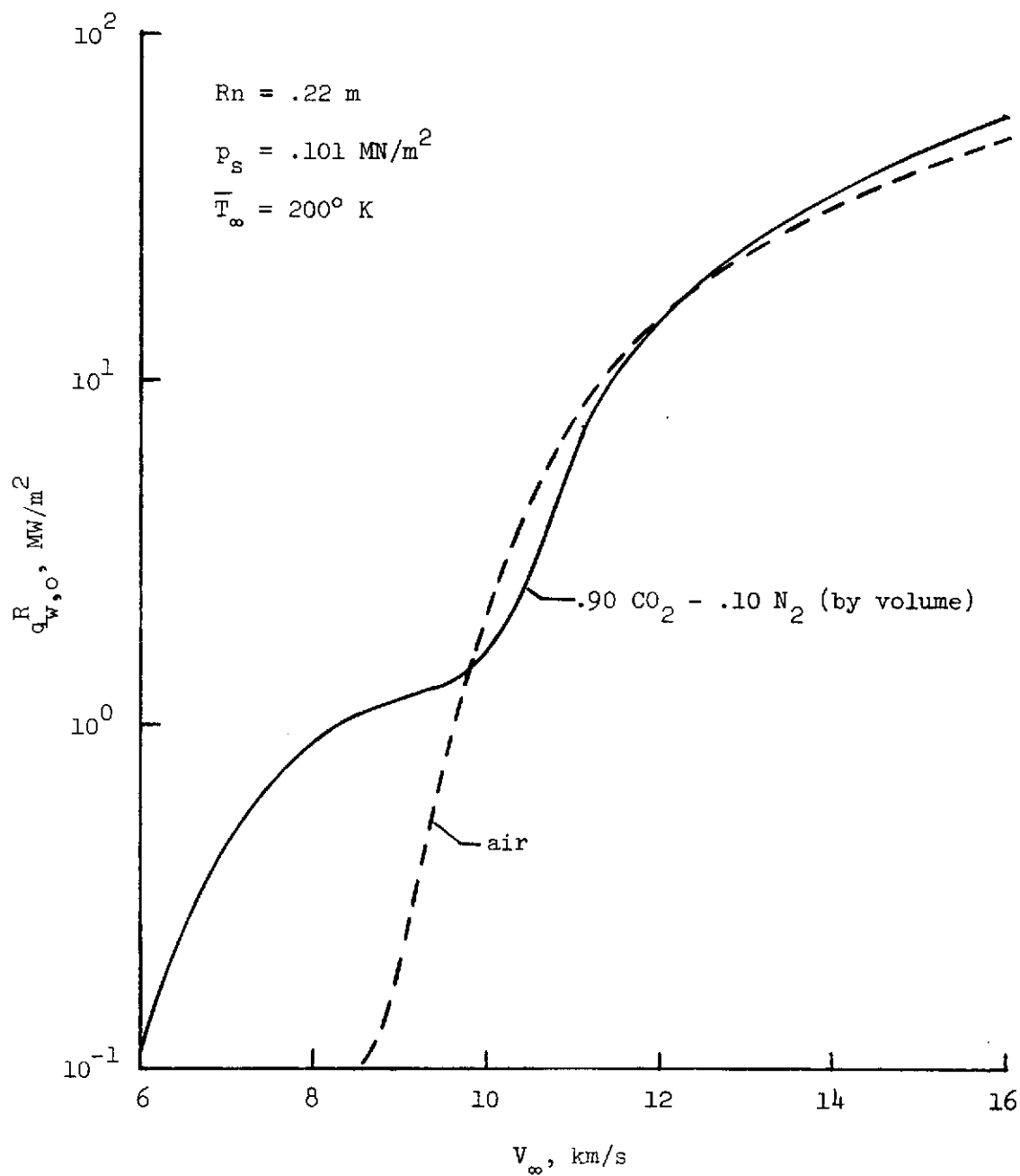
Figure 10. - A comparison of the stagnation-point, radiative
heating rates for entries in air and in a
.90 CO_2 - .10 N_2 (by volume) gas mixture.

θ_c	$q^R_{w,o}$, MW/m^2	δ_o/Rn	at s/Rn=3.0		
			δ/Rn	$\overline{T}_\delta/\overline{T}_s$	$\theta+\beta$
60°	11.39	.0435	.1893	.9058	63.33°
55°	11.35	.0434	.1606	.8514	57.77°
50°	11.33	.0434	.1382	.7644	52.23°
45°	11.33	.0435	.1155	.6276	46.59°

$V_\infty = 12.20$ km/s

$\rho_\infty = 2.744 \times 10^{-4}$ kg/m^3

$p_\infty = 20.01$ N/m^2

$Rn = 2.00$ m

$\overline{T}_s = 12175°$ K
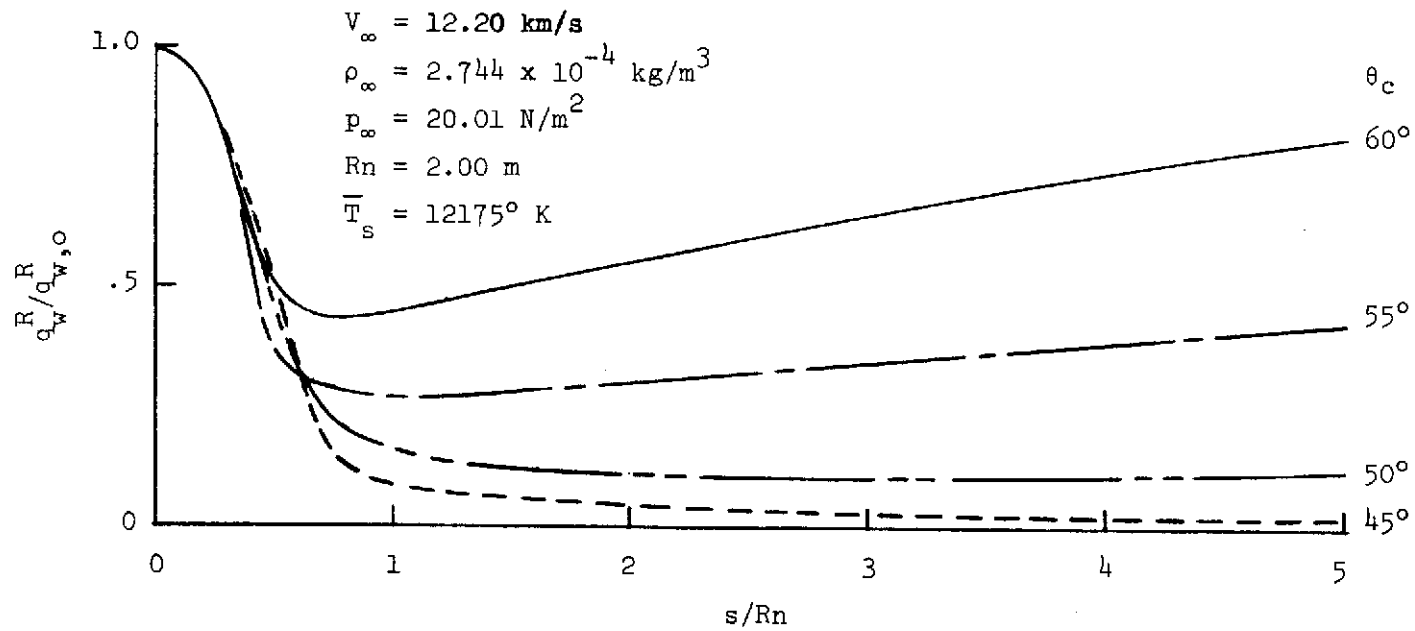
Figure 11. - The distribution of radiative heating along spherically-capped, conical bodies for entry in air.
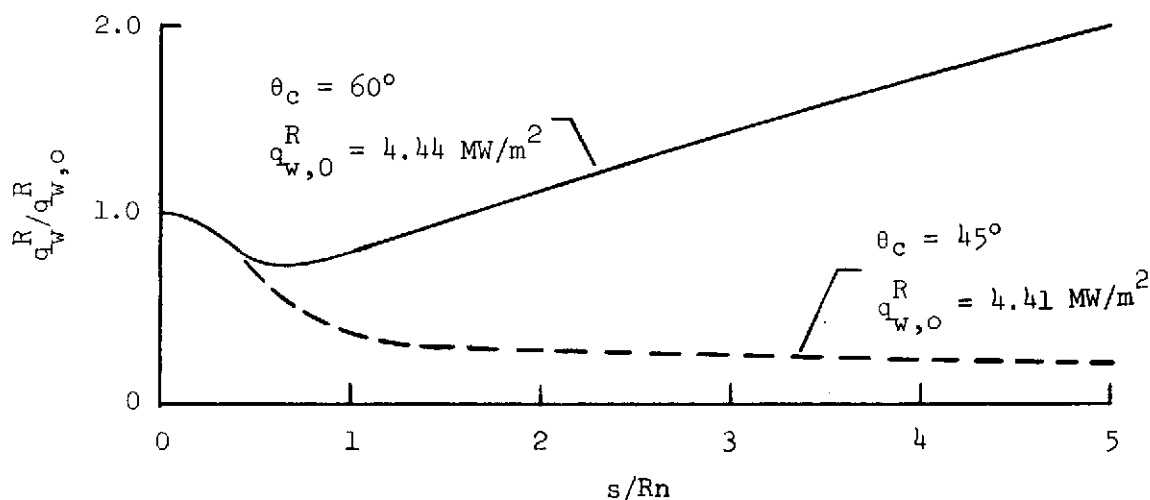
(a) $V_\infty = 8.740$ km/s ; $\rho_\infty = 3.294 \times 10^{-3}$ kg/m^3 ; $p_\infty = 130.6$ N/m^2

$h_\infty = -8.43$ MJ/kg ; $Rn = .3048$ m
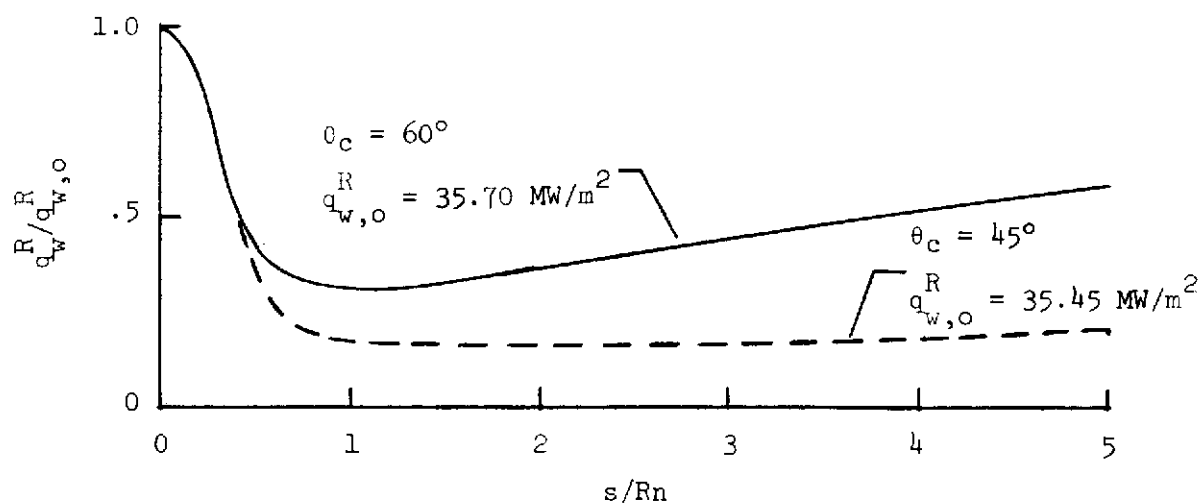
(b) $V_\infty = 11.175$ km/s ; $\rho_\infty = 2.850 \times 10^{-3}$ kg/m^3 ; $p_\infty = 117.3$ N/m^2

$h_\infty = -8.43$ MJ/kg ; $Rn = .3048$ m

Figure 12. - The distribution of radiative heating along spherically-capped, conical bodies for entry in a .90 CO_2 - .10 N_2 (by volume) gas mixture.

$V_\infty = 12.20 \text{ km/s}$; $\rho_\infty = 2.744 \times 10^{-3} \text{ kg/m}^3$

$p_\infty = 20.01 \text{ N/m}^2$; $\theta_c = 60°$
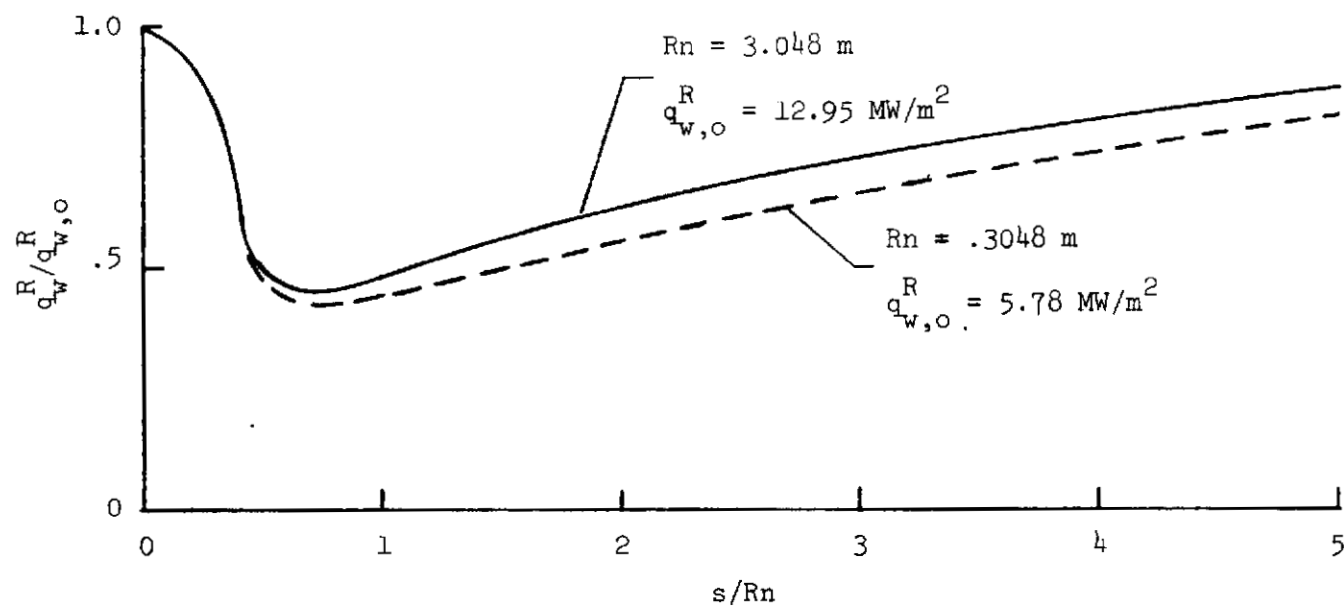
Figure 13. – The effect of nose radius on the distribution of radiative heating along a spherically-capped, conical body for entry in air.

Figure 14. — The effect of nose radius on the distribution of radiative heating along a spherically-capped, conical body for entry in a .90 CO_2 - .10 N_2 (by volume) gas mixture.
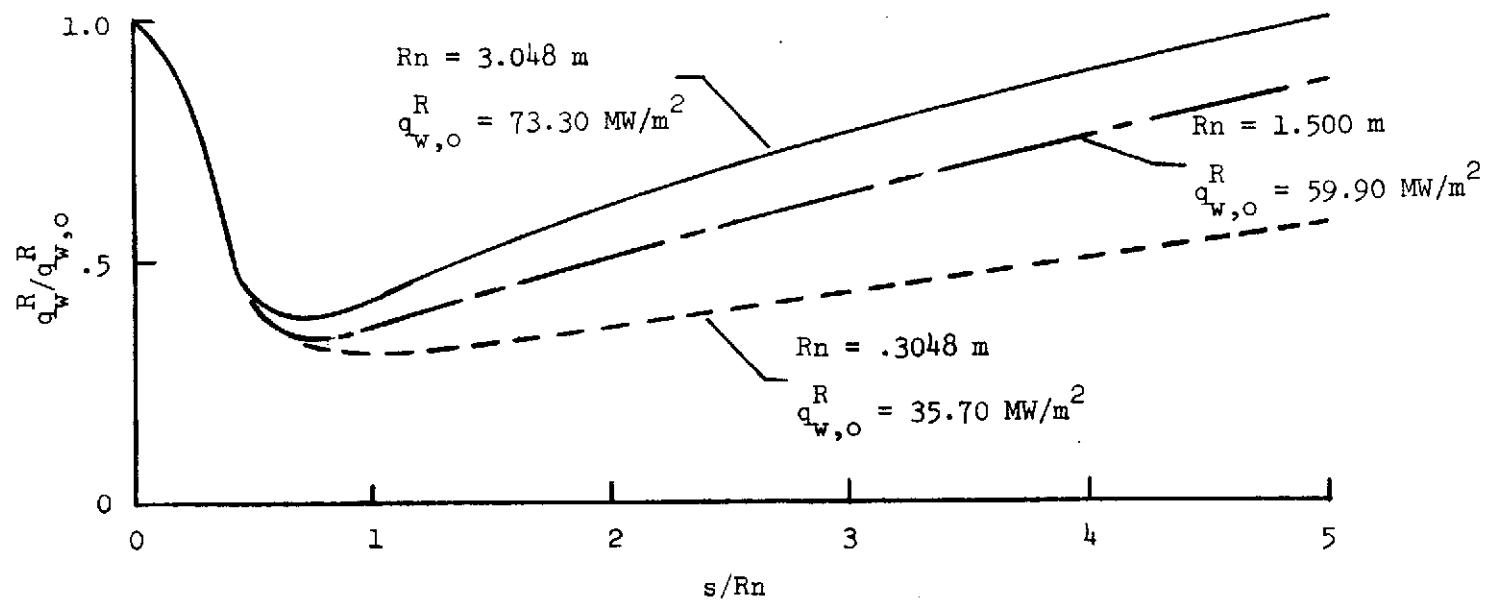
(b) $V_\infty = 11.175$ km/s ; $\rho_\infty = 2.850 \times 10^{-3}$ kg/m^3 ; $p_\infty = 117.3$ N/m^2

$h_\infty = -8.43$ MJ/kg ; $\theta_c = 60°$

Figure 14. - Concluded.
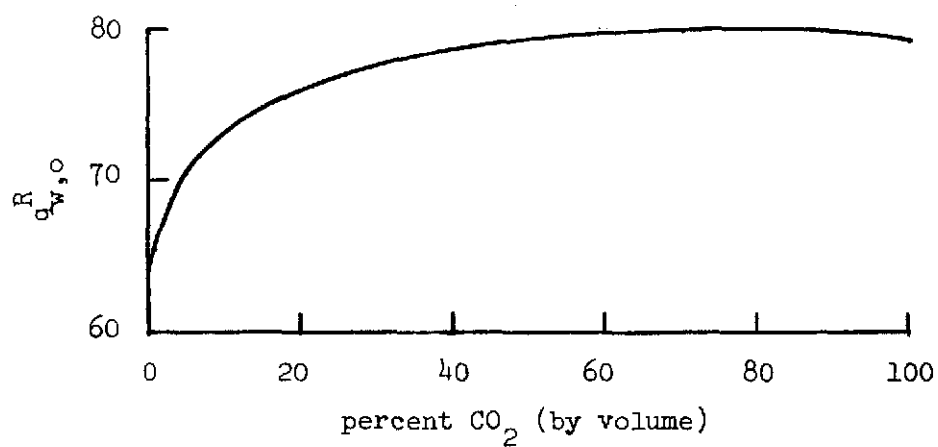
(a) $V_\infty = 12.0$ km/s ; $\rho_\infty = 2.99 \times 10^{-3}$ kg/m^3
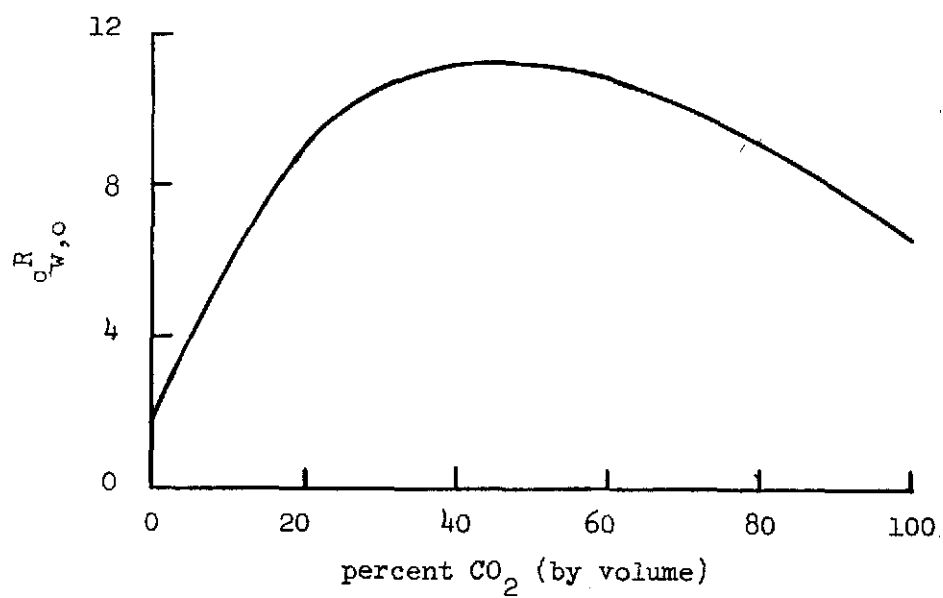
(b) $V_\infty = 9.0$ km/s ; $\rho_\infty = 5.31 \times 10^{-3}$ kg/m^3

Figure 15. – Stagnation-point, radiative heating rates in $CO_2 - N_2$ gas mixtures. Rn=.3048 m

Gas composition by volume

$.79 \, N_2 - .21 \, O_2$ (air)

$V_\infty = 15.250 \ km/s$

$\rho_\infty = 1.77 \times 10^{-4} \ kg/m^3$

$p_\infty = 12.3 \ N/m^2$

$h_\infty = 0.0 \ J/kg$

$Rn = 2.56 \ m$

Specified wall conditions

$\overline{T}_w = 3840 \ ^\circ K$

$(\rho v)_w = .205 \ kg/m^2\text{-}s$

Elemental mass fractions of
injected gas:

Carbon	.923
Oxygen	.058
Hydrogen	.018
Nitrogen	.001

(a) Free-stream conditions and specified wall conditions.

Figure 16. – Fully-coupled, stagnation-point solution for
Earth reentry. Present method is compared
with the method of Garrett (ref. 19).
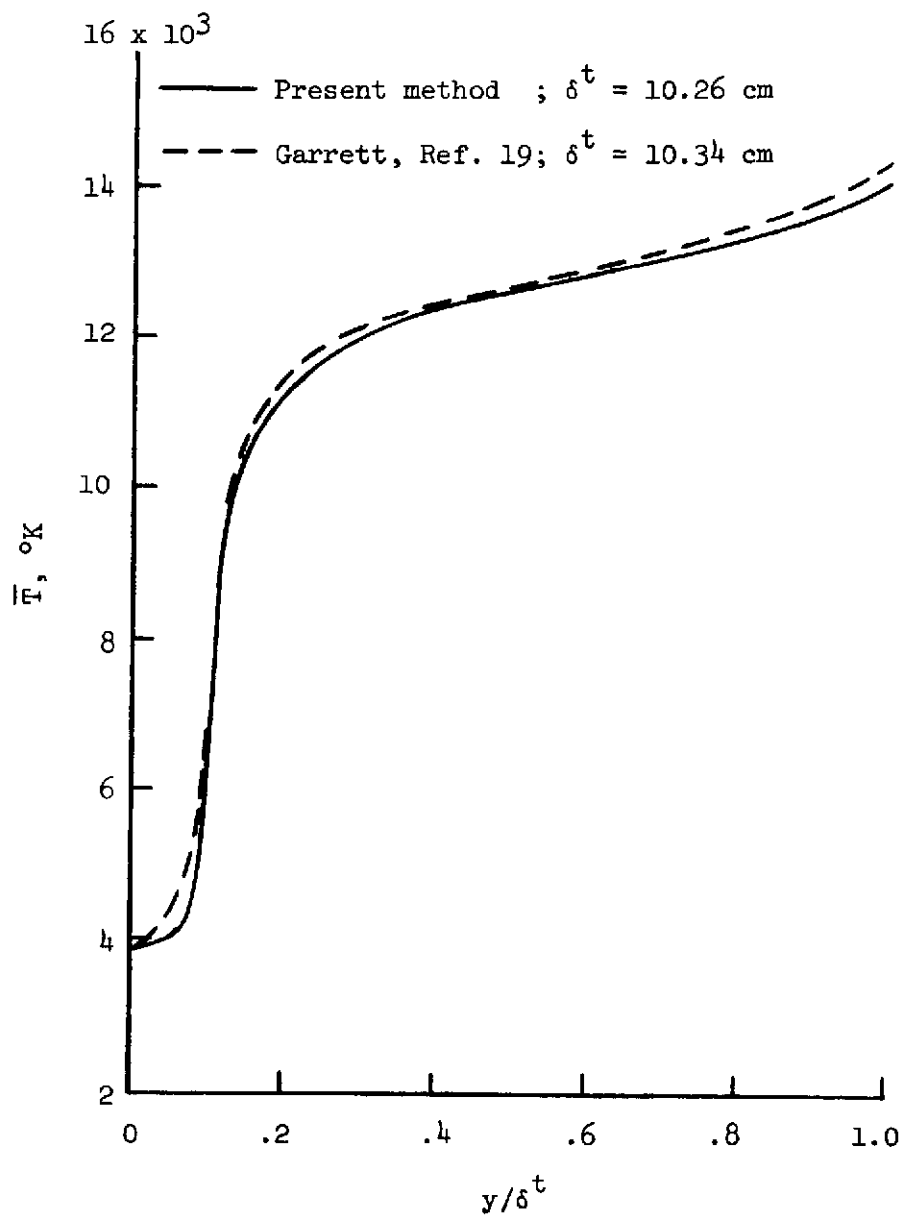
(b) Temperature profile through layer.

Figure 16. - Continued.
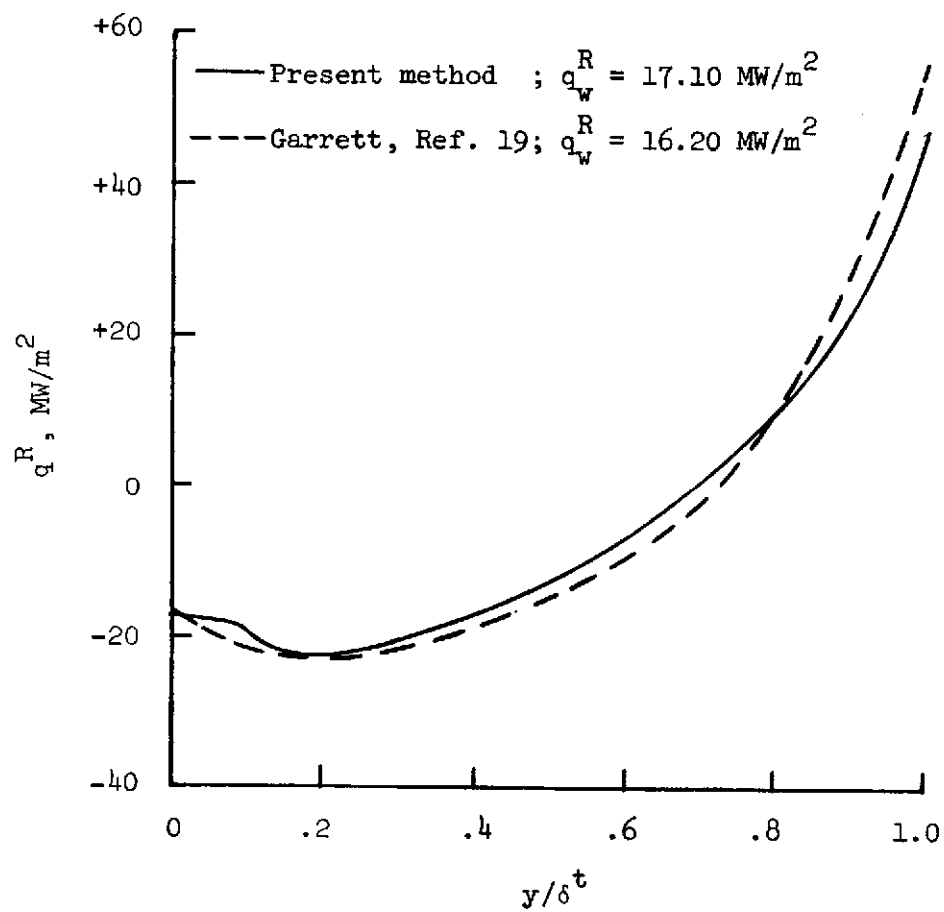
(c) Radiative heating profile through layer.
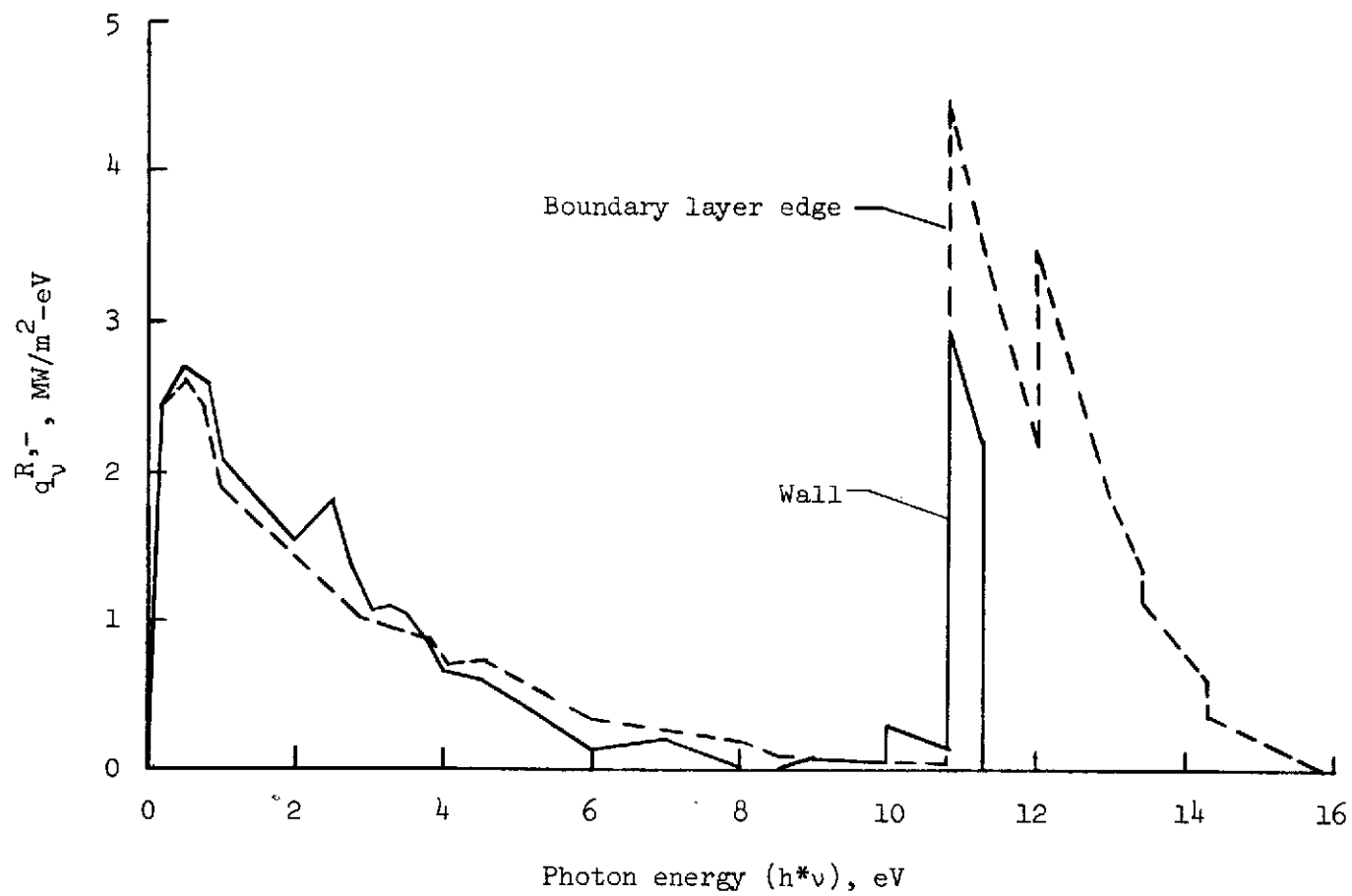
Figure 16. - Continued.

(d) Spectral distribution of radiative heating
toward the body due to continuum processes.

Figure 16. – Continued.
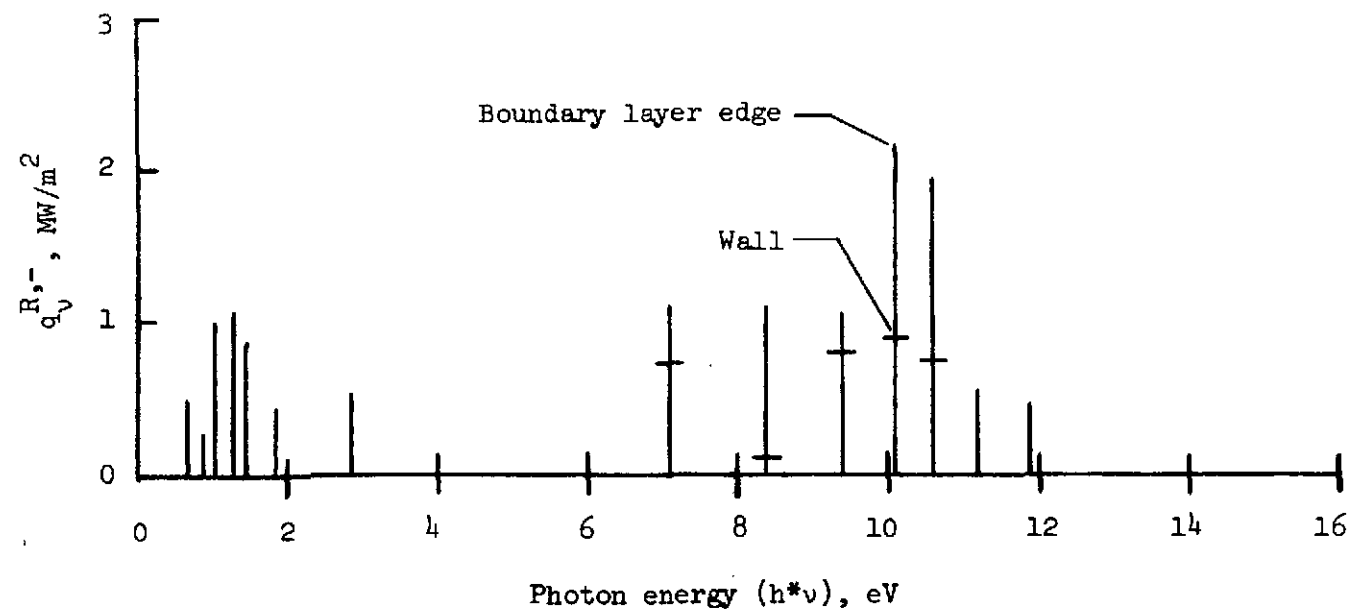
(e) Spectral distribution of radiative heating
toward the body due to line processes.

Figure 16. - Concluded.
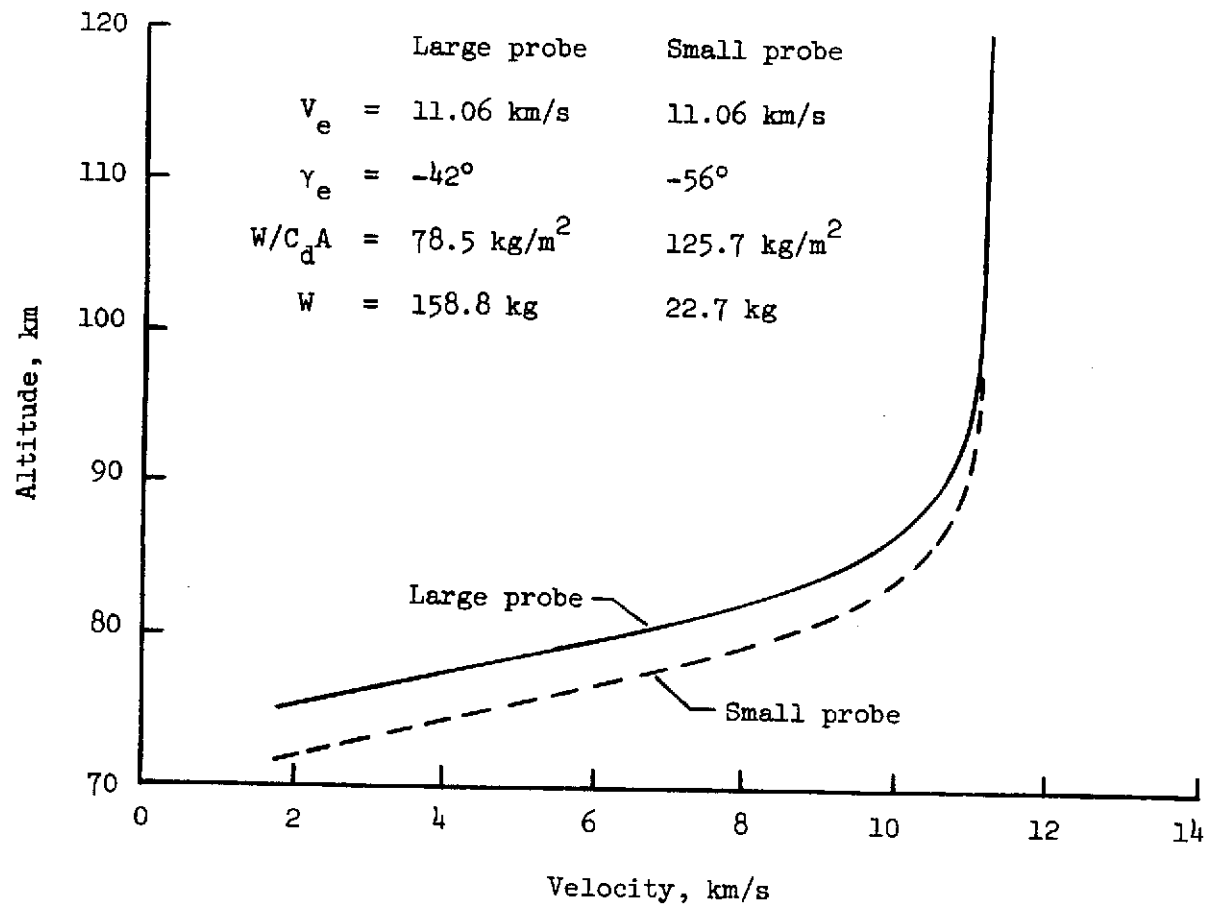
Figure 17. - Trajectories for large and small probes during entry to Venus.
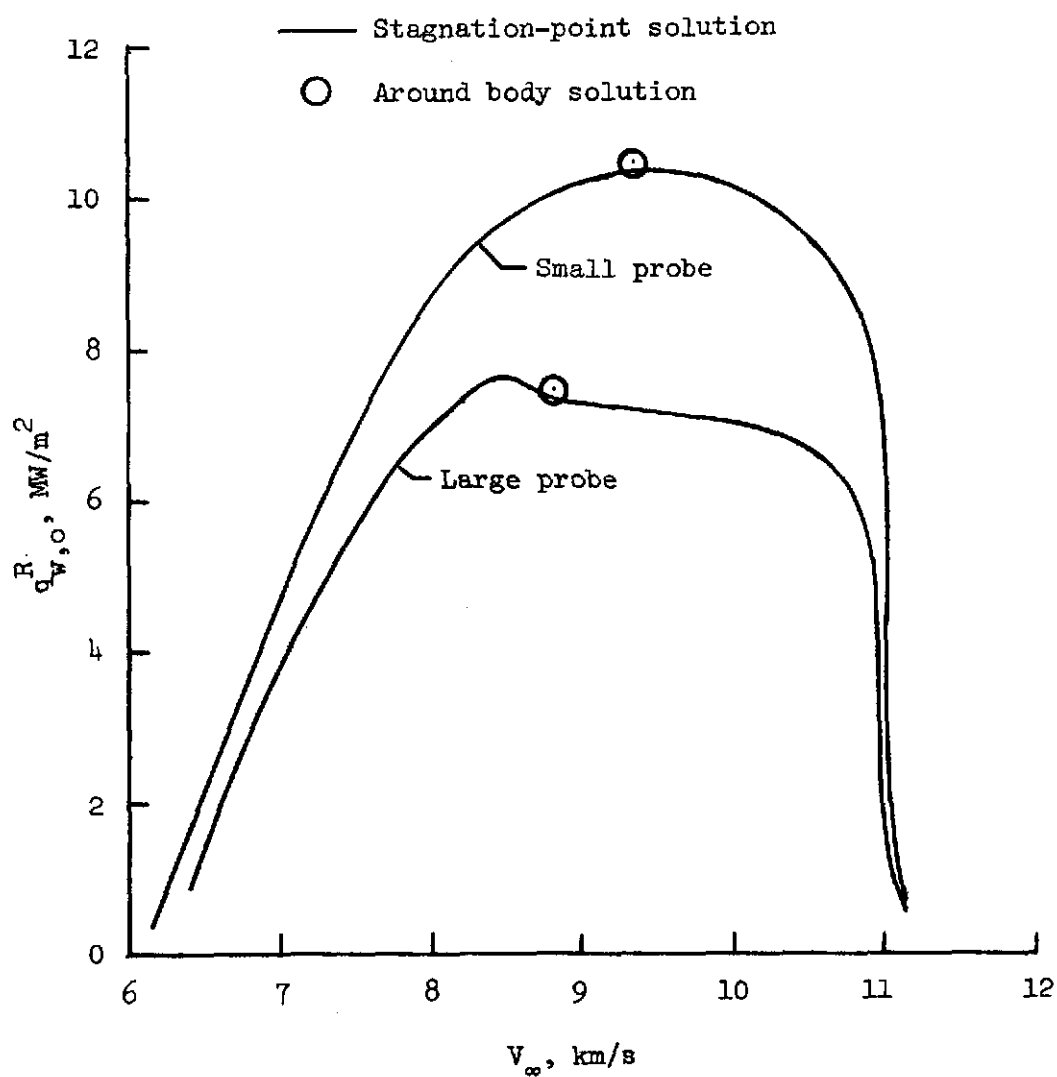
Figure 18. - Stagnation-point, radiative heating rates along
entry trajectories for large and small probes.
Results from radiating, inviscid flow solutions.

Gas composition by volume
.97 CO_2 - .03 N_2

$V_\infty = 8.803$ km/s

$\rho_\infty = 5.79 \times 10^{-3}$ kg/m^3

$p_\infty = 200.1$ N/m^2

$h_\infty = -8.86$ MJ/kg

Rn $= 0.3429$ m

$\theta_c = 60°$
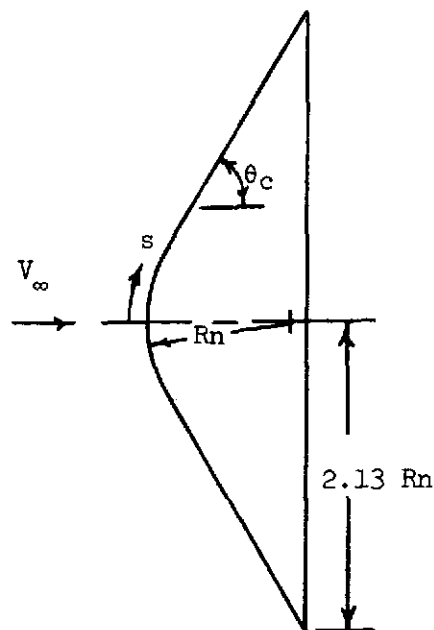
(a) Free-stream conditions and body shape.
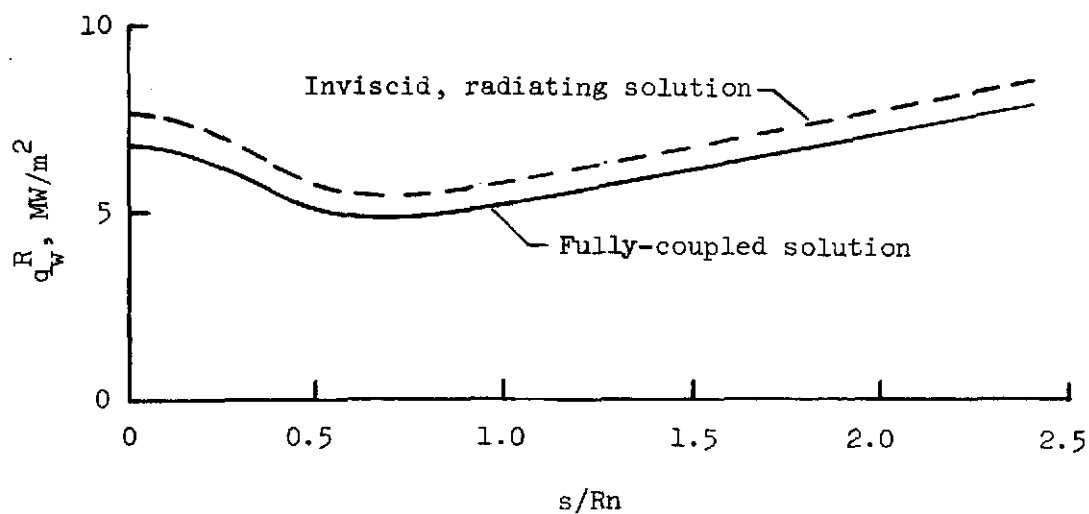
(b) Comparison of radiative heating.

Figure 19. - Fully-coupled, radiating flow solution with
steady-state ablation of carbon-phenolic
heatshield for large probe.
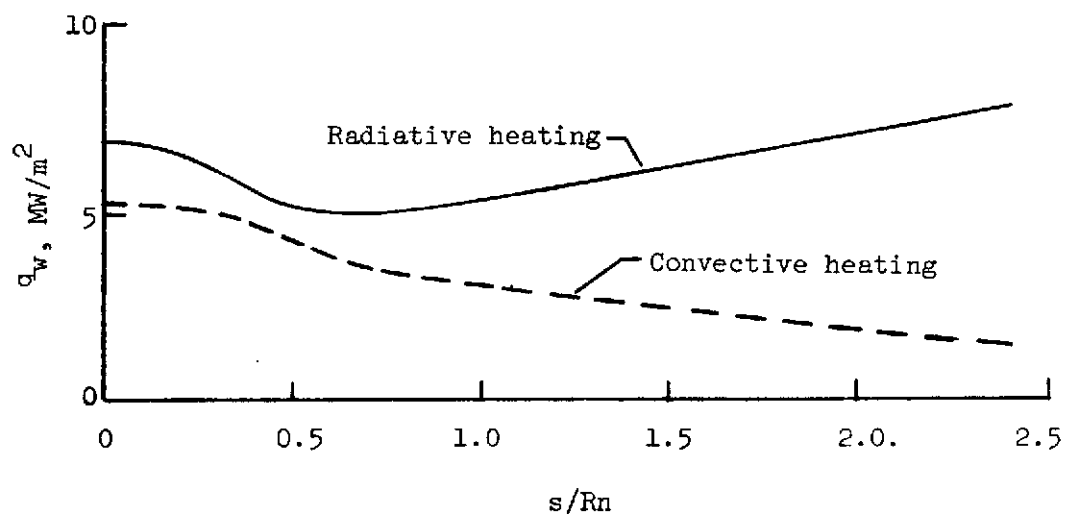
(c) Radiative and convective heating distribution.
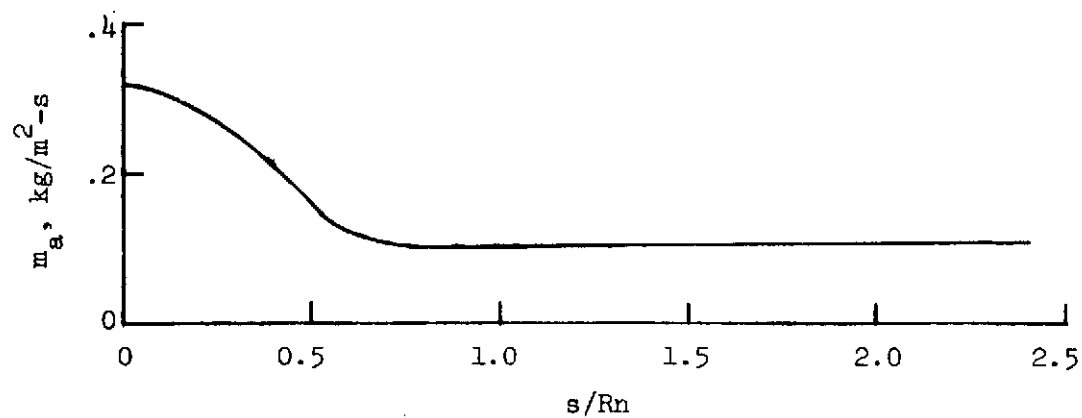
(d) Ablation rate distribution.

Figure 19. - Continued.

(e) Aerodynamic shear distribution.
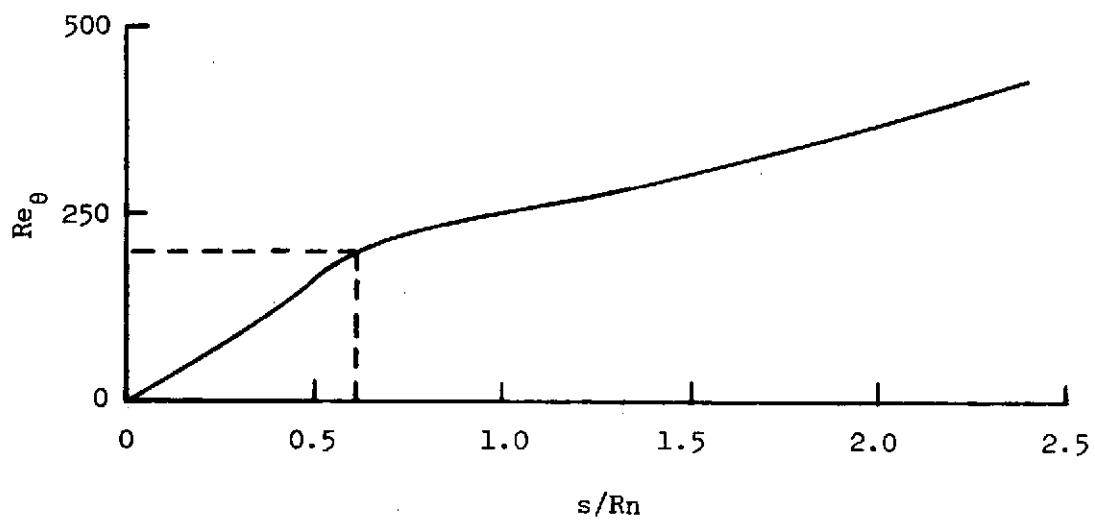
(f) Momentum thickness Reynolds number distribution.

Figure 19. - Continued.

(g) Spectral distribution of radiative heating
toward the body due to continuum processes.

Figure 19. - Concluded.
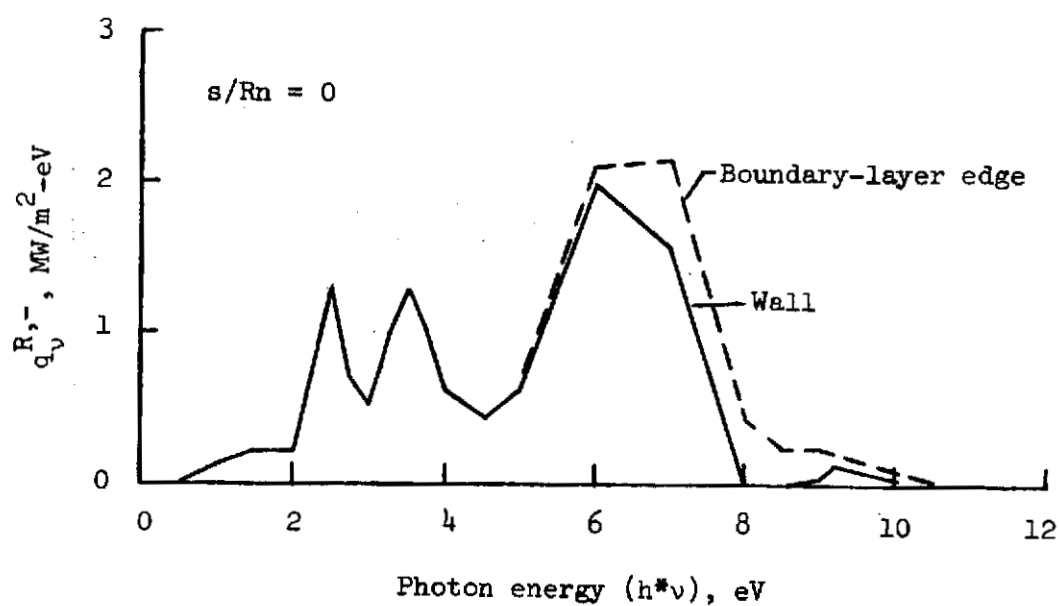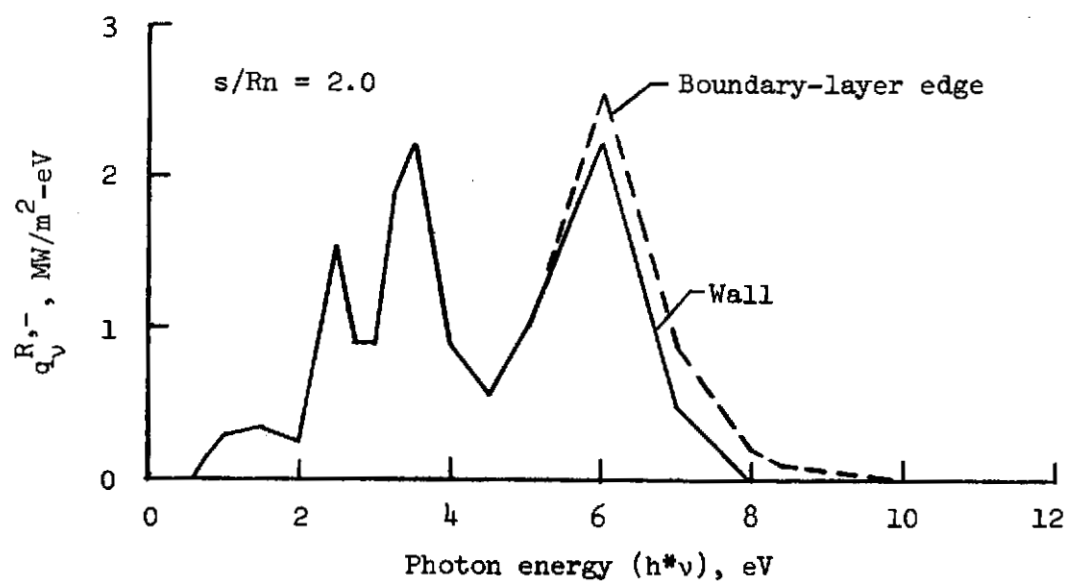
Gas composition by volume
.97 CO_2 - .03 N_2

V_∞ = 9.331 km/s

ρ_∞ = 9.32 x 10^{-3} kg/m^3

P_∞ = 330.4 N/m^2

h_∞ = -8.86 MJ/kg

Rn = 0.1397 m

θ_c = 45°

(a) Free-stream conditions and body shape.

Inviscid, radiating solution

Fully-coupled solution

q_w^R, MW/m^2

s/Rn
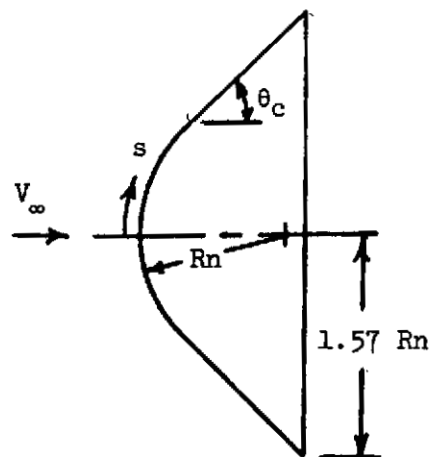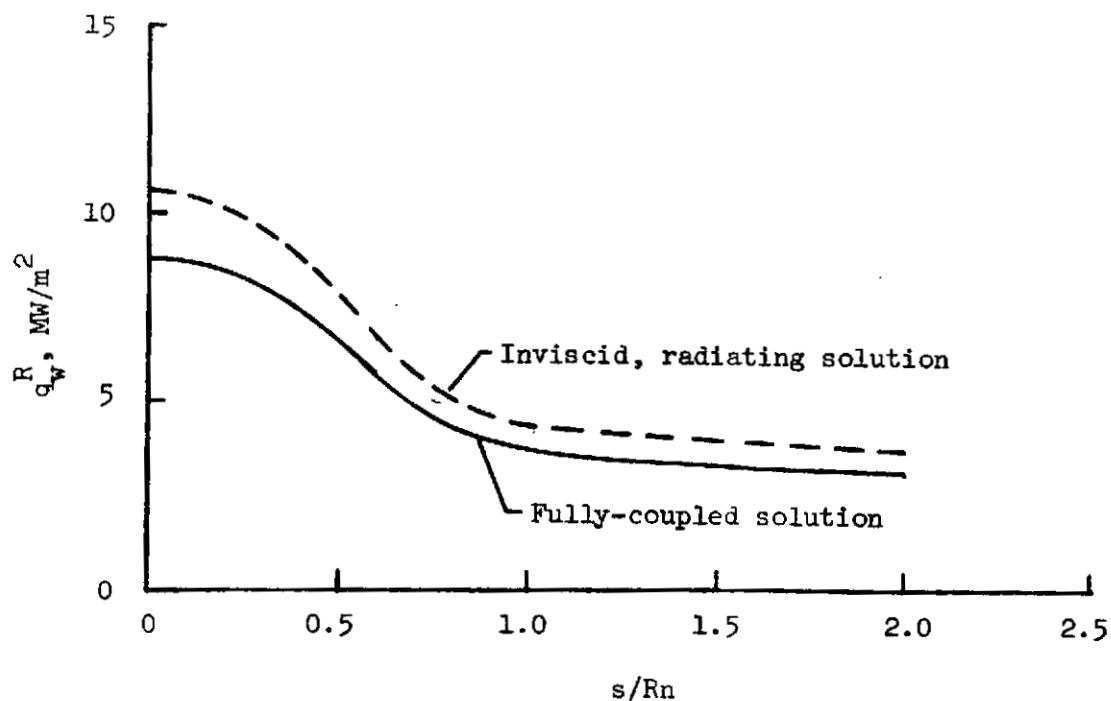
(b) Comparison of radiative heating.

Figure 20. - Fully-coupled, radiating flow solution with
steady-state ablation of carbon-phenolic
heatshield for small probe.
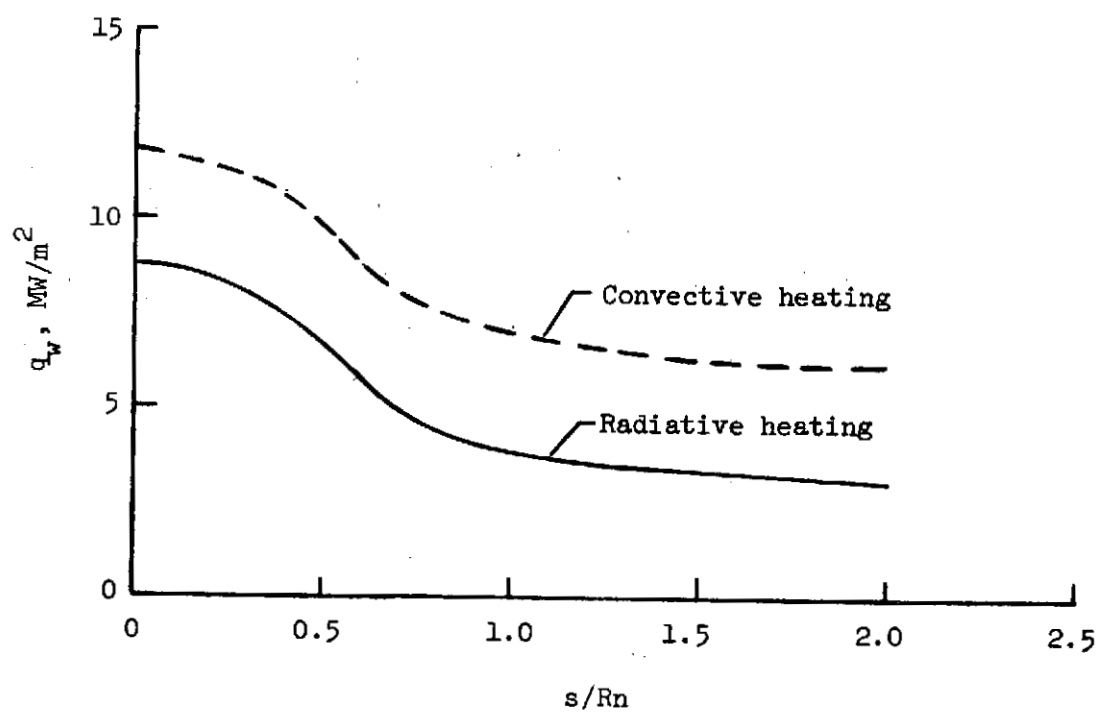
(c) Radiative and convective heating distribution.
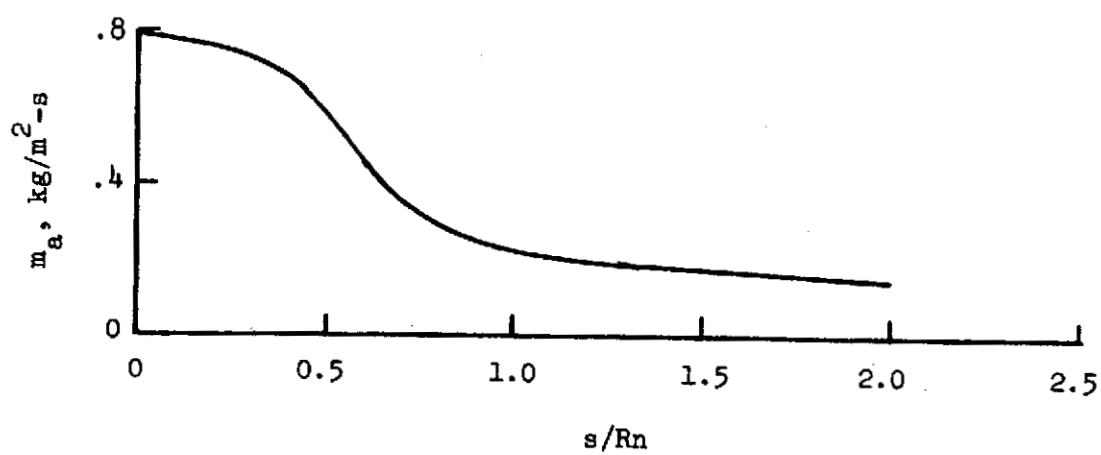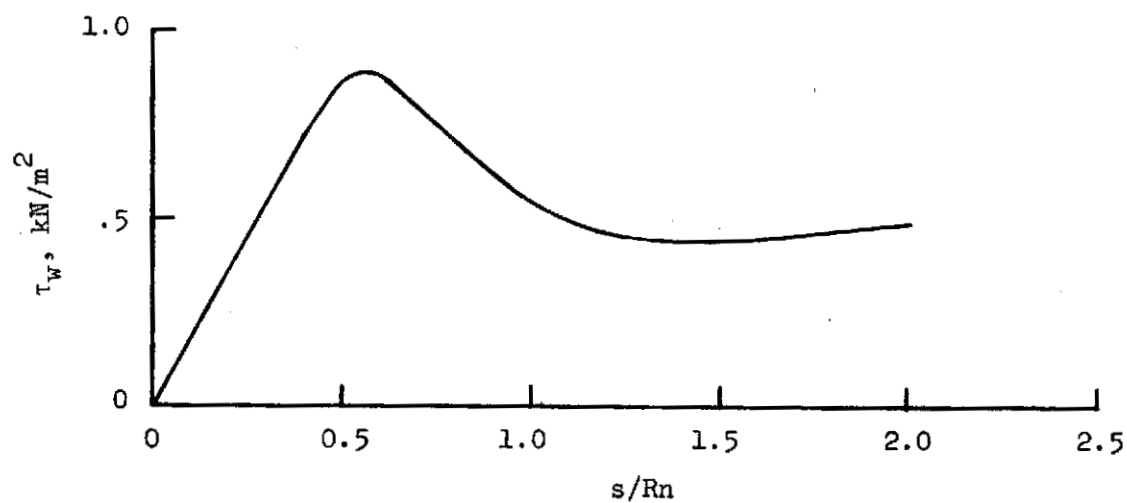
(d) Ablation rate distribution.

Figure 20. - Continued.

(e) Aerodynamic shear distribution.

(f) Momentum thickness Reynolds number distribution.
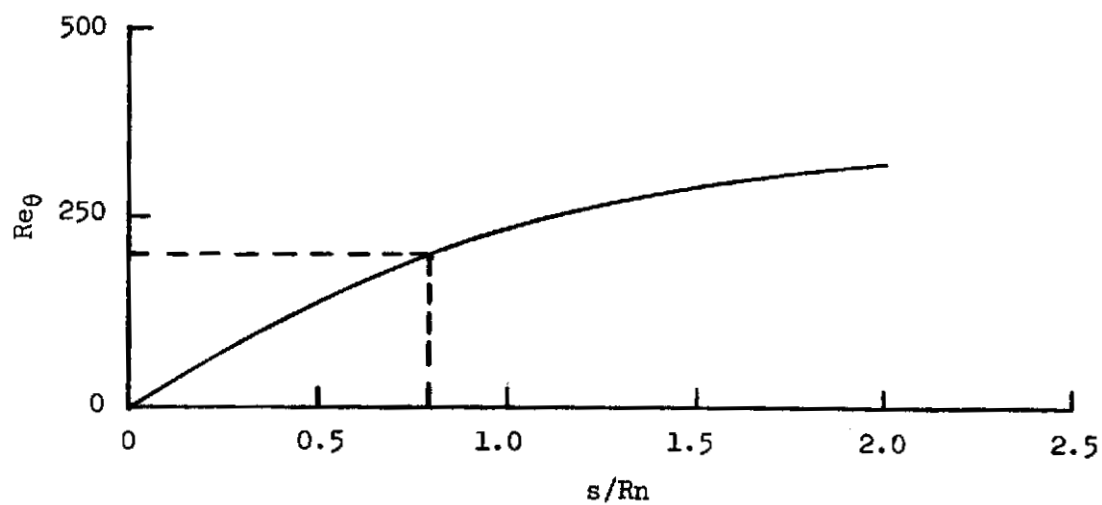
Figure 20. - Continued.
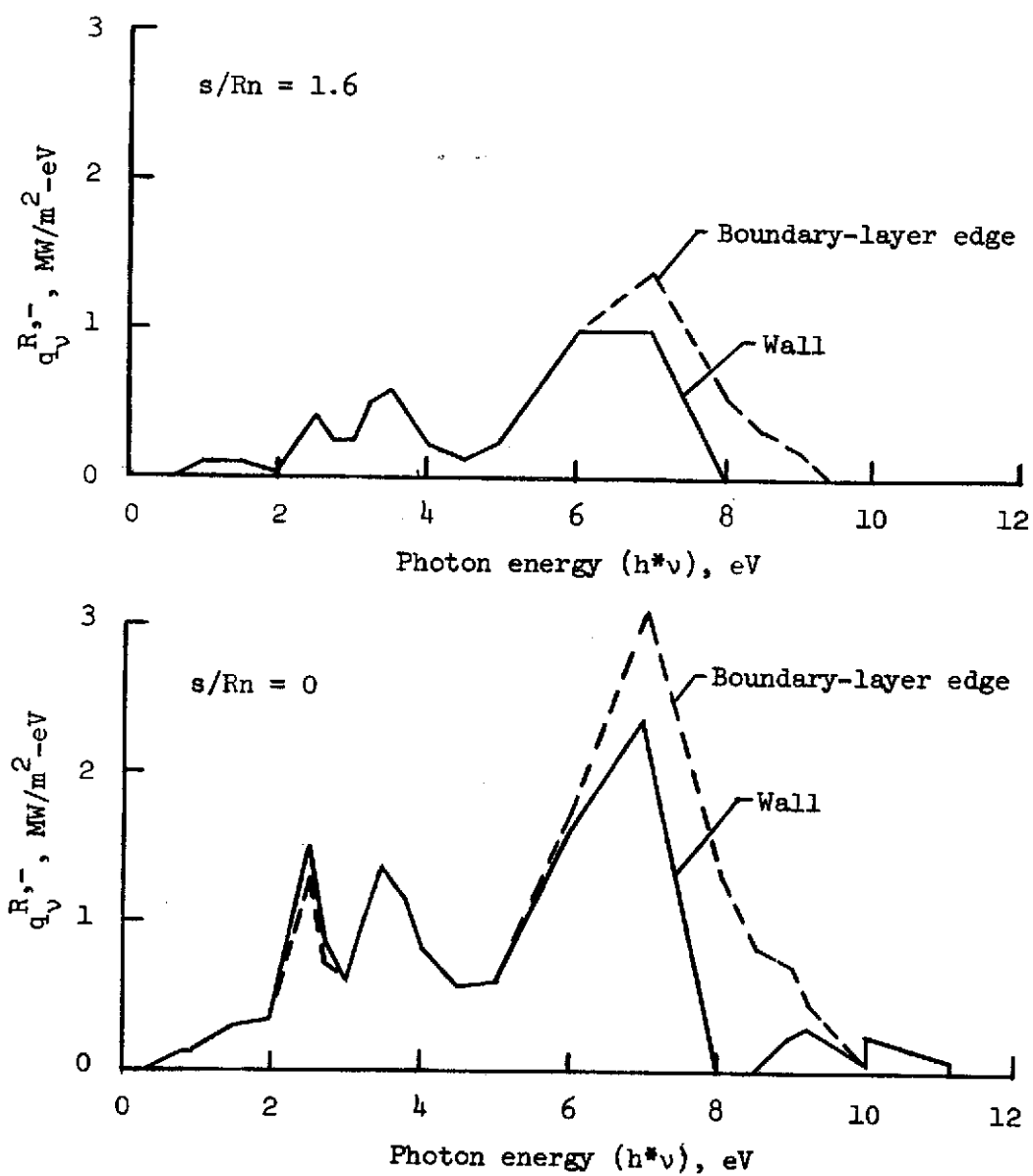
(g) Spectral distribution of radiative heating
toward the body due to continuum processes.

Figure 20.- Concluded.
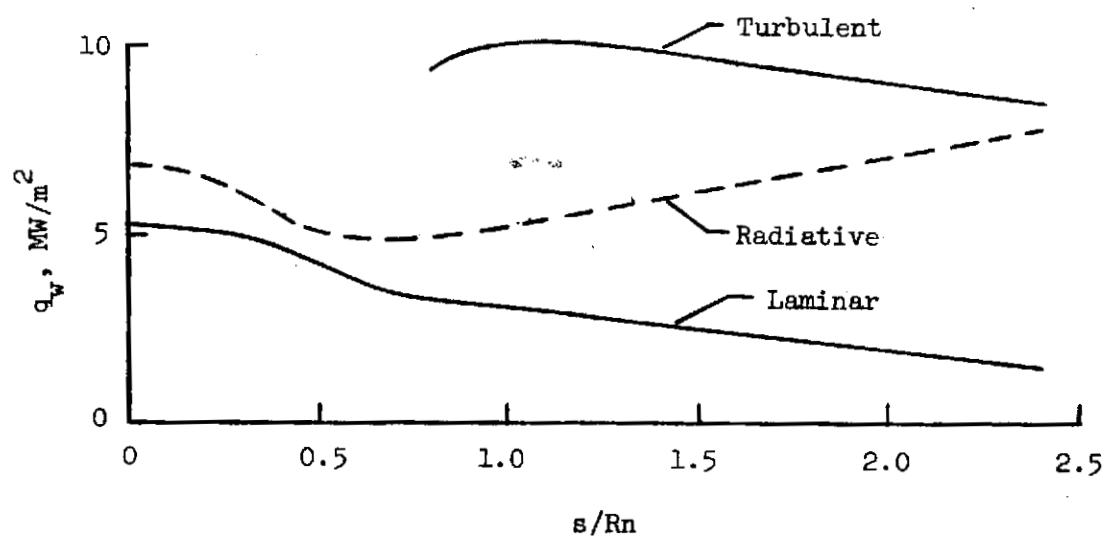
(a) Heating rate distribution.
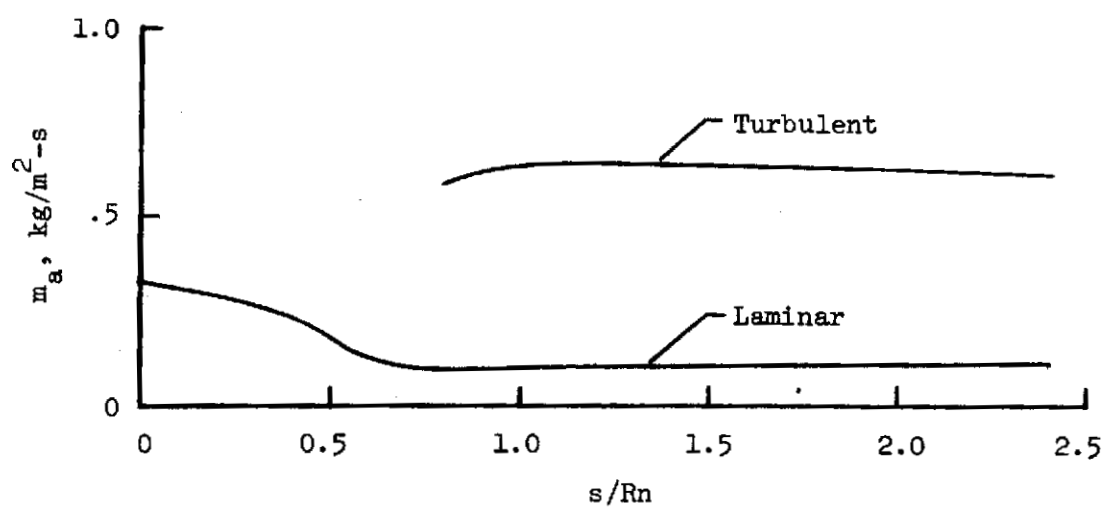
(b) Ablation rate distribution.

Figure 21. – Comparison between a turbulent and laminar
boundary layer for fully-coupled solution
for large probe.
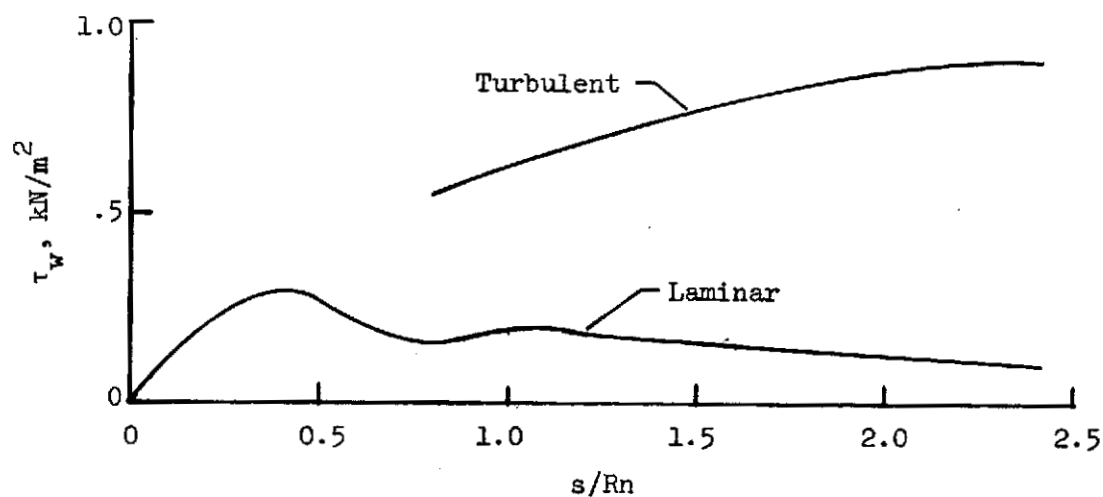
(c) Aerodynamic shear distribution.
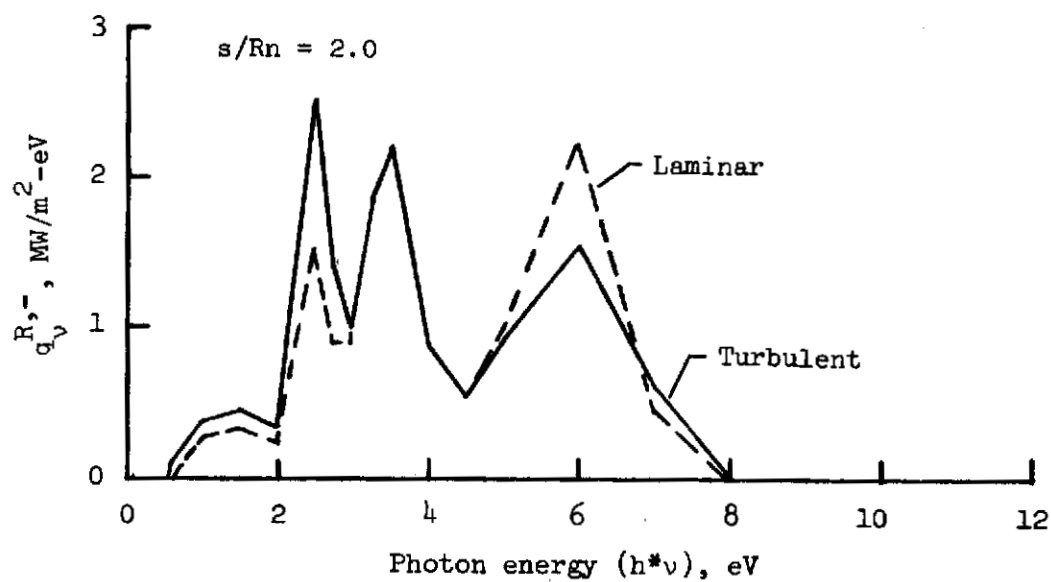
(d) Spectral distribution at the wall of radiative
heating toward the body due to continuum processes.

Figure 21. - Concluded.

Gas composition by volume
.97 CO_2 - .03 N_2

V_∞ = 11.175 km/s

ρ_∞ = 2.85 x 10^{-3} kg/m^3

p_∞ = 117.3 N/m^2

h_∞ = -8.86 MJ/kg

Rn = 0.3048 m

θ_c = 60°
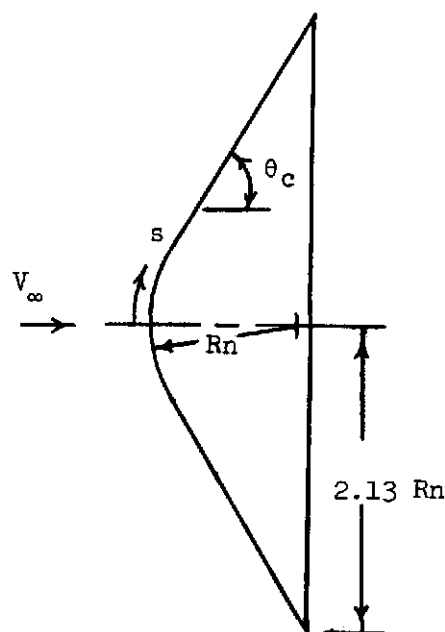
(a) Free-stream conditions and body shape.
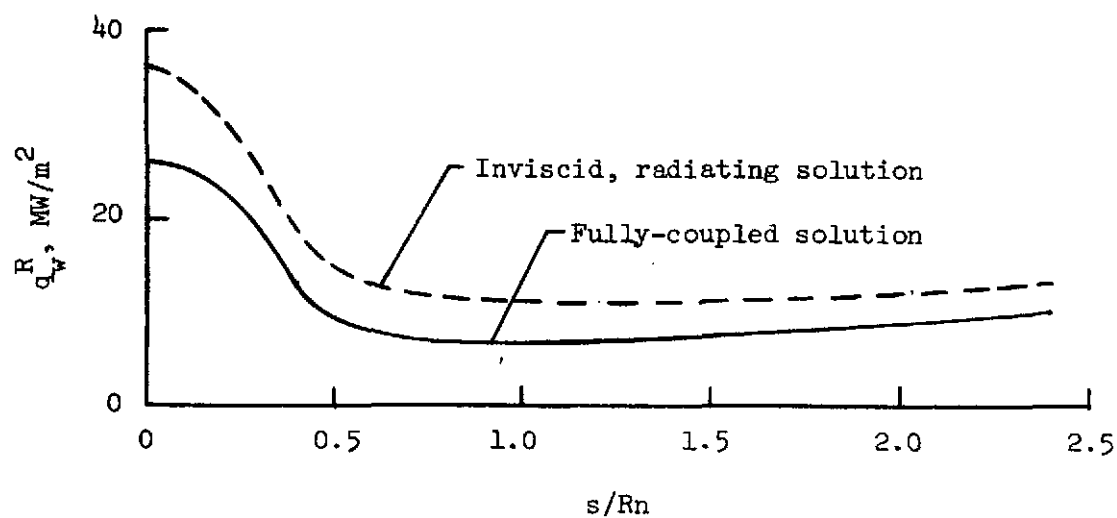
(b) Comparison of radiative heating.

Figure 22. — Fully-coupled, radiating flow solution with steady-state ablation of carbon-phenolic heatshield for high velocity entry.
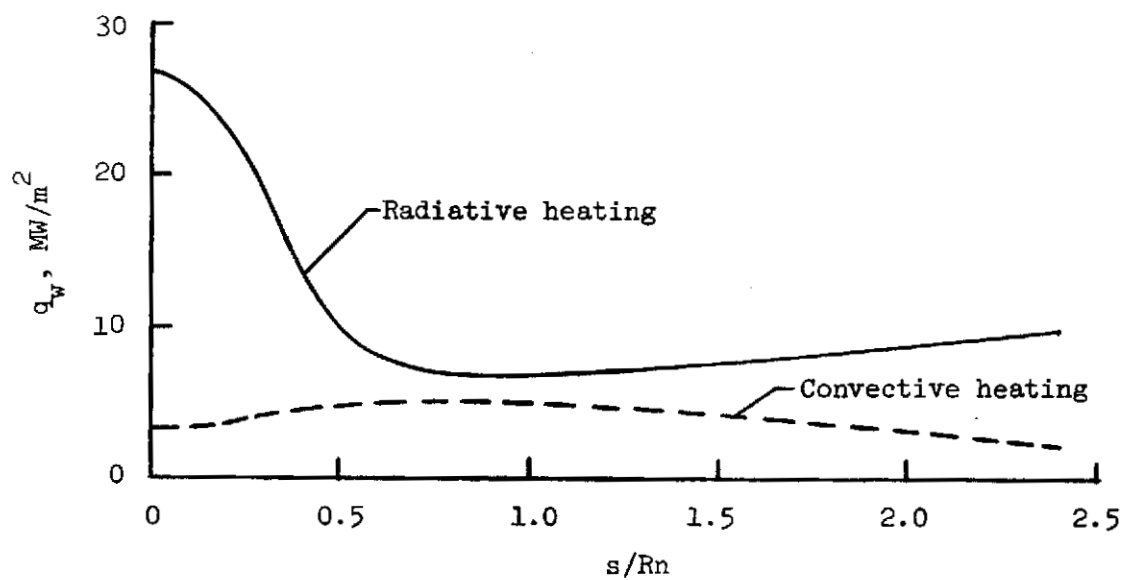
(c) Radiative and convective heating distribution.
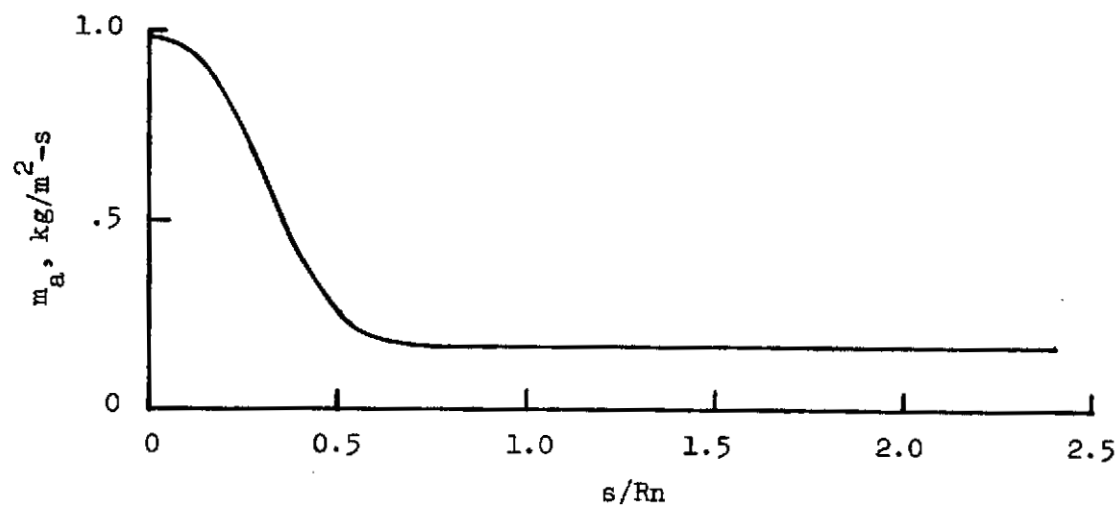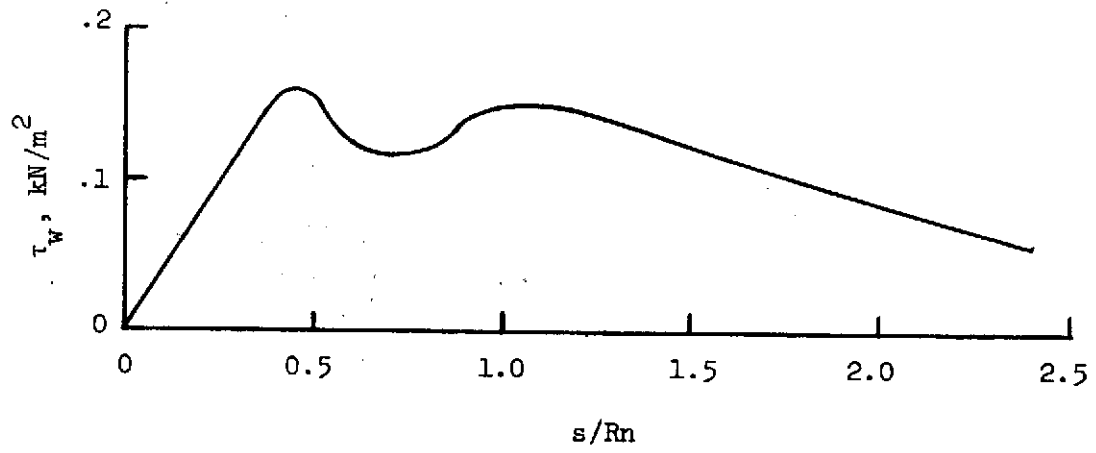
(d) Ablation rate distribution.

Figure 22. - Continued.

(e) Aerodynamic shear distribution.
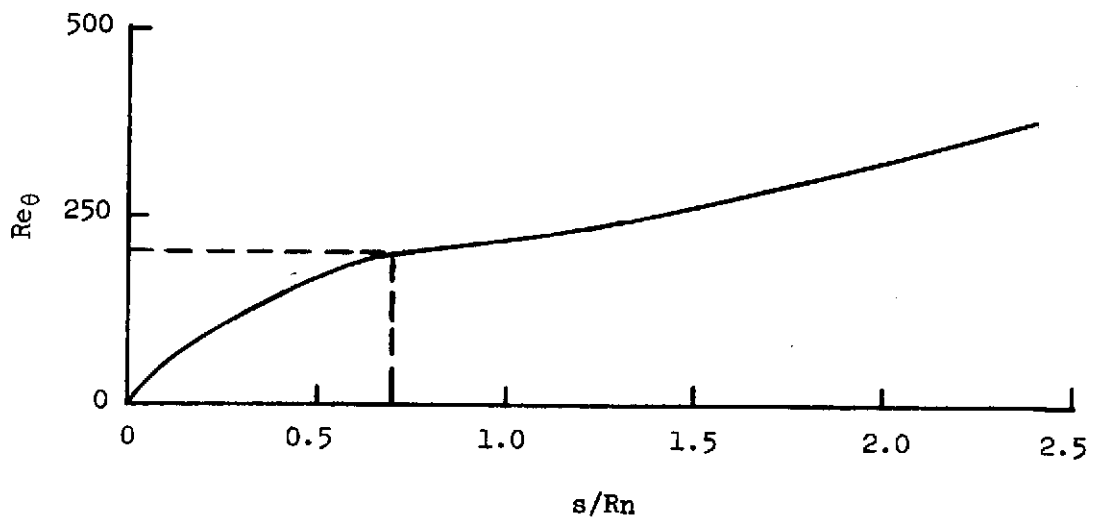
(f) Momentum thickness Reynolds number distribution.

Figure 22. - Continued.
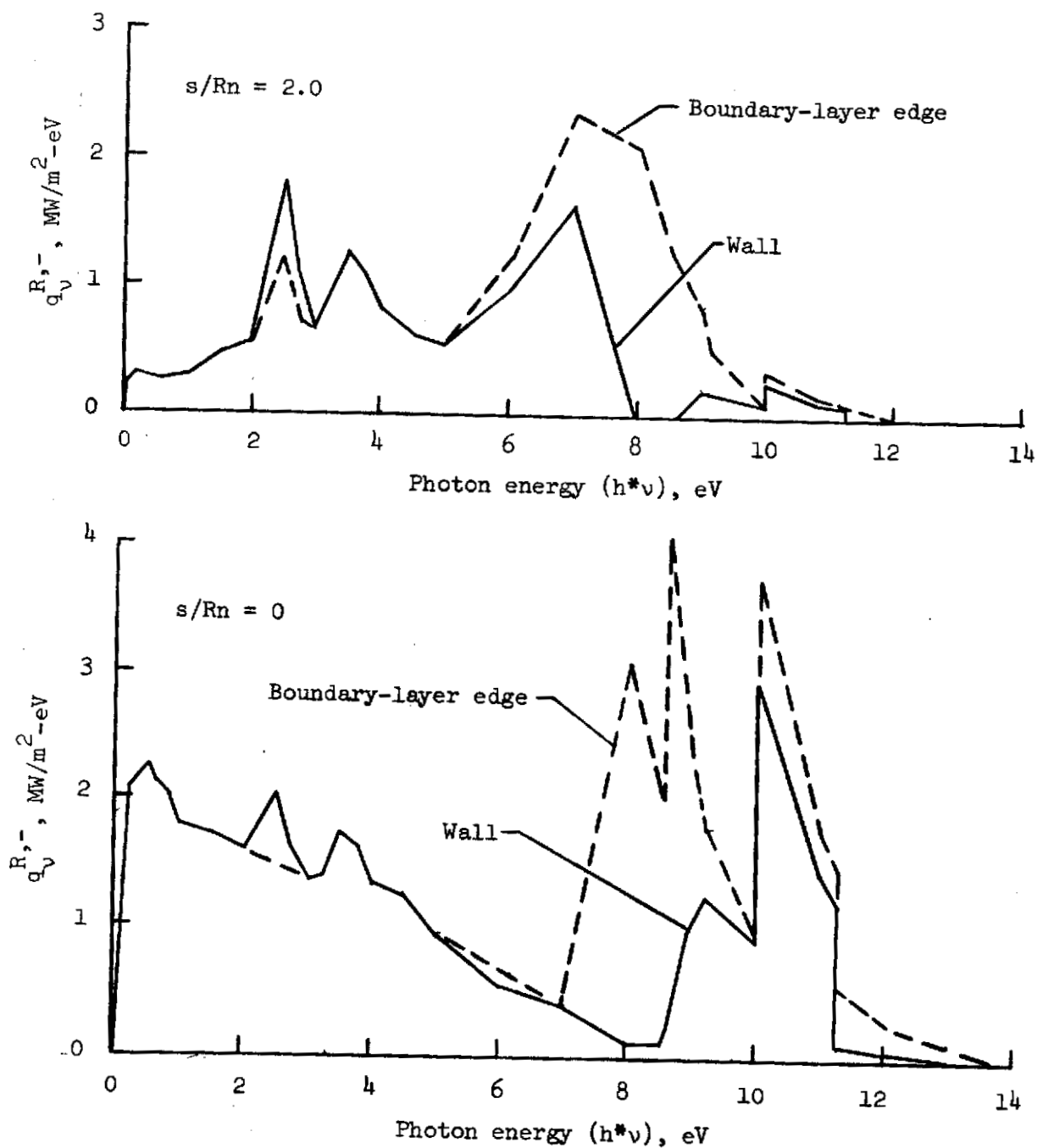
(g) Spectral distribution of radiative heating
toward the body due to continuum processes.

Figure 22. - Continued.
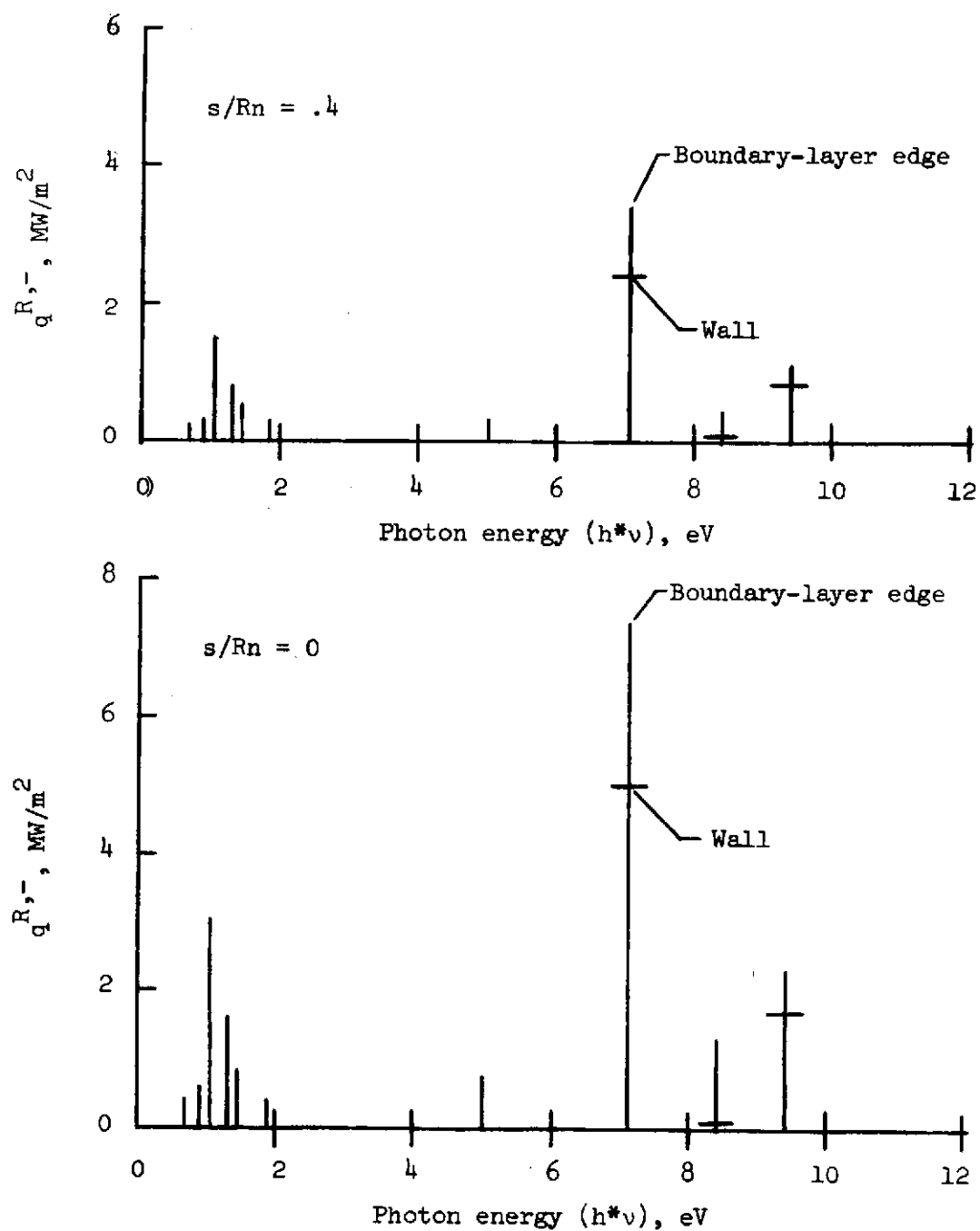
(h) Spectral distribution of radiative heating toward the body due to line processes.

Figure 22. - Concluded.

LIST OF REFERENCES

1. Hirschfelder, Joseph O.; Curtis, Charles F.; and Bird, Byron R. 1964. Molecular Theory of Gases and Liquids. John Wiley and Sons, Inc., New York.

2. Olstad, Walter B. 1971. Nongray Radiating Flow about Smooth Symmetric Bodies. AIAA J., vol. 9, no. 1: 122-130.

3. Callis, Linwood B. 1971. Coupled Nongray Radiating Flows about Long Blunt Bodies. AIAA J., vol. 9, no. 4: 553-559.

4. Page, William A. 1971. Aerodynamic Heating for Probe Vehicles Entering the Outer Planets. AAS Paper No. AAS-71-144.

5. Anderson, John D., Jr. 1969. An Engineering Survey of Radiating Shock Layers. AIAA J., vol. 7, no. 9: 1665-1675.

6. Moretti, Gino; and Abbett, Michael. 1966. A Time-Dependent Computational Method for Blunt Body Flows. AIAA J., vol. 4, no. 12: 2136-2141.

7. Callis, Linwood B. 1969. Solutions of Blunt-Body Stagnation Region Flows with Nongrey Emission and Absorption of Radiation by a Time-Asymptotic Technique. NASA Technical Report, NASA TR R-399.

8. Barlett, Eugene P.; and Kendall, Robert M. 1968. An Analysis of the Coupled Chemically Reacting Boundary Layer and Charring Ablator. Pt. III - Nonsimilar Solution of the Multicomponent Laminar Boundary Layer by an Integral Matrix Method. NASA Contractor Report, NASA CR-1062.

9. Nicolet, W. E. 1970. Advanced Methods for Calculating Radiation Transport in Ablation-Product Contaminated Boundary Layers. NASA Contractor Report, NASA CR-1656.

10. Walberg, Gerald D.; and Sullivan, Edward M. 1970. Ablative Heat Shields for Planetary Entries - A Technology Review. Presented at the ASTM/IES/AIAA Space Simulation Conference, Gaithersburg, Maryland.

11. Allen, H. Julian. 1964. Hypersonic Aerodynamic Problems of the Future, Chap. 1. In Wilbur C. Nelson (ed.). The High Temperature Aspects of Hypersonic Flow. Macmillan Co., New York.

12. Allen, H. Julian; Seiff, Alvin; and Winovich, Warren. 1963. NASA Technical Report, NASA TR R-185.

13. Penner, S. S.; and Olfe, Daniel B. 1968. Radiation and Reentry. Academic Press, New York.

14. Eggers, Alfred J., Jr. 1959. The Possibility of a Safe Landing, Chap. 13. In Howard S. Seifert (ed.), Space Technology. John Wiley and Sons, New York.

15. Lees, Lester. 1959. Recovery Dynamics - Heat Transfer at Hypersonic Speeds in a Planetary Atmosphere, Chap. 12. In Howard S. Seifert (ed.), Space Technology. John Wiley and Sons, New York.

16. Ehricke, Krafft A. 1959. Interplanetary Operations, Chap. 8. In Howard S. Seifert (ed.), Space Technology. John Wiley and Sons, New York.

17. Steg, L.; and Lew, H. 1964. Hypersonic Ablation, Chap. 32. In Wilbur C. Nelson (ed.), The High Temperature Aspects of Hypersonic Flow. Macmillan Co., New York.

18. Kendall, Robert M; Rindal, Roald A.; and Bartlett, Eugene P. 1967. A Multicomponent Boundary Layer Chemically Coupled to an Ablating Surface. AIAA J., vol. 5, no. 6: 1063-1071.

19. Garrett, Lloyd Bernard. 1971. An Implicit Finite Difference Solution to the Viscous Radiating Shock Layer with Strong Blowing. Unpublished Ph.D. Thesis, Department of Mechanical and Aerospace Engineering, North Carolina State University at Raleigh. University Microfilm, Ann Arbor, Michigan.

20. Kennet, H.; and Strack, S. L. 1961. Stagnation Point Radiative Heat Transfer. ARS J., vol. 31, no. 3: 370-372.

21. Koh, J. C. Y. 1962. Radiation From Nonisothermal Gases to the Stagnation Point of a Hypersonic Blunt Body. ARS J., vol. 32, no. 9: 1374-1377.

22. Hoshizaki, H.; and Lasher, L. E. 1968. Convective and Radiative Heat Transfer to an Ablating Body. AIAA J., vol. 6, no. 8: 1441-1449.

23. Chien, Kuei-Yuan. 1971. Application of the S_n Method to Spherically Symmetric Radiative-Transfer Problems. AIAA Paper No. 71-466.

24. Wilson, K. H. 1971. Evaluation of One-Dimensional Approximations for Radiative Transport in Blunt Body Shock Layers. LMSC N-EE-71-3, Lockheed Missiles and Space Co., Sunnyvale, California.

25. Boughner, Robert Eugene. 1969. Theoretical Predictions of Non-Gray Radiant Heat Transfer in High Temperature Nonisothermal CO_2-N_2 Mixtures. Unpublished Ph.D. Thesis, Mechanical Engineering Dept., Purdue University. University Microfilm, Ann Arbor, Michigan.

26. Olstad, Walter B. 1968. Blunt-Body Stagnation-Region Flow with Nongray Radiation Heat Transfer - A Singular Perturbation Solution. NASA Technical Report, NASA TR R-295.

27. Page, William A.; Compton, Dale L.; Borucki, William J.; and Cliffone, Donald L. 1968. Radiative Transport in Inviscid Nonradiabatic Stagnation-Region Shock Layers. AIAA Paper No. 68-784.

28. Smith, G. Louis; Suttles, John T.; Sullivan, Edward M.; and Graves, Randolph A., Jr. 1970. Viscous Radiating Flow Field on an Ablating Body. AIAA Paper No. 70-218.

29. Rigdon, W. S.; Dirling, R. B., Jr.; and Thomas, M. 1970. Stagnation Point Heat Transfer During Hypervelocity,Atmospheric Entry. NASA Contractor Report, NASA CR-1462.

30. Wilson, K. H. 1967. RATRAP - A Radiation Transport. Code. 6-77-67-12, Lockheed Missiles and Space Co., Sunnyvale, California.

31. Thomas, M. 1967. The Spectral Linear Absorption Coefficient of Gases - Computer Program SPECS (H 189). Douglas Report DAC-59135, McDonnell-Douglas Astronautics Co., Western Division, Santa Monica, California.

32. Nicolet, W. E. 1969. User's Manual for the Generalized Radiation Transfer Code (RAD/EQUIL). Aerotherm Report No. UM-69-9, Aerotherm Corp., Mountain View, California.

33. Suttles, John T. 1971. Comparison of the Radiative Flux Profiles and Spectral Detail from Three Detailed Nongrey Radiation Models at Conditions Representative of Hypervelocity Earth Entry. NASA Technical Memorandum, NASA TM X-2447.

34. Vincenti, Walter G.; and Kruger, Charles H., Jr. 1967. Introduction to Physical Gas Dynamics. John Wiley and Sons, New York.

35. Penner, S. S. 1959. Quantitative Molecular Spectroscopy and Gas Emmissivities. Addison-Wesley Publishing Co., Reading, Massachusetts.

36. Wilson, K. H.; and Grief, R. 1968. Radiation Transport in Atomic Plasmas. J. Quant. Spectry. Radiative Transfer, vol. 8, no. 4: 1061-1986.

37. Goulard, R. 1964. Fundamental Equations of Radiation Gas Dynamics, Chap. 27. In Wilbur C. Nelson (ed.), The High Temperature Aspects of Hypersonic Flow. Macmillan Co., New York.

38. Goulard, R.; and Goulard, M. 1960. One-Dimensional Energy Transfer in Radiant Media. Int. J. Heat Mass Transfer, vol. 1: 81-91.

39. Goulard, R.; Boughner, R. E.; Burns, R. K.; and Nelson, H. F. 1968. Radiating Flows During Entry into Planetary Atmospheres. IAF Paper No. RE70.

40. Howe, John T.; and Viegas, John R. 1963. Solutions of the Ionized Radiating Shock Layer, Including Reabsorption and Foreign Species Effects and Stagnation Region Heat Transfer. NASA Technical Report, NASA TR R-159.

41. Hoshizaki, H.; and Wilson, K. H. 1965. Viscous Radiating Shock Layer About a Blunt Body. AIAA J., vol. 3, no. 9: 1614-1622.

42. Hoshizaki, H.; and Wilson, K. H. 1967. Convective and Radiative Heat Transfer During Superorbital Entry. AIAA J., vol. 5, no. 1: 23-35.

43. Chin, Jin H. 1968. Radiation Transport for Stagnation Flows Including the Effect of Lines and Ablation Layer. AIAA Paper No. 68-664.

44. Wilson, K. H. 1970. Massive Blowing Effects on Viscous Radiating, Stagnation-Point Flow. AIAA Paper No. 70-203.

45. Burns, Raymond K.; and Oliver, Calvin C. 1968. Downstream Radiation Flux to Blunt Entry Vehicles. AIAA J., vol. 6, no. 12: 2452-2453.

46. Chou, Y. S. 1971. Locally Nonsimilar Solutions for Radiating Shock Layer about Smooth Axisymmetric Bodies. LMSC N-EE-71-2, Lockheed Missiles and Space Co., Sunnyvale, California.

47. Maslen, S. H. 1964. Inviscid Hypersonic Flow Past Smooth Symmetric Bodies. AIAA J., vol. 2, no. 6: 1055-1061.

48. Tauber, Michael E. 1969. Atmospheric Entry into Jupiter. J. Spacecraft, vol. 6, no. 10: 1103-1109.

49. Tauber, Michael E. 1971. Heat Protection for Atmospheric Entry into Saturn, Uranus, and Neptune. AAS Paper No. AAS-71-145.

50. Tauber, Michael E.; and Wakefield, Roy M. 1970. Heating Environment and Protection during Jupiter Entry. AIAA Paper No. 70-1324.

51. Perry, James C.; and Pasiuk, Lionel. 1966. A Comparison of Solutions to a Blunt Body Problem. AIAA J., vol. 4, no. 8: 1425-1426.

52. Barnwell, Richard W. 1971. A Time-Dependent Method for Calculating Supersonic Angle-of-Attack Flow about Axisymmetric Blunt Bodies with Sharp Shoulders and Smooth Nonaxisymmetric Blunt Bodies. NASA Technical Note, NASA TN D-6283.

53. Bohachevsky, Ihor O.; and Mates, Robert E. 1966. A Direct Method for Calculation of the Flow about an Axisymmetric Blunt Body at Angle of Attack. AIAA J., vol. 4, no. 5: 776-782.

54. VonNeumann, J.; and Richtmyer, R. D. 1950. A Method for the Numerical Calculation of Hydrodynamic Shocks. J. Appl. Phys., vol. 21: 232-237.

55. Lax, Peter D. 1954. Weak Solutions of Nonlinear Hyperbolic Equations and their Numerical Computation. Commun. Pure Appl. Math., vol. VII, no. 1: 159-193.

56. Lax, Peter D.; and Wendroff, Burton. 1964. Difference Schemes for Hyperbolic Equations with High Order of Accuracy. Commun. Pure Appl. Math, vol. XVII, no. 3: 381-398.

57. MacCormack, Robert W. 1969. The Effect of Viscosity in Hypervelocity Impact Cratering. AIAA Paper No. 69-354.

58. MacCormack, Robert W. 1970. Numerical Solution of the Interaction of a Shock Wave with a Laminar Boundary Layer. In Maurice Holt (ed.), Proceedings of the Second International Conference on Numerical Methods in Fluid Dynamics, 151-163. Springer-Verlag, New York.

59. Moretti, Gino; and Abbett, Michael. 1966. A Fast, Direct and Accurate Technique for the Blunt Body Problem. Technical Report No. 583, General Applied Science Laboratories, Westbury, N. Y.

60. Anderson, John D., Jr. 1970. Time-Dependent Solutions of Nonequilibrium Nozzle Flows - A Sequel. AIAA J., vol. 8, no. 12: 2280-2282.

61. National Academy of Sciences. 1970. Venus, Strategy for Exploration. Report of a Study by the Space Science Board. National Academy of Sciences, Washington, D. C.

62. Ames Research Center. 1972. Pioneer Venus. Report of a Study by the Science Steering Group. Ames Research Center, Moffett Field, California.

63. Ainsworth, J. E. 1970. Comprehensive Study of Venus by Means of a Low-Cost Entry-Probe and Orbiter Mission-Series. Report X-625-70-203, Goddard Space Flight Center, Greenbelt, Maryland.

64. Marcotte, Paul G. 1971. Planetary Explorer, Phase A Report and Universal Bus Description. Goddard Space Flight Center, Greenbelt, Maryland.

65. Jaworski, W.; and Nagler, R. G. 1970. A Parametric Analysis of Venus Entry Heat-Shield Requirements. Technical Report 32-1468, Jet Propulsion Laboratory, Pasadena, California.

66. Nagler, Robert G. 1970. A Systematic Review of Heat-Shield Technology for Extraterrestrial Atmospheric Entry. Technical Report 32-1436, Jet Propulsion Laboratory, Pasadena, California.

67. Norman, Herbert C.; and Hart, Paul M. 1968. Mission Influence on the Aerothermodynamic Environment for a Venus Entry Vehicle. AAS Paper No. 68-4-6.

68. Strauss, Eric L.; and Sparhawk, H. E. 1968. Ablative Heat Shields for Planetary Entry Vehicles. AAS Paper No. 68-8-5.

69. Spiegel, Joseph M.; Wolf, Fred; and Zeh, Dale W. 1968. Simulation of Venus Atmospheric Entry by Earth Re-Entry. AIAA Paper No. 68-1148.

70. Anon. 1968. Models of Venus Atmosphere (1968). NASA Special Publication, NASA SP-8011.

71. Deacon, H. J., Jr.; and Rumpel, W. F. 1971. Radiative Transfer Properties of a Shocked Venus Model Atmosphere. J. Spacecraft, vol. 8, no. 2: 177-182.

72. Livingston, F. R.; and Williard, J. 1971. Planetary Entry Body Heating Rate Measurements in Air and Venus Atmospheric Gas up to T=15,000 K. AIAA J., vol. 9, no. 3: 485-492.

73. Falanga, Ralph A.; and Sullivan, Edward M. 1970. An Inverse-Method Solution for Radiating, Nonadiabatic, Equilibrium Inviscid Flow over a Blunt Body. NASA Technical Report, NASA TN D-5907.

74. Hughes, William F.; and Gaylord, Eder W. 1964. Basic Equations of Engineering Science. Schaum Publishing Company, New York.

75. Isaacson, Eugene; and Keller, Herbert Bishop. 1966. Analysis of Numerical Methods. John Wiley and Sons, New York.

76. Inouye, Mamoru. 1965. Blunt Body Solutions for Spheres and Ellipsoids in Equilibrium Gas Mixtures. NASA Technical Note, NASA TN D-2780.

77. Graves, Randolph A., Jr. 1970. Diffusion Model Study in Chemically Reacting Air Couette Flow with Hydrogen Injection. NASA Technical Note, NASA TR R-349.

78. Kendall, Robert M.; and Bartlett, Eugene P. 1968. Nonsimilar Solution of the Multicomponent Laminar Boundary Layer by an Integral-Matrix Method. AIAA J., vol. 6, no. 6: 1089-1097.

79. Kendall, Robert M; Anderson, Larry W.; and Aungier, Ronald H. 1972. Nonsimilar Solution for Laminar and Turbulent Boundary-Layer Flows over Ablating Surfaces. AIAA J., vol. 10, no. 9: 1230-1236.

80. Kendall, Robert M. 1968. A General Approach to the Thermochemical Solution of Mixed Equilibrium-Nonequilibrium, Homogeneous or Heterogeneous Systems. Pt. V - An Analysis of the Coupled Chemically Reacting Boundary Layer and Charring Ablator. NASA Contractor Report, NASA CR-1064.

81. Bartlett, Eugene P.; Kendall, Robert M; and Rindal, Roald A. 1968. A Unified Approximation for Mixture Transport Properties for Multicomponent Boundary-Layer Applications. Pt. IV - An Analysis of the Coupled Chemically Reacting Boundary Layer and Charring Ablator. NASA Contractor Report, NASA CR-1063.

82. Grose, Ronald D.; and Kendall, Robert M. 1970. A Nonsimilar Solution for Laminar and Turbulent Boundary Layer Flows Including Entropy Layers and Transverse Curvature. NASA Contractor Report, NASA CR-73481.

83. Anderson, Larry W.; and Kendall, Robert M. 1970. A Nonsimilar Solution for Multicomponent Reacting Laminar and Turbulent Boundary Layer Flows Including Transverse Curvature. Technical Report No. AFWL-TR-69-106, Air Force Weapons Laboratory, Kirtland AFB, New Mexico.

84. Anderson, Larry W.; Bartlett, Eugene P.;and Kendall, Robert M. 1970. User's Manual - Volume I - Boundary Layer Integral Matrix Procedure (BLIMP). Technical Report No. AFWL-TR-69-114, Vol. I. Air Force Weapons Laboratory, Kirtland AFB, New Mexico.

85. Anderson, Larry W.; and Kendall, Robert M. 1970. User's Manual - Volume II - Boundary Layer Integral Matrix Procedure (BLIMP). Technical Report No. AFWL-TR-69-114, Vol. II. Air Force Weapons Laboratory, Kirtland AFB, New Mexico.

86. Anderson, Larry W.; and Morse, Howard L. 1971. User's Manual - Volume I - Boundary Layer Integral Matrix Procedure (BLIMP). Technical Report No. AFWL-TR-69-114. Vol. I (Supp.). Air Force Weapons Laboratory, Kirtland AFB, New Mexico.

87. Moyer, Carl B.; and Rindal, Roald A. 1968. Finite Difference Solution for the In-Depth Response of Charring Materials Considering Surface Chemical and Energy Balances. Pt. II - An Analysis of the Coupled Chemically Reacting Boundary Layer and Charring Ablator. NASA Contractor Report, NASA CR-1061.

88. Inouye, Mamoru; Rakich, John V.; and Lomax, Harvard. 1965. A Description of Numerical Methods and Computer Programs for Two-Dimensional and Axisymmetric Supersonic Flow Over Blunt-Nosed and Flared Bodies. NASA Technical Note, NASA TN D-2970.

89. Suttles, John T. 1969. A Method of Integral Relations Solution for Radiating, Nonadiabatic, Inviscid Flow over a Blunt Body. NASA Technical Note, NASA TN D-5480.

APPENDIX A

UNSTEADY CHARACTERISTICS SOLUTION

A quasi, one-dimensional unsteady characteristics solution is used for the shock points in the radiating, inviscid flow field solution. The present method for this solution is similar to the methods given by Callis (ref. 7) and by Moretti and Abbett (ref. 6). A brief development of the equations is given below and further details are available in the above mentioned reports.

In the analysis, the pertinent quantities considered are the normal component of the velocity and the Y-coordinate. Since the tangential velocity is unchanged across a shock wave, the tangential velocity is not considered a pertinent quantity and the S-momentum equation is neglected. Consequentially, the equations for mass, Y-momentum, and energy are considered as quasi, one-dimensional equations modified by forcing terms on the RHS of the equations. The forcing terms are the terms in the equations which do not contain derivatives, which contain derivatives with respect to the S-coordinate, and which contain the tangential velocity.

The mass equation (eq. 17) is written as

$$\rho_T^* + A\rho_Y^* + \frac{1}{\delta} v_Y = C_1 \tag{A1}$$

where the asterisk refers to the natural logarithm of ρ that is differentiated. The Y-momentum equation (eq. 19) is written as

$$v_T + Av_Y + \frac{1}{\rho\delta} p_Y = C_2 \tag{A2}$$

In the inviscid flow field analysis, the mass equation in terms of density and the energy equation in terms of enthalpy were combined to form a new equation in terms of pressure. This combined equation replaced the mass equation; however, in the characteristics development, the combined equation is used for the energy equation. Thus, the energy equation (eq. 30) is written as

$$p_T + Ap_Y + \frac{\rho P_3}{\delta} v_Y = C_3 \tag{A3}$$

The forcing terms are

$$C_1 = -\left(\frac{u}{\lambda} \rho_S^* - \frac{B}{\rho} u_Y + \frac{1}{\lambda} u_S + \frac{C}{\rho}\right) \tag{A4}$$

$$C_2 = -\left(\frac{u}{\lambda} v_S - E\right) \tag{A5}$$

$$C_3 = -\left[\frac{u}{\lambda} p_S + P_3 \left(\frac{\rho}{\lambda} u_S + C\right) - \frac{F^R}{P_1\rho} - P_3 Bu_Y\right] \tag{A6}$$

The forcing terms are considered as known quantities and the characteristics equations and the compatibility equations are solved for by standard procedure.

The differential relations for the variables ρ, p, and v of the independent variables Y and T are

$$\rho_T^* \, dT + \rho_Y^* \, dY = d\rho^* \tag{A7}$$

$$v_T \, dT + v_Y \, dY = dv \tag{A8}$$

$$p_T \, dT + p_Y \, dY = dp \tag{A9}$$

The equations A1 to A3 and A7 to A9 written in matrix form are

$$
\begin{vmatrix} \rho_T^* \\ \rho_Y^* \\ v_T \\ v_Y \\ p_T \\ p_Y \end{vmatrix} \quad x \quad
\begin{vmatrix}
dT & dY & 0 & 0 & 0 & 0 \\
0 & 0 & dT & dY & 0 & 0 \\
0 & 0 & 0 & 0 & dT & dY \\
1 & A & 0 & \frac{1}{\delta} & 0 & 0 \\
0 & 0 & v_T & A & 0 & \frac{1}{\rho\delta} \\
0 & 0 & 0 & \frac{\rho P_3}{\delta} & 1 & A
\end{vmatrix}
=
\begin{vmatrix} d\rho^* \\ dv \\ dp \\ C_1 \\ C_2 \\ C_3 \end{vmatrix}
\qquad (A10)
$$

The characteristics equations are found by setting the associated co-efficient determinant equal to zero.

$$
\begin{vmatrix}
dT & dY & 0 & 0 & 0 & 0 \\
0 & 0 & dT & dY & 0 & 0 \\
0 & 0 & 0 & 0 & dT & dY \\
1 & A & 0 & \frac{1}{\delta} & 0 & 0 \\
0 & 0 & v_T & A & 0 & \frac{1}{\rho\delta} \\
0 & 0 & 0 & \frac{\rho P_3}{\delta} & 1 & A
\end{vmatrix}
= 0
\qquad (A11)
$$

The solution of equation A11 is a cubic in dY/dT and the characteristics equations are

$$
\frac{dY}{dT} = A
\qquad (A12)
$$

$$
\frac{dY}{dT} = A \pm \frac{\sqrt{P_3}}{\delta}
\qquad (A13)
$$

Equation A12 is a trivial solution and is neglected. The compatibility equations are found by substituting a column of the associated coefficient determinant by the RHS of equation A10 and the determinant is set

equal to zero.

$$\begin{vmatrix} dT & dY & 0 & dp* & 0 & 0 \\ 0 & 0 & dT & dv & 0 & 0 \\ 0 & 0 & 0 & dp & dT & dY \\ 1 & A & 0 & C_1 & 0 & 0 \\ 0 & 0 & v_T & C_2 & 0 & \frac{1}{\rho\delta} \\ 0 & 0 & 0 & C_3 & 1 & A \end{vmatrix} = 0 \qquad (A14)$$

The solution of equation A14 is

$$\left(\frac{dY}{dT} - A\right)\frac{dv}{dT} + \frac{1}{\rho\delta}\frac{dp}{dT} = \left(\frac{dY}{dT} - A\right)C_2 + \frac{C_3}{\rho\delta} \qquad (A15)$$

and substituting for $\frac{dY}{dT}$ from equation A13, the compatibility equations

are

$$\frac{dv}{dT} \pm \frac{1}{\rho\sqrt{P_3}}\frac{dp}{dT} = C_2 \pm \frac{C_3}{\rho\sqrt{P_3}} \qquad (A16)$$

From equations A13 and A16, the right running characteristic is used in

the solution for the shock points and the equations are

$$\frac{dY}{dT} = A + \frac{\sqrt{P_3}}{\delta} \qquad (A17)$$

$$\frac{dv}{dT} + \frac{1}{\rho\sqrt{P_3}}\frac{dp}{dT} = C_2 + \frac{C_3}{\rho\sqrt{P_3}} \qquad (A18)$$

APPENDIX B

STAGNATION-POINT SOLUTION FOR RADIATING,

INVISCID FLOW FIELD

The equations for the radiating, inviscid flow field around an axisymmetric blunt body are reduced so that they are applicable for only a stagnation-point solution. Note, the equations presented in this section are not used for the stagnation point of the complete body solution but are used in a separate program when only a stagnation-point solution is required.

The following conditions, from symmetry of the body, exist at the stagnation line.

$$\left.\begin{array}{lll} u = 0 & v_S = 0 & \beta = 0 \\[2mm] u_Y = 0 & h_S = 0 & \theta = \pi/2 \\[2mm] \rho_S = 0 & p_S = 0 & K = 1 \end{array}\right\} \tag{B1}$$

With these conditions, the equations for mass, Y-momentum, and energy (eqs. 30, 19, and 20) become

mass:

$$p_T = -\left[Ap_Y + P_3\left(\frac{2\rho}{\lambda}u_S + \frac{\rho}{\lambda}v_Y + \frac{2\rho v}{\lambda}\right) - \frac{F^R}{P_1\rho} \right] \tag{B2}$$

Y-momentum:

$$v_T = -\left(Av_Y + \frac{1}{\rho\delta}p_Y\right) \tag{B3}$$

energy:

$$h_T = -\left(Ah_Y - \frac{1}{\rho}p_T - \frac{A}{\rho}p_Y + \frac{F^R}{\rho}\right) \tag{B4}$$

The equation for S-momentum (eq. 18) is degenerate at the stagnation line; but, by differentiation of equation 18 with respect to S and applying the symmetry conditions the following equation is obtained

S-momentum:

$$u_{ST} = -\left(Au_{SY} + \frac{1}{\lambda} u_S^2 + \frac{v}{\lambda} u_S + \frac{1}{\rho\lambda} p_{SS}\right) \qquad (B5)$$

The S derivative of the tangential velocity, u_S, is used in the stagnation-point solution rather than the tangential velocity. The parameters in the equations are

$$A = \frac{v}{\delta} - \frac{Y}{\delta} \delta_T \qquad (B6)$$

$$F^R = \frac{1}{\delta} q_Y^R + \frac{2}{\lambda} q^R \qquad (B7)$$

$$\lambda = 1 + \delta Y \qquad (B8)$$

In order to solve the set of equation an expression is needed for p_{SS}. An approximation for this parameter is taken from Newtonian theory

$$p_{SS} = -2 \qquad (B9)$$

The characteristic equation and the compatibility equation for the unsteady characteristic solution at the shock location become

$$\frac{dY}{dT} = A + \frac{\sqrt{P_3}}{\delta} \qquad (B10)$$

$$\frac{dv}{dT} + \frac{1}{\rho\sqrt{P_3}} \frac{dp}{dT} = \frac{C_3}{\rho\sqrt{P_3}} \qquad (B11)$$

where

$$C_3 = -\left[\frac{2\rho}{\lambda} P_3 (u_S + v) - \frac{F^R}{P_1\rho}\right] \qquad (B12)$$

The equations presented in this section are non-dimensionalized by the expression given in equation 14. Indeterminate terms were evaluated by the L'Hospital rule.

APPENDIX C

COMPUTER PROGRAM FOR RADIATING, INVISCID

FLOW FIELD SOLUTION

A program listing and a description of inputs are given for the computer program developed for the radiating, inviscid flow field solution. The program is written in FORTRAN IV language for CDC 6000 series computers. In order to run the program, all variables have to be initially set to zero by means external to the program. A system subroutine called by a SETCORE control card is used for this external initialization for the computer system used in the present study.

The inputs and printed outputs for a sample case are also given. The sample case is a radiating solution for a .97 CO_2 - .03 N_2 (by volume) gas composition. The body shape is a hemispherical nose, .3048 meter radius, with a 60° half-angle, conical afterbody.

PROGRAM LISTING

```
PROGRAM SUTFLO(INPUT,OUTPUT,TAPE5=INPUT,TAPE6=OUTPUT,PUNCH)          1
REAL R                                                               2
COMMON/SUT2/  VY(15),SY(15),KY(15),THETA(15),BETA(15),RB(15),       3
1DELTA(15),DELTAY(15),XB(15)                                         4
COMMON/SUT3/  RHO(15,11),U(15,11),VY(15,11),PY(15,11),HY(15,11),    5
1T(15,11),SX(15,11),PA(15,11),VAM(15,11),PY(15,11),HM(15,11),       6
2TAU(15,11)                                                          7
COMMON/SUT4/ RHOB(15,11),UB(15,11),VBY(15,11),PB(15,11),            8
1HB(15,11),OELS1(15),OELS2(15),OELS3(15),OELS4(15),OELS5(15),       9
2DELY1(11),DELY2(11),DELY3(11),DELY4(11),DELY5(11)                  10
DIMENSION DELY6(11),DELY7(11),DELY8(1)                              11
DIMENSION DELS6(15),DELS7(15),DELS8(15)                             12
COMMON/SUT5/ RHOF(15,11),UY(15,11),VY(15,11),PY(15,11),HY(15,11)    13
COMMON/SUT6/  OP(15,11),OH(15,11),OH(15,11),QD(15,11)               14
1             ,QHY(15),QHC(15),QHL(15)                              15
COMMON/SUT7/ VELZ(15),SA2Z(15)                                      16
COMMON/RAD/AHY(90),AHVL(25),SKEP(45)      ,DELTR,GPSE(56),PP(900),  17
1FHV(29),FHVC(50),FHMM(25),FMMP(25),FEME(11),FTP(11),FL1,FL2,FLG,   18
2FLG1,GAMP(300),GEE(56),X2(16),R2(16),HAFS,HBLP,NO(300),MTC,MICH(1) 19
3),MIHVC,MHV,NUI(29),NY,PRE(11),TPE(11),VOL(11),XRQ,HQ(7,1),YDELT   20
4,VY(11),CASE(9),TMSH(50),THSHL(25),YW                              21
COMMON/LINE/HVL(500),R1,R2,YLCH(11),YLCP(11),HMH(16,11),HAF,TA(9)   22
1,N1,XHOL(300),GUP(900)                                             23
COMMON/RADCOR/FRE(8,11),TT(11),YMW(11),HM(11),SP(1,11,0)            24
1     ,THETR,SY1,SP1,SR1,HSS                                        25
COMMON/INTCOR/XR(20),N,M                                            26
COMMON/EQFCOR/FSC1( 62),FSC0(33),FSC2(24),FSC1(16),15,              27
1       16C2(62) ,FSC3( 249)  ,FPSC3(169),                         28
2       1SC3(4),FSC4,(SC4,FSC5( 44),1SP2,PAMDA(31),PAMD6(51)       29
3       ,ESP,MICK,FSC0(3),KIN,KOUT,KKR(20),FSC1 01                 30
COMMON/SUTCOM/TKS,PKS,HKS,HEPKS,STPKS,HMKS,CPFKS,CSPKS,ALPKS,       31
1BETHKS,GAMKS,VEL,SA2,KYS                                           32
DIMENSION GF(11)                                                    33
DIMENSION KOS(10)                                                   34
DIMENSION CC(3,5)                                                   35
DIMENSION CH(3,3)                                                   36
DIMENSION IKSU(6),ITCU(5),IRCU(5)                                   37
DIMENSION YAUM(15)                                                  38
NAMELIST/NAME1/ VF,PF,RHOF,HF,RM,KYS,KSE,Y                          39
NAMELIST/NAME2/ TIPRAC,IKSC,CC1,CCF,ICC,IKSF,IOUTH,IOUTP,ITC,IRC,   40
1IKSU,ITCU,IRCU,NCTS,LSC,CC1                                        41
READ(5,940) KOS(1),KOS(2),KOS(3),KOS(4),KOS(5),CASE                42
940 FORMAT(5I1,15A5)                                                43
VDRAD = KOS(5)                                                      44
VDEL = KOS(2)                                                       45
READ(5,NAME1)                                                       46
READ(5,911) (THETA(KS),SEKS,RB(KS),XB(KS),K(KS), KS=1,KSE)          47
911 FORMAT(5P15,7)                                                  48
LS = -1                                                             49
LSC = 1500                                                          50
CCS = .0005                                                         51
TIPRAC = .8                                                         52
IKSC=500                                                            53
CC1 = .0001                                                         54
CCF = .95                                                           55
ICC = 50                                                            56
IKSF = 1500                                                         57
IOUTH = 100                                                         58
IOUTP = 99                                                          59
ITC = 50                                                            60
IRC = 100                                                           61
IKSU(1) = 100                                                       62
IKSU(2) = 200                                                       63
IKSU(3) = 400                                                       64
IKSU(4) = 600                                                       65
IKSU(5) = 800                                                       66
ITCU(1) =ITC                                                        67
ITCU(2) =ITC                                                        68
ITCU(3) =ITC                                                        69
ITCU(4) =ITC                                                        70
ITCU(5) =ITC                                                        71
IRCU(1) = IRC                                                       72
IRCU(2) = IRC                                                       73
IRCU(3) = IRC                                                       74
IRCU(4) = IRC                                                       75
IRCU(5) = IPC                                                       76
NCTS = 0                                                            77
IF(KOS(1).EQ.0)  GO TO 4                                            78
READ(5,NAME2)                                                       79
4 CONTINUE                                                          80
IKSUE6 = IKSF                                                       81
READ(5,9905) IKS,TAUT,TT1,TR1,YO,Y9                                 82
IF(IKS.EQ.0)  GO TO 9901                                            83
READ(5,9906) (BETA(KS), KS=1,KSF)                                   84
READ(5,9906) (DELTA(KS), KS=1,KSE)                                  85
READ(5,9906) (DELTAT(KS), KS=1,KSE)                                 86
DO 9945  KS=1,KSE                                                   87
DO 9945  KY=1,KYS                                                   88
READ(5,9906) PY(KS,KY),RHO(KS,KY),H(KS,KY),U(KS,KY),V(KS,KY),       89
1VA(KS,KY),PY(KS,KY),OD(KS,KY)                                      90
9945 CONTINUE                                                       91
9905 FORMAT(I5,E15.8,I5,I5,E15.6,(5)                                92
9906 FORMAT(5P15.8)                                                 93
IF(VDEL.EQ.0) GO TO 9991                                            94
CL = ABS(DELTATE(1)                                                 95
IF(IKS.GE.LSC.AND.CL.LE.CCS) LS=0                                   96
9991 CONTINUE                                                       97
KYS1=KYS-1                                                          98
KSE1 = KSE-1                                                        99
KYC = KYS/2                                                        100
XCC1 = 3.*KSE                                                      101
IOUT = IOUTP                                                       102
TC = 0                                                             103
CALL INPUT                                                        104
IF(NORAD.EQ.0)  GO TO 11                                           105
NY = KYS                                                          106
NI = NY                                                           107
NIC = NY                                                          108
DO 83  I=1,NY                                                     109
NICH(I) = I                                                       110
YY(I) = Y(I)                                                      111
83 CONTINUE                                                        112
DO 3  I=1,20                                                      113
XR(I) = 0                                                         114
3 CONTINUE                                                        115
KR(1) = 1                                                         116
KR(3) = KOS(4)                                                    117
KR(4) = KOS(5)                                                    118
KR(7) = I                                                         119
KR(11) = 1                                                       120
KR(12) = 1                                                       121
CALL RADIN                                                       122
11 CONTINUE                                                      123
SY1 = VF/.3048                                                   124
SP1 = PF/101325.                                                 125

SR1 = RHOF/16.018463                                            126
HSS = HF*(1.8/4184.)                                            127
WRITE(6,900) CASE                                               128
900 FORMAT(1H1,//ZX,*CASE= *,15A5)                              129
WRITE(6,995) VF,RHOF,PF,HF,RM                                   130
995 FORMAT(//ZX,*FREESTREAM PARAMETERS*,5X,*VELOCITY = *,E11.4,1X, 131
1HR/S*,/2X,*DENSITY = *,E11.4,1X,*KG/M3*,/2X,*PRESSURE = *,   132
2E11.4,1X,*N/M2*,/2X,*ENTHALPY = *,E11.4,1X,*J/KG*,/2X,*NOSE RADI  133
3US = *,E11.4,1X,*M*,)                                         134
WRITE(6,956)                                                    135
956 FORMAT(//2X,*BODY SHAPE, NONDIMENSIONAL BY NOSE RADIUS*,    136
1           /10X,**S*,6X,*S*,9X,*XBOD*,7X,*YBOD*,             137
2YX,*THETA*,7X,*R*)                                            138
WRITE(6,957) (KS,S(KS),XB(KS),PB(KS),THETA(KS),R(KS), KS=1,KSE) 139
957 FORMAT(10X,I2,5X,F8.6,5X,F8.6,3X,F8.6,3X,F8.6,3X,F8.6)      140
DO 5  I=1,10                                                    141
KOS(I)=0                                                        142
5 CONTINUE                                                       143
KOS(1)=2                                                        144
KOS(2)=L                                                        145
KOS(5)=KOS(2)                                                   146
DELS1(1) = S(2)-S(1)                                            147
DELS2(1) = DELS1(1)                                             148
DELS3(1) = 1.                                                   149
DELS4(1) = 1.                                                   150
DELS5(1) = 1./DELS1(1)                                          151
DELS1(KSE) = S(KSE)-S(KSE1)                                     152
DELS2(KSE) = DELS1(KSE)                                         153
DELS3(KSE) = 1.                                                 154
DELS4(KSE) = 1.                                                 155
DELS5(KSE) = 1./DELS1(KSE)                                      156
DO 81  KS=2,KSE1                                                157
DELS1(KS) = S(KS+1)-S(KS)                                       158
DELS2(KS) = S(KS)-S(KS-1)                                       159
DELS3(KS) = (DELS1(KS)*DELS1(1))/(DELS2(KS)*DELS2(KS))          160
DELS4(KS) = DELS3(KS)-1.                                        161
DELS5(KS) = 1./(DELS1(KS)+(DELS3(KS)*DELS2(KS)))                162
81 CONTINUE                                                      163
DELY1(1) = Y(2)-Y(1)                                            164
DELY2(1) = DELY1(1)                                             165
DELY3(1) = 1.                                                   166
DELY4(1) = 1.                                                   167
DELY5(1) = 1./DELY1(1)                                          168
DELY1(KYS) = Y(KYS)-Y(KYS1)                                     169
DELY2(KYS) = DELY1(KYS)                                         170
DELY3(KYS) = 1.                                                 171
DELY4(KYS) = 1.                                                 172
DELY5(KYS) = 1./DELY1(KYS)                                      173
DO 60  KY=2,KYS1                                                174
DELY1(KY) = Y(KY+1)-Y(KY)                                       175
DELY2(KY) = Y(KY)-Y(KY-1)                                       176
DELY3(KY) = (DELY1(KY)*DELY1(1))/(DELY2(KY)*DELY2(KY))          177
DELY4(KY) = DELY3(KY)-1.                                        178
DELY5(KY) = 1./(DELY1(KY)+(DELY3(KY)*DELY2(KY)))                179
60 CONTINUE                                                      180
DO 86  KY=1,KYS                                                 181
IF(KY.GE.KYS1) GO TO 87                                         182
G1 = DELY1(KY) + DELY1(KY+1)                                    183
DELY6(KY) = (G1*G1)/(DELY1(KY)*DELY1(KY))                       184
DELY7(KY) = DELY6(KY) - 1.                                      185
DELY8(KY) = 1./(G1-(DELY6(KY)*DELY1(KY)))                       186
GO TO 86                                                       187
87 CONTINUE                                                      188
G1 = DELY2(KY) + DELY2(KY-1)                                    189
DELY6(KY) = (G1*G1)/(DELY2(KY)*DELY2(KY))                       190
DELY7(KY) = DELY6(KY) - 1.                                      191
DELY8(KY) = 1./(G1-(DELY6(KY)*DELY2(KY)))                       192
86 CONTINUE                                                      193
DO 89  KS=1,KSE                                                 194
IF(KS.GT.2) GO TO 88                                            195
G1 = DELS1(KS) + DELS1(KS-1)                                    196
DELS6(KS) = (G1*G1)/(DELS1(KS)*DELS1(KS))                       197
DELS7(KS) = DELS6(KS) - 1.                                      198
DELS8(KS) = 1./(G1-(DELS6(KS)*DELS1(KS)))                       199
GO TO 89                                                       200
88 CONTINUE                                                      201
G1 = DELS2(KS) + DELS2(KS-1)                                    202
DELS6(KS) = (G1*G1)/(DELS2(KS)*DELS2(KS))                       203
DELS7(KS) = DELS6(KS) - 1.                                      204
DELS8(KS) = 1./(G1-(DELS6(KS)*DELS2(KS)))                       205
89 CONTINUE                                                      206
IF(IKS.NE.0) GO TO 9992                                         207
IT1 = 0                                                        208
IP1 = 0                                                        209
IHS = 0.                                                       210
TAUT = 0.                                                      211
J9 = 1                                                         212
DO 13  KS=1,KSE                                                213
KOS(5)=2                                                       214
IF(KS-1) 14,14,15                                              215
14 THETR=0.                                                     216
BETA(1) = 0.                                                   217
TT(1)=18000.                                                   218
PPES(1)=1.0                                                    219
CALL EQUIL(KQS,1,PRES(1))                                      220
VEL2(1) = VEL*.3048/VF                                         221
SA2Z(1) = SA2                                                  222
RHO(1,KYS) = (RHRES*16.018463)/RHOF                            223
DELTA(1) = 0.78/RHO(1,KYS)                                     224
TO=TRS                                                         225
H(1,KYS) = (HEPKS*4184.)/(VF*VF)                               226
P(1,KYS) = (PKS*101325.)/(RHOF*VF*VF)                          227
VEL(KYS) = -VEL*COS(SA2)*.3048/VF                              228
U(1,KYS) = 0.                                                  229
HCL(1) = HE(1,KYS) + (VY(1,KYS)*VY(1,KYS)/2.)                  230
P(1,1) = P(1,KYS) + (RHO(1,KYS)*V(1,KYS)*V(1,KYS)/2.)          231
U(1,1) = 0.                                                    232
VY(1,1) = 0.                                                   233
GO TO 16                                                       234
15 TT(1) = 1.80*KS                                              235
PPES(1) =PKS                                                   236
THETR = 1.5707963 - THETA(KS)                                  237
CALL EQUIL(KQS,1,PRES(1))                                      238
VEL2(KS) = VEL*.3048/VF                                        239
SA2Z(KS) = SA2                                                 240
H(KS,KYS) = (HEPKS*4184.)/(VF*VF)                              241
P(KS,KYS) = (PKS*101325.)/(RHOF*VF*VF)                         242
V(KS,KYS) = -VEL*COS(SA2)*.3048/VF                             243
U(KS,KYS) = VEL*SIN(SA2)*.3048/VF                              244
P(KS,1) = P(1,1)*COS(THETR)*COS(THETR)                         245
HE(KS,1) = H(KS-1,1)*(P(KS,1)/P(KS-1,1))**GAMRA)               246
U(KS,1) = SQRT(2.0*(HE(1,1)-H(KS,1)))                          247
V(KS,1) = 0.                                                   248
16 CONTINUE                                                      249
KOS(9)= 0                                                      250
```

```
      I = 0
      DO 249  KY=KYS1,KYS                                            521
      I = I+1                                                        522
      G1 = 1.0 + (K(I)*V(KYJ*DELTAC(I)                               523
      G4 = (VEL,KY)- (Y(KY)*DELTAC(I))/DELTAC(I)                     524
      CHC1,I) = G4 + (VA(I),KY)/DELTAC(I)                            525
      CHC2,I) = 1.7(RHO(1,KYI*VA(1,KY)                               526
      S2 = U(2,KY)/S(2)                                             527
      CH(5,I) = -(I2.*RHO(I),KY)*VA(I,KY)/VA(I,KY)/G1)*IS2* (K(I)*VI, 528
      (KY)))  + (00(I,KY)/(P(I(,KY)*RHO(1,KY))                       529
      CHC3,I) + CH(5,I)*CHC2,I)                                      530
  249 CONTINUE                                                       531
  239 CONTINUE                                                       532
      JSTOP = JSTOP + 1                                              533
      IF(JSTOP.GT.21) GO TO 470                                      534
      GO TO 475                                                      535
  470 KS = 1                                                         536
  471 WRITE(6,495) KS,(KS,JSTOP                                      537
  495 FORMAT(1H1,//////LOX,*SHOCK PROPERTIES DID NOT CONVERGE IN 25 ITE 538
     1RATIONS*,///13X,*BODY LOCATION =*,F3,3X,*TIME ITERATIONS =*,I4, 539
     23X,*SHOCK ITERATIONS =*,I5)                                    540
      CALL OUTPUT(IKS,TAUT,KSE,KYS)                                  541
      STOP                                                           542
  475 CONTINUE                                                       543
      DELTAG = DELTA(I) + ((CG6*DELTAT(I))*.5*TAUM)                  544
      IF(JSTOP.EQ.11  GO TO 240                                      545
      SY1 = (1.+ DELTAT(I))*(VF/.3048)                               546
      (QS(5) = 0.                                                    547
      THETR = 1                                                      548
      TT(1) = T(1,KYS)*TO*1.8                                        549
      PRES(1) = (P(1,KYS)*RHOF*VF*VF)/101325.                        550
      CALL EQUIL(KQS,1,PRES(1))                                      551
      VFL2(I) = VEL*.3048/VF                                         552
      SA22(I) = SA2                                                  553
      CG2 = -(VEL*.3048/VF) + DELTAT(I)                              554
      CG1 = (RHRKS*16.018463)/RHOF                                   555
      CG3 = (PKS*101325.)/(RHOF*VF*VF)                               556
      CG4 = (H(PKS*46186.1/(VF*VF)                                   557
  240 CONTINUE                                                       558
      G1 = 1.0 + (K(KS)*DELTAG                                       559
      CH(1,3) = (CG2-DELTAT(I)*VA(1,KYS))/DELTAG                     560
      CH(2,3) = 1./(CG1*VA(1,KYS)                                    561
      CH(5,3) = -((2.0*CG1*VA(1,KYS)*VA(1,KYS)/G1)*(S2*(K(1)*CG2))   562
     1* (00(I,KYS)/(P(I(1,KYS)*CG1)                                  563
      CH(3,3) = CH(5,3)*CH(2,3)                                      564
      SY1 = (41.0-V(KYS)))*(I2./TAUM)- CH(1,3)-CH(1,1))* (V(KYS)*    565
     1(CH(1,2)-CH(1,1))                                              566
      SY2 = (2.*(1.0-V(KYS))/TAUM) + CH(1,2) - CH(1,1)               567
      SY1 = SY1/SY2                                                  568
      SY2 = (SY1-V(KYS))/(1.0-V(KYS))                                569
      C4 = VF(,KYS)+(SY2*VI(,KYS)-VF(,KYS))                          570
      C5 = PI(,KYS)+(SY2*(PI(,KYS)-PI(,KYS))                         571
      G6 = (CH(2,3)*CH(2,1)+(SY2*(CH(2,3)-CH(2,1)))/2.               572
      C1 = (CH(3,3)*CH(3,1)+(SY2*(CH(3,3)-CH(3,1)))/2.               573
      C9 = C4 + (C1*TAUM)- (C6*(CG3-C5)                              574
      C10 = ABS((CG2-C9)/CG2)                                        575
      IF(C10-.0001) 236,256,235                                      576
  235 CONTINUE                                                       577
      IF(JSTOP.GT.1)  GO TO 234                                      578
      ERR2 = CG2 - C9                                                579
      DTAT2 = DELTAT(I)                                              580
      DELTAT(I) = 1.2*DELTAT(I)                                      581
      IF(DELTAT(I).EQ.0.) GO TO 238                                  582
      GO TO 239                                                      583
  238 DELTAT(I) = -.002                                              584
      GO TO 239                                                      585
  236 CONTINUE                                                       586
      ERR1 = ERR2                                                    587
      DTAT1 = DTAT2                                                  588
      ERR2 = CG2 - C9                                                589
      DTAT2 = DELTAT(I)                                              590
      DELTAT(I) = DTAT2 - ((ERR2*(DTAT2-DTAT1))/(ERR2-ERR1))         591
      GO TO 239                                                      592
  236 DELTR(I) = DELTAG                                              593
      RHOR(I,KYS) = CG1                                              594
      UR(I,KYS) = 0.                                                 595
      VB(I,KYS) = CG2                                                596
      PB(I,KYS) = CG5                                                597
      HB(I,KYS) = C64                                                598
      DO 350  KS=2,KSE                                               599
      JSTOP = 0                                                      600
      TAUM = TAUNS(KS)                                               601
      CG5 = DELTA(KS)                                                602
      CG6 = DELTAT(KS)                                               603
      G2 =(1.0 + (K(KS)*DELTA(KS))*TAN(THETA(KS))                    604
      I = 0                                                          605
      DO 349  KY=KYS1,KYS                                            606
      I = I+1                                                        607
      IF(KS.EQ.KSE)  GO TO 2200                                      608
      S2 = (U(KS*1,KY)+(DELS4(KS)*U(KS,KY)-(DELS3(KS)*U(KS-1,KY))*   609
     1DELS5(KS)                                                      610
      S3 = (V(KS*1,KY)+(DELS4(KS)*V(KS,KY)-(DELS3(KS)*V(KS-1,KY))*   611
     1DELS5(KS)                                                      612
      S4 = (P(KS*1,KY)+(DELS4(KS)*P(KS,KY)-(DELS3(KS)*P(KS-1,KY))*   613
     1DELS5(KS)                                                      614
      GO TO 2201                                                     615
 2200 S2=(-(DELST(KSE)*U(KSE,KY) +(DELS6(KSE)*U(KSE),KY)) -U(KSE-2,KY 616
     1)*DELSB(KSE)                                                   617
      S3=(-(DELST(KSE)*V(KSE,KY) +(DELS6(KSE)*V(KSE),KY) -V(KSE-2,KY 618
     1)*DELSB(KSE)                                                   619
      S4=(-(DELST(KSE)*P(KSE,KY) +(DELS6(KSE)*P(KSE),KY) -P(KSE-2,KY 620
     1)*DELSB(KSE)                                                   621
 2201 CONTINUE                                                       622
      IF(KY.EQ.KYS)  GO TO 2210                                      623
      S2 = (U(KS,KY+1)+(DELY6(KY)*U(KS,KY)-(DELY3(KY)*U(KS,KY-1))*   624
     1DELY5(KY)                                                      625
      GO TO 2211                                                     626
 2210 S2=(-(DELY7(KY)*U(KS,KYS) +(DELY6(KY)*U(KS,KYS))  -U(KS,KYS-2)  627
     1)*DELY8(KY)                                                    628
 2211 CONTINUE                                                       629
      G1 = 1.0 + (K(KS)*V(KY)*DELTA(KS)                              630
      R = RB(KS) + (V(KY)*DELTAT(KS)*COS(THETA(KS))                  631
      G3 = (Y(KY)*G2)/G1                                             632
      G4 = (V(KS,KY)- (Y(KY)*DELTA(KS))- (U(KS,KY)*G3))/DELTA(KS)    633
      G5 = (Y(KY)*DELTAT(KS))/DELTA(KS)                              634
      G6 = (RHO(KS,KY)*U(KS,KY)*SIN(THETA(KS))/R) + (RHO(KS,KY)*V(KY 635
     1(K(KS)/G1)*COS(THETA(KS))/(Y(KY)                              636
      G8 = K(KS)*U(KS,KY)*U(KS,KY)/G1                                637
      CHC1,I) = G4 + (VA(KS,KY)/DELTA(KS))                          638
      CHC2,I) = 1./(RHO(KS,KY)*V(KS,KY)                             639
      G3 = -(U(KS,KY)*G3)/G1)*G8                                    640
      G7 = -(U(KS,KY)*S4/G1) -(VA(KS,KY)*VA(KS,KY)*(RHO(KS,KY)*S2/G1 641
     1*G6)) +(00(KS,KY)/(P(KS,KY)*RHO(KS,KY))) + (VA(KS,KY)*VA(KS,KY 642
     2(G5*Y2)                                                       643
      CH(3,3) = G3 + (G7*CH(2,I))                                    644
  349 CONTINUE                                                       645
  339 CONTINUE                                                       646
      JSTOP = JSTOP +1                                               647
      IF(JSTOP.GT.26) GO TO 471                                      648
      DELTAG = DELTA(KS) + (((CG6*DELTAT(KS))*.5*TAUM)               649
      G1 = 1.0 + (K(KS)*DELTAG                                       650
      IF(KS.GT.2) GO TO 460                                          651
      S1 = (DELTAG-DELTA(I))*(2./S(2))                               652
      GO TO 461                                                      653
  460 S1 = (-(DELST(KS)*DELTAG) +(DELS6(KS)*DELTA(KS-1)) -DELTA(KS-2)* 654
                                                                     655
```

```
      IDELSB(KS)                                                     656
  461 BETAR(KS) = ATAN(S1/G1)                                        656
      SVI = 1. + I2.*DELTAT(KS)*SIN(THETA(KS)) + (DELTA(KS)*         657
     IDELTAT(KS)(                                                    658
      SVI = SQRT(SVI)*VF/.3048                                       659
      GAMMA = (DELTAT(KS)*COS(THETA(KS))/(1.+DELTAT(KS)*SIN          660
     ITHETA(KS)(                                                     661
      THETR = 1.5707963 -THETA(KS)-BETA(KS)- ATAN(GAMMA)             662
      KQS(5) = 1                                                     663
      TT(1) = T(KS,KYS)*TO*1.8                                       664
      PRES(1) = P(KS,KYS)*RHOF*VF*VF/101325.                         665
      CALL EQUIL(KQS,1,PRES(1))                                      666
      VEL2(KS) = VEL*.3048/VF                                        667
      SA22(KS) = SA2                                                 668
      GAMMA = SA2 + BETA(KS)                                         669
      CG2 = -(VEL*COS(GAMMA)*.3048/VF) + DELTAT(KS)                  670
      CG1 = VEL*SIN(GAMMA)*.3048/VF                                  671
      CG3 = RHRKS*16.018463/RHOF                                     672
      CG3 = (PKS*101325.)/(RHOF*VF*VF)                               673
      CG4 = (H(PKS*46186.1/(VF*VF)                                   674
      R = RB(KS) + (DELTAG*COS(THETA(KS))                            675
      G3 = TAN(BETA(KS))                                             676
      G4 = (CG2 -DELTAT(KS))- (CG7*CG3))/DELTAG                      677
      G5 = CG1*G3/DELTAG                                             678
      G6 = (CG1*COS(THETA(KS))/R) + (CG1*CG2*((K(KS)/G1)+(           679
     1COS(THETA(KS)))/R))                                            680
      G8 = K(KS)*CG3*CG7/G1                                          681
      CHC1,5) = G4 + (VA(KS,KYS)/DELTAG)                             682
      CHC2,5) = 1./(CG1*VA(KS,KYS)                                   683
      G3 = -(CG7*G3/G1)*G8                                           684
      G7 = (CG3*G4/G1) - (VA(KS,KYS)*VA(KS,KYS)*((CG1*S2/G1)+G6)) +  685
     1(00(KS,KYS)/(VA(KS,KYS)*G1)) + (VA(KS,KYS)*VA(KS,KYS)*G5*Y2)   686
      CH(5,3) = G3 + (G7*CH(2,3))                                    687
      SY1 = ((1.0-V(KYS)))*((2./TAUM)-CH(1,3)-CH(1,1)))+ (V(KYS)*    688
     1(CH(1,2)-CH(1,1)))                                             689
      SY2 = (2.0*(1.0-V(KYS))/TAUM) + CH(1,2) -CH(1,1)               690
      SY1 = SY1/SY2                                                  691
      SY2 = (SY1-V(KYS))/(1.0-V(KYS))                                692
      C4 = V(KS,KYS)+(SY2*(V(KS,KYS)-V(KS,KYS))                      693
      C5 = P(KS,KYS)+(SY2*(P(KS,KYS)-P(KS,KYS))                      694
      G6 = (CH(2,3)+ CH(2,1)+ (SY2*(CH(2,3)-CH(2,1)))/2.             695
      C1 = (CH(3,3)+CH(3,1)+(SY2*(CH(3,3)-CH(3,1)))/2.               696
      C9 = C4 + (C1*TAUM)- (C6*(CG3-C5))                             697
      C10 = ABS((CG2-C9)/CG2)                                        698
      IF(C10-.0001) 336,356,335                                      699
  336 CONTINUE                                                       700
      IF(JSTOP.GT.1)  GO TO 334                                      701
      ERR2 = CG2 - C9                                                702
      DTAT2 = DELTAT(KS)                                             703
      DELTAT(KS) = 1.2*DELTAT(KS)                                    704
      IF(DELTAT(KS).EQ.0.) GO TO 338                                 705
      GO TO 339                                                      706
  338 DELTAT(KS) = -.002                                             707
      GO TO 339                                                      708
  334 CONTINUE                                                       709
      ERR1 = ERR2                                                    710
      DTAT1 = DTAT2                                                  711
      ERR2 = CG2 - C9                                                712
      DTAT2 = DELTAT(KS)                                             713
      DELTAT(KS) = DTAT2 - ((ERR2*(DTAT2-DTAT1))/(ERR2-ERR1))        714
      GO TO 339                                                      715
  336 DELTA(KS) = DELTAG                                             716
      RHOR(KS,KYS) = CG1                                             717
      UR(KS,KYS) = CG7                                               718
      VB(KS,KYS) = CG2                                               719
      PB(KS,KYS) = CG5                                               720
      HB(KS,KYS) = C64                                               721
  350 CONTINUE                                                       722
      C1 = ABS(DELTAT(I)(                                            723
      IF((KS.GE.LSC.AND.C1.LE.CC5)  LS=0                             724
      GO TO 4500                                                     725
 4500 CONTINUE                                                       726
      DELTA(KS) = 0.                                                 727
      KQS(5) = 1                                                     728
      SY1 = VF/.3048                                                 729
      THETR = 0.                                                     730
      TT(1) = T(1,KYS)*TO*1.8                                        731
      PRES(1) = P(1,KYS)*RHOF*VF*VF/101325.                          732
      CALL EQUIL(KQS,1,PRES(1))                                      733
      VEL2(I) = VEL*.3048/VF                                         734
      SA22(I) = SA2                                                  735
      VB(1,KYS) = -VEL2(I)                                           736
      UB(1,KYS) = 0.                                                 737
      RHOR(1,KYS) = RHRKS*16.018463/RHOF                             738
      PB(1,KYS) = (PKS*101325.)/(RHOF*VF*VF)                         739
      HB(1,KYS) = (H(PKS*46186.3/(VF*VF)                             740
 4400 CONTINUE                                                       741
      DO 107  KS=2,KSE                                               742
      C2 = RB(KS) + (DELTA(KS)*COS(THETA(KS)))                       743
      SF(I) = 0.                                                     744
      C5 = RB(KS)*RHO(KS,1)*U(KS,1)                                  745
      DO 106  KY=2,KYS                                               746
      R = RB(KS) + (Y(KY)*(C2-RB(KS))                                747
      C4 = R*RHO(KS,KY)*U(KS,KY)                                     748
      SF(KY) = ((C4*C3)*.9*DELY2(KY)) + SF(KY-1)                     749
      C3 = C4                                                        750
  106 CONTINUE                                                       751
      DELTA(KS) = 0.                                                 752
      C5 = (SF(KYS)-(RB(KS)*COS(THETA(KS))))*2.                      753
      DELTA(KS) = RB(KS)*RHO(KS)/C5                                  754
  107 CONTINUE                                                       755
      DO 108  KS=2,KSE                                               756
      G1 = 1.0 + (K(KS)*DELTA(KS))                                   757
      S1 =(-(DELST(KS)*DELTA(KS)*G1) +(DELS6(KS)*DELTA(KS)-((        758
     1-(DELTA(KS)*-2)*DELTA(KS)(                                     759
      DELTA(KS) = ATAN(S1/G1)                                        760
  108 BETA(KS) = ATAN(S2/G1?                                         761
      G1 = 1.0 + (K(KSE)*DELTA(KS))                                  762
      S1 =(-(DELST(KSE)*DELTA(KS)*G1) +(DELS6(KSE)*DELTA(KSE-1))     763
     1-DELTA(KSE-2))*DELS8(KSE)                                      764
      BETA(KSE) = ATAN(S1/G1?                                        765
      DO 109  KS=2,KSE                                               766
      KQS(5) = 1                                                     767
      SY1 = VF/.3048                                                 768
      THETR = 1.5707963 - THETA(KS) - BETA(KS)                       769
      TT(1) = T(KS,KY)*TO*1.8                                        770
      PRES(1) = P(KS,KY)*RHOF*VF*VF/101325.                          771
      CALL EQUIL(KQS,1,PRES(1))                                      772
      VEL2(KS) = VEL*.3048/VF                                        773
      SA22(KS) = SA2                                                 774
      GAMMA = SA2 + BETA(KS)                                         775
      V(KS,KYS) = -VEL2(KS)*SIN(GAMMA)                               776
      U(KS,KYS) = VEL2(KS)*SIN(GAMMA)                                777
      RHOR(KS,KYS) = RHRKS*16.018463/RHOF                            778
      PB(KS,KYS) = (PKS*101325.)/(RHOF*VF*VF)                        779
      HB(KS,KYS) = (H(PKS*46186.1/(VF*VF)                            780
  109 CONTINUE                                                       781
      IF(LS.EQ.21 GO TO 4500                                         782
      LS = +1                                                        783
                                                                     784
```

```
      WRITE(6,4130)
4130  FORMAT(1H1,////////////20X,10H**********,///20X,*PROGRAM WAS SWITCHE
     1D TO MASS BALANCE OPTION*,///20X,10H**********)
      CALL OUTPUT(KS,TAUY,RSF,KYS)
4500  CONTINUE
      DO 103   KS=1,KSE
      TAUR = TAUMS(KS)
      DO 103   KY=1,KYS
```

```
9940 CONTINUE
     STOP
1901 CONTINUE
     GO TO 1
 381 CONTINUE
     IKS = -IKS
     CALL OUTPUT(IKS,TAUT,KSE,KYS)
     STOP
     END
C
     SUBROUTINE OUTPUT(IKS,TAUT,KSF,KYS)
     REAL X
     COMMON/SUT2/  YE(1),S(15),K1(15),THETA(15),BETA(15),RB(15),
    1OELTA(15),DELTA(15),RBI(15)
     COMMON/SUT3/  RHOI(15,11),UI(15,11),VI(15,11),PI(15,11),HE(15,11),
    1TE(15,11),SX(15,11),VR(15,11),VAM(15,11),PI(15,11),WM(15,11),
    2TAU(15,11)
     COMMON/SUT4/ RHOB(15,11),UB(15,11),VB(15,11),PB(15,11),
    1HB(15,11),DELS1(15),DELS2(15),OELS3(15),DELS4(15),DELS5(15),
    2DELV1(11),DELY2(11),DELY3(11),DELY4(11),DELYS(11)
     COMMON/SUT5/ RHOF(15,11),UF(15,11),VF(15,11),PT(15,11),HF(15,11)
     COMMON/SUT6/   QM(15,11),QM(15,11),QM(15,11),QOE(15,11)
    1            QNTE(15),QMC(15),QML(15)
     COMMON/SUT7/ VEL2(15),SA22(15)
     DIMENSION SF(11)
     I = 1
     J = KYS
     IF(IKS) 14,13,13
  13 CONTINUE
     WRITE(6,1050) IKS,TAUT
1050 FORMAT(1H1,//2X,*NON-CONVERGED OUTPUT*,10X,*ITERATIONS =*,14,10X,
    1*TIME =*,E10.3,///)
     GO TO 15
  14 CONTINUE
     WRITE(6,1051) IKS,TAUT
1051 FORMAT(1H1,//2X,*CONVERGED OUTPUT*,10X,*ITERATIONS =*,15,10X,
    1*TIME =*,E10.3,///)
  15 CONTINUE
     DO 1300   KS=1,KSE
     C1=RB(KS)-(DELTA(KS) * SINE(THETA(KS)))
     C2=RB(KS) + (DELTA(KS) * COSE(THETA(KS)))
     IF(IKS.EQ.1) GO TO 1296
     S(1) = 0.
     C3 = RB(KS)*RHO(KS,1)*U(KS,1)
     DO 1295 KY=2,KYS
     W = RB(KS) + (Y(KY)*(C2-RB(KS)))
     C6 = RHO(KS,KY)*U(KS,+Y)
     SF(KY) = ((C4+C3)*.5*DELY2(KY)) + SF(KY-1)
     C3 = C4
1295 CONTINUE
     AMF = ((C2*C2)/2.*DELTA(KS))
     C5 = (SF(KYS) -(RB(KS)*COSE(THETA(KS))))*2.
     DELTAM = RB(KS)*RB(KS)/C5
     GO TO 1297
1296 CONTINUE
     DO 1298 KY=1,KYS
1298 SF(KY) = 0.
     AMF = 0.
     DELTAM = DELTA(1)
1297 CONTINUE
     WRITE(6,971) KS,S(KS),THETA(KS),DFTA(KS),DELTA(KS),DELTAT(KS),
    1RB(KS),RBE(KS),C1,C2,QNTE(KS),QMC(KS),QML(KS)
 971 FORMAT(//2X,*BODY STATION *,17,*X,*C =*,F8.4,*5X,*THETA =*,F8.4,*9X
    1,*BETA =*,F8.4,5X,*DELTA =*,F8.4,*5X,*DELTAT =*,F10.5,//2X,22X,
    2*XBOD =*,F8.4,5X,*YBOD =*,F8.4,5X,*RSHOK =*,F8.4,5X,*YSHOK =*,
    3F8.4,//2X,22X,*QUF =*,F10.5,5X,*QMC =*,F10.5,5X,*QML =*,E10.3,//)
     WRITE(6,972) VEL2(KS),SA22(KS)
 972 FORMAT(2X,22X,*VFL2 =*,F10.5,5X,*SA2 =*,E10.3,//)
     WRITE(6,1101) (KY, KY=1,J)
     WRITE(6,1102)      (Y(KY)    ,KY=I,J)
     WRITE(6,1103)      (P(KS,KY)  ,KY=I,J)
     WRITE(6,1104)      (RHO(KS,KY) ,KY=I,J)
     WRITE(6,1105)      (HE(KS,KY)  ,KY=I,J)
     WRITE(6,1106)      (U(KS,KY)   ,KY=I,J)
     WRITE(6,1107)      (VI(KS,KY)  ,KY=I,J)
     WRITE(6,1108)      (VAM(KS,KY) ,KY=I,J)
     WRITE(6,1109)      (T(KS,KY)   ,KY=I,J)
     WRITE(6,1110)      (WM(KS,KY)  ,KY=I,J)
     WRITE(6,1111)      (SX(KS,KY)  ,KY=I,J)
     WRITE(6,1112)      (VA(KS,KY)  ,KY=I,J)
     WRITE(6,1113)      (P(KS,KY)   ,KY=I,J)
     WRITE(6,1114)      (OP(KS,KY)  ,KY=I,J)
     WRITE(6,1115)      (QM(KS,KY)  ,KY=I,J)
     WRITE(6,1116)      (QM(KS,KY)  ,KY=I,J)
     WRITE(6,1117)      (QO(KS,KY)  ,KY=I,J)
     WRITE(6,1131)      (RM(KS,KY)  ,KY=I,J)
     WRITE(6,1132)      (U(KS,KY)   ,KY=I,J)
     WRITE(6,1133)      (VT(KS,KY)  ,KY=I,J)
     WRITE(6,1134)      (FF(KS,KY)  ,KY=I,J)
     WRITE(6,1135)      (NT(KS,KY)  ,KY=I,J)
     WRITE(6,1151)      (TAU(KS,KY),KY=I,J)
     WRITE(6,1137)      (SF(KY), KY=1,J)
1137 FORMAT(2X,THSF   ,11(E10.3,1X))
     WRITE(6,974) ARF,SF(KYS),DELTAM
 976 FORMAT(//15X,*MASS BALANCE*,5X,*FREESTREAM =*,E10.5,5X,*SHOCK LAYE
    1R =*,E10.5,5X,*DELTA MASS =*,F10.3)
1101 FORMAT(2X,IONKY   ,11(17, 9X))
1102 FORMAT(2X,THY     ,11(E10.3,1X))
1103 FORMAT(2X,THP     ,11(E10.3,1X))
1104 FORMAT(2X,THRHO   ,11(E10.3,1X))
1105 FORMAT(2X,THH     ,11(E10.3,1X))
1106 FORMAT(2X,THU     ,11(E10.3,1X))
1107 FORMAT(2X,THV     ,11(E10.3,1X))
1108 FORMAT(2X,THM     ,11(E10.3,1X))
1109 FORMAT(2X,THE     ,11(E10.3,1X))
1110 FORMAT(2X,THWM    ,11(E10.3,1X))
1111 FORMAT(2X,THSX    ,11(E10.3,1X))
1112 FORMAT(2X,THVA    ,11(E10.3,1X))
1113 FORMAT(2X,THP1    ,11(E10.3,1X))
1114 FORMAT(2X,THQP    ,11(E10.3,1X))
1115 FORMAT(2X,THQM    ,11(E10.3,1X))
1116 FORMAT(2X,THQN    ,11(E10.3,1X))
1117 FORMAT(2X,THQD    ,11(E10.3,1X))
1131 FORMAT(2X,THRHOT  ,11(E10.3,1X))
1132 FORMAT(2X,THUT    ,11(E10.3,1X))
1133 FORMAT(2X,THVT    ,11(E10.3,1X))
1134 FORMAT(2X,THFF    ,11(E10.3,1X))
1135 FORMAT(2X,THNT    ,11(E10.3,1X))
1151 FORMAT(2X,THTAU   ,11(E10.3,1X))
1300 CONTINUE
     RETURN
     END
C
C    . . . . . . . . . . . . . . . . . . . . . . . . . . .
C
C    SUBROUTINES FOR CHEMICAL EQUILIBRIUM CALCULATIONS AND SOLUTION OF
C    RANKINE-HUGONIOT EQUATIONS.
C
C    . . . . . . . . . . . . . . . . . . . . . . . . . . .
C
     SUBROUTINE INPUT
     INTEGER FAMDA,FAMOB,CHAR,BLANK
     INTEGER AMDA,AMOB
     COMMON/RADCON/FRE(31,11),ETT(11),VMN(11),HM(11),SPI1,(1,8)
    1            ,THETA,SV1,SP1,SB1,HS
```

```
     COMMON /EQPCOM/ RB(31,21),        IFC(31),ATA(8),ATB(8),WAT(8),
    1  KAT(8),TM(8),IS,KM(LD),CAM(8),P,RC(31,21),
    2  RD(31,2),RE(31,21),RP(31,2),Y,TK(8,8),TO(8,8),
    3  TU(1,2),VM(31),VNU(31,8),L2,L3,TPF,KM2,MCM,MCV,
    4  WM,WTM(31),YI(31),YN(31),3SPZ,FAMDA(31),FAMOB(31),
    5  ISP,M,WT31,KIN,KOUT,KAM(20),ATC(8)
     COMMON /EQTCOM/ SIP,HIP,EL,ENL,FLIQ,CPF,IRE,IER,AA,FT3,IN,TL,TT,
    1  MODE,MMELT,SMELT,TMAX,TMIN,MELT,SUMM,SUM,I884),
    2  E8(8),ERL(8),A(14,14),B(16),EPC(32),ALPC(8),FMU(8),
    3  GAMH(8),GAMF(8),JC,MG,     CPG,DY(31),CP(31),
    4  HI(31),SB(31),IC(31),WLNK(31),EI(31),TTMIN,TTMAX,
    5  FNUS(8),US,WSS,ISPO,BC(8),ALMK(8),BY(8),IBC(8),
    6  SI,RRJ,SVA,SVB,SVC,SVO,SUMC,    RV,CMF,EP,IFCJC,
    7  NTG,WTL,JJ(8),BE(8),LEF(8)
     COMMON/SUTCOM/TKS,PKS,WPKS,HEPKS,SEPKS,RHRKS,CPPKS,CSPKS,ALFKS,
    1BETMKS,GAMKS,VEL,SA2,KYS
     DIMENSION CI,JI 3L,1),TF(1)
     DIMENSION JICP(512)
     DIMENSION UM(  8, 8)
     EQUIVALENCE(TU( 32),TF),(VMU,CIJ)
     DIMENSION SORCE(8), FM(8), JAT(7), ALPT(7), TAU(8,8),
    1CC( 8),KPMAIZI,RAI21
     DIMENSION         IC( 8),LIM( 8, 8)
 301 FORMAT(13)
 302 FORMAT(2E9.6,4,2P6.0.11)
3020 FORMAT(1XE12.5,F10.4,Y2/1X6E12.5,F10.4,F11.4,I2)
 303 FORMAT(1H  /IH )
 304 FORMAT(13,344,F9.3,7E8.3)
 306 FORMAT(7(F1.0,1)),AZ,9A4)
     DATA CHAR,BLANK/4HCHAR,4H    /
     KIN = 5
     KOUT = 6
     KP(3)=2
     KP(2) = 1
3047 M=0
     P=1.
     VENT=P*1.F-6
     PINT=ALOG(VENT)
     KPRG=1.
     READ(KIN,301) IS
     JATLB1=0
     IX=1
     IF (IS-10) 311,311,399
 311 READ(KIN,304) (KAT(J), ATA(J), ATB(J), ATC(J), WAT(J), ITK(J,1),
    1  I=1,7),J=1,IS)
     DO 59   I=1,IS
     DO 59   J=1,15
     SPI1,I,J)=ABS(TK(J,I))
  59 CONTINUE
     DO 45   J=1,IS
     TK(J,I)=0.
  45 CONTINUE
     DO 327 K=1,7
     VA=0.
     DO 322 J=1,IS
     IF(KAT(J)-90) 3111,325,3111
3111 IF(TK(J,K)) 324,322,325
 324 VA=VA-TK(J,K)
     TK(J,K)=-TK(J,K)/WAT(J)
     GO TO 322
 325 VA=VA+TK(J,K)
 322 CONTINUE
     IF(VA) 326,327,326
 326 DO 325 J=1,IS
 325 TK(J,I)=TK(J,K)/VA
 327 CONTINUE
     IX=ISC1
     IF(KP(3)) 399,399,394
 334 IF(MX)=0.
     AAA=0.
     X=0
     II=ISP
     J=1
 342 READ(KIN,306)(ALPT(K),JAT(K),K=1,7),SORCE,AMDA,AMOB
     IF(ALPT(8)) 344,399,344
 344 DO 345 K=1,IS
 345 C(K)=0.
     DO 349 J=1,7
     IF(JAT(I)) 346,349,346
 346 DO 347 K=1,IS
     IF(JAT(I)-KAT(K)) 347,348,347
 347 CONTINUE
     READ(KIN,301)
     GO TO 342
 348 C(K)=ALPT(J)
 349 CONTINUE
     NT=0.
     L=1
     LAMK=0
     DO 388 I=1,IS
     IF(C(I)) 387,388,387
 387 LAMK=LAMK+L
     NT=NT+C(I) * WAT(I)
 388 CONTINUE
     L=L*L
     IF(J-IS) 360,360,349
 360 JM=J-1
     DO 3601 L=1,IS
3601 C(J,L,J)=C(L)
     LARK(J) = LAMK
     IF (J-M) 320,320,313
 313 DO 314 L=1,JM
     IM=I+M
     UGM=C(IM,)
     UMEL,J)=0.
     IF(UGM) 353,314,353
 353 DO 395 I=1,L
 395 UM(I,J)=UM(I,J)-UME(I,L)*UGH
     DO 396 I=IM,IS
 396 UM(I,J)=0.
 394 C(I)=C(I)-TAU(I,L)*UGH
 314 UM(J,L)=0.
 320 DO 316 I=1,IS
     IF(ABS(C(I))-.001)316,316,317
 316 TAU(I,J)=C(I)-.001*316,316,317
     DO 396 I=1,JM
 906 VMU(I,II)=-UM(I,J)
     DO 397 I=2,IS
 397 VM(I,II)=0.
     LAMK(II)=LAMK
     GO TO 370
 517 IM(J)=F
     JM(J,J)=1.
     DO 398 L=1,J
 398 UM(L,J)=UM(L,J)/C(I)
     DO 320 L=1,IS
 328 TAU(L,J)=C(L)/C(I)
     YC=VINT
     KM=J
     J=J+1
     IF(J-IS) 372,372,329
 329 DO 330 L=2,IS
     JM=ISP-L
     JM=IM+L
     IM=IM(JM+1)
     DO 330 K=1,JM
     UGM=TAU(IM,K)
     DO 390 I=1,IS
```

```
 35      DYI=X(I+2)
         IF (IFC(I)+1) 275,40,40
 40      IF (IFC(I)) 205,95,250
 45      IF (IFC(I)+2) 75,50,50
 50      IF (IFC(I)) 70,55,85
 55      VA=E(I)-TC(I)*X(I)
         DO 65 J=1,I5
         IF (I8C(J)) 60,60,65
 60      VA=VA+VNU(I,J)*X(J+2)
 65      CONTINUE
         DYI=VA
         GO TO 95
 70      IF (IK-IRF) 75,80,15
 75      DYI=0.
         GO TO 275
 80      IFC(I)=1
         DYI=X(IR)
         GO TO 230
 85      L=L+1
         IF (L-IER) 90,85,90
 90      DYI=X(I)
         GO TO 230
 95      WFG=DWTG+VNE(I)*DYI*WTME(I)
         IF (IPI(I)) 100,105,100
100      IF (IK-M) 105,145,105
105      IF (VNE(I)-DUMP) 110,140,140
110      IF (MOE) 195,195,115
115      IF (DYI) 120,275,125
120      IF (VNE(I)/RUMP-.9999995-CNF*DYI) 275,275,130
125      IF (BUMP/VN(I)-1.-CNF*DYI) 135,275,275
130      CNF=(VNI(I)/RUMP-.99999995)/DYI
         GO TO 275
135      CNF=(BUMP/VNI(I)-1.)/DYI
         GO TO 275
140      IF (MOE) 175,175,150
145      X1=X1+1
         M=IR+ME(I)
150      IF (DYI) 155,275,160
155      IF (DYI*CNF+.990) 165,275,275
160      IF (DYI*CNF-9.) 275,275,170
165      CNF=-.990/DYI
         GO TO 275
170      CNF=9./DYI
         GO TO 275
175      IF (DYI*CNF-2.303) 180,190,190
180      IF (DYI*CNF+6.909) 185,275,275
185      CNF=-6.909/DYI
         GO TO 275
190      CNF=2.303/DYI
         GO TO 275
195      IF (Y(I)-BULP+ABS(DYI)*CNF) 275,200,200
200      CNF=(Y(I)-BULP)/ABS(DYI)
         GO TO 275
C        NON-PRESENT BASE
209      CONTINUE
215      IF (Y(I)+CNF*DYI-0.1) 275,220,220
220      DUM1=(.1-Y(I))/DYI
         IF (DUM1-.0001) 275,275,275
225      CNF=DUM1
         GO TO 275
230      DWTL=DWTL+DYI*WTME(I)
         IF (DYI) 215,275,250
235      IF (VNE(I)) 250,250,240
240      IF (VNE(I)+DYI*CNF) 245,250,250
245      CNF=-VNI(I)/DYI*1.00001)
250      CONTINUE
265      IF (ABS(CNF*DYI)-P) 275,275,270
270      CNF=P/ABS(DYI)
275      CNFF(I)=CNF
280      DYI(X)=DYI
290      IF (X(671)-1) 315,315,300
295      FORMAT (13Z(MXZHVN9XLHTRE*HDYZA5HSCALF7XLH6SXAMIFL 1H1/11X46,5F10.
        13+13+12.1X,46,5E10.3,13,1211)
300      X0=1
         WRITE (XOUT,2951  IFANDAE(I),VNE(I),Y(I),DYA(J,LI),CNFF(J),F(J),IFC(J
        1),1P(J),I,J=1,Y0)
         WRITE (XOUT,3103 (E8(I),I=1,I5)
         WRITE (XOUT,510) (X(I),I=1,IXPO)
         WRITE (XOUT,305( (IR(I),I=1,I5)
305      FORMAT (10I5)
310      FORMAT (8E12,4)
         CONTINUE
         IF (X(I)) 320,360,320
320      X1=X(I)*CNF
         ABX=ABS(X(I))
         IF (IABS(X)-.5) 330,910,425
325      CNF=.5/ABX
         X1=CNF*X(I)
330      IF (X1) 360,360,335
335      TM=TMAX
         X1=AMINI(1.2,X1)
         GO TO 345
340      TM=TMIN
         X1=AMAX1(-0.2,X1)
345      DTM=(TM-T)/(TMAX(I)
         IF (DTM-1.1) 350,355,355
350      CNF=DTM*CNF
         T=TM
         GO TO 360
355      T=T/(1.-X1)
360      AA=AA*EXP(CNF*X(2))
         MI=1
         N=IR(1)
         WTL=0.
         WTG=0.
         I=1
         LIM=IKR(N)+N
         DO 495 (K=1,LIM
         DYI=CNF*DYI(K)
         IF (DYI) 395,390,395
390      IF (IFC(I)) 495,435,485
395      IF (IFC(I)) 455,400,480
400      IF (IPI(I)) 405,430,405
405      IF (M-IK) 410,415,410
410      IF (MOE) 430,430,470
415      MI=MI+1
         M=IR(M(I)
420      VNC(I)=VN(I)*E(I,+DYI)
         IF (VNI(I)) 430,430,425
425      Y(I)=ALOG(VNI(I))
         GO TO 435
430      Y(I)=Y(I)+DYI
         VNI(I)=EXP(Y(I))
435      VA=WTME(I)+VNE(I)
         WTG=WTG+VA
         IF (IK-I5) 440,440,445
440      PNUS(I)=VNI(I)
         GO TO 495
445      DO 450 K=1,I5
         VA=VNU(I,K)+VNE(I)
         PNUS(K)=PNUS(K)+VA
450      CONTINUE
         GO TO 495
C        NON-PRESENT BASE CORRECTIONS AND TESTS
455      Y(I)=Y(I)+DYI
```

```
         IF (Y(I)) 495,460,460
460      IF (IFC(I)+1) 495,465,465
465      CONTINUE
475      Y(I)=0.
         IFC(I)=1
         GO TO 495
480      VNE(I)=VN(I)*DYI
         IF (VN(I)) 490,490,485
485      WTL=WTL+VN(I)*WTME(I)
         GO TO 495
490      VN(I)=0.
         IFC(I)=-1
495      I=I+1
         RETURN
         END
C
         SUBROUTINE THERM
         INTEGER FN
         INTEGER FANQ0,FANOM
         COMMON/RADCOM/FR(3),E(I),TT(I),VNME(I),MH(I),SP(I,IL,R)
        L          ,THETA,SV1,SP1,SR1,HS
         COMMON /EOPCOM/ R8(31,2),           IFC(31),ATA(8),ATN(8),WAT(8),
        1          KAT(8),CN(8),TS,KR(10),LAN(3(5),P,RCC(8),Z5,
        2          RDC(31,2),RF(31,7),RF(31,2),T,TK(8,8),FQ(8,8),
        3          TU(3),Z),VN(I),VNU(3),I,L2,L3,ITFF,RR2,HCH,NEV,
        4          WN,WTM(3),Y(31),YX(31),J5P2,FANOAI3),FANOBI31),
        5          ISP,M,M(X),KFN,KOUF,KKR(20),ATC(4)
         COMMON /EOFCOM/ SSP,H3P,F(,FN(,FL(Q,CPF,DF,IER,AA,ITS,IN,IL,ET,
        1          MODE,HM(I),SMFLT,TMAX,IMIN,MFLT,SUMN,SUML,IRF(6),
        2          ER(8),FQL(4),RF(4,16),RC(24),CP3(E),ALP(4),FNU(4),
        3          GAMH(8),GAMF(4),JC,HG,        CPG,DY(31),CP3(I),
        4          H(31),SR(31),TC(31),VMK(31),EE5(1),TTMN,TFMAX,
        5          PNUS(4),V5,V55,I5PQ,RC(4),BLVK(8),BY(8),I8C(8),
        6          B1,XKJ,VA,SVA,SVC,SVD,SUNC,       RV,CNF,FP,IFCJC,
        7          WTG,WTL,J,J5+1,RF(4),LFF(R)
         DIMENSION CEJ( 31,1),TF(1)
         EQUIVALENCE(TU( 323,TF),(VNU,CEJ)
  5      MODE=KR(1)
         IF (ITS) 50,10,50
 10      WTG=0.
         WTL=0.
         IF (RR(1R) 40,40,15
 15      IF (IFC(M+1)-1) 25,20,25
 20      IF (TR-.00)-TF(M+X1) 75,25,30
 25      IFC(N+1)=1
         VNME(I)=0.
 30      DO 35 K=1,I5
 35      VNU(N+1,K)=-TQ(K,31)
         WTL=-VN(N+1)
 40      CONTINUE
         SUMN=0.
         DO 45 I=1,I5
         PNUS(I)=0.
 45      CONTINUE
 50      HMELT=0.
         FL1Q=0.
         SMFLT=0.
         MFLT=1
         TMIN=TTMIN
         TMAX=TFMAX
         TFMAX=500.
         VA=ALOG(TF*3000.)
         VB=T-3000.
         VC=(T*3000.)/2.
         VD=T43000.
         VF=VC/(VD+VD)
         PT=1.986*RF
         I=1
         DO 235 IK=1,N
         J=2
         IF (IFC(I)+1) 165,45,45
 85      IF (IFC(I)) 90,95,120
 90      IF (MODE-I) 185,160,185
 95      IF (ITS) 165,100,165
100      SUMN=SUMN+VN(I)
         DUML=WTME(I)*VNE(I)
         WTG=WTG+DUML
         IF (IK-I5) 105,105,110
105      PNUS(I)=VNE(I)
         GO TO 115
110      DO 115 K=1,I5
         DUM1=VNU(I,K)*VNE(I)
         PNUS(K)=PNUS(K)+DUM1
115      CONTINUE
         GO TO 165
120      IF (IFC(I)-1) 125,125,165
125      IF(ITS) 150,145,150
145      WTL=WTL+VN(I)*WTME(I)
150      IF (MODE-1) 165,155,165
155      TMIN=AMAX1(TMIN,TF(I))
160      TFMAX=AMAX1(TF(I),TFMAX)
165      IF (T-ABSE(U(I,1)) 170,175,175
170      J=1
175      CP(I)=RC(I,J)+FNRQ(I,J)+PF(C,J)/((T+E)
         H(I)=RB(I,J)+VR*RCR(C,J)+RF(I,J)+VC*RF(I,J)/V0)
         SB(I)=RF(I,J)+RC(I,J)+VA+VN+RF(I,J)+EE(I,J)*VE)
         IF (MODE-2) 210,160,180
180      IF (IFC(I)-1) 210,195,210
185      IF (ETU(I,1)) 190,210,210
190      IF (T+FU(I,1) 200,195,205
195      HMELT=-H(I)+HMELT
         SMFLT=-SR(I)+SMELT
         MFLT=I
         IF (J-2) 210,170,210
200      TMAX=AMIN1(TMAX,-TU(I,1))
         GO TO 210
205      TMIN=AMAX1(TMIN,-TU(I,1))
210      TC(I)=-H(I)/RV
         VLMK(I)=TC(I)+SB(I)/(1.986*
         IF (IK-I5) 215,215,220
215      BLNK(I)=VLNK(I)
         IRC(I)=IFC(I)
         BC(I)=TC(I)
         GO TO 235
220      DO 230 K=1,I5
         IF (IRC(K)+1) 230,225,225
225      VLNK(I)=VLNK(I)-VNU(I,K)*BLNK(K)
         TC(I)=TC(I)-VNU(I,K)*BC(K)
230      CONTINUE
235      I=I+1
         IF (MODE-1) 250,240,250
240      IF (TFMAX-T) 245,250,250
245      T=TFMAX
         IF(T-500.) 240,240,5
248      WRITE(KOUT,249)
         STOP
249      FORMAT(///38H NO AVAILABLE SURFACE SPECIES. . .STOP)
250      IF (ITS) 385,255,385
255      AA=P*WN
365      SUMN=SUMN/P
         SUML=ALOG(SUMN)
         WTG=WTG/SUMN
         WTL=WTL/SUMN
         SUMC=1.0
385      RETURN
```

```
C
      SUBROUTINE MATER
      INTEGER FAMOA,FAMOR
      DIMENSION ECCI(31),EESF(31)
      DIMENSION EBS(16)
      COMMON /RADCOM/FR(31,11),TF(11),VMN(11),HHE(11),SP(1,11,8)
     1             ,THETA,SV1,SPL,SR1,HS
      COMMON /EOPCOM/ CHE31,21,              IFC(31),ATAI8),ATB(8),MAT(8),
     1      KAZ(R),IREP1,IS,RC(10),LAM1T(11),P,RC(31,2),
     2      RO(31,2),4E(31,2),RF(31,2),T,TK(8,8),TQ(8,8),
     3      TU(31  2),VN(31),VNU(31,8),L2,L3,TFF,KR2,MCH,NCV,
     4      MN,MYM(3),YI(31),VM(31),1SP2,FAMOA(3),FAMOR(31),
     5      ISP,N,WC(3),KEN,KRUT,KKR(20),ATC(8)
      COMMON /EOTCOM/ SIP,HIP,FL,EML,FLIQ,CPF,IRC,ERR,AA,TYS,IN,IL,IT,
     1      MODE,HMLT,SMFLT,TMAX,TREM,MELT,SUMN,SUMR,IR(9),
     2      ER(8),ER1(8),44(6,(4),8I(4),1P(31),ALP(8),FNU(8),
     3      GANH(8),GANF(9),JC,HG,            CPG,DY(31),CP1(31),
     4      HI(9),SBI3(1),TC(31),VLNE(31),E(31),TFMIN,FTMAX,
     5      PNUS(8),NS,WSS,ISPO,BCL8),NLNK(8),BV(8),IBC(8),
     6      R1,KKJ,SV4,SVN,SVC,SVD,SUMC,        NV,CMF,EP,IFC,JC,
     7      MYG,MTL,JJ181,AF(R),LFF(8)
      DIMENSION VLAN(31,1),X(14)
      DIMENSION CEJ( 31,1),TF(11)
      EQUIVALENCE(TU( 32),TF1,(VNU,C(J)
      WSS=WS
      DO 5 I=1,IS
      IBC(I)=IFC(I)
    5 
   40 RV=WSS-WTL/WTG
      IF (ERR(T)-1) 70,45,50
   45 IF (IT5) 70,60,70
   50 CONTINUE
      KRF7)=KR(71-1
      IF (KRFT)-1) 70,60,70
   60 WRITE (KRUT,65) IT,I=1,IS)
   65 FORMAT (50H1FT5 TEMP   PRES=HVT  EQUIL FR  MASRAL ER  SCALE  7(I3,
     17H MASRAL)/90X3(I5,7H MASRAL))
C     INITIALIZE
   70 FL=0.
      CPG=0.
      EP=0
      CPF=0.
      JC=0
      JCS=0
      ISP=IS+1
      ISPO=IS+2
      B(1)=0.
      B(2)=0.
      A(1,1)=0.
      A(1,2)=0.
      A(2,1)=0.
      A(2,2)=0.
C     -----INITIALIZE CONTRIBUTION OF MOST SIGNIFICANT SPECIES IN EACH M
      DO 75 I=1,IS
      FN(I)=0.
   75 F(I)=KA*PL*(I)
      ISP2=ISPO
C     -- - MAIN BASE SPECIES LOOP
      DO 125 TK=1,IS
      I=2-IR(IK)
      IF (KAT(IK)-99) 85,80,85
   80 PNUS(I-2)=0.
C     ZERO MATRIX
   85 DO 90 K=1,ISPO
   90 A(K,I)=0.
      IF (IT5) 110,95,110
C     NORMALIZE ON PRESSURE ON FIRST PASS
   95 VN(I-2)=VN(I-2)/SUMN
      EBL(I-2)=0.
      IF (IBC(I-2)) 110,100,105
  100 V(E-2)=TF(I-2)-SUMR
      GO TO 110
  105 VN(I-2)=VN(I-2)/SUMC
C     INITIALIZE SOMF HORF
  110 A(I)=0.
      A(1,1)=0.
      IF(I-2)=0.
C     SET FLAG INDICATING SIGNIFICANCE OF SPECIES IN MASS
C     BALANCE(S) AND INCREMENT EQUIV ON SIGNIFICANT SPECIES
      IF (VN(I-2)-EBL(I-2)) 120,120,115
  115 IF(I-2)=I-1
C     TREAT BASE SPECIES CONTAINING BUT NOT REPRESENTING NON-PRESENT
C     ELEMENTS IN SAME MANNER AS NON-PRESENT CONDENSED SPECIES
  120 IF (IBC(I-2)*L) 325,125,125
  125 IF (IBC(I-2)) 100,215,130
  130 A(1,1)=1.
      VA=VN(I-2)
      IF (1ABS((BC(I-2-31-1) 135,710,140
  135 A(2,2)=1.0
      GO TO 290
  140 IF (EBC(I-2)-ABS(VR)) 145,150,150
  145 FB(I-2)=ABS(VA)
      IB(I-2)=T-2
  150 F(I-2)=F(I-2)-VA
  155 IF (MODE-1) 280,170,280
  170 TMIN=AMAX1(TMIN,TF(I-2)
      IF (T-TF(I-2+.03)) 175,175,160
  175 A(1,1)=1.0F+10
      F(I-2)=-VN(I-2)*1.00IE+10
      MODE=0
  180 IF (MODE-1) 185,190,185
  185 IF (KR(8)) 280,280,190
  190 IF (TF(I-2)+.001-T) 325,195,195
  195 IF (JC) 205,205,200
  200 IF (Y(I-2)-BJC) 325,325,705
  205 BJC=Y(I-2)
      JCS=JC
      TMAX=TF(I-2)
      JC=I-2
      IFC(JC=IBC(I-2)
      IF (KR(8)) 210,210,280
  210 A(1,JCS=2)=0.
      A(1,I)=-1.0.
      GO TO 325
C     -----GAS PHASE
  215 VA=VN(I-2)
      CPG=CPG+VA*CP(I-2)
      A(1,1)=VA
      A(2,1)=VA
      EP=EP-VA
  275 FN(I-2)=ABS(VA)
      IB(I-2)=I-2
      F(I-2)=F(I-2)-VA
  280 IF (MODE-2) 320,300,285
  285 IF (IBC(I-2)) 325,205,290
  290 HOS=SB(I-2)
      GO TO 305
  295 HOS=SB(I-2)-1.98690*Y(I-2)-1.0869
      GO TO 310
  300 HOS=H(I-2)
      IF (IBC(I-2)) 325,310,305
  305 A(1,I)=HOS
      GO TO 315
  310 A(1,1)=HOS*VN(I-2)
  315 A(1,2)=A(1,2)-HOS*VN(I-2)
```

```
  320 CPF=CPF+CP(I-2)*VN(I-2)
  325 CONTINUE
      DO 330 I=1,IS
      NEE(I)=E(I)
  330 BY(I)=T(I)
      IER=0
      IRE=0
      EER=0.
C     --- MAIN NON-BASE SPECIES LOOP
  350 LIM=NKKR(8)
      IF (ILIM-TSP) 730,355,355
  355 J=ISP
      DO 725 IA=ISP,LIM
      IF (ITK-N) 365,365,340
  360 F(J)=1.E-10
      IF (IFC(J)) 410,725,445
  365 IF (IFC(J)+1) 725,370,370
  370 IF (IT5) 390,375,390
  375 VN(J)=VN(J)/SUMN
      IF (IFC(J)) 390,385,380
  380 VN(J)=VN(J)/SUMC
      GO TO 390
  385 Y(J)=Y(J)-SUMR
  390 F(J)=VLNK(J)-Y(J)
      DO 405 I=1,IS
      IF (IBC(I)) 400,400,395
  395 FNU(I)=0.
      GO TO 405
  400 FNU(I)=VNU(J,I)
      F(J)=F(J)+FNU(I)*NYI(I)
  405 CONTINUE
  409 EAB=ABS(F(J))
      IF (IFC(J)) 410,590,445
C     CONDENSED SPECIES
  410 EAB=E(J)
  425 IF (E(J)-ERR) 531,535,430
  430 EER=E(J)
      IF (ITE8) 435,435,440
  435 ISPO=ISPO*L
      IER=ISPO
  440 IF=IER
      IRE=IN
      GO TO 450
  445 ISPO=ISPO+1
      IF=ISPO
  450 ATR=0.
  460 DO 465 I=3,ISPO
      A(I,IE)=0.
  467 A(IE,I)=0.
      DO 480 K=1,IS
      DUMI=VNU(J,K)
      IF (IBC(K)-1) 470,470,480
  470 VA=DUR(PVN(J)
      A(K+2,YE)=DUR1-WTR+PNUS(K)+GAMF(K)+WTG)
      9FCK)=9F(K)-VA
      IF (ABS(VA)-ER(K)) 480,4*),475
  475 E(IN)=ABS(VA)
      IR(N)=IR
  480 CONTINUE
      K=IF-ISP2
      IF (IK-N) 505,505,485
  485 JJ(K)=JC
      B(EES)=Y(JC)
      IF (JC-IS) 495,495,470
  490 A(IF,3)=TC(JC)
      B(IE)=Y(JC)
  495 EAB=-R(IF)
      IF (IFC,JC) 715,715,500
  500 EAB=ABS(FAB)
      GO TO 715
  505 JJ(K)=J
      JJ(K)=J
      A(IF,1)=TC(J)
      B(IE)=E(J)
      IF (IK+.001-TF(J)) 515,510,510
  510 IF (KR(8)) 530,510,540
  515 IF(MDOF-1) 530,525,530
  525 A(IE,IE)=1.E+10
      B(IF)=-VN(J)*1.00E+10
      MODE=0
  530 IF (MODE-2) 535,575,540
  535 IF (MODE-2) 715,540,715
  540 IF (T-TF(J)-.001) 545,545,560
  545 IF (JC) 555,555,550
  550 IF (E(J)-BJC) 725,725,555
  555 BJC=E(J)
      JC=IA
      IFC,JC=TFC(JC)
      TMAX=TF(J)
      IF (KR(8)) 565,565,560
  560 IF (MDOF-2) 725,575,580
  564 A(1)=BJC
      DO 570 K=1,IS
  570 A(1,K+2)=-FNU(K)
      A(1,J3=TC(J)
      GO TO 725
  575 HOS=H(J)
      GO TO 585
  580 HOS=SB(J)
  585 A(1,1E)=HHS
      A(1,2)=A(1,2)-VN(J)*HHS
      CPF=CPF+CP(J)*VN(J)
      GO TO 715
C     GAS PHASE SPECIES
  590 TF(J)=0
      IF (VN(J)) 595,715,595
  595 1=0
      CPG=CPG+VN(J)*CP(J)
  625 DO 690 K1=1,IS
      I=2-TR(K1)
      VA=VNU(J,1-2)*VN(J)
  445 SF(I-2)=B(I-2)-VA
      ARSVA=ABS(VA)
  650 IF (ABS(VA-FNL(I-2)) 660,660,655
  655 ID=1
      IF (ABS(VA)-ER(I-2)) 670,670,665
  660 IF (ABS(VA)-EBL(I-2)) 680,680,670
  665 EB(I-2)=ARSVA
      IB(I-2)=IN
  670 DO 675 K=3,ISP2
  675 A(1,K)=A(1,K)+VA*FNU(K-2)
      B(I)=B(I)+VA*E(J)
      A(1,1)=A(1,1)+VA*TC(J)
      A(2,1)=A(2,1)+VN(J)*FNU(I-2)
  680 CONTINUE
      IF (IQ) 715,715,685
  685 EP=EP-VN(J)
      IF(J)=-1
      B(2)=B(2)-VN(J)*E(J)
      A(2,1)=A(2,1)-VN(J)*TC(J)
      IF (MODE-2) 710,690,695
  690 HHS=H(J)*VN(J)
      GO TO 700
  695 HOS=VN(J)*SB(J)-1.98690*Y(J)-1.0869)
  700 DO 705 I=3,ISP2
```

```
705   A(1,1)=HOS*FMU(I-2)*A(1,1)
      A(1,2)=A(1,2)-HOS
      A(3,1)=A(1,1)-HOS*TC(J)
      B(1)=B(1)-HOS*E(J)
710   CPF=CPF+VN(J)*CP(J)
715   IF (IEL-EAB) 720,725,725
720   FL=EAB
725   J=J+1
710   CONTINUE
      ISP3=I6+3
      IF (MODE-2) 745,735,760
735   CPA=CPF+T
      SHMLT=HMFLT*VN(MELT)
      EHS=AA*HIP*A(1,2)
      IF (IKMJ+1) 750,740,750
740   OUM1=SVA/AA*T*T
      EHS=AA*SVC-OUM1+A(1,2)
      HIP=-A(1,2)/AA
      A(1,2)=-AA*SVC-OUM1
      CPA=(CPF*2.+OUM1/T)*T
      OUM2=SVB/AA*T
      P=P-EP
      EP=0.
      IF (ABS(EHS/AA-10.) 765,765,740
745   EP=-P+SVD-OUM2
      A(2,1)=A(2,1)+OUM2
      A(2,2)=-OUM2
750   IF (RR(2)-RMODE) 765,755,765
755   A(1,2)=-AA*HIP
      GO TO 765
760   CPA=CPF
      SHMLT=SMELT*VN(MELT)
      EHS=AA*SIP+A(1,2)-1.9869*(P-CP)
      A(1,2)=-AA*SIP
765   B(1)=B(1)+EHS
      A(1,1)=A(1,1)+CPA
      IF (SHMLT) 785,785,770
770   IF (FHS) 785,785,775
775   EHS=P+HS-SHMLT
      A(1)=B(1)-SHMLT
      IF (FHS) 780,785,785
780   FLTO=1.+FHS/SHMLT
      MODE=0
      A(1,1)=1.E+10
      TMIN=500.
      TMAX=5000.
785   ENL=ABS(EP)/P*100.
      DO 810 I=3,ISP2
      A(I-2)=DE(I-2)
      ENL(I-2)=EB(I-2)+1.F-7
      A(I,2)=AA*ALP(I-2)
      IF (IPC(I-2)-E) 795,795,799
790   WP=WFN+1
      GO TO 810
795   CONTINUE
805   ER=A(I-2)
      ADER=ABS(ER)/(DB(I-2)+1.F-20)
      ENL=AMAX1(ADER,ENL)
      A(I)=B(I)+ER
810   CONTINUE
      IF (ISP2-ISP0) 815,800,800
815   IV=0
      JZ=0
C     ADD CONDENSED NONBASE SPECIES TO ARRAY
      DO 840 IE=ISP3,ISP0
      J=IF+ISP2
      J=JJ(J)
      IF (J-IS) 820,820,830
820   DO 825 K=1,IS
      A(I(K,4+2)=0.
      A(I(K,J+2)=-1.0
      GO TO 840
830   DO 835 K=1,IS
835   A(I(K,4+2)=-VNU(J,K)
840   CONTINUE
C     ELIMINATE TERMS CORRESPONDING TO PRESENT BASE CONDENSED
      DO 855 K=1,IS
      IF (IFCC(K)) 855,855,845
845   DO 850 IE=ISP3,ISP0
850   A(I(E,K+2)=0.
855   CONTINUE
880   B(I2)=EP+B(I2)
      A(I2)=1
      IF (RODE-I) 910,990,885
885   IF (ABS(EHS/A(1,1))-.0001) 910,910,920
890   IF (IFCJC) 895,900,905
895   IF (JC-IRE) 900,900,900
905   MODE=0
      TMIN=TTMIN
      TMAX=TTMAX
900   IF (ABS(B(1))-1.5-4) 910,910,920
910   IF (EL-1.E-4) 915,915,920
915   IF (FML-1.E-5) 935,955,920
920   IN=ISP0
      IL=1
      IF (MODE) 925,925,930
925   IN=ISP0-1
      IT=2
      K(I)=0.
      RETURN
930   IT=ITS+1
935   ITS=-1
      GO TO 930
      END
C
      SUBROUTINE RERATX(N,C,NN,D,NNN,LS,IS,NS)
C     DIRECT INVERSION PROCEDURE  --  C IS REPLACED BY CNN-1
      DIMENSION D(14,2),SD(80),C(14,1),L(60),S(60),LL(60),LLL(60),LS(1)
      KIN=3
      KOUT=6
      NI=N+1
      NP=N+NN
      DO 11 I=1,NP
      LLL(I)=1
      IF(L(S(I))) 113,113,112
112   L(I)=L(S(I))
      GO TO 11
113   L(I)=I
11    CONTINUE
      IX=-1
      IF(IS+2) 111,109,111
106   FORMAT(11H  L(I),J=1,13,5X (30I3))
107   FORMAT(15H  L(C(I),J),J=1,13,12H) ,D(C(J),J=1,I3, 6H),I=1,I3,15H)
      IFORE RERAYS
108   FORMAT(2X, 1LELO.3/(12X, 10F10.3))
109   WRITE(KOUT,107) NP,NNN,N
      WRITE(KOUT,106)(L(I),I=1,NP)
      IX=0
      DO 110 I=1,N
110   WRITE(KOUT,108)(C(I,J),J=1,NP),(D(I,J),J=1,NNN)
111   IS=-L
C     TRIANGULATE MATRIX
      DO 19 I=L,N
      DO 160 M=1,NP
160   S(M)=ABS(C(I,M))
      IF(IS) 16,16,16
```

```
18    IS=0
      SD(I)=1.
      GO TO 12
C     REDUCE ROW I BY PRECEEDING ROWS
16    DO 17 J=2,I
      K=L(J-1)
      DIV=-C(I,K)
      IF(DIV) 161,17,161
161   C(I,K)=0.
      DO 162 M=1,NP
      DIVC=DIV*C(J-1,M)
      S(M)=AMAX1(S(M),ABS(DIVC))
162   C(I,M)=C(I,M)+DIVC
      IF(NNN) 17,17,163
163   DO 164 M=1,NNN
164   D(I,M)=D(I,M)+DIV*D(J-1,M)
17    CONTINUE
C     SEEK MAXIMUM PIVOT
12    DIV=0.
      DO 13 JJ=I,N
      M=L(JJ)
      IF(ABS (C(I,M))-DIV*S(I,I3,12)
121   DIV=ABS (C(I,M))
      K=M
      J=JJ
13    CONTINUE
      IF(IK) 130,131,130
130   SD(I) = DIV/S(K)
      L(JJ)=L(I)
      L(I)=K
      IF(SD(I)-1.E-8) 131,131,14
C     SINGULAR MATRIX RETURN
131   IS=-I
      WRITE(KOUT,151) (I,L(I),SD(I),IT=1,I)
      RETURN
14    DIV=C(I,K)
      C(I,K)=1.0
      K=L(L(J)
      L(L(I))=LL(I)
      LLL(I)=M
      LL(M)=I
C     NORMALIZE ROW
      IF(NNN) 143,143,141
141   DO 142 J=1,NNN
142   D(I,J)=D(I,J)/DIV
143   DO 15 J=1,NP
15    C(I,J)=C(I,J)/DIV
      IF(IX) 192,150,192
151   FORMAT(12H*  PIVOT  ROW/COL/RES.RATIO S(I6,2H/I3,1H/E0.2,1H,)
190   WRITE(KOUT,151) (I,L(I),SD(I),I=1,NP)
C     DIAGONALIZE MATRIX
192   NNN=I
      DO 20 I=1,N
      K=L(I+1)
      DO 20 J=1,I
      DIV=-C(J,K)
      IF(DIV)19,19,19
19    C(J,K)=0.
      IF(NNN) 191,191,192
192   DO 195 M=1,NNN
195   D(J,M)=D(J,M)+DIV*D(I+1,M)
191   DO 201 M=1,NP
201   C(J,M)=C(J,M)+DIV*C(I+1,M)
20    CONTINUE
C     INTERCHANGE COLUMNS
      DO 30 I=1,NP
      I=I
71    J=L(I)
      L(I)=I
      IF(J-I)22,30,22
22    IF(IS)23,23,25
23    DO 24 M=1,N
      S(M)=C(M,I)
24    C(M,I)=C(M,J)
      I=J
      GO TO 21
25    IF(I-J)26,25,26
26    DO 27 M=1,N
27    C(M,I)=C(M,J)
      I=J
      GO TO 28
28    DO 29 M=1,N
29    C(I,M)=S(M)
30    I=0
30    CONTINUE
C     INTERCHANGE ROWS
      DO 40 I=1,N
      I=I
81    J=LL(I)
      LL(I)=I
      IF(J-I)32,40,32
32    IF(IS)33,33,35
33    DO 34 M=1,NP
      S(M)=C(I,M)
34    C(I,M)=C(J,M)
      IF(NNN) 343,34,341
341   DO 342 M=1,NNN
      SD(M)=D(I,M)
342   D(I,M)=D(J,M)
343   I=J
      GO TO 31
35    IF(I-J)36,35,36
36    DO 37 M=1,NP
37    C(I,M)=C(J,M)
      IF(NNN) 373,375,371
371   DO 372 M=1,NNN
372   D(I,M)=D(J,M)
375   I=J
      GO TO 31
38    DO 39 M=1,NP
39    C(I,M)=S(M)
      IF(NNN) 393,393,391
391   DO 392 M=1,NNN
392   D(I,M)=SD(M)
393   IS=0
40    CONTINUE
      IF(IX) 411,409,411
407   FORMAT(15H  ((C(I,J),J=1,I3,12H),(D(I,J),J=1,I3, 6H),I=1,I3,15H) AF
      ITEH RERAY  )
409   WRITE(KOUT,407) NP,NNN,N
      DO 410 I=1,N
410   WRITE(KOUT,108)(C(I,J),J=1,NP),(D(I,J),J=1,NNN)
411   RETURN
      END
C
C     * * * * * * * * * * * * * * * * * * * * * * * * * * * * * * * *
C
C     SUBROUTINES FOR RADIATIVE TRANSPORT CALCULATIONS.
C
C     * * * * * * * * * * * * * * * * * * * * * * * * * * * * * * * *
C
      SUBROUTINE RADIN
```

DESCRIPTION OF INPUT

CARD SET 1 - CONTROL CARD AND CASE IDENTIFICATION
  CARD 1, FORMAT(5I1,15A5)
    FIELD 1, (COLUMNS 1-5) KQS
      COLUMN 1   DETERMINES IF CHANGES ARE TO BE MADE FOR PARAMETERS IN
                NAMELIST NAME2. SEE CARD SET 4.
         0   NO CHANGES IN NAME2
         1   CHANGES IN NAME2
      COLUMN 2   DETERMINES IF MASS BALANCE OPTION TO BE USED. SEE ALSO THE
                PARAMETERS LSC AND CGS IN NAME2 OF CARD SET 4.
         0   MASS BALANCE NOT USED
         1   MASS BALANCE USED
      COLUMN 3   DETERMINES IF RADIATIVE TRANSPORT IS CONSIDERED.
         0   NO RADIATIVE TRANSPORT
         1   RADIATIVE TRANSPORT
      COLUMN 4   DETERMINES IF MOLECULES ARE TO BE INCLUDED IN RADIATIVE
                TRANSPORT.
         0   MOLECULES INCLUDED (SEE CARD SET 7)
         1   MOLECULES NOT INCLUDED
      COLUMN 5   DETERMINES HOW THE LINE CONTRIBUTIONS ARE CALCULATED IN THE
                RADIATIVE TRANSPORT.
         0   INCLUDE LINES, WEAK LINES TREATED APPROXIMATELY
         1   INCLUDE LINES IN FULL DETAIL
         2   EXCLUDE LINES
    FIELD 2, (COLUMNS 6-80) CASE
      CASE IDENTIFICATION (ALPHANUMERIC).

CARD SET 2 - FREESTREAM CONDITIONS, NUMBER OF NODES, NOSE RADIUS.
  CARDS AS REQUIRED, NAMELIST FROMAT (NAME1)
    VF   FREESTREAM VELOCITY, METERS PER SECOND
    RHOF FREESTREAM DENSITY, KILOGRAMS PER CUBIC METER
    PF   FREESTREAM PRESSURE, NEWTONS PER SQUARE METER
    HF   FREESTREAM ENTHALPY, JOULES PER KILOGRAM
    RN   BODY RADIUS AT STAGNATION POINT (NOSE RADIUS), METERS
    KYS   NUMBER OF NODES THROUGH LAYER INCLUDING WALL AND SHOCK LOCATIONS.
         MAXIMUM OF 11.
    Y(I) ARRAY OF NONDIMENSIONAL LOCATION OF NODES THROUGH LAYER (I=1,KYS).
         Y(1)=0 AT WALL AND Y(KYS)=1 AT SHOCK.
    KSE   NUMBER OF NODES AROUND BODY. MAXIMUM OF 15.

CARD SET 3 - SPECIFICATION OF BODY SHAPE AT NODES AROUND BODY.
  CARDS AS REQUIRED AND EQUAL TO KSE, FORMAT(5F15.7). ONE CARD FOR EACH BODY
  LOCATION. BEGIN AT S=O. LENGTHS TO BE NONDIMENSIONAL BY RN AND ANGLES IN
  RADIANS.
    COLUMN 1-15   THETA, BODY ANGLE
    COLUMN 16-30   S, DISTANCE ALONG BODY FROM STAGNATION POINT
    COLUMN 31-45   RB, RADIUS OF BODY PERPENDICULAR TO AXIS.
    COLUMN 46-60   XB, AXIAL DISTANCE FROM STAGNATION POINT
    COLUMN 61-75   K, BODY CURVATURE TERM

CARD SET 4 - CONVERGENCE TERMS, OUTPUT, MASS BALANCE TERMS, ETC.
        SKIP THIS SET IF KQS(1)=0.
  CARDS AS REQUIRED, NAMELIST FORMAT(NAME2)
    VALUES FOR THE PARAMETERS IN NAME2 ARE SET IN THE PROGRAM, BUT ARE NOT
    NECESSARILY GOOD VALUES FOR ALL PROBLEMS. TO CHANGE ANY OF THEM,
    SET KQS(1)=1 AND READ IN THE VALUES FOR THE PARAMETERS WHICH ARE TO BE
    CHANGED. FOR NO CHANGES, SET KQS(1)=0 AND SKIP THIS CARD SET.
      DF1   MULTIPLY OF CORRELATION FOR INITIAL SHOCK STAND-OFF DISTANCE.
      TIFRAC   MULTIPLY OF VALUE FOR GETTING TIME STEP. MUST BE LESS THAN 1.0.
      IKSC   THE ITERATION TO BEGIN CHECKING FOR CONVERGENCE.
      CC1   CONVERGENCE CRITERION. THE CHANGE IN ENTHALPY BETWEEN
             ITERATIONS, (H(N+1)-H(N))/H(N), MUST BE LESS THAN CC1 FOR
             CONVERGENCE.
      CCF   FRACTION OF NODES POINTS ALONG WALL, SHOCK, AND LAYER MIDPOINT
             FOR WHICH THE CONVERGENCE CRITERION MUST BE MET. VALUE FOR
             CCF MUST BE LESS THAN 1.0.
      ICC   CONSECUTIVE NUMBER OF ITERATIONS FOR WHICH THE ERROR CRITERION
             MUST BE MET.
      IKSF   MAXIMUM NUMBER OF ITERATIONS TO BE ALLOWED. CARDS ARE PUNCHED
             TO PICK UP CASE BY ANOTHER RUN. SEE CARD SET 5.
      IOUTN   PRINTED OUTPUT IS GIVEN FOR CONVERGED SOLUTION.
             FOR INTERMEDIATE OUTPUT, IOUTN IS THE NUMBER OF ITERATIONS
             BETWEEN OUTPUT.

      IOUTF   IF THE INITIAL VALUES (FIRST GUESS VALUES) ARE TO BE PRINTED,
             SET THE VALUE OF IOUTF TO IOUTN MINUS ONE. IF NOT, SET IOUTF
             EQUAL TO ZERO.
      ITC   NUMBER OF ITERATIONS BETWEEN CALCULATION OF THERMODYNAMIC
             PROPERTIES.
      IRC   NUMBER OF ITERATIONS BETWEEN CALCULATION OF RADIATIVE
             TRANSPORT.
      IKSU(I) ARRAY FOR VALUES OF ITERATIONS AT WHICH THE VALUES FOR ITC
             AND IRC CAN BE CHANGED DURING SOLUTION. MAXIMUM OF 5.
      ITCU(I) ARRAY OF VALUES FOR ITC WHICH CORRESPONDS TO IKSU(I).
      IRCU(I) ARRAY OF VALUES FOR IRC WHICH CORRESPONDS TO IKSU(I).
      NCTS   IF NCTS EQUALS ZERO, THE TIME STEP CAN VARY AROUND BODY AND
             SOLUTION WILL GENERALLY CONVERGE FASTER. IF NCTS IS NOT EQUAL
             TO ZERO, THE MINIMUM TIME STEP IS USED AT ALL BODY LOCATIONS.
      CGS   CRITERION TO BE MET BEFORE MASS BALANCE OPTION CAN BE USED.
             THE SHOCK VELOCITY AT THE STAGNATION POINT (DELTAT(1)) MUST BE
             LESS THAN THE SET VALUE FOR CGS BEFORE THE MASS BALANCE
             OPTION CAN BE USED FOR CALCULATING THE SHOCK STAND-OFF
             DISTANCE AROUND BODY. THIS IS BECAUSE THE SHOCK STAND-OFF
             DISTANCE AT THE STAGNATION POINT MUST BE CONVERGED BEFORE USING
             THE MASS BALANCE OPTION.
      LSC   THE MINIMUM ITERATION AT WHICH THE MASS BALANCE OPTION CAN BE
             USED.

CARD SET 5 - INPUT FOR THE PICK UP OF A SOLUTION.
  THE PROGRAM IS WRITTEN SO THAT A SOLUTION CAN BE PICKED UP FROM A SPECIFIED
  ITERATION.
  FOR A NEW CASE, A BLANK CARD IS INSERTED FOR THIS CARD SET.
  IF THE NUMBER OF ITERATIONS REACHES THE VALUE SET FOR IKSF (CARD SET 4)
  THEN A CONVERGED SOLUTION WAS NOT OBTAINED WITHIN THE SPECIFIED NUMBER OF
  ITERATIONS AND A SET OF CARDS ARE PUNCHED OUT. THIS SET OF PUNCHED OUTPUT
  CAN BE INSERTED FOR CARD SET 5 AND THE SOLUTION CAN BE PICKED UP BY ANOTHER
  RUN AT THAT ITERATION. FOR A PICK UP CASE, IKSF AND IKSC (CARD SET 4) MUST
  BE GREATER THAN THE VALUE OF IKSF FROM THE PRIOR RUN)

CARD SET 6, 7 AND 8.
  THESE CARD SETS ARE THE CHEMISTRY INPUTS FOR THE CHEMICAL EQUILIBRIUM
  CALCULATIONS AND THE BASIC RADIATION AND SPECTROSCOPIC DATA FOR THE
  RADIATIVE TRANSPORT CALCULATIONS. THE INPUTS FOR THE CARD SETS ARE DESCRIBED
  IN THE REPORT - NICOLET, W.E.   USER#S MANUAL FOR THE GENERALIZED RADIATION
  TRANSFER CODE (RAD/EQUIL). AEROTHERM REPORT NUMBER UM-69-9. AEROTHERM
  CORPORATION, MOUNTAIN VIEW, CALIFORNIA.
  CARD SET 6 IS READ IN THE SUBROUTINE INPUT. CARD SETS 7 AND 8 ARE READ IN
  SUBROUTINE RADIN.

CARD SET 6 - CHEMISTRY INPUT.
  THE INPUTS FOR THIS CARD SET ARE DESCRIBED IN GROUP 3 AND GROUP 4 OF DECK B
  IN THE REPORT BY NICOLET.
  MODIFICATIONS
    GROUP 3   IN COLUMNS 25-30 ON EACH ELEMENT CARD, EXCEPT ELECTRON, GIVE THE
             ELEMENTAL MASS FRACTION FOR THAT ELEMENT. (AS A NEGATIVE NUMBER)
             NOTE, MASS FRACTION OF ELEMENT.
    GROUP 4   THE THERMODYNAMIC INPUT DATA (3 CARD SET) FOR THE ATOMIC SPECIES
             OF THE ELEMENTS MUST BE ARRANGED FIRST IN THE SAME ORDER AS
             GIVEN BY GROUP 3. THE DATA FOR THE ELECTRON AND IONIZED SPECIES
             ARE STILL AT THE END. CONDENSED SPECIES ARE NOT ALLOWED.
             MAXIMUM NUMBER OF SPECIES IS 40. A BLANK CARD MUST BE PLACED
             AT THE END OF GROUP 4 AS STATED BY NICOLET.

CARD SET 7 - CONTINUUM CONTRIBUTIONS TO RADIATIVE TRANSPORT. SKIP THIS CARD
             SET IF KQS(3)=0.
  THE INPUTS FOR THIS CARD SET ARE DESCRIBED IN GROUP 6, CARD 3 OF DECK B
  IN THE REPORT BY NICOLET.
  IDENTIFIES WHICH CONTINUUM CONTRIBUTIONS ARE TO BE INCLUDED IN THE
  CALCULATION OF RADIATIVE TRANSPORT.

CARD SET 8 - RADIATION AND SPECTROSCOPIC DATA. SKIP THIS CARD SET IF KQS(3)=0.
  THE INPUTS FOR THIS CARD SET ARE DESCRIBED IN DECK A (ENTIRE DECK) IN THE
  REPORT BY NICOLET.

```
11101      .97 CO2 - .03 N2 (BY VOLUME), 60 DEG. CONICAL BODY, HIGH VEL.        1
$NAME1   VF=11175., RHOF=.00285, PF=117.3, HF=-8860000., RN=.1048, KSE=10.      2
         KYS=9, Y(1)=0.,.125,.250,.375,.500,.625,.750,.875,1.000, $END          3
1.570796    0.           0.          0.         1.0                             4
1.370796    .2          .198669    -.019933     1.0                             5
1.170796    .4          .389418     .078939     1.0                             6
1.047198    .6          .566165     .172175     0.                             7
1.047198    .8          .739171     .272175     0.                             8
1.047198   1.2         1.085781     .472175     0.                             9
1.047198   2.0         1.778601     .872175     0.                            10
1.047198   3.0         2.644426    1.372175     0.                            11
1.047198   4.0         3.510652    1.872175     0.                            12
1.047196   5.0         4.376677    2.372175     0.                            13
$NAME2   LSC=600, IKSF=1200, ITC=100, IRCU(1)=200,200,200,200,100,            14
         IOUTN=200, IOUTF=199  $END                                           15
   0                                                                           16
   4                                                                           17
 6 CARBON     12.011    -.2676                                                 18
 7NITROGEN    14.007    -.0193                                                 19
 8 OXYGEN     16.000    -.7131                                                 20
99ELECTRON     .00055                                                          21
1006                              JANAF 03/61              C                   22
170886+6 135500+5 444633+1 228125-3 40983046 49287042  500. 3000.1  0.C       23
170886+6 135500+5 412212+1 261908-3 262886+7 492670+2 3000. 5000.1  0.C       24
1007                              JANAF 03/61              N                   25
112965+6 134370+5 486944+1 383516-4 958460+5 480900+2  500. 3000.1  0.N       26
112965+6 134370+5 428957+1 240844-3 41727346 480900+2 3000. 5000.1  0.N       27
1008                              JANAF 06/62              O                   28
595590+5 135220+5 497228+1 390768-5 156749+5 500960+2  500. 3000.1  0.0       29
595590+5 135220+5 657489+1-224268-3-891782+7 500960+2 3000. 5000.1  0.0       30
 2  7                             JANAF 9-30-65            N2                   31
     0+0 221649+5 793097+1 319649-3-31429546 63765042  500  30001  -ON2        32
     0+0 221649+5 878236+1 68 810-4-119262+7 63765042  3000 60001  -ON2        33
 2  8                             JANAF 9-30-65            O2                   34
     0+0 234545+5 808690+1 497028-3-742932+6 674972+2  500  30001  -OO2        35
     0+0 234545+5 1009242+2 636677-4-659192+7 674972+2 3000 60001  -OO2        36
 1 6  1  7                        JANAF 12-31-66           CN                   37
110999+6 232619+5 706816+1 994584-3-107243+6 669760+2  500  30001  -OCN        38
110999+6 232479+5 126220+2-176667-3-184680+8 669760+2 3000 60001  -OCN        39
 1 6  1  8                        JANAF 9-30-65            CO                   40
-264169+5 223569+5 808732+1 281527-3-13212+46 65369942  500  30001  -OCO       41
-264169+5 223569+5 885923+1 582009-6-124951+7 653609+2 3000 60001  -OCO       42
 1 6  2  8                        JANAF 9-30-65            CO2                  43
-940539+5 365349+5 135296+2 479823-3-865470+6 798480+2  500  30001  -OCO2      44
-940539+5 365349+5 144884+2 176547-3-130622+7 798480+2 3000 60001  -OCO2      45
 2  6                             JANAF 12/69      KS       C2                  46
200223+6 246779+5 776530+1 671194-3 208014+6 68559042  300  30001  10C2       47
200221+6 246779+5 843360+1 447514-3 259636+6 68559042  3030 60001  10C2       48
 2  6  1  7                       JANAF 3-31-67            C2N                  49
133000+6 384599+5 146553+2 722952-4-54212746 86627042  500  30001  -0C2N      50
133006+6 384599+5 145950+2 590928-4 356595+6 866270+2 3000 60001  -0C2N       51
 2  6  1  8                       JANAF 9-30-66            C2O                  52
684999+5 306079+5 142061+2 468192-3-780511+6 86446042  500  30001  -0C2O      53
684999+5 306079+5 162297+2-141246-3-253785+7 864460+2 3000 60001  -0C2O       54
 3  6                             JANAF 12/69      KS       C3                  55
199999+6 309579+5 996626+1 976478-3-168296+6 81235942  300  30001  10C3       56
199999+6 309579+5 129505+2 166809-3-516560+7 81235942  3000 60001  10C3       57
 4  6                             JANAF 12/69      KS       C4                  58
231999+6 510959+5 183531+2 744725-3-67781+46 94893942  300  30001  10C4       59
231999+6 510959+5 208450+2 244726-5-306350+7 94893942  3000 60001  10C4       60
 5  6                             JANAF 12/69      KS       C5                  61
213999+6 653359+5 234751+2 992624-3-936491+6 10912843  300  30001  10C5       62
238999+6 653359+5 267963+2 382130-5-412893+7 109128+3 3000 60001  10C5        63
1007 01 08                        JANAF 06/63              NO                  64
215800+6 227000+5 877623+1 849031-4-78965646 48840042  500. 3000.1  0.NO      65
215800+6 227000+5 916260+1 467885-5-21251947 488490+2 3000. 5000.1  0.NO      66
 1  7  2  8                       JANAF 9-30-64            NO2                  67
790999+4 344819+5 131500+2 215749-3-804084+6 847950+2  500  30001  -0NO2      68
790999+4 344819+5 139044+2 720659-6-169730+7 847950+2 3000 60001  -0NO2       69
 2  7  1  8                       JANAF 12-31-64           N2O                 70
196099+6 365529+5 137618+2 322928-3-82699746 81590042  500  30001  -0N2O      71
196099+6 365529+5 148858+2 232425-3-228472+7 815909+2 3000 60001  -0N2O       72
 1  99                            JANAF 3-31-65            E-                  73
     0+0 134229+5 496800+1 000000-0-700991-3 16458942  500  30001  -0E-       74
     0+0 134229+5 496799+1 000000-0 216303-0 16458942  3000 60001  -0E-       75
```

```
 1  8  1  99                      JANAF 6-30-65                   D-             76
242999+5 136819+5 497358+1-566327-6 190609+5 492849+2  500  30001  -0D-        77
242999+5 136819+5 496546+1 402558-6 349305+5 492849+2  3000 60001  -0D-        78
 2  8  1  99                      JANAF 12-31-66                  O2-            79
-113099+5 235849+5 977974+1 127404-3-269662+6 693049+2  500  30001  -0O2-      80
-113099+5 235849+5 865325+1 136181-3 631793+6 693049+2  3000 60001  -0O2-      81
 1  6  1  99                      CONVAIR ZPH-122 12/61            C+            82
+428995+6 150120+5 489657+1 180700-4-348000+5 484232+2 22000. 10000.1   C+     83
+428995+6 150120+5 489657+1 180700-4-348000+5 484232+2 22000. 10000.1   C+     84
 1  6  1  8  1  99                CONVAIR ZPH-122 12/61           CO+            85
+294283+6 243830+5 893619+1 378000-4-150900+7 666595+2 22000. 10000.1  CO+     86
+294283+6 243830+5 893619+1 378000-4-150900+7 666595+2 22000. 10000.1  CO+     87
 1  7  1  99                      CONVAIR ZPH-122 12/61            N+            88
+446641+6 151310+5 501751+1 617100-4-184100+7 496847+2 22000. 10000.1   N+     89
+446641+6 151310+5 501751+1 617100-4-184100+7 496847+2 22000. 10000.1   N+     90
 1  7  1  8  1  99                JANAF 6-30-66                   NO+            91
236659+6 221499+5 792263+1 320385-3-313163+6 653320+2  500  30001  -0NO+      92
236659+6 221499+5 892163+1 385863-4-164555+7 653320+2  3000 60001  -0NO+      93
 2  7  1  99                      CONVAIR ZPH-122 12/61           N2+            94
+357258+6 251470+5 136508+2-327940-3-225630+8 656601+2 22000. 10000.1  N2+     95
+357258+6 251470+5 136508+2-327940-3-225630+8 656601+2 22000. 10000.1  N2+     96
 1  8  1  99                      CONVAIR ZPH-122 12/61            O+            97
+371999+6 149290+5 336271+1 306710-3 590200+7 484849+2 22000. 10000.1   O+     98
+371999+6 149290+5 336271+1 306710-3 590200+7 484849+2 22000. 10000.1   O+     99
 2  8  1  99                      CONVAIR ZPH-122 12/61           O2+           100
+279695+6 248710+5 594789+1 626340-3 103500+8 677731+2 22000. 10000.1  O2+    101
+279695+6 248730+5 547789+1 626340-3 103500+8 677731+2 22000. 10000.1  O2+    102
 1  6  1  7  1  99                JANAF 6/69       KS      CN+                  103
429399+6 238459+5 811795+1 517816-3-130663+6 702739+2  300  30001  -0CN+      104
429399+6 238459+5 102410+2-992339-5-499752+7 702739+2  1000 60001  -0CN+      105
 1  6  1  7  1  99                JANAF 6/69       KS      CN-                  106
159999+5 222629+5 761849+1 420233-3-100744+6 648930+2  300  30001  10CN-      107
159999+5 222629+5 892372+1 373764-4-152872+7 648930+2  3000 60001  10CN-      108
```

```
 1  1  1  1  1  1  1  1  1  1  1  1  1  0  1  1  1  1  1  0  1                  110
2056 4                                                                        111
   0.40  +01  0.10  +02  0.60  +01  0.18  +02  0.54  +02  0.90  +02            112
   0.00  +00  0.00  +00  0.90  +01  0.50  +01  0.10  +01  0.50  +01            113
   0.30  +01  1.53  +31  0.90  +01  0.40  +01  0.90  +01  0.50  +01            114
   0.12  +01  0.50  +01  0.12  +02  0.15  +02  0.36  +02  0.00  +00            115
   0.20  +01  0.80  +01  0.18  +02  3.32  +01  0.00  +00  0.00  +00            116
   0.00  +00  0.00  +00  0.90  +01  0.00  +00  0.00  +00  0.00  +00            117
   0.01  +00  0.00  +00  0.00  +00  0.00  +00  0.40  +01  0.00  +00            118
   0.03  +00  0.00  +00  0.00  +00  0.00  +00  0.00  +00  0.00  +00            119
   0.60  +01  0.00  +00  0.00  +00  0.00  +00  0.00  +00  0.00  +00            120
   0.03  +00  0.00  +00  0.00  +00  0.00  +00  0.00  +00  0.00  +00            121
   0.00  +00  0.2984+01  0.3576+01  0.1045+02  0.1188+02  0.1300+02            122
   0.00  +00  0.90  -07  0.1967+01  0.4189+01  0.9144+01                       123
   0.9519+01  0.1074+02  0.1099+02  0.1208+02  0.00  +01  1.2639+00            124
   2.6839+00  4.1625+00  7.5351+00  7.9461+00  8.6442+00  0.00  +00            125
   0.00  +00  0.1020+02  0.1208+02  0.1274+02  0.00  +00  0.00  +00            126
```

```
   0.60  +00  0.81  +30  0.96  +00  0.12  +01  0.14  +01  0.162 +01            132
   0.24  +01  0.34  +01  0.40  +01  0.62  +01  0.80  +01  0.90  +01            133
   0.97  +01  0.1045+02  0.1080+02  0.1170+02  0.1210+02  0.1280+02            134
   0.1340+02  0.1380+02  0.00  +00  0.00  +00  0.00  +00  0.00  +00            135
   0.80  +00  0.95  +00  0.12  +01  0.14  +01  0.16  +01  0.24  +01            136
   0.3500+01  0.40  +01  0.60  +01  0.80  +01  0.90  +01  0.97  +01            137
   0.1045+02  0.1080+02  0.1170+02  0.1210+02  0.1280+02  0.1340+02            138
   0.1340+02  0.1450+02  0.00  +00  0.00  +00  0.00  +00  0.00  +00            139
   0.69  +00  0.89  +00  0.1050+01  0.1290+01  0.1460+01  0.1850+01            140
   0.2850+01  0.3700+01  0.5000+01  0.7110+01  0.8400+01  0.94  +01            141
   0.1007+02  0.1062+02  0.1120+02  0.1190+02  0.1241+02  0.1304+02            142
   0.1358+02  0.1470+02    .      .      .      +      .      .                143
 6 71316                                                                       144
 6 8  6  5  6  5  1  1 810 1212 712 8  9  4  4  4                              145
27        0.660       0.8421       5.67E  -20                                 146
16        0.685       0.198        110E-21 6.                                  147
27        0.6859      0.044        32LE-21 3.                                  148
 6        0.689       0.1597       187E-20 6.                                  149
23        0.710       0.208        639E-18 4.                                  150
```

161

						#
5	0.7525	0.0149	446E-21			
22	0.844	3.0808	412E-21	3.		
21	0.852	0.0687	108E-21			
5	0.875	0.0366	380E-21	4.		
15	0.8840	0.1570	367E-21			
4	0.9158	0.00847	759E-22			
6	0.9304	0.0253	387E-20	2.		
6	0.965	0.0262	387E-20	4.		
16	0.991	0.0805	309E-20	2.		
23	1.019	0.0329	205E-19	4.		
5	1.0355	0.0735	331E-21	7.		
22	1.079	0.1008	320E-21	8.		
15	1.0980	0.7490	344E-21			
14	1.1320	0.2010	367E-21			
21	1.163	0.474	108E-21			
22	1.224	0.0285	262E-21			
5	1.2610	0.118	312E-21	3.		
4	1.3190	0.1833	984E-22			
21	1.326	0.206	138E-21	3.		
14	1.3380	0.9130	342E-21			
5	1.3677	0.0387	292E-21			
4	1.4380	0.256	824E-22	3.		
13	1.4670	0.9900	865E-22			
21	1.487	0.0405	218E-21			
5	1.5527	0.0030	293E-20			
12	1.594	1.0300	709E-22			
4	1.6630	0.0923	998E-22			
15	1.767	0.0224	275E-20	3.		
22	1.814	0.0039	350E-20	5.		
5	1.8357	0.00566	293E-20	5.		
26	1.888	0.4407				
14	2.015	0.0258	275E-20	3.		
26	2.549	0.1193				
4	2.925	0.0070	106E-20	3.		
13	3.0	0.010	810E-21	2.		
12	3.167	0.00826	520E-21			
4	3.4724	0.00861	452E-20	3.		
12	3.7110	0.0149	110E-20			
19	5.002	0.0676	113E-21			
18	6.424	0.07290	113E-21			
19	7.013	0.01410	500E-21			
19	7.078	0.0748	262E-21			
3	07.111	0.0634	912E-22			
11	7.481	0.105	673E-22			
19	7.717	0.00534	220E-20			
19	7.721	0.0367	109E-19			
17	7.947	0.283	208E-22			
19	8.030	0.50457	690E-19			
19	8.191	0.0116	130E-18			
19	8.203	0.00147	119E-19			
19	8.302	0.00831	538E-18			
2	08.3021	0.0740	912E-22			
18	8.368	0.011	214E-21			
19	8.377	0.00501	677E-18			
18	8.433	0.0142	500E-21			
18	8.474	0.0625	268E-21			
3	08.781	0.0435	661E-22			
18	9.137	0.00526	228E-20			
18	9.141	0.0362	109E-19			
3	09.301	0.0166	446E-21			
17	9.332	0.203	557E-23			
3	09.394	0.0119	229E-21			
18	9.450	0.0218	690E-19			
3	09.460	0.0360	338E-21			
09	9.5010	0.0471	548E-22			
15	9.611	0.0114	130E-18			
18	9.623	0.00143	119E-19			
17	9.697	0.01950	500E-21			
17	9.698	0.0038	235E-21			
17	9.709	0.0767	235E-21			
18	9.722	0.0001	538E-18			
18	9.797	0.00488	677E-18			
17	9.834	0.026	293E-21			
2	09.973	0.0890	661E-22			
3	10.102	0.0374	293E-20			

#					#
151	11	10.182	0.1510	653E-22	226
152	25	10.196	0.4162		227
153	1	10.332	0.1840	621E-22	228
154	17	10.401	0.30719	220E-20	229
155	17	10.405	0.0495	109E-19	230
156	3	10.418	0.0225	537E-20	231
157	2	10.493	0.0187	446E-20	232
158	3	10.585	0.0131	796E-20	233
159	2	10.619	0.0533	312E-21	234
160	3	10.662	0.00819	268E-19	235
161	17	10.714	0.0298	690E-19	236
162	3	10.757	0.00518	437E-19	237
163	10	10.761	0.1200	653E-22	238
164	18	10.873	0.705	630E-21	239
165	17	10.875	0.0155	130E-18	240
166	17	10.887	0.00195	119E-19	241
167	1	10.927	0.4540	161E-23	242
168	17	10.986	0.011	253E-19	243
169	11	11.007	0.0185	367E-21	244
170	17	11.061	0.00659	677E-18	245
171	3	11.200	0.0200	446E-21	246
172	2	11.243	0.0418	293E-20	247
173	3	11.310	0.0254	323E-21	248
174	7	11.424	0.2260	143E-23	249
175	2	11.609	0.0250	532E-20	250
176	2	11.778	0.0220	796E-20	251
177	11	11.806	0.0049	145E-20	252
178	09	11.852	0.0199	367E-21	253
179	2	11.874	0.0091	268E-19	254
180	2	11.948	0.00575	437E-19	255
181	3	12.000	0.0269	290E-20	256
182	09	12.067	0.0218	344E-21	257
183	25	12.084	0.0791		258
184	11	12.160	0.0019	128E-20	259
185	14	12.181	1.05	159E-22	260
186	3	12.316	0.0136	696E-20	261
187	10	12.404	0.0461	653E-22	262
188	2	12.414	0.0574	390E-21	263
189	2	12.511	0.0279	337E-21	264
190	09	12.521	0.0775	633E-22	265
191	09	12.651	0.00924	145E-20	266
192	25	12.745	0.02899	4.59E-20	267
193	1	12.877	0.0233	446E-21	268
194	1	13.004	0.1320	294E-21	269
195	17	13.119	0.379	101E-21	270
196	2	13.190	0.0489	299E-20	271
197	2	13.508	0.0291	696E-19	272
198	7	13.543	0.1610	950E-24	273
199	18	13.601	0.295	159E-22	274
200	1	13.677	0.0957	293E-20	275
201	1	13.993	0.0584	532E-20	276
202	1	14.160	0.0342	796E-20	277
203	1	14.257	0.0212	268E-19	278
204	1	14.332	0.0138	437E-19	279
205	48				280

#						
206	0.02	0.1	0.2	0.5	0.6	0.8
207	1.00	1.50	2.00	2.5	2.75	3.0
208	3.25	3.50	3.75	4.0	4.5	5.0
209	6.00	7.00	8.00	8.50	8.52	8.98
210	9.00	9.19	9.21	9.99	10.01	10.79
211	10.81	11.00	11.25	11.27	11.99	12.01
212	12.18	12.20	12.99	13.00	13.39	13.41
213	13.59	13.61	14.29	14.31	14.55	15.00

OUTPUT FOR SAMPLE CASE

CASE — .97 CO2 — .03 N2 (BY VOLUME), 60 DEG. CONICAL BODY, HIGH VEL.

FREESTREAM PARAMETERS
VELOCITY = 1.1175E+04 M/S
DENSITY = 2.8500E-03 KG/M3
PRESSURE = 1.1730E+02 N/M2
ENTHALPY = -8.6600E+04 J/KG
NOSE RADIUS = 3.0480E-01 M

BODY SHAPE, NONDIMENSIONAL BY NOSE RADIUS

NS	S	XBOD	YBOD	THETA	K
1	0.0000	0.0000	0.0000	1.5708	1.0000
2	.2000	.0199	.1987	1.3708	1.0000
3	.4000	.0789	.3894	1.1708	1.0000
4	.6000	.1722	.5662	1.0472	0.0000
5	.8000	.2722	.7394	1.0472	0.0000
6	1.2000	.4722	1.0858	1.0472	0.0000
7	2.0000	.8722	1.7786	1.0472	0.0000
8	3.0000	1.3722	2.6446	1.0472	0.0000
9	4.0000	1.8722	3.5107	1.0472	0.0000
10	5.0000	2.3722	4.3767	1.0472	0.0000

PARAMETERS FOR NONDIMENSIONALIZATION
VF = 1.1175E+04 M/S
RHUF = 2.8500E-03 KG/M3
VF*VF = 1.24881E+08 J/KG
RHOF*VF*VF = 3.55910E+05 N/M2
RHOF*VF*VF*VF = 3.97729E+09 W/M2
TS = 1.1816E+04 K
VF*VF/TS = 1.05683E+04 J/(KG-K)
RN = 3.0480E-01 M
RN/VF = 2.72352E-05 S

NORMAL SHOCK PROPERTIES — NONDIMENSIONAL
PRESSURE = .9375
DENSITY = 15.45
ENTHALPY = .4269
TEMPERATURE = 1.000
VELOCITY = -.0627
MOLECULAR WT. = 13.39
ENTROPY = 1.592
SONIC VELOCITY = .2700

NAME2
TIFRAC = 0.8E+00,
IMSC = 500,
CGI = 0.1E-03,
CCF = 0.95E+00,
ICC = 50,
IKSF = 1200,
IOUTN = 200,
IOUTF = 100,
ITG = 100,
IRG = 100,
IKSU = 100, 200, 400, 600, 800, 1000,
ITGU = 50, 50, 50, 50, 50,
IRGU = 200, 200, 200, 200, 100,
MCTS = 0,
LSC = 800,
CCS = 0.5E-03,
6END

CONVERGED OUTPUT   ITERATIONS = -843   TIME = 1.519E+01

BODY STATION 1   S = 0.0000   THETA = 1.5708   BETA = 0.0000   DELTA = .0456   DELTAT = 0.

XBOD = 0.0000   YBOD = 0.0000   XSHOC = -.0456   YSHOC = .0000

QNT = 8.916E-03   QNL = 4.739E-03   QML = 4.176E-03

VELZ = 6.270E-02   SA2 = 0.

MASS BALANCE   FREESTREAM = 0.   SHOCK LAYER = 0.   DELTA MASS = 4.557E-02

BODY STATION 2   S = .2000   THETA = 1.3708   BETA = .0119   DELTA = .0468   DELTAT = 0.

XBOD = .0199   YBOD = .1987   XSHOC = -.0259   YSHOC = .2080

QNT = 7.693E-03   QNC = 4.139E-03   QML = 3.554E-03

VELZ = 1.966E-01   SA2 = 1.256E+00

MASS BALANCE   FREESTREAM = 4.623E-01   SHOCK LAYER = 4.614E-01   DELTA MASS = 4.477E-02

163

BODY STATION 3   S = .4000   THETA = 1.1700   BETA = .0136   DELTA = .0505   DELTAF = 0.

XBOD = .0789   YBOD = .3894   XSHOC = .0324   YSHOC = .4093

QMI = 4.713E-03   QWC = 2.770E-03   QWL = 1.943E-03

VELZ = 3.806E-03   SAZ = 1.429E+00

KY	1	2	3	4	5	6	7	8	9
Y	0.	1.250E-01	2.500E-01	3.750E-01	5.000E-01	6.250E-01	7.500E-01	8.750E-01	1.000E+00

MASS BALANCE   FREESTREAM = 1.466E+00   SHOCK LAYER = 1.452E+00   DELTA MASS = 5.054E-02

BODY STATION 4   S = .6000   THETA = 1.0472   BETA = .0187   DELTA = .0525   DELTAF = 0.

XBOD = .1722   YBOD = .5462   XSHOC = .1247   YSHOC = .5924

QMI = 3.176E-03   QWL = 2.240E-03   QWL = 9.364E-04

VELZ = 4.061E-01   SAZ = 1.472E+00

KY	1	2	3	4	5	6	7	8	9
Y	0.	1.250E-01	2.500E-01	3.750E-01	5.000E-01	6.250E-01	7.500E-01	8.750E-01	1.000E+00

MASS BALANCE   FREESTREAM = 3.342E+00   SHOCK LAYER = 3.335E+00   DELTA MASS = 5.256E-02

BODY STATION 5   S = .8000   THETA = 1.0472   BETA = .0338   DELTA = .0580   DELTAF = 0.

XBOD = .2722   YBOD = .7394   XSHOC = .2219   YSHOC = .7604

QMI = 2.682E-03   QWL = 2.172E-03   QWL = 7.097E-04

VELZ = 4.779E-01   SAZ = 1.468E+00

KY	1	2	3	4	5	6	7	8	9
Y	0.	1.250E-01	2.500E-01	3.750E-01	5.000E-01	6.250E-01	7.500E-01	8.750E-01	1.000E+00

MASS BALANCE   FREESTREAM = 5.088E+00   SHOCK LAYER = 5.080E+00   DELTA MASS = 5.802E-02

BODY STATION 6   S = 1.2000   THETA = 1.0472   BETA = .0484   DELTA = .0745   DELTAF = 0.

XBOD = .4722   YBOD = 1.0858   XSHOC = .4059   YSHOC = 1.1241

QMI = 2.803E-03   QWL = 2.221E-03   QWL = 5.761E-04

VELZ = 4.801E-01   SAZ = 1.465E+00

KY	1	2	3	4	5	6	7	8	9
Y	0.	1.250E-01	2.500E-01	3.750E-01	5.000E-01	6.250E-01	7.500E-01	8.750E-01	1.000E+00

MASS BALANCE   FREESTREAM = 8.254E+00   SHOCK LAYER = 8.244E+00   DELTA MASS = 7.654E-02

```
BODY STATION  7        S =  2.0000      THETA =  1.0472      BETA =   .0534      DELTA =  .1186      DELTAT = 0.
                       XBOD =   .8722      YBOD =  1.7786      XSHOC =   .7693      YSHOC =  1.8380
                       QWT = 3.094E-03     QWC = 2.533E-03      QWL = 5.612E-04

                       VEL2 = 4.558E-01   SA2 = 1.462E+00

KY         1           2           3           4           5           6           7           8           9
Y     0.          1.250E-01   2.500E-01   3.750E-01   5.000E-01   6.250E-01   7.500E-01   8.750E-01   1.000E+00
P     7.643E-01   7.582E-01   7.577E-01   7.567E-01   7.548E-01   7.529E-01   7.505E-01   7.477E-01   7.509E-01
RHO   2.256E+01   1.815E+01   1.857E+01   1.859E+01   1.849E+01   1.836E+01   1.822E+01   1.806E+01   1.803E+01
H     2.589E-01   3.245E-01   3.193E-01   3.188E-01   3.195E-01   3.208E-01   3.221E-01   3.235E-01   3.250E-01
U     1.104E-01   3.865E-01   4.505E-01   4.554E-01   4.573E-01   4.560E-01   4.558E-01   4.552E-01   4.551E-01
V     0.         -1.082E-03  -6.109E-03  -9.804E-03  -1.313E-02  -1.649E-02  -1.984E-02  -2.324E-02  -2.519E-02
M     6.385E-01   1.705E+00   2.014E+00   2.041E+00   2.045E+00   2.036E+00   2.026E+00   2.016E+00   2.010E+00
T     6.950E-01   7.784E-01   7.688E-01   7.674E-01   7.690E-01   7.712E-01   7.735E-01   7.760E-01   7.792E-01
MW    1.613E+01   1.473E+01   1.482E+01   1.484E+01   1.482E+01   1.480E+01   1.477E+01   1.475E+01   1.473E+01
SX    1.399E+00   1.489E+00   1.482E+00   1.481E+00   1.483E+00   1.485E+00   1.486E+00   1.488E+00   1.490E+00
VA    1.985E-01   2.200E-01   2.237E-01   2.232E-01   2.237E-01   2.244E-01   2.252E-01   2.259E-01   2.268E-01
PL   -4.006E-01  -2.944E-01  -3.038E-01  -3.058E-01  -3.045E-01  -3.026E-01  -3.008E-01  -2.992E-01  -2.950E-01
QP    0.          1.154E-03   1.752E-03   2.142E-03   2.477E-03   2.794E-03   3.098E-03   3.396E-03   3.691E-03
QH    3.094E-03   3.315E-03   2.986E-03   2.712E-03   2.441E-03   2.164E-03   1.645E-03   1.095E-03   0.
QN   -3.094E-03  -2.160E-03  -1.234E-03  -5.702E-04   4.580E-05   6.895E-04   1.918E-03   2.300E-03   3.693E-03
DD    6.230E-02   6.207E-02   5.321E-02   4.293E-02   4.243E-02   4.619E-02   5.455E-02   7.721E-02   1.114E-01
RHOT  1.079E-02   1.234E-03   8.508E-04   2.928E-04  -2.145E-04  -1.887E-04   2.244E-05   9.654E-06   0.
UT   -1.039E-04   5.963E-05   1.544E-05   7.482E-06   1.608E-06  -4.934E-06  -7.427E-06  -9.446E-06   0.
VT    0.          3.634E-08  -3.138E-08   6.421E-07   7.724E-07   1.033E-06   1.474E-06   1.880E-06   0.
PT    2.390E-05  -7.344E-06   4.954E-06   1.561E-06   9.403E-07   1.689E-07  -7.531E-07  -1.698E-06   0.
HT   -1.567E-04  -1.465E-05  -1.084E-05  -3.766E-06   3.610E-06   2.998E-06  -6.094E-07   1.613E-06   0.
TAU   5.985E-02   5.343E-02   5.617E-02   5.814E-02   5.988E-02   6.165E-02   6.351E-02   6.549E-02   6.699E-02
SF    0.          1.110E+00   2.880E+00   4.721E+00   6.630E+00   8.537E+00   1.043E+01   1.232E+01   1.420E+01

            MASS BALANCE      FREESTREAM = 1.422E+01      SHOCK LAYER = 1.420E+01      DELTA MASS = 1.188E-01

BODY STATION  8        S =  3.0000      THETA =  1.0472      BETA =   .0543      DELTA =  .1730      DELTAT = 0.
                       XBOD =  1.3722      YBOD =  2.6444      XSHOC =  1.2223      YSHOC =  2.7511
                       QWT = 3.622E-03     QWC = 3.040E-03      QWL = 5.823E-04

                       VEL2 = 4.550E-01   SA2 = 1.462E+00

KY         1           2           3           4           5           6           7           8           9
Y     0.          1.250E-01   2.500E-01   3.750E-01   5.000E-01   6.250E-01   7.500E-01   8.750E-01   1.000E+00
P     7.654E-01   7.548E-01   7.560E-01   7.534E-01   7.557E-01   7.539E-01   7.517E-01   7.492E-01   7.516E-01
RHO   2.368E+01   1.874E+01   1.884E+01   1.866E+01   1.852E+01   1.838E+01   1.825E+01   1.810E+01   1.802E+01
H     2.420E-01   3.157E-01   3.158E-01   3.170E-01   3.194E-01   3.208E-01   3.220E-01   3.235E-01   3.254E-01
U     1.320E-01   4.263E-01   4.591E-01   4.545E-01   4.550E-01   4.543E-01   4.542E-01   4.541E-01   4.543E-01
V     0.         -1.648E-03  -6.054E-03  -9.419E-03  -1.265E-02  -1.597E-02  -1.928E-02  -2.265E-02  -2.486E-02
M     6.901E-01   1.925E+00   2.072E+00   2.041E+00   2.035E+00   2.026E+00   2.020E+00   2.013E+00   2.004E+00
T     6.814E-01   7.623E-01   7.622E-01   7.659E-01   7.687E-01   7.712E-01   7.734E-01   7.760E-01   7.799E-01
MW    1.656E+01   1.489E+01   1.489E+01   1.485E+01   1.482E+01   1.480E+01   1.478E+01   1.475E+01   1.472E+01
SX    1.375E+00   1.478E+00   1.477E+00   1.480E+00   1.483E+00   1.484E+00   1.486E+00   1.488E+00   1.491E+00
VA    1.933E-01   2.217E-01   2.216E-01   2.228E-01   2.237E-01   2.244E-01   2.251E-01   2.259E-01   2.270E-01
PL   -4.076E-01  -3.128E-01  -3.116E-01  -3.074E-01  -3.045E-01  -3.021E-01  -3.005E-01  -2.987E-01  -2.941E-01
QP    0.          1.356E-03   2.046E-03   2.557E-03   3.013E-03   3.434E-03   3.843E-03   4.217E-03   4.606E-03
QH    3.622E-03   3.931E-03   3.622E-03   3.318E-03   2.973E-03   2.580E-03   2.098E-03   1.406E-03   0.
QN   -3.622E-03  -2.575E-03  -1.574E-03  -7.596E-04   3.902E-05   8.543E-04   1.737E-03   2.811E-03   4.606E-03
DD    4.889E-02   4.685E-02   4.171E-02   3.425E-02   3.744E-02   3.940E-02   4.555E-02   6.803E-02   1.005E-01
RHOT  9.330E-03   4.004E-04  -9.613E-05  -4.389E-04  -6.606E-04  -6.190E-04  -4.900E-04  -4.934E-04   0.
UT   -3.418E-04   1.423E-05  -1.099E-05  -1.129E-05  -1.599E-05  -1.810E-05  -1.693E-05  -1.662E-05   0.
VT    0.          6.198E-06   2.760E-06   3.149E-06   3.014E-06   2.979E-06   3.034E-06   2.999E-06   0.
PT    2.185E-05  -1.545E-05  -1.175E-06  -2.956E-06  -2.910E-06  -3.149E-06  -3.595E-06  -3.992E-06   0.
HT   -1.303E-04  -7.649E-06   1.250E-06   5.613E-06   9.020E-06   8.294E-06   6.195E-06   7.260E-06   0.
TAU   8.951E-02   7.968E-02   8.265E-02   8.476E-02   8.709E-02   8.963E-02   9.236E-02   9.524E-02   9.748E-02
SF    0.          1.842E+00   4.609E+00   7.469E+00   1.030E+01   1.313E+01   1.594E+01   1.874E+01   2.154E+01

            MASS BALANCE      FREESTREAM = 2.156E+01      SHOCK LAYER = 2.154E+01      DELTA MASS = 1.730E-01

BODY STATION  9        S =  4.0000      THETA =  1.0472      BETA =   .0542      DELTA =  .2275      DELTAT = 0.
                       XBOD =  1.8722      YBOD =  3.5107      XSHOC =  1.6752      YSHOC =  3.6244
                       QWT = 4.164E-03     QWC = 3.556E-03      QWL = 6.075E-04

                       VEL2 = 4.550E-01   SA2 = 1.462E+00

KY         1           2           3           4           5           6           7           8           9
Y     0.          1.250E-01   2.500E-01   3.750E-01   5.000E-01   6.250E-01   7.500E-01   8.750E-01   1.000E+00
P     7.652E-01   7.549E-01   7.546E-01   7.572E-01   7.557E-01   7.540E-01   7.519E-01   7.493E-01   7.515E-01
RHO   2.450E+01   1.902E+01   1.893E+01   1.872E+01   1.857E+01   1.843E+01   1.829E+01   1.813E+01   1.803E+01
H     2.296E-01   3.114E-01   3.141E-01   3.169E-01   3.186E-01   3.201E-01   3.215E-01   3.231E-01   3.254E-01
U     1.153E-01   4.412E-01   4.566E-01   4.535E-01   4.541E-01   4.538E-01   4.539E-01   4.541E-01   4.543E-01
V     0.         -1.481E-03  -6.028E-03  -9.311E-03  -1.256E-02  -1.588E-02  -1.919E-02  -2.256E-02  -2.488E-02
M     7.249E-01   2.012E+00   2.078E+00   2.041E+00   2.036E+00   2.027E+00   2.021E+00   2.015E+00   2.005E+00
T     6.722E-01   7.550E-01   7.590E-01   7.643E-01   7.673E-01   7.699E-01   7.724E-01   7.752E-01   7.798E-01
MW    1.690E+01   1.497E+01   1.492E+01   1.487E+01   1.484E+01   1.481E+01   1.479E+01   1.476E+01   1.472E+01
SX    1.357E+00   1.472E+00   1.475E+00   1.479E+00   1.482E+00   1.484E+00   1.486E+00   1.488E+00   1.491E+00
VA    1.897E-01   2.194E-01   2.208E-01   2.223E-01   2.232E-01   2.240E-01   2.248E-01   2.257E-01   2.270E-01
PL   -4.089E-01  -3.227E-01  -3.151E-01  -3.094E-01  -3.062E-01  -3.038E-01  -3.016E-01  -2.996E-01  -2.942E-01
QP    0.          6.590E-04   2.332E-03   2.945E-03   3.492E-03   3.987E-03   4.474E-03   4.948E-03   5.413E-03
QH    4.164E-03   4.539E-03   4.209E-03   3.842E-03   3.427E-03   2.844E-03   2.410E-03   1.662E-03   0.
QN   -4.164E-03  -2.999E-03  -1.876E-03  -8.965E-04   4.522E-05   1.033E-03   2.056E-03   3.277E-03   5.413E-03
DD    4.115E-02   3.908E-02   3.674E-02   3.405E-02   3.396E-02   3.517E-02   3.476E-02   5.948E-02   9.198E-02
RHOT  1.162E-02  -1.618E-04  -4.450E-04  -6.599E-04  -7.206E-04  -6.658E-04  -6.144E-04  -6.369E-04   0.
UT   -4.484E-04  -7.228E-06  -1.644E-05  -1.466E-05  -1.729E-05  -1.737E-05  -1.569E-05  -1.553E-05   0.
VT    0.          6.428E-06   2.649E-06   2.824E-06   2.529E-06   2.211E-06   2.141E-06   1.884E-06   0.
PT    1.860E-05  -1.969E-05  -5.487E-06  -7.024E-06  -6.923E-06  -7.125E-06  -7.502E-06  -7.829E-06   0.
HT   -1.620E-04  -1.942E-06   5.150E-06   7.540E-06   8.502E-06   7.590E-06   6.696E-06   7.710E-06   0.
TAU   1.199E-01   1.060E-01   1.091E-01   1.117E-01   1.147E-01   1.180E-01   1.216E-01   1.253E-01   1.282E-01
SF    0.          2.578E+00   6.245E+00   1.015E+01   1.392E+01   1.767E+01   2.141E+01   2.513E+01   2.884E+01

            MASS BALANCE      FREESTREAM = 2.887E+01      SHOCK LAYER = 2.884E+01      DELTA MASS = 2.279E-01

BODY STATION 10        S =  5.0000      THETA =  1.0472      BETA =   .0538      DELTA =  .2816      DELTAT = 0.
                       XBOD =  2.3722      YBOD =  4.3767      XSHOC =  2.1281      YSHOC =  4.5175
                       QWT = 4.662E-03     QWC = 4.025E-03      QWL = 6.369E-04

                       VEL2 = 4.554E-01   SA2 = 1.462E+00

KY         1           2           3           4           5           6           7           8           9
Y     0.          1.250E-01   2.500E-01   3.750E-01   5.000E-01   6.250E-01   7.500E-01   8.750E-01   1.000E+00
P     7.649E-01   7.549E-01   7.585E-01   7.571E-01   7.557E-01   7.540E-01   7.519E-01   7.494E-01   7.512E-01
RHO   2.519E+01   1.922E+01   1.901E+01   1.878E+01   1.863E+01   1.848E+01   1.834E+01   1.816E+01   1.803E+01
H     2.195E-01   3.083E-01   3.128E-01   3.158E-01   3.177E-01   3.193E-01   3.208E-01   3.226E-01   3.252E-01
U     1.367E-01   4.492E-01   4.572E-01   4.548E-01   4.539E-01   4.538E-01   4.540E-01   4.543E-01   4.547E-01
V     0.         -1.721E-03  -6.019E-03  -9.266E-03  -1.294E-02  -1.587E-02  -1.919E-02  -2.257E-02  -2.503E-02
M     7.582E-01   2.063E+00   2.078E+00   2.044E+00   2.039E+00   2.032E+00   2.025E+00   2.019E+00   2.007E+00
T     6.652E-01   7.501E-01   7.575E-01   7.629E-01   7.657E-01   7.685E-01   7.711E-01   7.743E-01   7.795E-01
MW    1.718E+01   1.503E+01   1.494E+01   1.489E+01   1.485E+01   1.482E+01   1.480E+01   1.477E+01   1.472E+01
SX    1.342E+00   1.468E+00   1.474E+00   1.478E+00   1.480E+00   1.483E+00   1.485E+00   1.487E+00   1.490E+00
VA    1.869E-01   2.178E-01   2.201E-01   2.217E-01   2.227E-01   2.236E-01   2.244E-01   2.254E-01   2.269E-01
PL   -4.078E-01  -3.298E-01  -3.179E-01  -3.118E-01  -3.081E-01  -3.053E-01  -3.030E-01  -3.004E-01  -2.946E-01
QP    0.          1.705E-03   2.591E-03   3.242E-03   3.917E-03   4.497E-03   5.047E-03   5.583E-03   6.138E-03
QH    4.662E-03   5.105E-03   4.746E-03   4.318E-03   3.845E-03   3.301E-03   2.690E-03   1.876E-03   0.
QN   -4.662E-03  -3.402E-03  -2.155E-03  -1.026E-03   8.204E-05   1.196E-03   2.357E-03   3.706E-03   6.138E-03
DD    3.550E-02   3.526E-02   3.354E-02   3.170E-02   3.161E-02   3.248E-02   3.597E-02   5.414E-02   8.509E-02
RHOT  1.326E-02  -4.497E-04  -6.094E-04  -7.338E-04  -7.164E-04  -6.649E-04  -6.688E-04  -7.090E-04   0.
UT   -4.877E-04  -1.571E-05  -1.668E-05  -1.470E-05  -1.619E-05  -1.557E-05  -1.419E-05  -1.447E-05   0.
VT    0.          5.581E-06   2.301E-06   2.296E-06   1.923E-06   1.622E-06   1.344E-06   9.978E-07   0.
PT    1.195E-05  -2.155E-05  -8.548E-06  -5.698E-06  -9.623E-06  -9.888E-06  -1.021E-05  -1.052E-05   0.
HT   -1.824E-04   9.953E-07   6.224E-06   7.699E-06   7.469E-06   6.681E-06   6.550E-06   7.406E-06   0.
TAU   1.506E-01   1.322E-01   1.354E-01   1.365E-01   1.422E-01   1.463E-01   1.507E-01   1.552E-01   1.587E-01
SF    0.          3.327E+00   6.095E+00   1.205E+01   1.755E+01   2.224E+01   2.691E+01   3.157E+01   3.620E+01

            MASS BALANCE      FREESTREAM = 3.624E+01      SHOCK LAYER = 3.620E+01      DELTA MASS = 2.816E-01
```